

PSR Report 1122

ANALYSIS OF LARGE URBAN FIRES

By

R. D. Small
D. A. Larson
H. L. Brode

September 1981

Final Report
Contract EMW-C-0309, Work Unit 2564E

For
Federal Emergency Management Agency
Washington, D.C. 20472

FEMA Review Notice

This report has been reviewed in the Federal Emergency Management Agency and approved for publication. Approval does not signify that the contents necessarily reflect the views and policies of the Federal Emergency Management Agency.

Approved For Public Release: Distribution Unlimited



PACIFIC • SIERRA RESEARCH CORP.

1456 Cloverfield Blvd. Santa Monica, California 90404

NOTICE

THIS DOCUMENT HAS BEEN REPRODUCED FROM THE BEST COPY FURNISHED US BY THE SPONSORING AGENCY. ALTHOUGH IT IS RECOGNIZED THAT CERTAIN PORTIONS ARE ILLEGIBLE, IT IS BEING RELEASED IN THE INTEREST OF MAKING AVAILABLE AS MUCH INFORMATION AS POSSIBLE.

BLOCK 20 (Cont.)

dependent volume heat source. The theory of large area fires thus developed is applicable to arbitrarily large fires and, in the lower limit, to scale fires the size of the multiple-fuel-bed Flambeau experiments.

The boundary value problem and solution algorithm for computation of the velocities and thermodynamic variables in and around the burning zone are detailed. Numerical results are given for the nominal case of a 10 km fire. The influence of radiation, turbulent diffusion of heat and momentum, and heat addition rate are explored and analyzed. The results show a large-velocity horizontal inflow being turned in the burning (heat addition) region to a vertical column flow, the convection column having a width comparable to that of the fire. The numerical results reveal the nonlinear interchanges of momentum and energy in the burning region and the early plume. An experimental multiple-fuel-bed Flambeau fire is also analyzed. For that case, the equations describing the convection column are shown to reduce to the classical plume equations. Numerical results are consistent with experimental observations, and resemble those obtained for the 10 km fire.

iii

PREFACE

This report continues Pacific-Sierra Research Corporation's model development and analysis of large urban fires. Analysis and results are presented for a nominal 10 km area fire and a multiple-fuel-bed Flambeau fire. Portions of this report will be submitted for presentation and publication to the Nineteenth International Symposium on Combustion, sponsored by The Combustion Institute.



EXECUTIVE SUMMARY

Large urban fires have resulted from natural disasters, explosions, and wartime actions. In many cases, entire urban areas were totally destroyed despite firefighters' efforts to contain the flames. The World War II firebombing raids on European and Japanese population centers caused immense damage and hundreds of thousands of casualties. Several ignited firestorms, with hurricane-force winds, high street-level temperatures, high concentrations of carbon monoxide, and complete burning of all combustible materials within the firestorm boundaries. Firestorms also produced a high number of casualties, seldom ameliorated even by concerted rescue efforts.

Large urban fires are a much greater threat in the age of nuclear weapons than ever before. Hundreds of square kilometers of an urban (or wildland) area can be ignited simultaneously by a single-megaton nuclear weapon. Indeed, superfires of unprecedented size could dwarf the tremendous fires of World War II.

After the firestorm in Hamburg, civil defense leaders in Germany addressed the problem of protecting the cities and the civilian population from such fierce fires. On the basis of the meager technical information then available, guidelines for rescue operations were outlined. However, the physical characteristics of the firestorm environment had not yet been defined--e.g., winds, temperatures, gas concentrations, sizes of combustible areas, and populations at risk. Such information is essential if planners are to design procedures for fire suppression/containment and population protection/rescue.

Today, years later, we are still without a complete and accurate picture of the superfire environment. No analysis has ever focused on the nature of the flow in and around the fire itself--which is the most vital information. Most studies have simply attempted to extrapolate results from classical plume theories, known to be valid only well above a small free-burning fire.

This report uses a new analytical approach to analyze the superfire environment. Our approach is based on a "component" model in

Preceding page blank

which different sets of equations are employed to represent the fundamentally different physics in separate parts of the fire-generated flow. Asymptotic analysis is used to derive the individual equation sets from standard conservation laws.

The "component" approach allows us to consider in detail the nature of the superfire environment in the critical region in and around the fire itself. Our analysis of that "combustion" region constitutes the first--and most interesting--model component.

The intensity and extent of the fires in the combustion region largely determine the characteristics of the entire flow field. Cold air is drawn into the burning zone and heated by the ongoing combustion processes. The heated air rises buoyantly, establishing a natural convection column. The buoyant air in the column cools and expands until a local equilibrium is established either in the upper atmosphere or at an inversion layer (of sufficient magnitude). Finally, a mesoscale recirculation pattern is established similar to a nocturnal urban heat island flow. Analyses of the convection column and recirculation flows produce the other basic model components.

We focus on the combustion region. Our analysis is valid in the upper limit for large urban fires with horizontal dimensions on the order of tens of kilometers and in the lower limit for fires the size of the multiple-fuel-bed Flambeau fires.

The first predictions concern the environment for a nominal large urban fire (with a 10 km radius). The sensitivity of the predictions to changes in model parameters is then considered. An experimental Flambeau fire (of radius ~ 0.25 km) is also analyzed. The results show reasonable agreement in all parameters when inflow horizontal velocities are selected to correspond to those observed.

Numerical simulation also shows that the type of plume observed over the Flambeau fire (i.e., with a width comparable to that of the fire) can be established only if turbulent mixing plays a major role in the combustion region dynamics. We anticipate that turbulence will play such a role in large urban fires.

CONTENTS

PREFACE	iii
EXECUTIVE SUMMARY	v
FIGURES	ix
TABLES	xiii
Section	
I. INTRODUCTION	1
Technical background	2
Summary of analysis	3
II. MODELING AND ANALYSIS	5
Physics	6
Basic equations and scaling	8
Asymptotic analysis	11
Combustion layer	13
Convection column	16
Special case of Flambeau fires	21
Combustion products	27
Cylindrical symmetry	28
III. COMBUSTION-LAYER BOUNDARY-VALUE PROBLEM	30
Analysis	30
Numerical solution	33
Results	36
IV. DISCUSSION	97
Appendix	
A. SYMBOLS	103
B. ANALYTIC DEVELOPMENT FOR CONVECTION COLUMN MODEL	109
C. ALGORITHM DOCUMENTATION	112
REFERENCES	171

FIGURES

1. Schematic of large area fire	5
2. Components of large urban fire model	7
3. Matching diagram for asymptotic solution of model equations	12
4. Sketch of a typical multiple-fuel-bed Flambeau fire ...	22
5. Boundary conditions for leading-order combustion- layer equations	31
6. Macro flowchart of solution algorithm for basic combustion-layer problem	35
7. Vertical velocity profiles used along inlet boundary ..	38
8. Velocity fields generated for different inlet velocity magnitudes	39
9. Temperature and pressure contours generated for dif- ferent inlet velocity magnitudes	40
10. Center-line velocities and temperatures generated for different inlet velocity magnitudes	41
11. Horizontal velocity profiles generated for different inlet velocity magnitudes	43
12. Vertical velocity profiles generated for different inlet velocity magnitudes	44
13. Velocity fields generated for different values of common heat/momentum diffusion coefficients	52
14. Temperature and pressure contours generated for dif- ferent values of common heat/momentum diffusion coefficients	53
15. Center-line velocities and temperatures generated for different values of common heat/momentum diffusion coefficients	54
16. Horizontal velocity profiles generated for different values of common heat/momentum diffusion coefficients	56

Preceding page blank

17. Vertical velocity profiles generated for different values of common heat/momentum diffusion coefficients	57
18. Velocity fields generated for selected diffusion coefficient mixes	58
19. Temperature and pressure contours generated for selected diffusion coefficient mixes	59
20. Center-line velocities and temperatures generated for selected diffusion coefficient mixes	60
21. Horizontal velocity profiles generated for selected diffusion coefficient mixes	61
22. Vertical velocity profiles generated for selected diffusion coefficient mixes	62
23. Spatial distributions of heat-release-rate variations .	64
24. Velocity fields generated for different spatially uniform heat release rates	65
25. Temperature and pressure contours generated for different spatially uniform heat release rates	66
26. Center-line velocities and temperatures generated for different spatially uniform heat release rates	67
27. Horizontal velocity profiles generated for different spatially uniform heat release rates	68
28. Vertical velocity profiles generated for different spatially uniform heat release rates	69
29. Velocity fields generated for uniform and two-cycle oscillatory heat release rates	73
30. Temperature and pressure contours generated for uniform and two-cycle oscillatory heat release rates	74
31. Center-line velocities and temperatures generated for uniform and two-cycle oscillatory heat release rates	75
32. Horizontal velocity profiles generated for uniform and two-cycle oscillatory heat release rates	76
33. Vertical velocity profiles generated for uniform and two-cycle oscillatory heat release rates	77

34. Velocity fields generated for uniform and ten-cycle oscillatory heat release rates	79
35. Temperature and pressure contours generated for uniform and ten-cycle oscillatory heat release rates ...	80
36. Center-line velocities and temperatures generated for uniform and ten-cycle oscillatory heat release rates	81
37. Horizontal velocity profiles generated for uniform and ten-cycle oscillatory heat release rates	82
38. Vertical velocity profiles generated for uniform and ten-cycle oscillatory heat release rates	83
39. Velocity fields generated for uniform and dead-zone heat release rates	84
40. Temperature and pressure contours generated for uniform and dead-zone heat release rates	85
41. Center-line velocities and temperatures generated for uniform and dead-zone heat release rates	86
42. Horizontal velocity profiles generated for uniform and dead-zone heat release rates	87
43. Vertical velocity profiles generated for uniform and dead-zone heat release rates	88
44. Velocity field predicted for typical multiple-fuel-bed Flambeau fire	92
45. Temperature and pressure contours predicted for typical multiple-fuel-bed Flambeau fire	93
46. Center-line velocities and temperatures predicted for typical multiple-fuel-bed Flambeau fire	94
47. Horizontal velocity profiles predicted for typical multiple-fuel-bed Flambeau fire	95
48. Vertical velocity profiles predicted for typical multiple-fuel-bed Flambeau fire	96
49. Classification of possible convection plumes	100
C.1. Flowchart of main program	119
C.2. Finite difference grid and stencils for numerical solution of leading-order combustion-layer problem ..	122

C.3. Macro flowchart of subroutine MSWEEP	124
C.4. Flow diagram of basic Newton step used in subroutine MSWEEP	125

TABLES

1. Parameter combinations considered	36
2. Ground-level numerical predictions for baseline parameter case A	45
3. 600-m-altitude numerical predictions for baseline parameter case A	46
4. Ground-level numerical predictions for parameter case B (increased magnitude of inlet vertical velocity)	47
5. 600-m-altitude numerical predictions for parameter case B (increased magnitude of inlet vertical velocity)	48
6. Ground-level numerical predictions for parameter case C (decreased magnitude of inlet vertical velocity)	49
7. 600-m-altitude numerical predictions for parameter case C (decreased magnitude of inlet vertical velocity)	50
8. Ground-level numerical predictions for parameter case M (increased uniform heat release rate)	71
9. 600-m-altitude numerical predictions for parameter case M (increased uniform heat release rate)	72
10. Ground-level numerical predictions for parameter case Q (dead-zone fire)	90
11. 600-m-altitude numerical predictions for parameter case Q (dead-zone fire)	91
C.1. Sample FIRE code output	116
C.2. Listing of FIRE code	142
C.3. Listing of FIRE2 code	156

I. INTRODUCTION

Each year, fires cause a tremendous loss of life and property in the United States. The spread of most urban structure fires is readily controlled by local firefighters, although there have been several notable exceptions [Lowe, 1979; Brode, 1980]. However, simultaneous fires such as those caused by natural and other disasters--e.g., earthquakes, explosions--often overwhelm local firefighters and destroy entire urban tracts. The extensive acreages annually burned by wildland fires would be even larger without coordinated action by great numbers of firefighters [Emmons, 1963, 1978].

An ordinary urban fire usually involves relatively few structures. In wartime, however, fires are deliberately set with the intention of burning whole cities. Multiple fires in large urban areas have proven extremely difficult to combat. Indeed, some have become superfires governed by phenomena not present in small urban fires.

The incendiary raids in Europe and Japan during World War II set multiple fires over fairly large urban tracts [Bond, 1951; Irving, 1963]. Several raids with highly concentrated bombing ignited firestorms that totally destroyed entire city sections (Hamburg, Dresden, Kassel, Darmstadt). Postwar studies based on survivor reports described fires simultaneously burning over tens of square kilometers (Hiroshima, 12 km^2 ; Dresden, 21 to 28 km^2 ; Hamburg, 21 km^2) and consuming all combustible materials within their boundaries. Hurricane-force winds, high-level street temperatures, and combustion intensities never previously observed were reported. Those experiences demonstrate that large area fires engender phenomena radically different from those of smaller fires.

Modern nuclear weapons can set fires over far larger areas than affected by any previous warfare or natural disaster. The thermal reach of megaton-size weapons can cause fires over more than 100 km^2 . For example, a one-megaton explosion (height of burst 700 m) can irradiate an area 7 km from ground zero with 30 cal/cm^2 of thermal

radiation. This is more than sufficient to ignite lightweight household materials and many typical exterior materials [Glasstone and Dolan, 1977]. The many thousands of simultaneous ignitions that will occur within seconds of the weapon burst over extensive urban areas could cause firestorms that would dwarf those that occurred in World War II.

This report presents a method for analyzing large area fires. A large area fire is herein defined as one with a flame height much smaller than its horizontal extent, and a convection column height comparable to a scale height of the atmosphere. Our analytical method should be applicable in the lower limit to fires the size of the multiple-fuel-bed *Flambeau* experiments [Countryman, 1969] and to nuclear-weapon-induced fires in the upper limit--as well as to city fires caused by natural disasters and wildland fires involving large areas.

TECHNICAL BACKGROUND

Most previous research concerning free-burning fires has been restricted to small fires and their plumes. There are significant phenomenological differences between small and large fires as well as between line and area fires [Lee, 1972; Small and Brode, 1980]. For example, the flow phenomena observed in small, free-burning fires can be related to local entrainment of ambient air [Cox and Chitty, 1980; McCaffrey, 1979], whereas additional mechanisms apparently are present in larger fires. This is evident from the large wind velocities observed in the World War II firestorms and in large wildland fires.

Similarly, the characteristics of line fires--such as occur in some wildlands or in urban fires (e.g., Tokyo, 1945)--are controlled by phenomena different from those of an area fire. A line fire is spread by local mechanisms such as conduction, convection, and radiation into the unburned regions [Emmons, 1963]. Area fires can be more nearly stationary and their behavior determined largely by integral properties--e.g., fire size, total heat release, and general atmospheric conditions.

Modeling of fires is extraordinarily complex, and a complete analysis would include description of both microscale and macroscale

phenomena. Indeed, many of the phenomena (e.g., chemistry and kinetics of fires, radiation, turbulence) that play a role in even a "simple" fire can still be described only qualitatively.

The plumes generated by free-burning fires have been the subject of several analyses. Similarity solutions [Morton, Taylor, and Turner, 1956; Morton, 1959; Yokoi, 1960] have been obtained using either an entrainment law or a mixing-length hypothesis. Such solutions are applicable for long, thin plumes and only well above the fire zone. Improvements to the basic plume theories have included piecewise integration of the solution through a real atmosphere [Murgai and Emmons, 1960], inclusion of radiation effects [Murgai, 1962; Smith, 1967], and consideration of the effects of combustion and variable gas composition [Nielsen and Tao, 1965].

The simple plume theories postulate relatively low inflow velocities at the edge of the convective plume and cannot be extrapolated to account for the higher velocity flows that occur in the fire zone. Even stoichiometric combustion in large, free-burning fires would require higher velocities than can be obtained through an edge effect such as entrainment. Simple scaling arguments [Byram, 1966; Small and Brode, 1980] suggest that the inflow velocities depend on the fire intensity and size.

The computations of Smith, Morton, and Leslie [1975] provide a first treatment of fire-generated winds near the fire zone as well as above it. Their results indicate a strong coupling of dynamic forces with the induced fire wind, even though density changes are assumed small (Boussinesq approximation) and the combustion processes are represented only by a heat addition rate at the ground boundary.

Our analysis provides detailed treatment of a finite-volume combustion zone and resolution of the dynamics and thermodynamics in and around the fire.

SUMMARY OF ANALYSIS

Our analytical approach is to consider the special features of each region (combustion zone, convection column, and far field of a superfire) and to use asymptotic expansions for formulating the appropriate equation sets. Scaled equations of mass, momentum, and energy

conservation, and an equation of state are introduced for each region, and an overall description of the flow is obtained by matching at the boundaries of those separate regions.

The basic features of the entire flow field are determined by the interactions in the combustion zone. Although that region is considerably smaller than the others (the convection column and the mesoscale atmospheric recirculation regions), the accurate resolution of its dynamics and thermodynamics are of primary importance in the modeling. The use of a component model facilitates such resolution and represents a significant departure from previous fire research [Morton, Taylor, and Turner, 1956; Murgai and Emmons, 1960; Nielsen and Tao, 1965; Smith, Morton, and Leslie, 1975].

Accordingly, we have emphasized the analysis of the combustion zone in our theoretical and numerical development. The heat release generated by the fires is modeled by a spatially-dependent volume heat source. Since density and temperature changes can be large, the conservation equations for a compressible gas are applied without the Boussinesq approximation. This allows coupling of the fire heat release, buoyancy, and pressure fields. Our analysis shows that several solutions can be obtained consistent with either a "thin" plume or a "thick" plume. Since large, free-burning fires usually engender convection column widths comparable to the horizontal fuel-bed dimension, we emphasize the "thick" column solution.

The theory is applied to a 10 km urban fire and one Flambeau experimental fire. The computed results detail the dynamics and thermodynamics of the combustion zone and clearly show the turning of a horizontal inflow velocity by the heat release and strong buoyancy into a vertical column flow. The calculation is carried vertically to approximately ten flame heights, and the results prescribe the initial conditions for the convective plume flow.

II. MODELING AND ANALYSIS

Our analysis considers an urban area covered by fire; the burning region need not be uniform. Such fires have resulted from natural disasters, wartime fire bombing, and the detonation of a nuclear weapon. The hot combustion products rise in the atmosphere and form a convection column above the burning region. The column height depends on conditions in the atmosphere as well as in the burning region. The initial temperature and momentum imparted to the gas in the burning region and the density difference between the hot column and the surrounding atmosphere all influence the height and character of the smoke column. The gases eventually establish equilibrium with the local atmosphere and spread laterally at the top of the column. A mesoscale far-field recirculation develops, similar to urban heat island flows [Delage and Taylor, 1970]. Figure 1 illustrates the basic features of a large area fire.

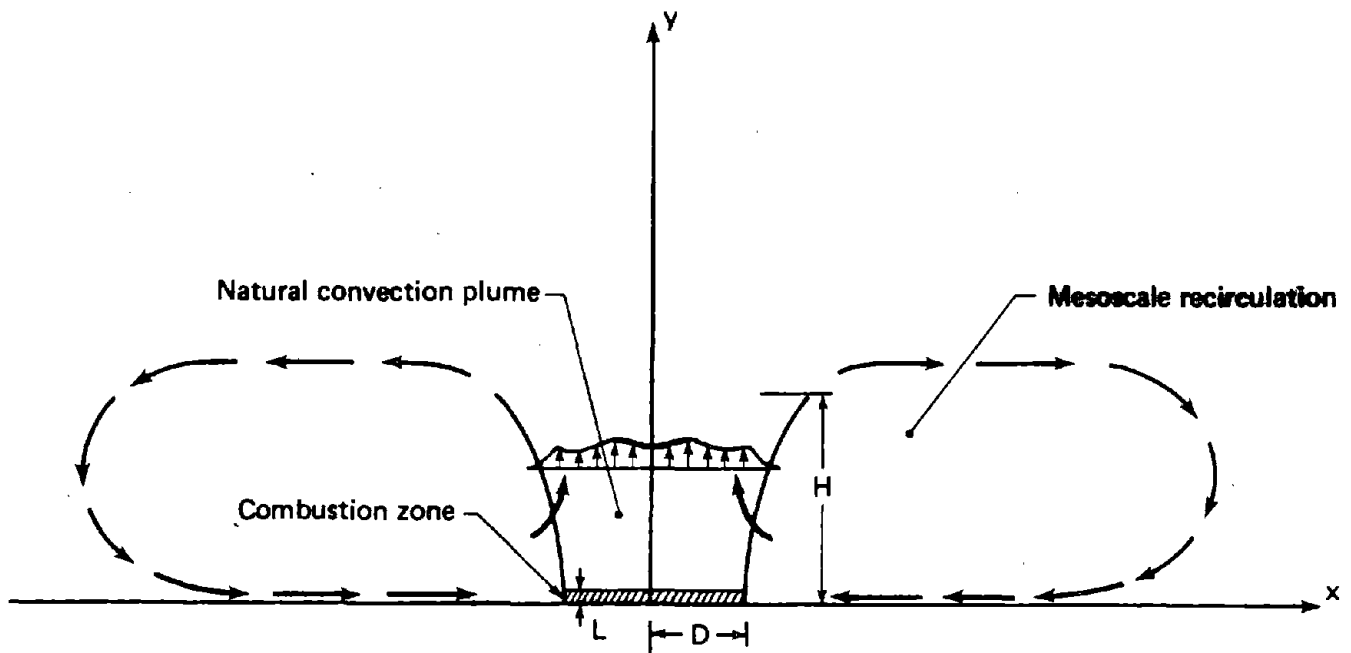


Fig. 1--Schematic of large area fire

The combustion zone is characterized by a heating zone of height L and half-width D . Considering a large area fire, then, the combustion-zone aspect ratio (L/D) forms a small parameter

$$\epsilon = L/D ,$$

which approaches zero in the limit of an infinite fire. The half-width D can be of the same order as the convection column height H , implying a convection-column aspect ratio (D/H) of order unity.

PHYSICS

The dominant physical effect in the combustion zone is the heat generated by the fire. Heated by the ongoing combustion, air becomes buoyant and rises, carrying with it smoke particulates and other by-products of combustion. The resulting flow is turbulent, and experiences radiation losses.

The complex combustion mechanisms are not considered in detail here. We model the overall effect of the burning by using a spatially dependent volumetric heat addition rate in the combustion zone. It is tacitly assumed that the buoyancy generated by the burning processes is reproduced by this volume addition. A more detailed description of the combustion physics may be introduced as a model refinement in a subsequent report.

In and around the combustion zone, the mean fire-generated flow is taken to be that of an ideal, compressible gas. Since that flow is expected to experience large changes in temperature but only small changes in pressure, the Boussinesq approximation is not employed. We take into account the effects of gas radiation, because experimental [McCaffrey, 1979] and analytical [Murgai, 1962; Smith, 1967] work suggests that radiation plays a significant role in reducing local air temperatures to nearly atmospheric values within a few flame heights above the fire. For simplicity, radiation losses are now modeled as being grey body, or "transparent" [Murgai, 1962]. Finally, analysis also shows that turbulent (Reynolds) stresses have an

important effect at least in the neighborhood of the symmetry axis. Standard eddy diffusivities are used in modeling the stresses. More detailed descriptions of the radiation and turbulence effects may be introduced later.

In the natural convection plume, hot, buoyant air from the combustion zone rises, mixes, spreads, and finally spills out laterally as it passes an equilibrium level in the upper atmosphere. The characteristics of the column depend critically on its aspect ratio D/H . Significant mixing occurs across long, narrow, Flambeau-type plumes, and the plume width at the top is greater than at the bottom. For larger urban fire plumes, which are as wide as they are tall, entrainment and mixing occur principally very near the sides of the plume and the flow is basically one-dimensional, with only a slight spreading along the sides. Figure 2 illustrates model components of a large urban fire.

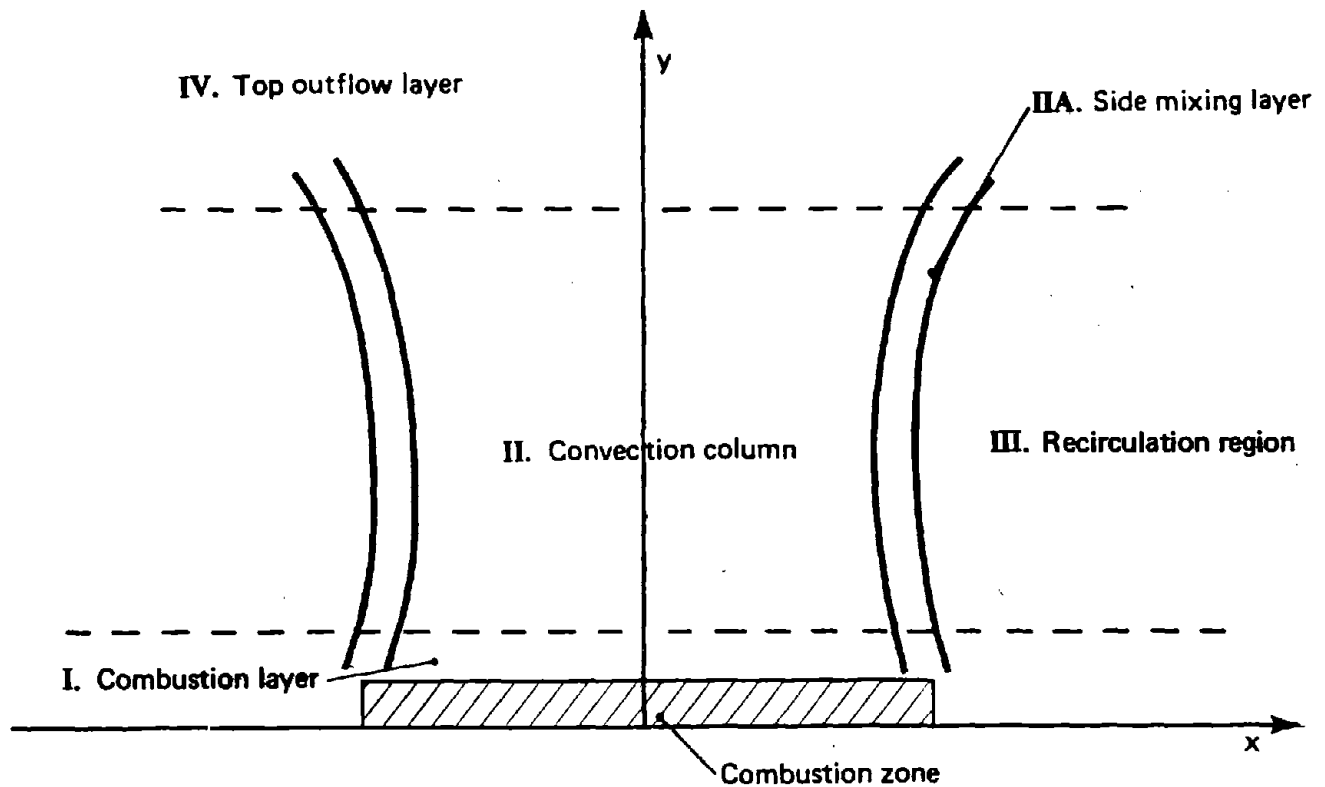


Fig. 2--Components of large urban fire model

BASIC EQUATIONS AND SCALING

The conservation equations for mass, momentum, and energy, and an equation of state appropriate for the steady-state description of a two-dimensional, large area fire are as follows:

$$\frac{\partial}{\partial x} (\rho u) + \frac{\partial}{\partial y} (\rho v) = 0 ;$$

$$\rho \left(u \frac{\partial u}{\partial x} + v \frac{\partial u}{\partial y} \right) = - \frac{\partial P}{\partial x} + \zeta_{11} \frac{\partial^2 u}{\partial x^2} + \zeta_{12} \frac{\partial^2 u}{\partial y^2} ;$$

$$\rho \left(u \frac{\partial v}{\partial x} + v \frac{\partial v}{\partial y} \right) = - \left(\frac{\partial P}{\partial y} + g\rho \right) + \zeta_{21} \frac{\partial^2 v}{\partial x^2} + \zeta_{22} \frac{\partial^2 v}{\partial y^2} ;$$

$$\begin{aligned} \rho C_P \left(u \frac{\partial T}{\partial x} + v \frac{\partial T}{\partial y} \right) = & \left(u \frac{\partial P}{\partial x} + v \frac{\partial P}{\partial y} \right) + Q \cdot q(x, y) - (4\pi\hat{\sigma}k^*) [T^4 - T_{\infty}^4(y)] \\ & + k_1 \frac{\partial^2 T}{\partial x^2} + k_2 \frac{\partial^2 T}{\partial y^2} ; \end{aligned}$$

$$P = \rho RT . \tag{2.1}$$

The diffusion coefficients ζ_{ij} and k_i represent all dissipative processes (both molecular and turbulent) for momentum and heat. The Reynolds stresses are assumed to be proportional to appropriate second-derivative terms. The term $Q \cdot q(x, y)$ is the heat addition rate due to combustion, with Q representing the mean rate and $q(x, y)$ a specified spatial distribution. The radiation loss is modeled by $(4\pi\hat{\sigma}k^*) [T^4 - \hat{T}_{\infty}^4(y)]$ [Murgai, 1962], where $(k^*)^{-1}$ and $\hat{\sigma}$ are the emission mean free path of the radiation and the Stefan constant, respectively, and $\hat{T}_{\infty}(y)$ is the far-field ambient temperature.

Pressure (P), density (ρ), and temperature (T) are expected to be of the same order of magnitude in all regions of interest as they are in the far-field atmosphere. Ground-level atmospheric values hence serve as nominal scales for these variables. Since the driving force for the entire flow field lies in the combustion zone, the characteristic dimensions and flow speeds of that zone are used

as nominal scales (denoted by braces) for spatial coordinates and velocities, as follows:

$$\begin{aligned} \{x\} &= D, \{y\} = L ; & \{P\} &= P_a, \{\rho\} = \rho_a, \{T\} = T_a ; \\ \{u\} &= U, \{v\} = \epsilon U, & U &\text{ yet to be chosen .} \end{aligned} \quad (2.2)$$

The subscript a refers to ground-level atmospheric values, ϵ is the combustion-zone aspect ratio ($\epsilon \ll 1$), and U is to be chosen so as to balance the terms for convective transport and heat addition in the energy equation (i.e., so that the equation represents a flow driven by combustive heating). The scaling for u and v is chosen to preserve the two-dimensional structure of the continuity equation [Eq. (2.1)], subject to the x and y scalings.

The nominal scalings in Eq. (2.2) are appropriate for the study of region I (Fig. 2). Other regions require rescalings. For example, for $H \sim D$ and $\epsilon = L/D$, the appropriate scaling for y in regions II and III is $\{y\} = H$, in contrast to Eq. (2.2). All rescalings are discussed as needed in our analysis.

The nondimensional version of Eq. (2.1), obtained by scaling Eqs. (2.1) using Eqs. (2.2), is

$$\begin{aligned} \frac{\partial}{\partial x} (\rho u) + \frac{\partial}{\partial y} (\rho v) &= 0 ; \\ \rho \left(u \frac{\partial u}{\partial x} + v \frac{\partial u}{\partial y} \right) &= - \left(\frac{1}{\delta_1} \right) \frac{\partial P}{\partial x} + M_{11} \frac{\partial^2 u}{\partial x^2} + M_{12} \frac{\partial^2 u}{\partial y^2} ; \\ \rho \left(u \frac{\partial v}{\partial x} + v \frac{\partial v}{\partial y} \right) &= - \left(\frac{1}{\epsilon^2 \delta_1} \right) \frac{\partial P}{\partial y} - \left(\frac{1}{\epsilon \delta_2} \right) \rho + M_{21} \frac{\partial^2 v}{\partial x^2} + M_{22} \frac{\partial^2 v}{\partial y^2} ; \\ \rho \left(u \frac{\partial T}{\partial x} + v \frac{\partial T}{\partial y} \right) &= \left(\frac{\gamma - 1}{\gamma} \right) \left(u \frac{\partial P}{\partial x} + v \frac{\partial P}{\partial y} \right) + \beta \{ q(x, y) - \sigma [T^4 - T_\infty^4(y)] \} \\ &\quad + K_1 \frac{\partial^2 T}{\partial x^2} + K_2 \frac{\partial^2 T}{\partial y^2} ; \\ P &= \rho T ; \end{aligned} \quad (2.3)$$

where

$$\begin{aligned}
 \delta_1 &= U^2/P_a/\rho_a ; & \delta_2 &= U^2/gD ; \\
 M_{1j} &= \epsilon \mathcal{C}_{1j}/\rho_a UL \quad \text{for } j = 1, 2 ; & K_1 &= \epsilon k_1/\rho_a UL ; \\
 M_{2j} &= \mathcal{C}_{2j}/\epsilon \rho_a UL \quad \text{for } j = 1, 2 ; & K_2 &= k_2/\epsilon \rho_a UL ; \\
 \sigma &= 4\pi \hat{\sigma} k^* T_a^4/Q ; & T_\infty(y) &= \hat{T}_\infty(y)/T_a ; \\
 \beta &= (\gamma - 1)/\gamma \cdot QD/P_a U ; & \gamma &= 1.4 ;
 \end{aligned} \tag{2.4}$$

and $q(x, y)$ can be varied, subject only to

$$q(x, y) \equiv 0 \quad \text{for } y > 1 \quad \text{and/or} \quad |x| > 1 . \tag{2.5}$$

Setting $\beta = 1$, so that the convective terms in the energy equation [Eq. (2.3)] are balanced with the heat source term, we find the nominal horizontal velocity scale U [Eq. (2.2)] to be

$$U = \left(\frac{\gamma - 1}{\gamma} \right) \left(\frac{QD}{P_a} \right) = \left(\frac{\gamma - 1}{\gamma} \right) \left(\frac{QL}{P_a \epsilon} \right) . \tag{2.6}$$

For $QL \sim 5.8 \times 10^{+4}$ cal/m²-sec [DCPA, 1973], $L \sim 10^2$ m, and $D \sim 10^4$ m, then

$$U \sim 67 \frac{\text{m}}{\text{sec}} \tag{2.7}$$

and increases (or decreases) proportionately with QL and inversely with ϵ .

Using the values for U , L , D , P_a , ρ_a , and g , then from Eq. (2.4) $\delta_1, \delta_2 \sim 0(\epsilon)$. Equations (2.3) can thus be rewritten in final form as

$$\frac{\partial}{\partial x} (\rho u) + \frac{\partial}{\partial y} (\rho v) = 0 ;$$

$$\rho \left(u \frac{\partial u}{\partial x} + v \frac{\partial u}{\partial y} \right) = - \frac{B}{\epsilon} \frac{\partial P}{\partial x} + M_{11} \frac{\partial^2 u}{\partial x^2} + M_{12} \frac{\partial^2 u}{\partial y^2} ;$$

$$\rho \left(u \frac{\partial v}{\partial x} + v \frac{\partial v}{\partial y} \right) = - \frac{B}{\epsilon^3} \left(\frac{\partial P}{\partial y} + \epsilon A \rho \right) + M_{21} \frac{\partial^2 v}{\partial x^2} + M_{22} \frac{\partial^2 v}{\partial y^2} ;$$

$$\begin{aligned} \rho \left(u \frac{\partial T}{\partial x} + v \frac{\partial T}{\partial y} \right) &= \frac{\gamma - 1}{\gamma} \left(u \frac{\partial P}{\partial x} + v \frac{\partial P}{\partial y} \right) + q(x, y) - \sigma [T^4 - T_{\infty}^4(y)] \\ &+ K_1 \frac{\partial^2 T}{\partial x^2} + K_2 \frac{\partial^2 T}{\partial y^2} ; \end{aligned}$$

$$P = \rho T , \quad (2.8)$$

where

$$\begin{aligned} A &= \frac{\delta_1}{\delta_2} \sim 1 , \quad B = \frac{\epsilon}{\delta_1} \sim 0.16 , \\ \sigma &\sim 0.023 \quad (\text{for } \hat{\sigma} = 1.354 \times 10^{-11} \text{ kcal/m}^2\text{-sec-(}^\circ\text{K)}^4 , \\ k^{*-1} &\sim 100 \text{ m}) . \end{aligned} \quad (2.9)$$

The coefficients M_{ij} and K_j , which characterize the turbulence effects, are left as parameters in this basic set of model equations. They are estimated as necessary in the analysis.

Most of our analysis and discussion concerns Eqs. (2.8). One section, however, presents a brief parallel analysis of a multiple-fuel-bed Flambeau fire. In this case, L and D differ significantly from the previous order estimates, so we consider a correspondingly revised version of Eq. (2.8).

ASYMPTOTIC ANALYSIS

Our component description of a large area fire involves asymptotic analysis in the limit where the combustion-zone aspect ratio ϵ ($=L/D$)

tends toward zero. Asymptotic expansions for the solution of the model equations in Eq. (2.8) are developed for each component region in Fig. 2 above, and the expansions are then suitably matched. The matching proceeds as diagrammed in Fig. 3.

The key asymptotic solution is that for region I, the combustion layer. Once it is developed, expansions for the convection column and side mixing layer (regions II and IIA, respectively) are found and

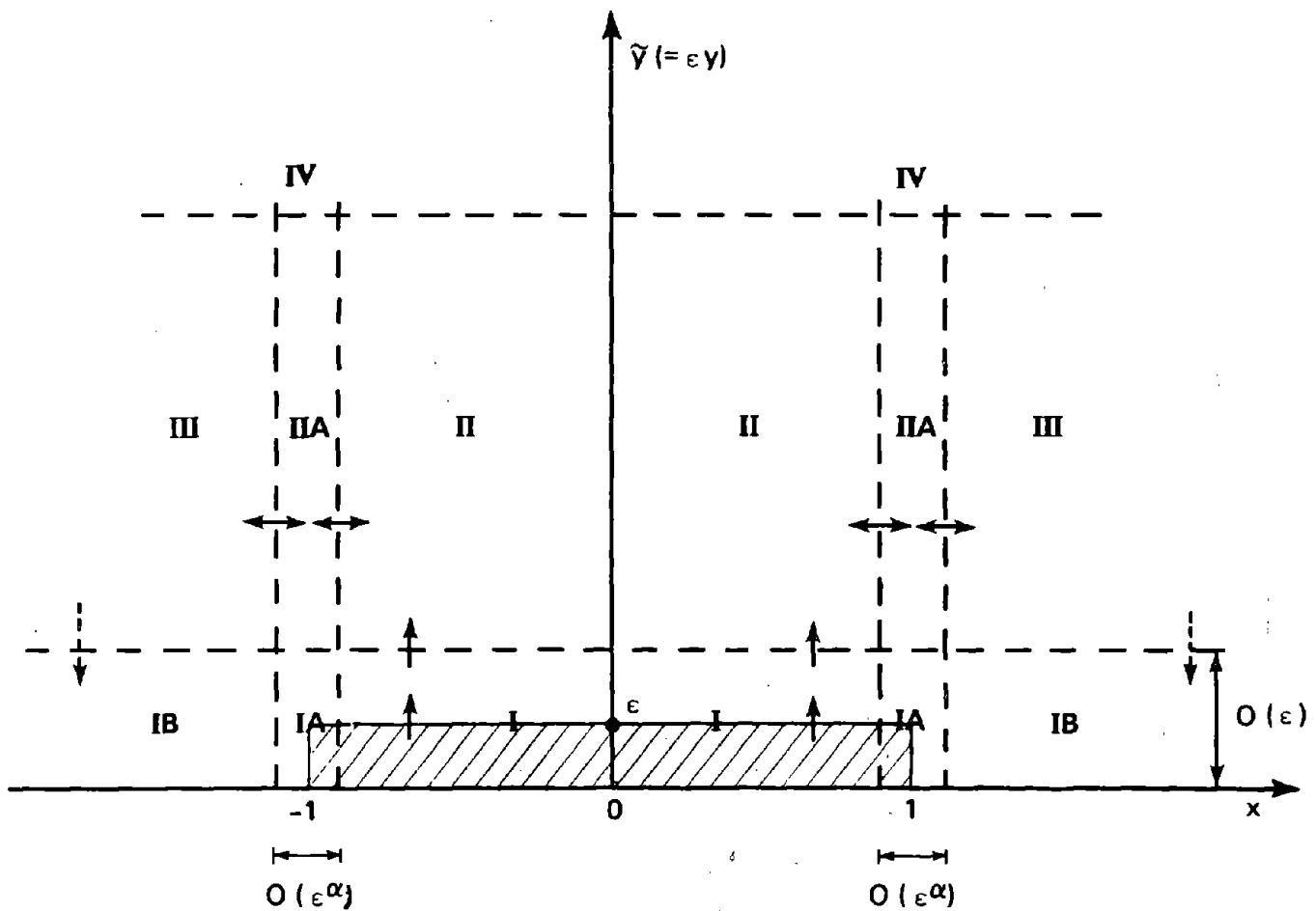


Fig. 3--Matching diagram for asymptotic solution of model equations

matched to it. Finally, expansions for the top outflow and recirculation regions (IV and III) must be successively developed and matched to the composite expansion for regions I, II, and IIA. This final matching may involve further intermediate analysis in one or both of regions IA and IB. For the moment, α (cf. Fig. 3) is left arbitrary.

The solution expansions for region I are based directly on equations (2.8). In other regions, expansions are derived from rescaled versions of those equations. In all regions, however, the expansions have the same general form--namely,

$$\begin{aligned} u &= u_0 + \epsilon u_1 + \epsilon^2 u_2 + \epsilon^3 u_3 + \dots ; \\ v &= v_0 + \epsilon v_1 + \epsilon^2 v_2 + \epsilon^3 v_3 + \dots ; \\ P &= P_0 + \epsilon P_1 + \epsilon^2 P_2 + \epsilon^3 P_3 + \dots ; \\ \rho &= \rho_0 + \epsilon \rho_1 + \epsilon^2 \rho_2 + \epsilon^3 \rho_3 + \dots ; \\ T &= T_0 + \epsilon T_1 + \epsilon^2 T_2 + \epsilon^3 T_3 + \dots . \end{aligned} \quad (2.10)$$

Below, we focus on determining the leading-order terms in the expansions. Equations for those terms (which describe the basic flow structure for a large area fire) are introduced and solutions discussed.

COMBUSTION LAYER

Substituting Eq. (2.10) into Eq. (2.8) produces the following leading-order equation set for region I:

$$\begin{aligned} \frac{\partial}{\partial x} (\rho_0 u_0) + \frac{\partial}{\partial y} (\rho_0 v_0) &= 0 ; \\ \rho_0 \left(u_0 \frac{\partial u_0}{\partial x} + v_0 \frac{\partial u_0}{\partial y} \right) &= -B \frac{\partial P_1}{\partial x} + M_{11} \frac{\partial^2 u_0}{\partial x^2} + M_{12} \frac{\partial^2 u_0}{\partial y^2} ; \\ \frac{\partial P_1}{\partial y} + A \rho_0 &= 0 ; \end{aligned}$$

$$\rho_0 \left(u_0 \frac{\partial T_0}{\partial x} + v_0 \frac{\partial T_0}{\partial y} \right) = q(x, y) - \sigma(T_0^4 - 1) + K_1 \frac{\partial^2 T_0}{\partial x^2} + K_2 \frac{\partial^2 T_0}{\partial y^2} ;$$

$$\rho_0 T_0 = P_0 = 1 . \quad (2.11)$$

The momentum balances here are actually first-order correction equations. The leading-order equations $\partial P_0 / \partial x = 0$ and $\partial P_0 / \partial y = 0$ imply that P_0 is constant with a value of one ground-level atmosphere, and changes in pressure are at most $O(\epsilon)$. Changes of such magnitude are consistent with experimental evidence on small, unenclosed fires [McCaffrey, 1979]. Further, since any far-field atmospheric temperature profile can vary only on the order of hundreds of degrees Kelvin over altitudes on the order of H ($\gg L$), then $T_\infty(y) \sim 1 + O(\epsilon y) + \dots$ for $y = O(1)$ and is hence replaced in this equation set by one.

The phenomenological coefficients M_{ij} and K_j describe the extent of the turbulent forces. At present, it is only possible to estimate their magnitudes, relying on physical understanding of the balance of forces and crude calculations to approximate the diffusion coefficients ζ_{ij} and k_j . Phenomenological theories such as mixing-length theory can provide useful approximations for the turbulent forces in most regions (II, III, IV) of this component model, but they are not applicable to the turbulence generated by the fire in region I. For the present, we adopt the following qualitative approximation:

$$M_{12} = K_2 = 0 . \quad (2.12)$$

This approximation may be removed in further research, but is not felt to be particularly restrictive. The approximation $M_{11} = K_1 = 0$ could alternatively be used in place of Eq. (2.12). However, we choose to proceed with Eq. (2.12), since horizontal diffusion due to turbulence certainly must be more than that in the vertical direction--at least in the central parts of the fire. The coefficients M_{11} and K_1 are then treated as parameters in the analysis of the combustion layer.

The resulting version of Eq. (2.11) must be solved subject to several types of boundary conditions. The solution must satisfy the following natural conditions:

$$\begin{aligned} \text{a. along } y = 0, \quad v_0 &= 0, \\ \text{b. along } x = 0, \quad u_0 &= 0, \quad \frac{\partial T_0}{\partial x} = 0. \end{aligned} \quad (2.13)$$

That is, there can be no flow into or out of the ground, and the flow is symmetric about the $x = 0$ axis (implying that $\partial \rho_0 / \partial x$, $\partial P_0 / \partial x$, and $\partial P_1 / \partial x$ as well as $\partial T_0 / \partial x$ are equal to zero there). If the solution is to be of a type that can be smoothly matched with solutions from regions III and II, respectively, it must also satisfy the following conditions:

$$\begin{aligned} \text{c. along } x = 1, \quad T_0 &= 1, \\ \text{d. as } y \rightarrow \infty, \quad u_0, \frac{\partial P_1}{\partial x}, \frac{\partial T_0}{\partial x}, \frac{\partial \rho_0}{\partial x} &\rightarrow 0. \end{aligned} \quad (2.14)$$

Condition c simply represents the expectation that the temperature is atmospheric to leading order in the bottom few hundred meters of the far-field recirculation region--and hence at the outer edge of the combustion layer. The first part of condition d, $u_0 \rightarrow 0$ as $y \rightarrow \infty$, implies that the horizontal velocity decays to a lower order term (equal to or less than the vertical velocity) above the combustion zone. The remaining terms are required to approach zero because, as Eq. (2.21) later shows, $\partial P_1 / \partial x \equiv \partial T_0 / \partial x \equiv \partial \rho_0 / \partial x \equiv 0$ in region II. Indeed, as shown in Sec. III, it turns out that $T_0, \rho_0 \rightarrow 1$ and $P_1 \sim \text{constant} - y$, so that $\partial P_1 / \partial x \rightarrow 0$ as $y \rightarrow \infty$. In view of Eq. (2.12), the no-slip condition, $u_0(x, 0) = 0$, is not required. Rescaling to include a viscous layer near $y = 0$ will be considered as a future model refinement.

The explicit analytic solution of Eq. (2.11) subject to Eqs. (2.12), (2.13), and (2.14) seems untenable. A computer code has therefore been developed to provide numerical solutions for this boundary value problem. Those solutions are discussed in Sec. III.

CONVECTION COLUMN

Since the characteristic height H of the urban fire convection column is on the order of D ($\sim 10^4$ m), its vertical spatial coordinate must be rescaled as

$$\tilde{y} = \epsilon y . \quad (2.15)$$

To preserve continuity in rescaling Eq. (2.8), we nominally assume $u = 0(\epsilon)$ in the column and introduce the further rescaling

$$\tilde{u} = \frac{u}{\epsilon} , \quad (2.16)$$

so that \tilde{u} is of order one. Subject to Eqs. (2.15) and (2.16), the nominal rescaling of Eq. (2.8) is then

$$\begin{aligned} \frac{\partial}{\partial x} (\rho \tilde{u}) + \frac{\partial}{\partial \tilde{y}} (\rho v) &= 0 ; \\ \rho \left(\tilde{u} \frac{\partial \tilde{u}}{\partial x} + v \frac{\partial \tilde{u}}{\partial \tilde{y}} \right) &= - \frac{B}{\epsilon^3} \frac{\partial P}{\partial x} + \left(\frac{M_{11}}{\epsilon} \right) \frac{\partial^2 \tilde{u}}{\partial x^2} + \epsilon M_{12} \frac{\partial^2 \tilde{u}}{\partial \tilde{y}^2} ; \\ \rho \left(\tilde{u} \frac{\partial v}{\partial x} + v \frac{\partial v}{\partial \tilde{y}} \right) &= - \frac{B}{\epsilon^3} \left(\frac{\partial P}{\partial \tilde{y}} + A \rho \right) + \left(\frac{M_{21}}{\epsilon} \right) \frac{\partial^2 v}{\partial x^2} + \epsilon M_{22} \frac{\partial^2 v}{\partial \tilde{y}^2} ; \\ \rho \left(\tilde{u} \frac{\partial T}{\partial x} + v \frac{\partial T}{\partial \tilde{y}} \right) &= \left(\frac{\gamma - 1}{\gamma} \right) \left(\tilde{u} \frac{\partial P}{\partial x} + v \frac{\partial P}{\partial \tilde{y}} \right) + \left(\frac{K_1}{\epsilon} \right) \frac{\partial^2 T}{\partial x^2} + \epsilon K_2 \frac{\partial^2 T}{\partial \tilde{y}^2} ; \\ P &= \rho T . \end{aligned} \quad (2.17)$$

(The term $q(x, y)$ is by definition zero in the convection column and $-\sigma[T^4 - T_\infty^4(y)]$ has been omitted above the combustion layer.) This version of Eq. (2.8) may in fact be appropriate for the study of the recirculation region (III) as well as the convection column, but it certainly must be further rescaled for the side mixing layer (region IIA), where turbulent shears and thermal gradients result in large horizontal derivatives. Such rescaling is discussed below (pp. 19-20).

The hierarchy of equation sets obtained in the asymptotic analysis of Eq. (2.17) of course depends on the magnitudes of the diffusion coefficients M_{ij} and K_j ; but there are neither data nor correlations from which to estimate these magnitudes. In developing the equation for the convection column, we therefore proceed noting that the results may be subject to modification once definitive large-plume turbulence data become available.

As shown in Appendix B, conventional mixing-length theory suggests that in region II we let

$$\frac{M_{11}}{\epsilon}, \frac{K_1}{\epsilon} = O(\epsilon); \quad M_{i2}, K_2 \ll 1 \text{ for } i = 1, 2. \quad (2.18)$$

Subject to this condition, the substitution of Eq. (2.10) into Eq. (2.17) with

$$u_0 = 0; \quad \tilde{u} = \frac{u}{\epsilon} = u_1 + \epsilon u_2 + \epsilon^2 u_3 + \dots \quad (2.19)$$

[cf. Eq. (2.16)] results in the following leading-order equation set:

$$\frac{\partial}{\partial x} (\rho_0 u_1) + \frac{\partial}{\partial \tilde{y}} (\rho_0 v_0) = 0;$$

$$\rho_0 \left(u_1 \frac{\partial u_1}{\partial x} + v_0 \frac{\partial u_1}{\partial \tilde{y}} \right) = -B \frac{\partial P_3}{\partial x};$$

$$\rho_0 \left(u_1 \frac{\partial v_0}{\partial x} + v_0 \frac{\partial v_0}{\partial \tilde{y}} \right) = -B \left(\frac{\partial P_3}{\partial \tilde{y}} + A \rho_3 \right);$$

$$\begin{aligned} \rho_0 \left(u_1 \frac{\partial T_3}{\partial x} + v_0 \frac{\partial T_3}{\partial \tilde{y}} \right) &= \left(\frac{\gamma - 1}{\gamma} \right) \left(u_1 \frac{\partial P_3}{\partial x} + v_0 \frac{\partial P_3}{\partial \tilde{y}} \right) - v_0 \left(\rho_1 \frac{\partial T_2}{\partial \tilde{y}} \right. \\ &\quad \left. + \rho_2 \frac{\partial T_1}{\partial \tilde{y}} + \rho_3 \frac{\partial T_0}{\partial \tilde{y}} \right); \end{aligned}$$

$$P_3 = \rho_0 T_3 + \rho_1 T_2 + \rho_2 T_1 + \rho_3 T_0; \quad (2.20)$$

where ρ_0 , T_0 , ρ_1 , T_1 , ρ_2 , and T_2 [and P_0 , P_1 , and P_2 in Eqs. (2.21) through (2.23) below] are all functions of \tilde{y} alone and satisfy

$$\begin{aligned}\frac{dP_0}{d\tilde{y}} + A\rho_0 &= 0, \\ \rho_0 \frac{dT_0}{d\tilde{y}} &= \left(\frac{\gamma - 1}{\gamma} \right) \frac{dP_0}{d\tilde{y}}, \\ P_0 &= \rho_0 T_0, \\ P_0(0) &= \rho_0(0) = T_0(0) = 1;\end{aligned}\tag{2.21}$$

$$\begin{aligned}\frac{dP_1}{d\tilde{y}} + A\rho_1 &= 0, \\ \rho_0 \frac{dT_1}{d\tilde{y}} &= \left(\frac{\gamma - 1}{\gamma} \right) \frac{dP_1}{d\tilde{y}} - \rho_1 \frac{dT_0}{d\tilde{y}}, \\ P_1 &= \rho_0 T_1 + \rho_1 T_0;\end{aligned}\tag{2.22}$$

and

$$\begin{aligned}\frac{dP_2}{d\tilde{y}} + A\rho_2 &= 0, \\ \rho_0 \frac{dT_2}{d\tilde{y}} &= \left(\frac{\gamma - 1}{\gamma} \right) \frac{dP_2}{d\tilde{y}} - \left(\rho_1 \frac{dT_1}{d\tilde{y}} + \rho_2 \frac{dT_0}{d\tilde{y}} \right), \\ P_2 &= \rho_0 T_2 + \rho_1 T_1 + \rho_2 T_0.\end{aligned}\tag{2.23}$$

It can easily be shown that the solution for Eq. (2.21) is

$$\begin{aligned}T_0 &= \left[1 - A \left(\frac{\gamma - 1}{\gamma} \right) \tilde{y} \right], \\ \rho_0 &= \left[1 - A \left(\frac{\gamma - 1}{\gamma} \right) \tilde{y} \right]^{\left(\frac{1}{\gamma - 1} \right)}, \\ P_0 &= \left[1 - A \left(\frac{\gamma - 1}{\gamma} \right) \tilde{y} \right]^{\left(\frac{\gamma}{\gamma - 1} \right)}.\end{aligned}\tag{2.24}$$

That is, as expected, the zeroth-order thermodynamic state is an adiabatic atmosphere and the column is only weakly buoyant. Subject to prescriptions of P_1 , T_1 , P_2 , and T_2 at $y = 0$, which must come from lower order analysis of the combustion layer equations, the linear systems in Eqs. (2.22) and (2.23) are then easily solved, and the description of the basic region II flow reduces to the solution of Eq. (2.20). This equation set is to be solved subject to

$$\begin{aligned} \text{a. along } \tilde{y} = 0, \quad v_0 &= v_\infty(x), \quad u_1 = u_{1\infty}(x), \text{ and (say)} \\ &P_3 = P_{3\infty}(x), \quad T_3 = T_{3\infty}(x), \\ \text{b. along } x = 0, \quad u_1 &= 0, \end{aligned} \tag{2.25}$$

where

$$v_\infty(x) = \lim_{y \rightarrow \infty} [v_0(x, y)]_{\text{region I}} \tag{2.26}$$

and $u_{1\infty}(x)$, $P_{3\infty}(x)$, and $T_{3\infty}(x)$ are to be similarly defined (subject to lower order analysis of the combustion layer equations). The edge of the convection column is marked (to leading order) by the free streamline that begins at $(x, \tilde{y}) = (1, 0)$ and is defined from the solution of Eqs. (2.20) and (2.25).

In region IIA (i.e., in the thin layer along the $y = \eta(y)$ streamline), the differences in velocities and thermodynamic states between the main convection column (region II) and the recirculation region (III) must be smoothed out. To leading order, then, appropriately rescaled equations for the flow in this region must represent a balance between the effects of buoyancy, mixing, and convection. That balance is obtained if the horizontal coordinate is rescaled as

$$\tilde{x} = \left(\frac{x - \eta(y)}{\sqrt{\epsilon}} \right), \tag{2.27}$$

so that the characteristic mixing-layer thickness is $O(\epsilon^{1/2})$ (i.e., defining α in Fig. 3 as $1/2$). As shown in Appendix B, the resulting leading-order equations for this layer are then

$$\frac{\partial}{\partial \tilde{x}} (\rho_0 \hat{u}_{3/2}) + \frac{\partial}{\partial \tilde{y}} (\rho_0 v_0) = 0 ;$$

$$u_1 = \left(\frac{d\eta}{d\tilde{y}} \right) v_0 ;$$

$$\rho_0 \left(\hat{u}_{3/2} \frac{\partial v_0}{\partial \tilde{x}} + v_0 \frac{\partial v_0}{\partial \tilde{y}} \right) = -B \left(\frac{dP_3}{d\tilde{y}} + A\rho_3 \right) + \tilde{M}_{21} \frac{\partial^2 v_0}{\partial \tilde{x}^2} ;$$

$$\begin{aligned} \rho_0 \left(\hat{u}_{3/2} \frac{\partial T_3}{\partial \tilde{x}} + v_0 \frac{\partial T_3}{\partial \tilde{y}} \right) &= \left(\frac{\gamma - 1}{\gamma} \right) \left(v_0 \frac{dP_3}{d\tilde{y}} \right) + \tilde{K}_1 \frac{\partial^2 T_3}{\partial \tilde{x}^2} - v_0 \left(\rho_1 \frac{\partial T_2}{\partial \tilde{y}} \right. \\ &\quad \left. + \rho_2 \frac{\partial T_1}{\partial \tilde{y}} + \rho_3 \frac{\partial T_0}{\partial \tilde{y}} \right) ; \end{aligned}$$

$$P_3 = \rho_0 T_3 + \rho_1 T_2 + \rho_2 T_1 + \rho_3 T_0 ; \quad (2.28)$$

where ρ_0 , T_0 , ρ_1 , T_1 , ρ_2 , T_2 , and P_3 [and P_0 , P_1 , and P_2] are all functions of \tilde{y} alone, and hence are as in region II [cf. Eqs. (2.21) through (2.24)]. The revised expansions for \tilde{u} and v [cf. Eqs. (2.10) and (2.19)] are

$$\begin{aligned} \tilde{u} &= u_1 + \epsilon^{1/2} u_{3/2} + \epsilon u_2 + \dots , \\ v &= v_0 + \epsilon^{1/2} v_{1/2} + \epsilon v_1 + \dots , \end{aligned} \quad (2.29)$$

with

$$\hat{u}_{3/2} = u_{3/2} - \left(\frac{d\eta}{d\tilde{y}} \right) v_{1/2} , \quad (2.30)$$

and

$$\begin{aligned}\tilde{M}_{i1} &= \left(\frac{M_{i1}}{\epsilon^2} \right) = O(1) \quad \text{for } i = 1, 2, \\ \tilde{K}_1 &= \left(\frac{K_1}{\epsilon^2} \right) = O(1)\end{aligned}\tag{2.31}$$

[cf. Eq. (2.18)]. In order that a solution of Eq. (2.28) match (as $\tilde{x} \rightarrow -\infty$) with the region II solution of Eq. (2.20) [as $x \rightarrow \eta(\tilde{y})$], it must satisfy the boundary conditions

$$\begin{aligned}\lim_{\tilde{x} \rightarrow -\infty} v_0(\tilde{x}, \tilde{y}) &= \lim_{x \rightarrow \eta(\tilde{y})} v_0^{(II)}(x, \tilde{y}), \\ \lim_{\tilde{x} \rightarrow -\infty} \left[\frac{\partial u_{3/2}}{\partial \tilde{x}}(\tilde{x}, \tilde{y}) \right] &= \lim_{x \rightarrow \eta(\tilde{y})} \left[\frac{\partial u_1^{(II)}}{\partial x}(x, \tilde{y}) \right], \\ \lim_{\tilde{x} \rightarrow -\infty} T_3(\tilde{x}, \tilde{y}) &= \lim_{x \rightarrow \eta(\tilde{y})} T_3^{(II)}(x, \tilde{y}),\end{aligned}\tag{2.32}$$

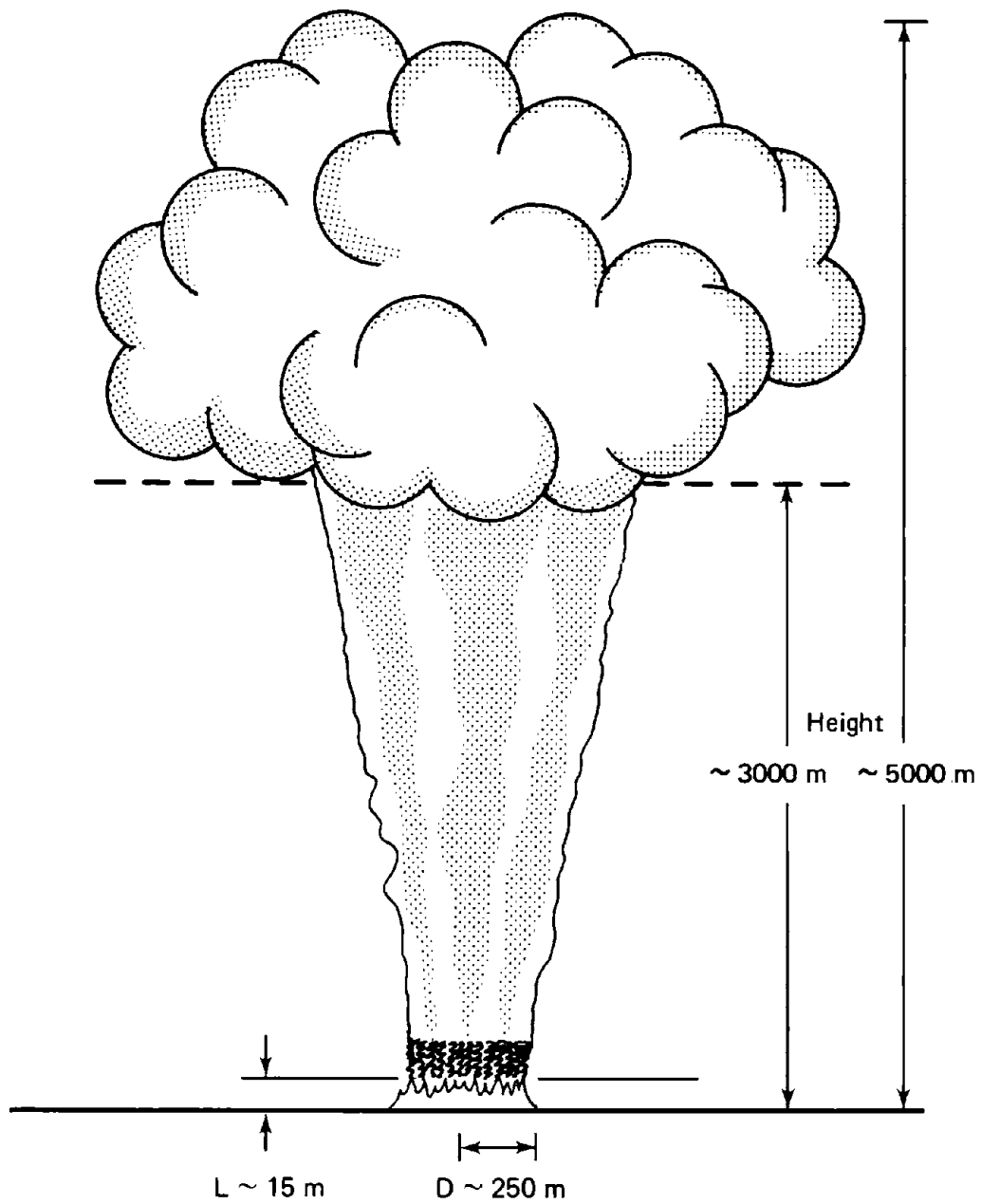
where the superscript (II) refers to the region II solution. Similar boundary conditions are required (as $\tilde{x} \rightarrow \infty$) for the solution of Eq. (2.28) to be matched to the solution of the equations that are ultimately introduced for the recirculation region. The solution of Eq. (2.28) subject to those boundary conditions must presumably be obtained by numerical methods. This task is left for future research.

SPECIAL CASE OF FLAMBEAU FIRES

The analysis presented so far is primarily applicable to a large area fire (i.e., $\epsilon \rightarrow 0$) with a convection-column aspect ratio $D/H \sim O(1)$. Here we apply the theory to the much smaller multiple-fuel-bed Flambeau fire [Countryman, 1969] illustrated in Fig. 4. Our analysis is based on the matching diagram in Fig. 3, but omits the side mixing layer, region IIA.

As shown in Fig. 4, $L \sim 15$ m, $D \sim 250$ m, and

$$\epsilon = 6 \times 10^{-2}.$$



Source: Countryman [1969].

Fig. 4--Sketch of a typical multiple-fuel-bed Flambeau fire

From Eq. (2.6), the indicated scale velocity is

$$U = 11.2 \text{ m/sec ;}$$

and, from Eq. (2.4), $\delta_1 \sim O(\epsilon^2)$ and $\delta_2 \sim O(\epsilon)$. By applying these scalings, the basic equation set is found to be the following slight revision of Eq. (2.8):

$$\frac{\partial}{\partial x} (\rho u) + \frac{\partial}{\partial y} (\rho v) = 0 ;$$

$$\rho \left(u \frac{\partial u}{\partial x} + v \frac{\partial u}{\partial y} \right) = - \left(\frac{B}{\epsilon^2} \right) \frac{\partial P}{\partial x} + M_{11} \frac{\partial^2 u}{\partial x^2} + M_{12} \frac{\partial^2 u}{\partial y^2} ;$$

$$\rho \left(u \frac{\partial v}{\partial x} + v \frac{\partial v}{\partial y} \right) = - \left(\frac{B}{\epsilon^4} \right) \left(\frac{\partial P}{\partial y} + \epsilon^2 A \rho \right) + M_{21} \frac{\partial^2 v}{\partial x^2} + M_{22} \frac{\partial^2 v}{\partial y^2} ;$$

$$\begin{aligned} \rho \left(u \frac{\partial T}{\partial x} + v \frac{\partial T}{\partial y} \right) &= \left(\frac{\gamma - 1}{\gamma} \right) \left(u \frac{\partial P}{\partial x} + v \frac{\partial P}{\partial y} \right) + q(x, y) - \sigma [T^4 - T_\infty^4(y)] \\ &\quad + K_1 \frac{\partial^2 T}{\partial x^2} + K_2 \frac{\partial^2 T}{\partial y^2} ; \end{aligned}$$

$$P = \rho T ; \tag{2.33}$$

where $A = \delta_1 / \epsilon \delta_2 \sim 0.52$, $B = \epsilon^2 / \delta_1 \sim 2.3$, and $\sigma \sim 0.023$ (for $k^{*-1} \sim 15$ m). The coefficients M_{ij} and K_j are taken to be of order one (since our analysis again shows that turbulent mixing is required for thick plume formation).

Substitution of Eq. (2.10) into Eq. (2.33) shows that the leading-order combustion-layer equation set for the Flambeau fire is that for large-scale urban fires, namely Eq. (2.11), except for changes in A , B , and σ (and possibly the diffusion coefficients). For convenience, we also make the qualitative simplification of Eq. (2.12) and seek a solution for the resulting equation set that satisfies the boundary conditions Eqs. (2.13) and (2.14).

We also, however, prescribe one further boundary condition for the Flambeau fire model. Prescription of u or $\partial u/\partial x$ is required along $x = 1$ (the inlet edge of the combustion region) if the solution for Eqs. (2.11), (2.12), (2.13), and (2.14) is to be unique. In general (cf. Sec. III), the inlet velocities should depend on the heat release and buoyancy generated in the combustion zone. That dependence holds even if the boundary prescription is applied as $x \rightarrow \infty$ [Smith, Morton, and Leslie, 1975].

For the Flambeau fire of Fig. 4, however, it appears that a reasonably accurate definition of u along $x = 1$ can be made from experimental data collected at several points on the fire periphery [Countryman, 1969]. Though these data are subject to scatter and may reflect some experimental error, horizontal velocity components at all collection points seem fairly constant (at about 10 m/sec) over the average flame height (~ 15 m). They then begin to decrease with increasing height above the flame region. The data suggesting such a decrease are for heights up to about 20 m. An exponential decrease above the fire zone is assumed, and the boundary condition is constructed as

$$\hat{c}. \text{ along } x = 1, \quad u = \begin{cases} u_I, & \text{for } 0 \leq y \leq 1 \\ u_I e^{-(y-1)}, & \text{for } y > 1 \end{cases},$$

$$u_I \sim 0.895 (\approx 10 \text{ m/sec}). \quad (2.34)$$

Numerical simulation shows that the combustion layer dynamics are fairly insensitive to quantitative changes in the exponential decay factor.

Since $D/H \sim O(\epsilon)$, the appropriate rescaling of Eq. (2.33) for the Flambeau convection-column region involves

$$\tilde{y} = \epsilon^2 y; \quad \tilde{u} = \frac{u}{\epsilon^2} = u_2 + \epsilon u_3 + \dots \quad (2.35)$$

The resulting equations describing the convection column are

$$\frac{\partial}{\partial x} (\rho \tilde{u}) + \frac{\partial}{\partial \tilde{y}} (\rho v) = 0 ;$$

$$\rho \left(\tilde{u} \frac{\partial \tilde{u}}{\partial x} + v \frac{\partial \tilde{u}}{\partial \tilde{y}} \right) = - \left(\frac{B}{\epsilon^6} \right) \frac{\partial P}{\partial x} + \frac{M_{11}}{\epsilon^2} \frac{\partial^2 \tilde{u}}{\partial x^2} + \epsilon^2 M_{12} \frac{\partial^2 \tilde{u}}{\partial \tilde{y}^2} ;$$

$$\rho \left(\tilde{u} \frac{\partial v}{\partial x} + v \frac{\partial v}{\partial \tilde{y}} \right) = - \left(\frac{B}{\epsilon^4} \right) \left(\frac{\partial P}{\partial \tilde{y}} + A\rho \right) + \frac{M_{21}}{\epsilon^2} \frac{\partial^2 v}{\partial x^2} + \epsilon^2 M_{22} \frac{\partial^2 v}{\partial \tilde{y}^2} ;$$

$$\rho \left(\tilde{u} \frac{\partial T}{\partial x} + v \frac{\partial T}{\partial \tilde{y}} \right) = \left(\frac{\gamma - 1}{\gamma} \right) \left(\tilde{u} \frac{\partial P}{\partial x} + v \frac{\partial P}{\partial \tilde{y}} \right) + \frac{K_1}{\epsilon^2} \frac{\partial^2 T}{\partial x^2} + \epsilon^2 K_2 \frac{\partial^2 T}{\partial \tilde{y}^2} ;$$

$$P = \rho T . \quad (2.36)$$

Since the convection-column aspect ratio in this case is small [i.e., $D/H = O(\epsilon)$], the column flow is expected to be that of a "standard" plume [Murgai and Emmons, 1960]. Indeed, Eq. (2.36) can be reduced to the usual set of plume equations in the following way. With $D \ll H$, the spread of energy and momentum horizontally is expected to be much greater than that in the vertical direction, and is assumed to balance the convective transfer of these quantities. The vertical diffusion terms [Eq. (2.36)] are therefore neglected and the following order estimates are made:

$$\begin{aligned} \frac{M_{11}}{\epsilon^2} = \tilde{M}_{11} = O(1) , \quad \frac{M_{21}}{\epsilon^2} = \tilde{M}_{21} = O(1) , \\ \frac{K_1}{\epsilon^2} = \tilde{K}_1 = O(1) . \end{aligned} \quad (2.37)$$

It is then inferred from the horizontal momentum equation [Eq. (2.36)] that P is a function of \tilde{y} alone through at least five orders in ϵ . Hence, from the vertical momentum balance, this function,

$$\tilde{P}(\tilde{y}) = \sum_{n=0}^5 \epsilon^n P_n ,$$

satisfies

$$\frac{d\tilde{P}}{d\tilde{y}} = -A\rho_{\infty}(\tilde{y}) , \quad (2.38)$$

where $\rho_{\infty}(\tilde{y})$ is the limiting density profile through five orders in ϵ as $|x| \rightarrow \infty$ (and $\tilde{u}, v \rightarrow 0$). Defining

$$\Gamma = \left(\frac{AB}{\epsilon^4} \right) \rho , \quad \Gamma_{\infty} = \left(\frac{AB}{\epsilon^4} \right) \rho_{\infty} , \quad (2.39)$$

and using Eqs. (2.37) and (2.38), then the following equation set is found to be valid to leading order in an $\epsilon \rightarrow 0$ expansion:

$$\begin{aligned} \frac{\partial}{\partial \tilde{x}} (\rho \tilde{u}) + \frac{\partial}{\partial \tilde{y}} (\rho v) &= 0 ; \\ \tilde{u} \frac{\partial v}{\partial \tilde{x}} + v \frac{\partial v}{\partial \tilde{y}} &= \frac{1}{\rho} (\Gamma_{\infty} - \Gamma) + \frac{1}{\rho} \left(\tilde{M}_{21} \frac{\partial^2 v}{\partial \tilde{x}^2} \right) ; \\ \tilde{u} \frac{\partial T}{\partial \tilde{x}} + v \frac{\partial T}{\partial \tilde{y}} + A \left(\frac{\gamma - 1}{\gamma} \right) v &= \frac{1}{\rho} \left(\tilde{K}_1 \frac{\partial^2 T}{\partial \tilde{x}^2} \right) . \end{aligned} \quad (2.40)$$

These are exactly the cartesian coordinate equivalents of the "standard" buoyant plume equations.

Similarity solutions of Eqs. (2.40) [Morton, Taylor, and Turner, 1956; Murgai and Emmons, 1960] require definition of the fire size, atmosphere, initial vertical velocity profile, initial buoyancy ($\Gamma_{\infty} - \Gamma$), and either an entrainment law or mixing-length hypothesis. Solution of the leading-order combustion-layer equation set [Eqs. (2.11) subject to Eqs. (2.12) through (2.14)] defines the vertical velocity profile. Prescription of the initial buoyancy requires lower order analysis of the combustion region. Computed results for the 250 m Flambeau combustion layer are presented in Sec. III.

COMBUSTION PRODUCTS

Once the heat release rate $Q \cdot q(x, y)$ is prescribed, the release rates for all other combustion end-products and the corresponding depletion rate for oxygen can be computed (at least approximately), assuming stoichiometric (or excess air) burning conditions. Simple uncoupled equations of mass conservation for individual reactant species can then be introduced and solved. For oxygen, carbon monoxide, carbon dioxide, and "smoke" (i.e., suspended solids)--four important reactant species in the basic large urban fire environment--these equations are

$$\rho \left(u \frac{\partial \phi_m}{\partial x} + v \frac{\partial \phi_m}{\partial y} \right) = \mathbf{s}_m \cdot \mathcal{R}_m(x, y) + D_{1m} \frac{\partial^2 \phi_m}{\partial x^2} + D_{2m} \frac{\partial^2 \phi_m}{\partial y^2}, \quad (2.41)$$

where m refers individually to oxygen, carbon monoxide, carbon dioxide, and smoke, and ϕ_m is the mass fraction of m in the flow. The various $\mathbf{s}_m \cdot \mathcal{R}_m(x, y)$ are source/sink rates due to the combustion processes, and the D_{1m} are turbulent diffusion coefficients. Consistent with the preceding analysis of Eq. (2.11), the qualitative approximation

$$D_{2m} = 0 \quad (2.42)$$

is made [cf. Eq. (2.12)]. The various D_{1m} are assumed to be order-one parameters.

To leading order (as $\varepsilon \rightarrow 0$), the solution of Eq. (2.41) is to be found subject to

$$u = u_0, \quad v = v_0, \quad \rho = \rho_0, \quad (2.43)$$

u_0 , v_0 , and ρ_0 coming from the solution of Eq. (2.11). The natural boundary conditions (using the same letter designations as on p. 15) for Eq. (2.41) are

$$\begin{aligned}
 \text{b. along } x = 0, \quad \frac{\partial \phi_m}{\partial x} &= 0, \quad \text{for all } m, \\
 \text{c. along } x = 1, \quad \phi_m &= 0.209, \quad \text{for } m = O_2, \\
 &\phi_m = 0, \quad \text{for } m = CO, CO_2, \text{ smoke} \quad (2.44)
 \end{aligned}$$

(i.e., symmetry at the center line and atmospheric values at the inlet edge). In view of Eq. (2.43), Eq. (2.41) is linear, and the boundary value problem is easily solved (numerically) once the ϕ_m are known along $y = 0$. But this information is also easily obtained. For $y = 0$, $v = 0$; thus, subject to Eq. (2.42), the leading-order version of Eq. (2.41) reduces to

$$(\rho_0 u_0) \frac{\partial \phi_m}{\partial x} = S_m \cdot R_m(x, 0) + D_{1m} \frac{\partial^2 \phi_m}{\partial x^2}, \quad (2.45)$$

which can then be solved subject to Eq. (2.44) as a standard ordinary-differential-equation, boundary-value problem. After the basic variables ρ_0 , u_0 , and v_0 are computed, predictions of oxygen depletion and carbon monoxide, carbon dioxide, and smoke contamination due to large fires can thus be made by solving Eq. (2.45) and then the leading-order versions of Eqs. (2.41) and (2.44).

CYLINDRICAL SYMMETRY

The procedure used in solving the two-dimensional problem can easily be adapted to the case of cylindrical symmetry. Subject again to Eq. (2.12), the leading-order equation set has the following form for a cylindrically symmetric fire:

$$\begin{aligned}
 \frac{\partial}{\partial r} (\rho_0 u_0 r) + \frac{\partial}{\partial y} (\rho_0 v_0 r) &= 0; \\
 \rho_0 \left(u_0 \frac{\partial u_0}{\partial r} + v_0 \frac{\partial u_0}{\partial y} \right) &= -B \frac{\partial P_1}{\partial r} + M_{11} \left(\frac{\partial^2 u_0}{\partial r^2} + \frac{1}{r} \frac{\partial u_0}{\partial r} \right);
 \end{aligned}$$

$$\frac{\partial P_1}{\partial y} + A\rho_0 = 0 ;$$

$$\rho_0 \left(u_0 \frac{\partial T_0}{\partial r} + v_0 \frac{\partial T_0}{\partial y} \right) = q(x, y) - \sigma(T_0^4 - 1) + K_1 \left(\frac{\partial^2 T_0}{\partial r^2} + \frac{1}{r} \frac{\partial T_0}{\partial r} \right) ;$$

$$\rho_0 T_0 = 1 . \quad (2.46)$$

Here, y is the vertical coordinate and r is the radial distance from the center of the fire. The boundary conditions in Eqs. (2.13) and (2.14) remain unchanged in this formulation, except that x is replaced by r .

III. COMBUSTION-LAYER BOUNDARY-VALUE PROBLEM

ANALYSIS

The use of asymptotic expansions for each region enables reduction of the conservation equations [Eq. (2.1)] to more concise statements of the balance of principal forces. For the combustion layer, the leading-order equations reduce to the following two first-order linear equations, two second-order nonlinear equations, and one equation of state:

$$\begin{aligned} \frac{\partial}{\partial x} (\rho_0 u_0) + \frac{\partial}{\partial y} (\rho_0 v_0) &= 0 ; \\ \rho_0 \left(u_0 \frac{\partial u_0}{\partial x} + v_0 \frac{\partial u_0}{\partial y} \right) &= -B \frac{\partial P_1}{\partial x} + M_{11} \frac{\partial^2 u_0}{\partial x^2} ; \\ \frac{\partial P_1}{\partial y} + A \rho_0 &= 0 ; \\ \rho_0 \left(u_0 \frac{\partial T_0}{\partial x} + v_0 \frac{\partial T_0}{\partial y} \right) &= q(x, y) - \sigma(T_0^4 - 1) + K_1 \frac{\partial^2 T_0}{\partial x^2} ; \\ \rho_0 T_0 &= 1 . \end{aligned} \tag{3.1}$$

Including the diffusion terms allows specification of a condition for u at both the symmetry line and the entrance to the combustion layer. An inviscid formulation [Larson and Small, 1980] results in a nontrivial (physically meaningful) solution only when x is re-scaled near the centerline as $\bar{x} = x/\epsilon^{3/2}$. This limitation implies an accelerating flow in the combustion layer, which slows and turns in the neighborhood of $x = 0$ and results in a high-velocity, thin (with respect to D) plume. Solutions of this type have been reported by, for example, Nielsen and Tao [1965].

Observations of large, free-burning fires [Countryman, 1969] indicate that the convection column thickness is of the same order as the horizontal fuel-bed dimension. Accordingly, we seek solutions

of Eq. (3.1) subject to the boundary conditions of Eqs. (2.13) and (2.14), and one further boundary condition along $x = 1$. The additional boundary condition is required because of the parabolic nature of the horizontal momentum equation. All boundary conditions are illustrated in Fig. 5.

It is clear from Eq. (3.1) that the effects of radiation and diffusion drive T_0 and ρ_0 to one as $y \rightarrow \infty$, and that $u_0 \rightarrow 0$ in this limit if $\partial P_1 / \partial x$ also does. All conditions in Eq. (2.14) are thus

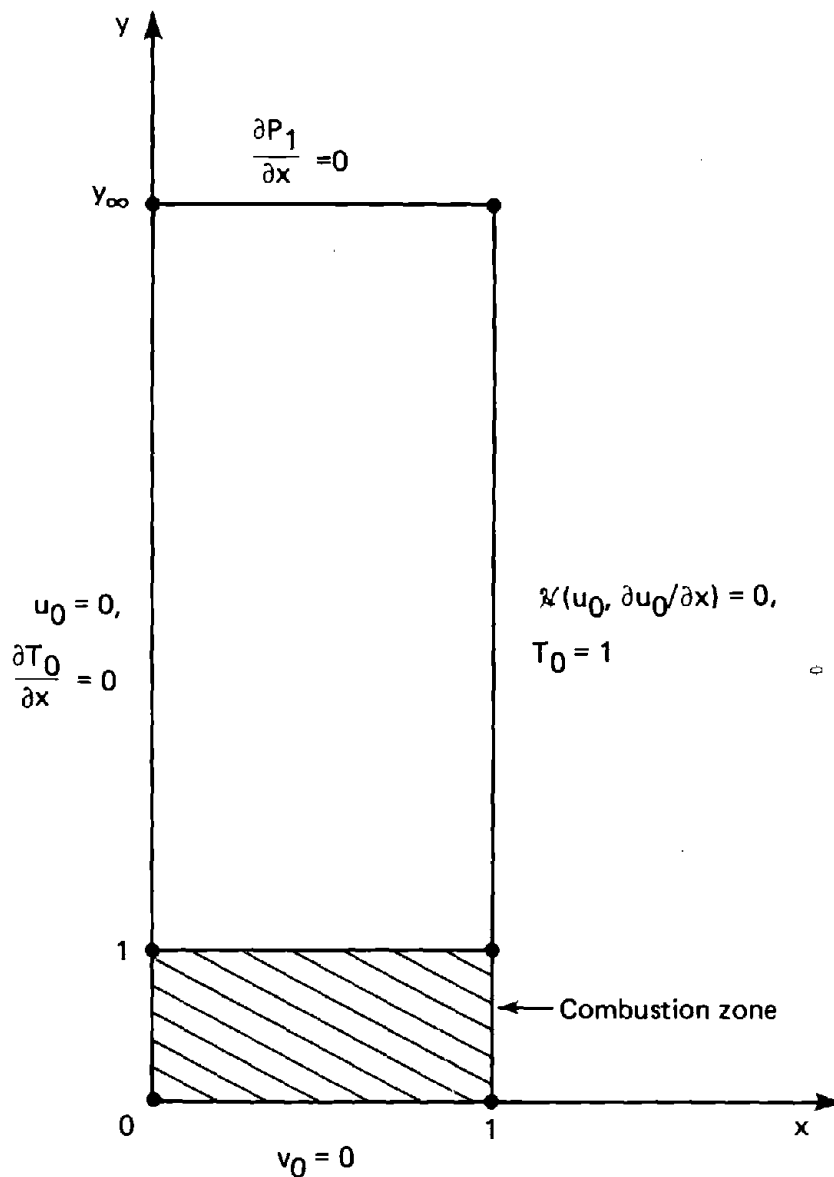


Fig. 5--Boundary conditions for leading-order combustion-layer equations

satisfied if either $u_0 = 0$ or $\partial P_1 / \partial x = 0$ is required as $y \rightarrow \infty$. The latter is chosen, since one boundary condition for P_1 is needed to complement the vertical momentum equation, which is of first order in P_1 . In practice, it was found sufficient to carry the calculation to $y \sim 8$ (eight flame heights) to satisfy the conditions at infinity.

The specific nature of the additional velocity boundary condition that must be posed along $x = 1$ is as yet unknown, and may be the subject of further research. The correct posing of this condition is prerequisite to answering two major practical questions: How fast are the maximum winds generated by a given fire intensity (i.e., heat release rate)? And, what is the horizontal extent of these winds beyond the fire and the associated collateral damage?

In modeling the Flambeau fire (see Sec. II, pp. 21-26), the horizontal velocity along the periphery of the burning area is defined by experimental data. For large urban fires, however, there is not yet any way to predict this velocity profile.

We suspect that the proper condition has the form

$$\mathcal{K} \left(u_0, \frac{\partial u_0}{\partial x} \right) = 0, \quad \text{along } x = 1, \quad (3.2)$$

where the functional form of \mathcal{K} is to be prescribed, possibly by general integral relations relating the inlet velocity to the buoyancy, pressure, and heat release rate. This question will be addressed by future research.

Alternatively, an empirical relation similar in concept to the plume entrainment laws might be developed to relate v_0 or $\partial v_0 / \partial y$ to a characteristic velocity of the local flow, e.g., $u_0(x, y)$. Such an inlet condition would have the form

$$-\frac{\partial}{\partial x} (\rho_0 u_0) = \frac{\partial v_0}{\partial y} = \mathcal{F}(u_0), \quad \text{along } x = 1. \quad (3.3)$$

Recent studies [Smith, Morton, and Leslie, 1975; Cox and Chitty, 1980] have noted that the entrainment laws [$u(1, y) \propto v(0, y)$] are not valid in the neighborhood of the combustion zone. Approximate relations for the mass flow into the burning zone have been suggested by Cox and Chitty [1980]. Future experimental work may allow definition of an empirical relation resembling Eq. (3.3).

At present, there is little justification for using any specific form for either \mathcal{M} or \mathcal{F} . Intuition suggests that $v_0(1, y)$ increases monotonically with increasing y at least to the top of the burning zone and remains constant to leading order for several flame heights above it. Accordingly, along $x = 1$, Eq. (3.3) is used to prescribe the combustion-zone inlet velocity with

$$v_0(1, y) = \hat{\alpha} \tanh(\hat{\beta}y/\hat{\alpha}) ,$$

$$\hat{\alpha} = \lim_{y \rightarrow \infty} v_0(1, y) , \quad \hat{\beta} = \frac{\partial v_0(1, 0)}{\partial y} . \quad (3.4)$$

NUMERICAL SOLUTION

The boundary value problem posed by Eqs. (3.1), (2.13), and (2.14), together with Eqs. (3.2) or (3.3), is unusual, and its solution is interesting. With the horizontal momentum and energy equations being parabolic for u_0 and T_0 , and the vertical momentum and continuity equations being first order for P_1 and v_0 , respectively, a "standard" boundary value problem for Eq. (3.1) would have u_0 , T_0 , and P_1 as well as v_0 prescribed as "initial data" on $y = 0$, u_0 and $\partial T_0/\partial x$ along $x = 0$, and $\mathcal{M}(u_0, \partial u_0/\partial x)$ and T_0 on $x = 1$, but no restrictions at all as $y \rightarrow \infty$. In contrast, both initial and "final" ($y = y_\infty$) data are prescribed (cf. Fig. 5), the difference between the two formulations being analogous to that between initial value problems and two-point boundary value problems for ordinary differential equations.

A standard method for solving two-point boundary value problems--"shooting" [Keller, 1968]--has thus been modified to provide numerical solutions to the problem posed above. The resulting scheme,

based on using solutions of the "standard" ("initial data") problem, is outlined in Fig. 6 and detailed in Appendix C.

The solution algorithm has been implemented on the Perkin-Elmer 3220 using both a prescribed inlet velocity and experimental data. In the first case, the numerical solution to the boundary value problem [Eqs. (3.1), (2.13), and (2.14)] is subject to the inlet-velocity boundary condition

$$\frac{\partial}{\partial x} (\rho_0 u_0) = \hat{\phi}(y) + \beta_0 u_0, \quad \text{along } x = 1, \quad (3.5)$$

with $\hat{\phi}(y)$ and β_0 prescribed as inputs. This case includes the general condition of Eq. (3.4), with

$$\hat{\phi}(y) = - \frac{\partial v_0}{\partial y}, \quad \beta_0 = 0, \quad (3.6)$$

and a special (sample) form of Eq. (3.3), where

$$\mathcal{F}(u_0) = \beta_0 u_0, \quad \hat{\phi}(y) = 0. \quad (3.7)$$

In the second case, the numerical solution is subject to

$$u_0 = \hat{g}(y), \quad \text{given, along } x = 1, \quad (3.8)$$

where $\hat{g}(y)$ is defined by the Flambeau fire experimental data [cf. Eq. (2.34)].

Stable, convergent computations have been carried out in both cases, complete solutions being generated in 4 to 12 min. However, convergence requires reasonable initial guesses for $P_1(x, 0)$, and also $T_0(x, 0)$ and $u_0(x, 0)$ --normal restrictions when nonlinear equations are solved by iterative methods. These codes are documented and further discussed in Appendix C.

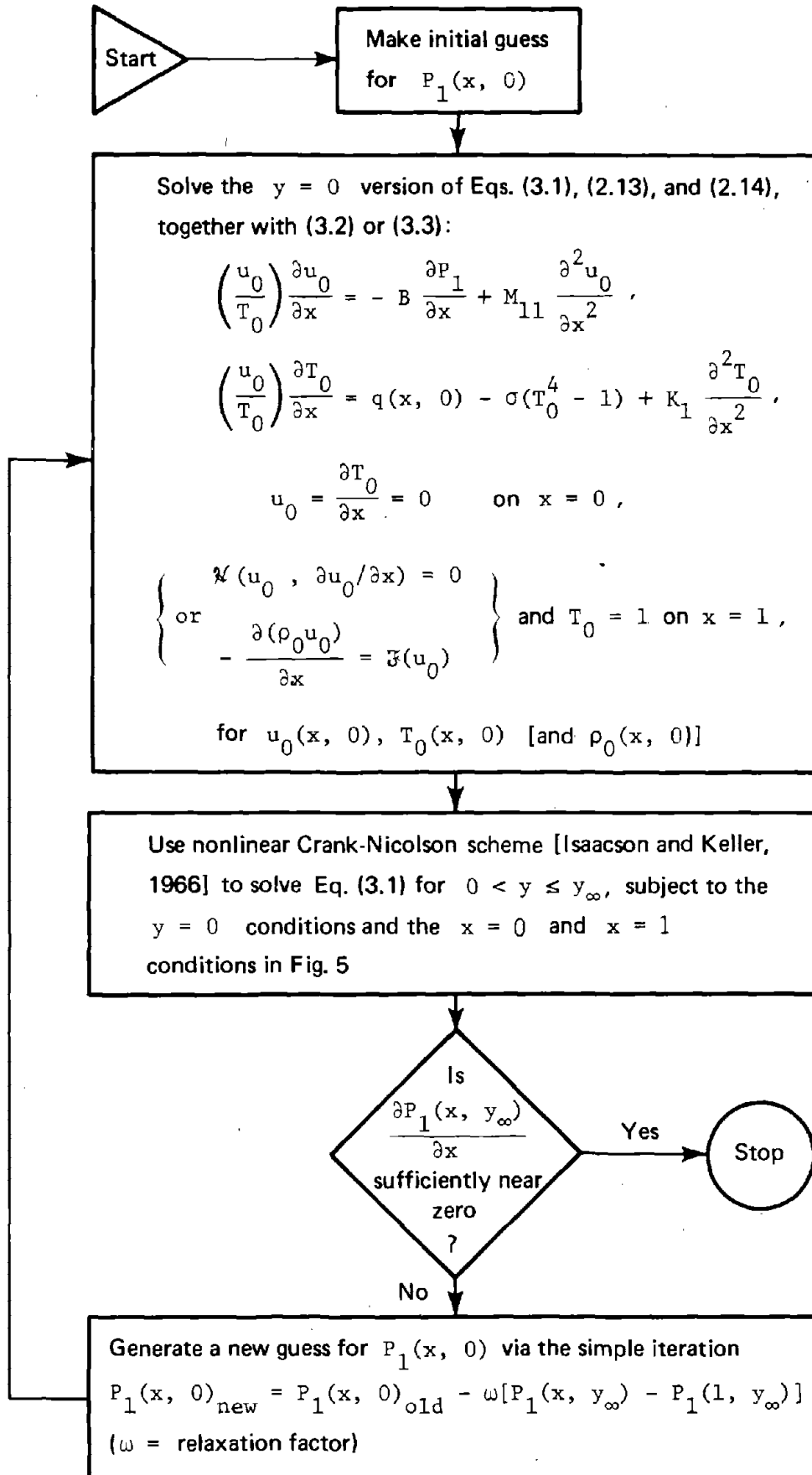


Fig. 6--Macro flowchart of solution algorithm for basic combustion-layer problem

RESULTS

A beginning series of parametric studies for the combustion-layer flow field, though incomplete, explains the gas dynamics in and near the burning region. These calculations explore some variations in the winds at the boundary, the turbulent viscosity, the heat diffusivity (due to turbulent mixing), the radiation losses, and the burning rate. Table 1 presents a partial list of calculations.

Table 1
PARAMETER COMBINATIONS CONSIDERED

Case	$\hat{\alpha}$	$\hat{\beta}$	σ	M_{11}	K_1	Remarks
A	1.0	1.5	0.023	0.5	0.5	Baseline case: $q(x, y) \equiv 1$
B	1.5	1.5	0.023	0.5	0.5	Higher vertical velocity input
C	0.5	1.5	0.023	0.5	0.5	Lower vertical velocity input
D	1.0	2.0	0.023	0.5	0.5	Increased gradient of vertical velocity input
E	1.0	1.0	0.023	0.5	0.5	Decreased gradient of vertical velocity input
F	1.0	1.5	0.05	0.5	0.5	Radiation increased
G	1.0	1.5	0.01	0.5	0.5	Radiation decreased
H	1.0	1.5	0.023	1.5	1.5	Diffusion increased
I	1.0	1.5	0.023	0.25	0.25	Diffusion decreased
J	1.0	1.5	0.023	0.10	0.10	Diffusion decreased
K	1.0	1.5	0.023	0.2	0.8	Variable diffusion coefficients
L	1.0	1.5	0.023	0.8	0.2	Variable diffusion coefficients
M	1.0	1.5	0.023	0.5	0.5	Double heating rate: $q(x, y) \equiv 2$
N	1.0	1.5	0.023	0.5	0.5	Halved heating rate: $q(x, y) \equiv 0.5$
O	1.0	1.5	0.023	0.5	0.5	Periodic fires (2): $q(x, y) = 1 - \cos 4\pi x$
P	1.0	1.5	0.023	0.5	0.5	Periodic fires (10): $q(x, y) = 1 - \cos 20\pi x$
Q	1.0	1.5	0.023	0.5	0.5	Ring ("inner dead zone") fire: $q(x, y) = 1.33; 1/3 \leq x \leq 1$

The variations represented by runs A, B, C, D, and E explore the influence of the boundary condition for vertical velocities at the outer edge of the fire and convection column. The horizontal inflow velocities at $x = 1$ are computed as part of the solution, and not a priori defined. The assumed form of the vertical velocity on the outer boundary is given by Eq. (3.4), in which the asymptotic value of the velocity

with height $y \rightarrow \infty$ is represented by $\hat{\alpha}$ and the initial slope of the velocity profile with altitude $y = 0$ is represented by $\hat{\beta}$. Figure 7 illustrates the boundary vertical velocity versus altitude for cases A through E. Case C has the lowest asymptotic velocity; case A, the standard intermediate value; and case B, the highest value. Similarly, case D has the highest initial slope, case A the intermediate slope, and case E the lowest or slowest initial slope.

Figure 8 compares the velocity fields for the three cases A, B, and C, but is rather difficult to interpret because the plots do not have the same scale for the velocities. The maximum velocities are approximately in the ratio 2:3:4 = C:A:B. One can deduce for case C (lowest boundary velocity) that the motion in the plume above the fire region is fairly vertical and has less horizontal inflow than either case A or B, where the boundary vertical velocities are higher and the horizontal velocities at $x = 1$ are appreciable well above the fire. It appears that the larger the vertical velocities at the boundary, the greater the mass flux into the plume well above the fire. The horizontal velocities coming in at the base of the fire are all approximately equal ($u \sim 2$), after the different scales in the plots have been normalized. The boundary condition is chosen somewhat arbitrarily, but it is evident that a qualitatively similar flow pattern develops for a fairly wide range of boundary velocities.

Figure 9 compares the temperature and pressure contours for cases A, B, and C. The temperature gradients increase as velocity decreases ($\hat{\alpha}$), but the pressure gradients appear to have equalized across the early plume somewhat more rapidly for the lowest-boundary-velocity case C.

Figure 10 compares temperature and velocity along the central axis of the fire for the same three cases. The center-line velocity continues to increase above the actual burning region in case B, where the boundary velocity is highest. The velocity along the center line levels off and increases only slightly above the burning region for the baseline calculation (case A). The velocity actually decreases above the top of the burning region in case C, where the boundary velocity is the least. The increased temperature peak in case C reflects

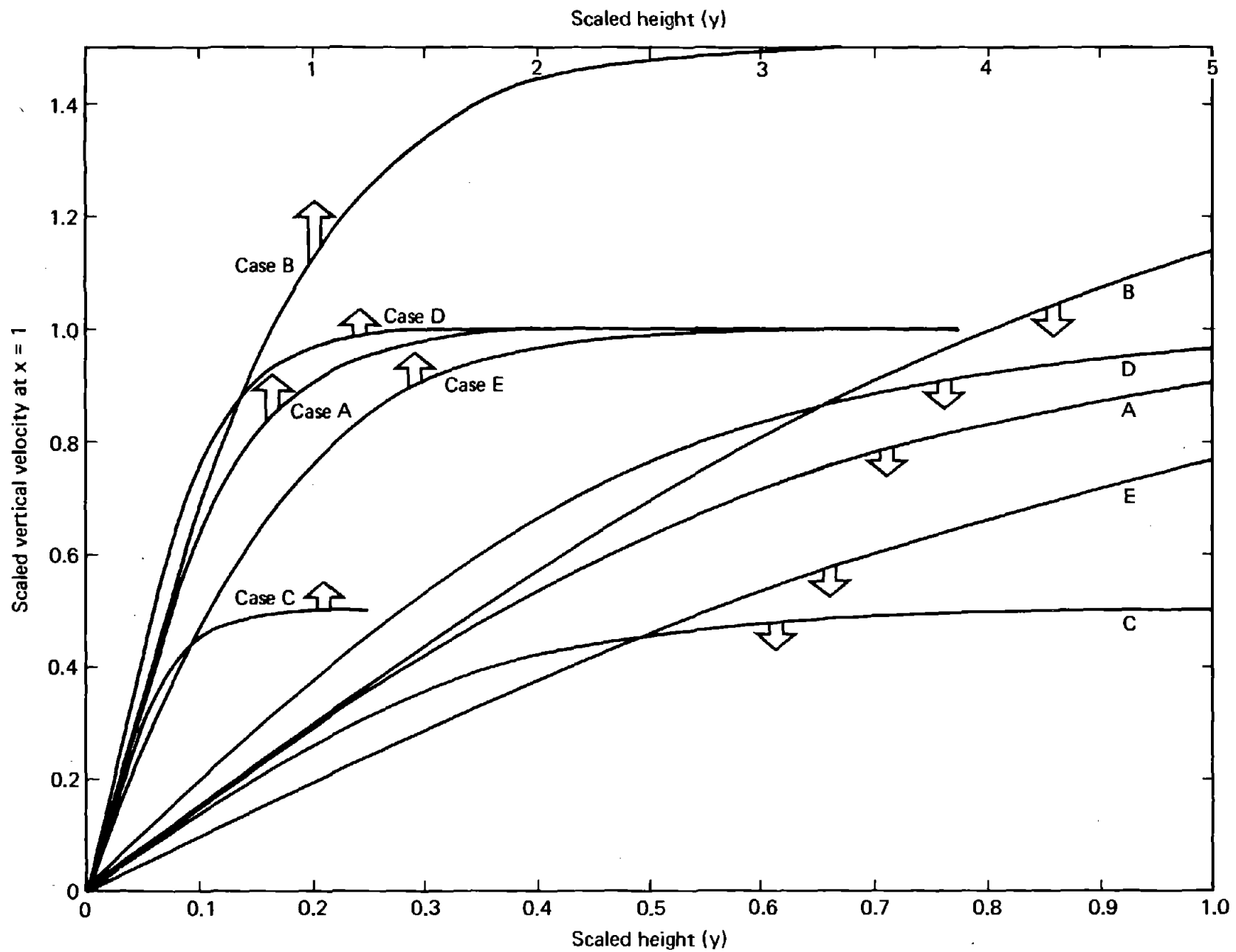


Fig. 7--Vertical velocity profiles used along inlet boundary

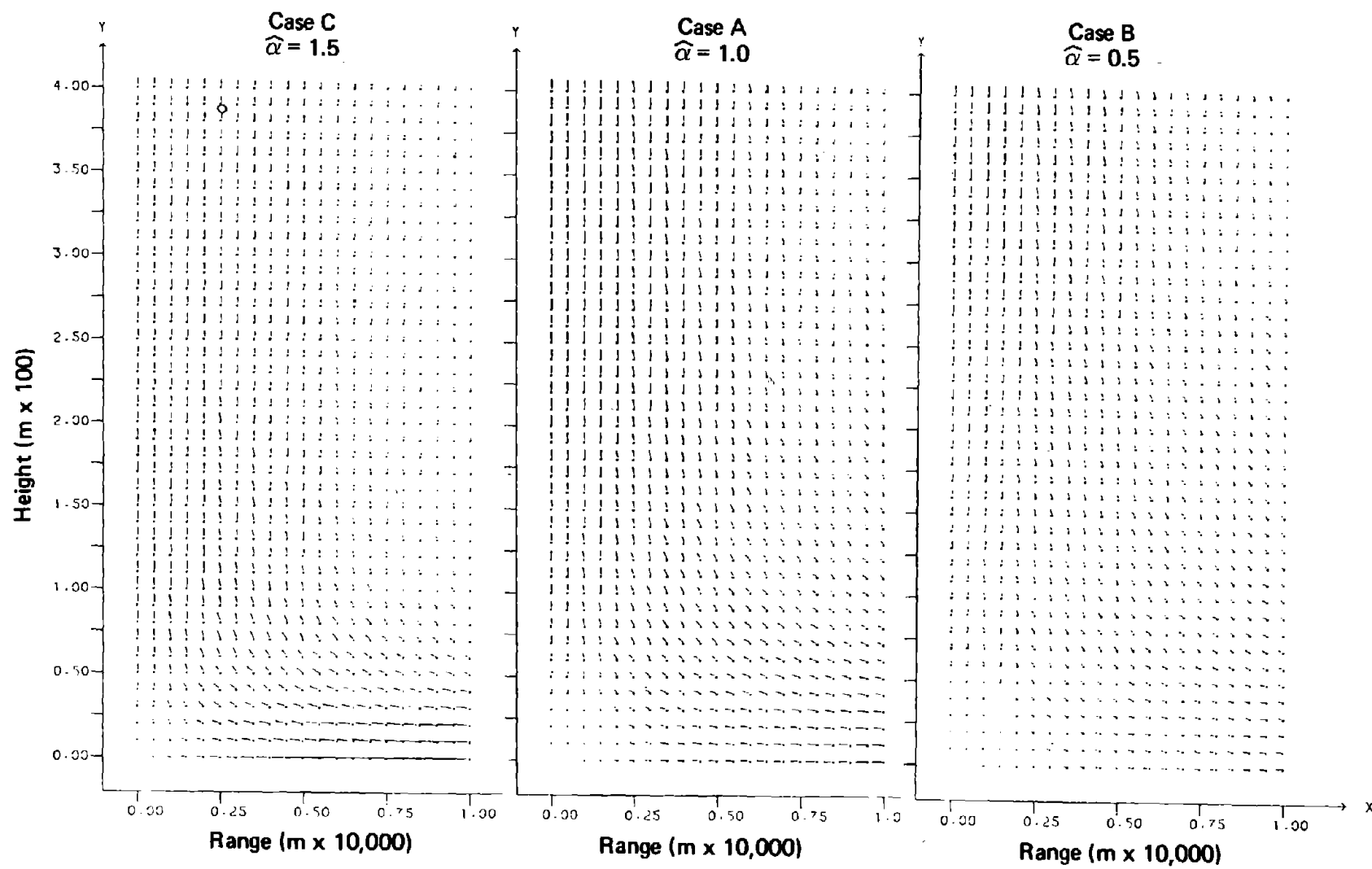


Fig. 8--Velocity fields generated for different inlet velocity magnitudes

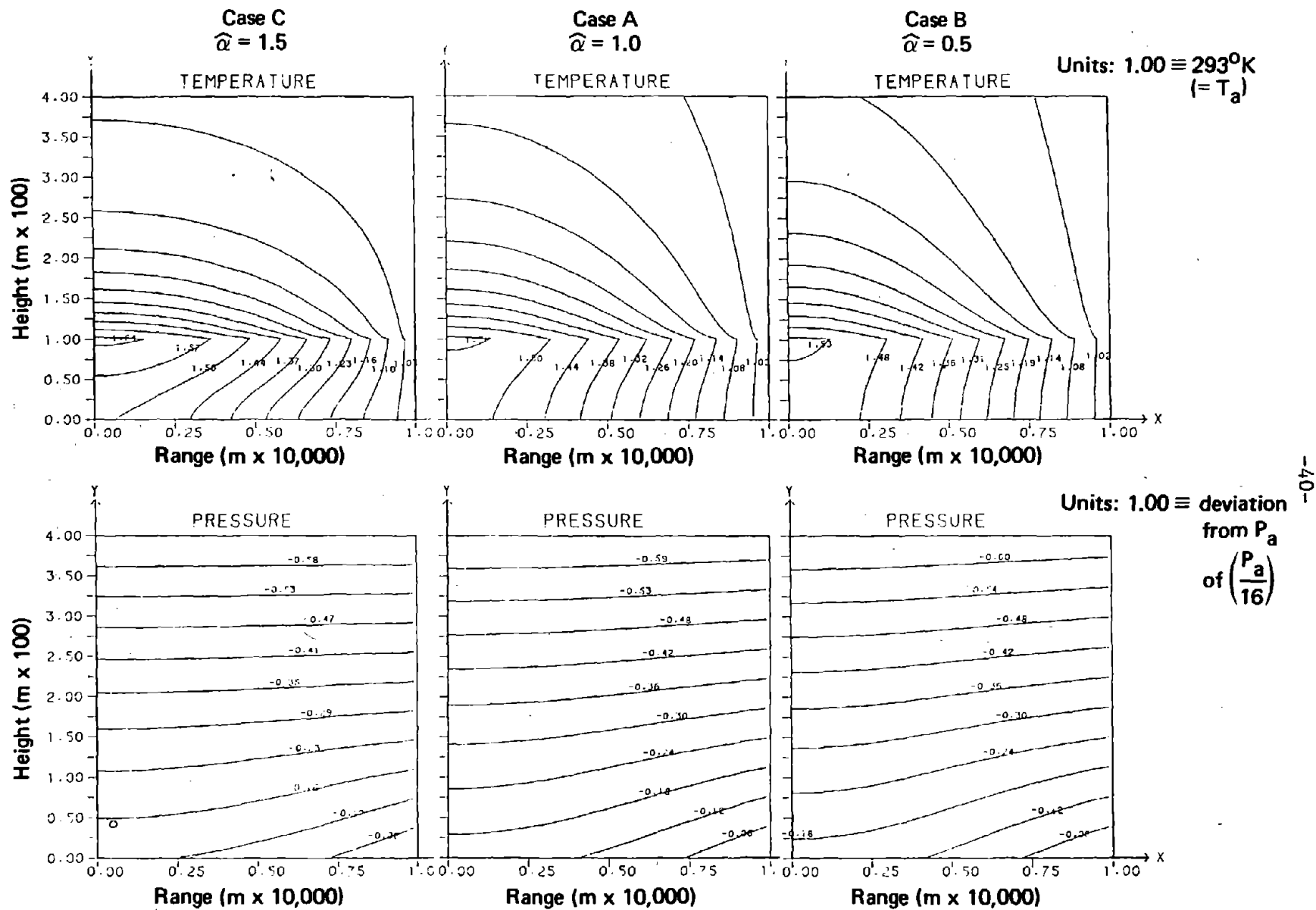


Fig. 9--Temperature and pressure contours generated for different inlet velocity magnitudes

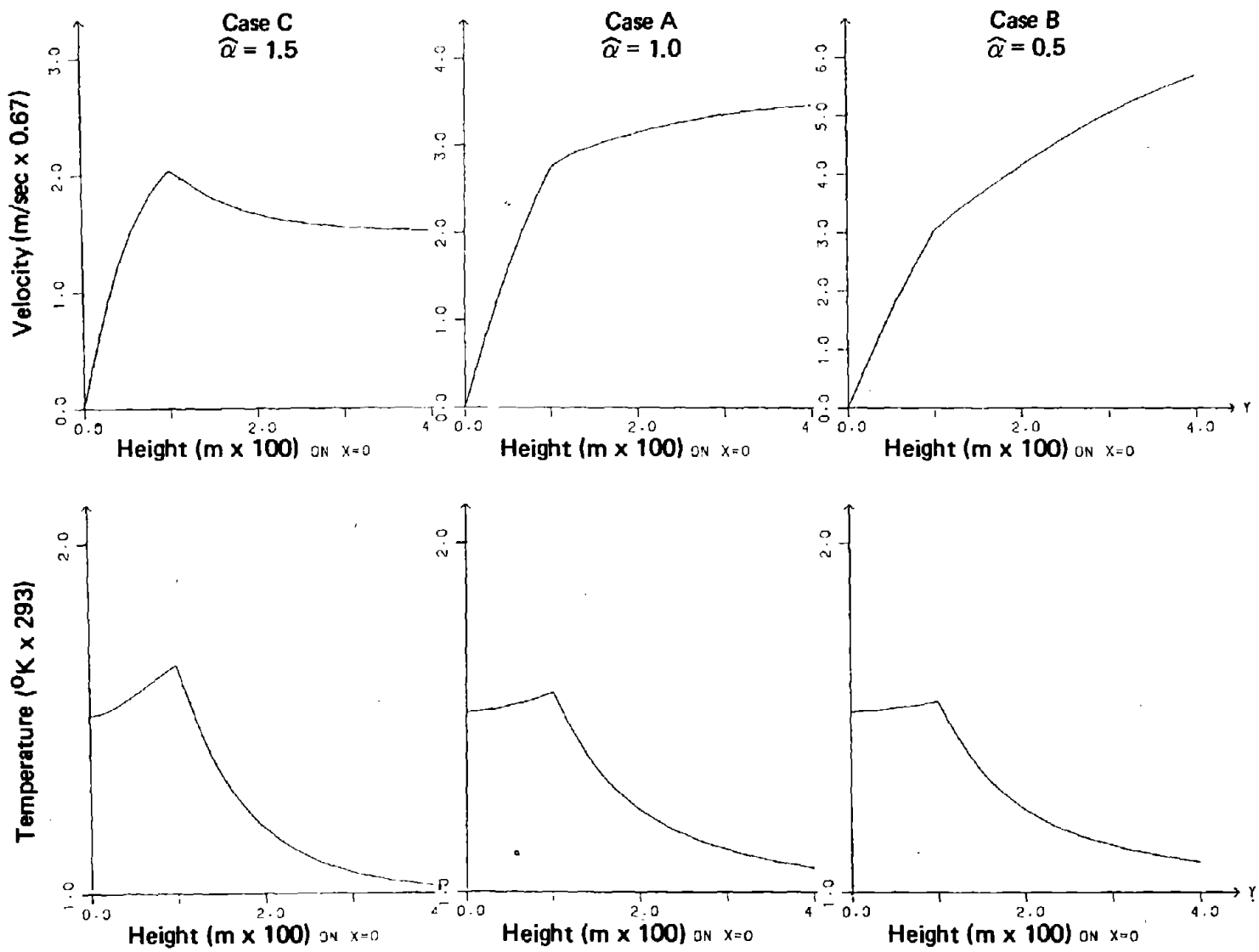


Fig. 10--Center-line velocities and temperatures generated for different inlet velocity magnitudes

the relatively longer fluid residence time in the burning region, whereas the more rapid decrease in temperature above the combustion zone indicates a higher radiative energy loss. In all cases, the temperature decreases rapidly above the burning region.

Figure 11 compares profiles of horizontal velocity as a function of the distance from the center line for the three cases, using comparable absolute values for the vectors. Velocities along the ground are similar in all three cases. However, the turning of the horizontal velocity to a vertical flow above the surface is much more rapid in the low-vertical-velocity case C than in the high-velocity case B. This reflects the interrelationship between the rising buoyant flow and the requirement for inflow air at the base of the column or in the fire region. When the column is rising vigorously (as in case B), the persistence of inward motion well above the surface is evident.

Figure 12 compares vertical velocities for the three cases as a function of horizontal range and altitude. The scale for each plot is expanded, so the plots do not have a single velocity amplitude measure. The maximum velocities are in the approximate ratio $2:3:4 = C:A:B$, the peak velocity of case C (at $y = 100$ m) being half the peak velocity of case B (at $y = 200$ m). The velocity across the plume does decelerate in the lowest-boundary-velocity case C, but continues to accelerate appreciably above the burn region in the highest-boundary-velocity case B. All cases show a similar distribution of velocities across the plume, reaching a maximum along the center line and decreasing toward the edge.

Tables 2 through 7 list the horizontal and vertical velocities (U , V), temperature (T), density (ρ), and pressure (P) for the bottom and uppermost rows of mesh points in each calculation (i.e., the points at the ground surface and those at six times the fire zone height, viz., 600 m). Also shown are the pressure gradient (P_X), the turbulent mixing rate as defined by the second derivative of the horizontal velocity ($NU * U_{XX}$), the thermal diffusion in terms of the second derivative of temperature ($K * T_{XX}$), and the net heat input rate, $Q(T)$.

A comparison of cases A, B, and C for the bottom mesh points (Tables 2, 4, and 6) shows remarkably similar temperature, density, and

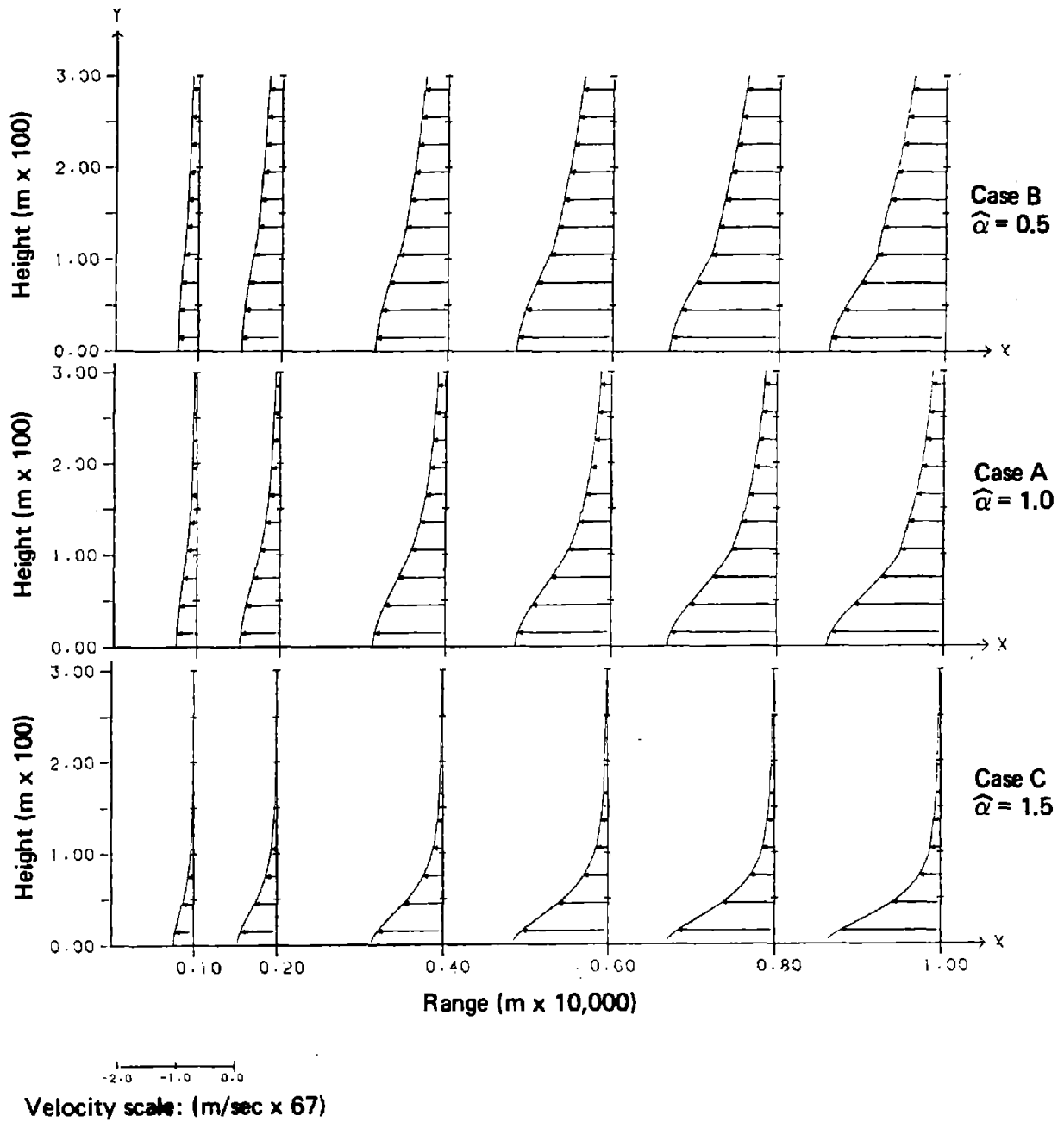
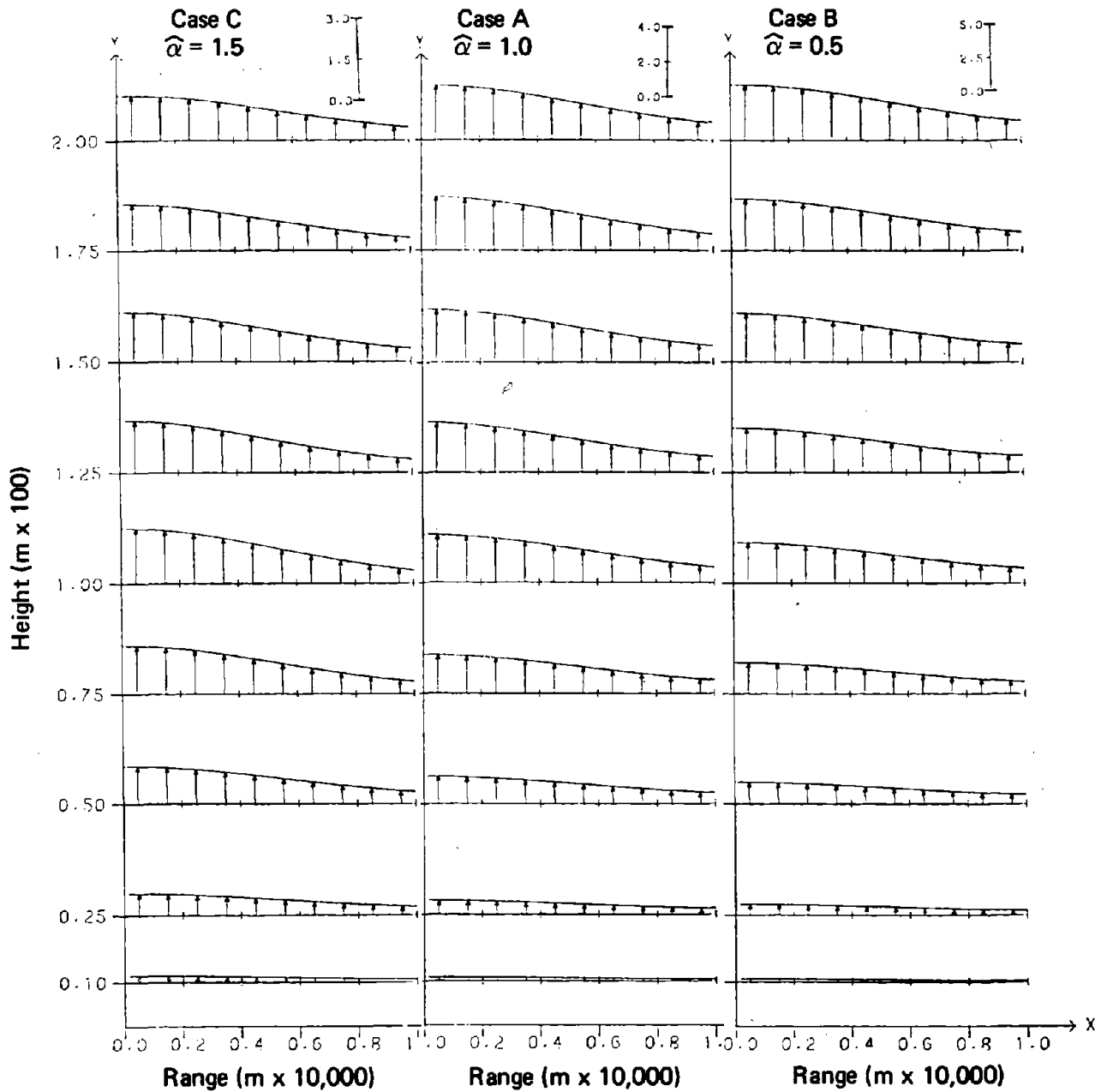


Fig. 11--Horizontal velocity profiles generated for different inlet velocity magnitudes



Velocity scale: (m/sec x 0.67)

Fig. 12--Vertical velocity profiles generated for different inlet velocity magnitudes

Table 2

GROUND-LEVEL NUMERICAL PREDICTIONS FOR BASELINE PARAMETER CASE A

SYSTEM PARAMETERS: A = 0.150 SIGMA = 0.023 NU = 0.500 K = 0.500

MESH: M = 40 DX = 0.025 N = 240 DY = 0.025

ITERATION PARAMETERS: ETLINE = 0.001000 MAXITL = 20 ETOLP = 0.005000 MAXITP = 20

INLET PARAMETERS: ALPHA = 1.000 BETA = 1.500 WLOSS = 0.000

FOR J = 1 (Y = 0.000):

I	X	U	V	T	RHO	P	PX	U(I+0.5X)	K*TX	Q(T)
1	0.000	0.000	0.000	1.516	0.660	-0.149	0.000	0.000	0.000	0.902
2	0.025	-0.084	0.000	1.516	0.660	-0.149	0.004	0.192	-0.900	0.902
3	0.050	-0.169	0.000	1.515	0.660	-0.149	0.014	0.388	-0.894	0.902
4	0.075	-0.252	0.000	1.512	0.661	-0.148	0.023	0.579	-0.884	0.903
5	0.100	-0.335	0.000	1.509	0.663	-0.147	0.031	0.764	-0.870	0.904
6	0.125	-0.417	0.000	1.505	0.665	-0.147	0.041	0.944	-0.849	0.905
7	0.150	-0.499	0.000	1.499	0.667	-0.145	0.051	1.116	-0.828	0.907
8	0.175	-0.577	0.000	1.493	0.670	-0.144	0.059	1.276	-0.800	0.909
9	0.200	-0.655	0.000	1.485	0.673	-0.142	0.067	1.426	-0.770	0.911
10	0.225	-0.731	0.000	1.477	0.677	-0.141	0.077	1.565	-0.736	0.914
11	0.250	-0.805	0.000	1.467	0.682	-0.139	0.085	1.689	-0.700	0.916
12	0.275	-0.877	0.000	1.457	0.686	-0.136	0.092	1.800	-0.661	0.919
13	0.300	-0.947	0.000	1.446	0.692	-0.133	0.102	1.899	-0.621	0.923
14	0.325	-1.014	0.000	1.434	0.697	-0.131	0.111	1.981	-0.578	0.926
15	0.350	-1.079	0.000	1.421	0.704	-0.128	0.118	2.051	-0.536	0.929
16	0.375	-1.142	0.000	1.408	0.710	-0.125	0.125	2.103	-0.492	0.933
17	0.400	-1.201	0.000	1.394	0.717	-0.122	0.132	2.147	-0.446	0.936
18	0.425	-1.258	0.000	1.380	0.725	-0.119	0.140	2.172	-0.400	0.940
19	0.450	-1.313	0.000	1.365	0.733	-0.115	0.146	2.183	-0.359	0.943
20	0.475	-1.364	0.000	1.349	0.741	-0.111	0.153	2.183	-0.314	0.947
21	0.500	-1.413	0.000	1.333	0.750	-0.108	0.161	2.174	-0.274	0.950
22	0.525	-1.459	0.000	1.317	0.759	-0.103	0.167	2.151	-0.231	0.954
23	0.550	-1.503	0.000	1.301	0.769	-0.099	0.174	2.119	-0.193	0.957
24	0.575	-1.545	0.000	1.284	0.779	-0.095	0.180	2.079	-0.153	0.960
25	0.600	-1.582	0.000	1.267	0.788	-0.090	0.185	2.027	-0.117	0.964
26	0.625	-1.617	0.000	1.250	0.799	-0.085	0.192	1.974	-0.084	0.967
27	0.650	-1.651	0.000	1.233	0.811	-0.081	0.195	1.908	-0.052	0.970
28	0.675	-1.681	0.000	1.216	0.822	-0.076	0.202	1.841	-0.021	0.973
29	0.700	-1.710	0.000	1.199	0.834	-0.071	0.209	1.772	0.005	0.976
30	0.725	-1.736	0.000	1.182	0.846	-0.065	0.211	1.693	0.033	0.978
31	0.750	-1.760	0.000	1.164	0.859	-0.060	0.215	1.616	0.054	0.981
32	0.775	-1.782	0.000	1.147	0.872	-0.055	0.222	1.539	0.077	0.983
33	0.800	-1.803	0.000	1.130	0.885	-0.049	0.228	1.460	0.095	0.985
34	0.825	-1.821	0.000	1.113	0.898	-0.043	0.230	1.377	0.111	0.988
35	0.850	-1.838	0.000	1.097	0.912	-0.037	0.234	1.298	0.128	0.990
36	0.875	-1.853	0.000	1.080	0.926	-0.031	0.242	1.223	0.140	0.992
37	0.900	-1.866	0.000	1.064	0.940	-0.025	0.246	1.145	0.151	0.994
38	0.925	-1.878	0.000	1.047	0.955	-0.019	0.248	1.067	0.161	0.995
39	0.950	-1.889	0.000	1.031	0.970	-0.013	0.252	0.996	0.169	0.997



Table 3

600-m-ALTITUDE NUMERICAL PREDICTIONS FOR BASELINE PARAMETER CASE A

FOR J = 241 (Y = 6.0000):

I	X	U	V	T	RHO	P	PX	NU*UXX	K*TX	Q(T)
1	0.000	0.000	3.528	1.026	0.975	-0.960	0.000	0.000	0.000	-0.003
2	0.025	-0.001	3.524	1.026	0.975	-0.960	0.000	0.003	-0.040	-0.003
3	0.050	-0.003	3.513	1.026	0.975	-0.960	0.001	0.007	-0.039	-0.002
4	0.075	-0.004	3.497	1.026	0.975	-0.960	0.000	0.009	-0.040	-0.002
5	0.100	-0.005	3.475	1.026	0.975	-0.960	-0.001	0.011	-0.037	-0.002
6	0.125	-0.007	3.447	1.026	0.975	-0.960	0.000	0.015	-0.039	-0.002
7	0.150	-0.008	3.413	1.025	0.975	-0.960	0.001	0.019	-0.037	-0.002
8	0.175	-0.009	3.373	1.025	0.976	-0.960	0.000	0.021	-0.035	-0.002
9	0.200	-0.010	3.329	1.025	0.976	-0.960	-0.001	0.023	-0.036	-0.002
10	0.225	-0.011	3.280	1.024	0.976	-0.960	0.000	0.026	-0.035	-0.002
11	0.250	-0.013	3.226	1.024	0.977	-0.960	0.000	0.027	-0.032	-0.002
12	0.275	-0.014	3.167	1.023	0.977	-0.960	-0.001	0.028	-0.031	-0.002
13	0.300	-0.015	3.105	1.023	0.978	-0.960	0.000	0.031	-0.031	-0.002
14	0.325	-0.016	3.039	1.022	0.978	-0.960	-0.001	0.034	-0.030	-0.002
15	0.350	-0.017	2.968	1.022	0.979	-0.960	0.000	0.035	-0.028	-0.002
16	0.375	-0.018	2.895	1.021	0.979	-0.960	-0.001	0.035	-0.028	-0.002
17	0.400	-0.019	2.819	1.021	0.980	-0.960	0.000	0.035	-0.025	-0.002
18	0.425	-0.020	2.741	1.020	0.981	-0.960	-0.001	0.037	-0.021	-0.002
19	0.450	-0.021	2.661	1.019	0.981	-0.960	0.000	0.037	-0.022	-0.002
20	0.475	-0.021	2.579	1.018	0.982	-0.960	-0.001	0.036	-0.018	-0.002
21	0.500	-0.022	2.496	1.017	0.983	-0.960	0.000	0.038	-0.020	-0.002
22	0.525	-0.023	2.411	1.017	0.983	-0.960	-0.001	0.037	-0.014	-0.002
23	0.550	-0.023	2.326	1.016	0.984	-0.960	0.000	0.038	-0.016	-0.002
24	0.575	-0.024	2.240	1.015	0.985	-0.960	-0.001	0.037	-0.013	-0.001
25	0.600	-0.024	2.154	1.014	0.986	-0.960	0.000	0.038	-0.013	-0.001
26	0.625	-0.025	2.068	1.014	0.987	-0.960	-0.001	0.037	-0.010	-0.001
27	0.650	-0.025	1.983	1.013	0.987	-0.960	0.000	0.033	-0.010	-0.001
28	0.675	-0.026	1.899	1.012	0.988	-0.960	-0.001	0.034	-0.009	-0.001
29	0.700	-0.026	1.815	1.011	0.989	-0.960	0.001	0.034	-0.006	-0.001
30	0.725	-0.026	1.733	1.010	0.990	-0.960	-0.001	0.031	-0.006	-0.001
31	0.750	-0.027	1.652	1.009	0.991	-0.960	0.000	0.029	-0.007	-0.001
32	0.775	-0.027	1.573	1.008	0.992	-0.960	-0.001	0.029	-0.003	-0.001
33	0.800	-0.027	1.495	1.007	0.993	-0.960	0.001	0.030	-0.003	-0.001
34	0.825	-0.027	1.419	1.006	0.994	-0.960	-0.001	0.026	-0.002	-0.001
35	0.850	-0.027	1.346	1.006	0.994	-0.960	0.000	0.024	-0.003	-0.001
36	0.875	-0.028	1.275	1.005	0.995	-0.960	-0.002	0.027	-0.001	0.000
37	0.900	-0.028	1.205	1.004	0.996	-0.960	0.000	0.025	-0.002	0.000
38	0.925	-0.028	1.138	1.003	0.997	-0.960	-0.001	0.021	0.002	0.000
39	0.950	-0.028	1.074	1.002	0.998	-0.960	0.000	0.019	-0.001	0.000
40	0.975	-0.028	1.012	1.001	0.999	-0.960	-0.002	0.025	0.001	0.000
41	1.000	-0.028	0.981	1.000	1.000	-0.960				

Table 4

GROUND-LEVEL NUMERICAL PREDICTIONS FOR PARAMETER CASE B
(INCREASED MAGNITUDE OF INLET VERTICAL VELOCITY)

SYSTEM PARAMETERS: A = 0.160 SIGMA = 0.023 NU = 0.500 K = 0.500

MESH: M = 40 DX = 0.025 H = 2.00 DY = 0.025

ITERATION PARAMETERS: ETOLME = 0.001000 MAXITL = 20 ETOLP = 0.005000 MAXITP = 20

INLET PARAMETERS: ALPHA = 1.500 BETA = 1.500 BLOSS = 0.000

FOR J = 1 (Y = 0.000):

I	X	U	V	T	RHO	P	PX	NU*UXX	K*TXX	Q(T)
1	0.000	0.000	0.000	1.516	0.660	-0.156	0.000	0.000	0.000	0.902
2	0.025	-0.045	0.000	1.516	0.660	-0.156	0.006	0.195	-0.900	0.902
3	0.050	-0.169	0.000	1.516	0.660	-0.156	0.017	0.393	-0.895	0.902
4	0.075	-0.253	0.000	1.512	0.661	-0.155	0.028	0.587	-0.883	0.903
5	0.100	-0.336	0.000	1.509	0.663	-0.154	0.039	0.776	-0.869	0.904
6	0.125	-0.418	0.000	1.508	0.665	-0.153	0.049	0.958	-0.851	0.905
7	0.150	-0.499	0.000	1.499	0.667	-0.152	0.060	1.131	-0.826	0.907
8	0.175	-0.579	0.000	1.492	0.670	-0.150	0.071	1.294	-0.800	0.909
9	0.200	-0.657	0.000	1.485	0.673	-0.148	0.081	1.445	-0.768	0.911
10	0.225	-0.733	0.000	1.476	0.677	-0.146	0.091	1.585	-0.737	0.914
11	0.250	-0.808	0.000	1.467	0.682	-0.144	0.101	1.711	-0.699	0.916
12	0.275	-0.880	0.000	1.457	0.687	-0.141	0.110	1.823	-0.661	0.919
13	0.300	-0.949	0.000	1.446	0.692	-0.138	0.119	1.922	-0.620	0.923
14	0.325	-1.017	0.000	1.434	0.698	-0.135	0.128	2.005	-0.578	0.926
15	0.350	-1.082	0.000	1.421	0.704	-0.132	0.137	2.072	-0.536	0.929
16	0.375	-1.144	0.000	1.408	0.710	-0.128	0.145	2.127	-0.491	0.933
17	0.400	-1.204	0.000	1.395	0.717	-0.124	0.152	2.165	-0.446	0.936
18	0.425	-1.261	0.000	1.379	0.725	-0.121	0.160	2.190	-0.403	0.940
19	0.450	-1.315	0.000	1.360	0.733	-0.116	0.167	2.203	-0.358	0.943
20	0.475	-1.366	0.000	1.340	0.741	-0.112	0.173	2.201	-0.315	0.947
21	0.500	-1.415	0.000	1.323	0.750	-0.108	0.180	2.188	-0.272	0.950
22	0.525	-1.461	0.000	1.317	0.759	-0.103	0.185	2.164	-0.232	0.954
23	0.550	-1.504	0.000	1.301	0.769	-0.099	0.191	2.130	-0.191	0.957
24	0.575	-1.545	0.000	1.284	0.779	-0.094	0.196	2.086	-0.154	0.960
25	0.600	-1.583	0.000	1.267	0.789	-0.089	0.200	2.034	-0.117	0.964
26	0.625	-1.618	0.000	1.250	0.800	-0.084	0.205	1.975	-0.084	0.967
27	0.650	-1.651	0.000	1.233	0.811	-0.079	0.208	1.910	-0.051	0.970
28	0.675	-1.682	0.000	1.216	0.822	-0.073	0.212	1.839	-0.022	0.973
29	0.700	-1.710	0.000	1.199	0.834	-0.068	0.215	1.766	0.005	0.976
30	0.725	-1.736	0.000	1.181	0.846	-0.063	0.218	1.688	0.031	0.978
31	0.750	-1.760	0.000	1.164	0.859	-0.057	0.220	1.608	0.055	0.981
32	0.775	-1.782	0.000	1.147	0.872	-0.051	0.223	1.527	0.076	0.983
33	0.800	-1.802	0.000	1.130	0.885	-0.046	0.225	1.445	0.095	0.985
34	0.825	-1.820	0.000	1.113	0.898	-0.040	0.226	1.363	0.111	0.988
35	0.850	-1.837	0.000	1.097	0.912	-0.035	0.227	1.281	0.127	0.990
36	0.875	-1.852	0.000	1.080	0.926	-0.029	0.229	1.202	0.140	0.992
37	0.900	-1.865	0.000	1.064	0.940	-0.023	0.230	1.122	0.150	0.994
38	0.925	-1.877	0.000	1.047	0.955	-0.017	0.231	1.047	0.161	0.995
39	0.950	-1.888	0.000	1.031	0.970	-0.012	0.231	0.971	0.167	0.997
40	0.975	-1.897	0.000	1.014	0.985	-0.006	0.232	0.900	0.175	0.999
41	1.000	-1.906	0.000	1.000	1.000	0.000	0.233	0.900	0.175	1.000

Table 5

600-m-ALTITUDE NUMERICAL PREDICTIONS FOR PARAMETER CASE B
(INCREASED MAGNITUDE OF INLET VERTICAL VELOCITY)

FOR J = 241 (Y = 6.000):

I	X	U	V	T	RHO	P	PX	NU*UXX	K*IXX	Q(T)
1	6.000	0.000	6.453	1.045	0.957	-0.960	0.000	0.000	0.000	-0.004
2	0.025	-0.006	6.446	1.045	0.957	-0.960	0.000	0.023	-0.077	-0.004
3	0.050	-0.016	6.425	1.045	0.957	-0.960	0.000	0.045	-0.077	-0.004
4	0.075	-0.025	6.392	1.045	0.957	-0.960	0.000	0.067	-0.076	-0.004
5	0.100	-0.033	6.347	1.045	0.957	-0.960	0.000	0.088	-0.075	-0.004
6	0.125	-0.041	6.290	1.044	0.957	-0.960	0.000	0.108	-0.073	-0.004
7	0.150	-0.048	6.222	1.044	0.958	-0.960	0.000	0.128	-0.070	-0.004
8	0.175	-0.056	6.142	1.043	0.958	-0.960	0.000	0.146	-0.069	-0.004
9	0.200	-0.064	6.053	1.043	0.959	-0.960	0.000	0.163	-0.066	-0.004
10	0.225	-0.071	5.953	1.042	0.960	-0.960	0.000	0.179	-0.063	-0.004
11	0.250	-0.078	5.843	1.041	0.960	-0.960	0.000	0.193	-0.060	-0.004
12	0.275	-0.085	5.725	1.040	0.961	-0.960	0.000	0.205	-0.057	-0.004
13	0.300	-0.091	5.599	1.039	0.962	-0.960	0.000	0.216	-0.054	-0.004
14	0.325	-0.098	5.464	1.038	0.963	-0.960	0.000	0.225	-0.050	-0.004
15	0.350	-0.104	5.323	1.037	0.964	-0.960	0.000	0.233	-0.047	-0.004
16	0.375	-0.109	5.176	1.036	0.965	-0.960	0.000	0.238	-0.043	-0.004
17	0.400	-0.115	5.023	1.035	0.966	-0.960	0.000	0.242	-0.040	-0.003
18	0.425	-0.120	4.866	1.034	0.967	-0.960	0.000	0.245	-0.034	-0.003
19	0.450	-0.125	4.704	1.032	0.969	-0.960	0.000	0.246	-0.030	-0.003
20	0.475	-0.129	4.539	1.031	0.970	-0.960	0.000	0.245	-0.028	-0.003
21	0.500	-0.133	4.372	1.030	0.971	-0.960	0.000	0.244	-0.024	-0.003
22	0.525	-0.137	4.204	1.029	0.972	-0.960	0.000	0.241	-0.024	-0.003
23	0.550	-0.141	4.034	1.027	0.974	-0.960	0.000	0.237	-0.017	-0.003
24	0.575	-0.144	3.864	1.025	0.975	-0.960	0.000	0.231	-0.018	-0.002
25	0.600	-0.147	3.694	1.024	0.977	-0.960	0.000	0.225	-0.011	-0.002
26	0.625	-0.151	3.525	1.023	0.978	-0.960	0.000	0.219	-0.011	-0.002
27	0.650	-0.152	3.359	1.021	0.979	-0.960	0.000	0.211	-0.007	-0.002
28	0.675	-0.155	3.194	1.019	0.981	-0.960	0.000	0.203	-0.006	-0.002
29	0.700	-0.157	3.032	1.018	0.982	-0.960	0.000	0.194	-0.004	-0.002
30	0.725	-0.158	2.873	1.016	0.984	-0.960	0.000	0.185	0.000	-0.002
31	0.750	-0.160	2.716	1.015	0.985	-0.960	0.000	0.176	-0.001	-0.001
32	0.775	-0.161	2.567	1.013	0.987	-0.960	0.000	0.167	0.003	-0.001
33	0.800	-0.162	2.420	1.012	0.988	-0.960	0.000	0.158	0.002	-0.001
34	0.825	-0.163	2.278	1.010	0.990	-0.960	0.000	0.149	0.005	-0.001
35	0.850	-0.163	2.141	1.009	0.991	-0.960	0.000	0.139	0.005	-0.001
36	0.875	-0.164	2.009	1.007	0.993	-0.960	0.000	0.131	0.006	-0.001
37	0.900	-0.164	1.883	1.006	0.994	-0.960	0.000	0.122	0.009	-0.001
38	0.925	-0.164	1.762	1.004	0.996	-0.960	0.000	0.113	0.005	-0.000
39	0.950	-0.164	1.646	1.003	0.997	-0.960	0.000	0.105	0.011	0.000
40	0.975	-0.164	1.536	1.001	0.999	-0.960	0.000	0.093	0.008	0.000
41	1.000	-0.164	1.431	1.000	1.000	-0.960	0.000	0.093	0.008	0.000

Table 6

GROUND-LEVEL NUMERICAL PREDICTIONS FOR PARAMETER CASE C
(DECREASED MAGNITUDE OF INLET VERTICAL VELOCITY)

FIRE: SOLUTION OF COMBUSTION LAYER BOUNDARY VALUE PROBLEM

SYSTEM PARAMETERS: A = 0.160 SIGMA = 0.023 NU = 0.500 K = 0.500

MESH: H = 40 DX = 0.025 N = 200 DY = 0.025

ITERATION PARAMETERS: FTOLP = 0.001000 MAXITL = 20 FTOLP = 0.005000 MAXITP = 20

INLET PARAMETERS: ALPHA = 0.500 BETA = 1.500 BLOSS = 0.000

FOR J = 1 (Y = 0.000):

T	X	H	V	T	RMU	P	PX	NU*UXX	K*TX	Q(T)
1	0.000	0.000	0.000	1.504	0.663	-0.125	0.000	0.000	0.000	0.904
2	0.025	-0.088	0.000	1.504	0.663	-0.125	0.003	0.207	-0.903	0.904
3	0.050	-0.175	0.000	1.504	0.664	-0.125	0.010	0.416	-0.896	0.905
4	0.075	-0.262	0.000	1.504	0.665	-0.124	0.016	0.620	-0.887	0.905
5	0.100	-0.349	0.000	1.501	0.666	-0.124	0.022	0.819	-0.870	0.906
6	0.125	-0.434	0.000	1.496	0.668	-0.123	0.029	1.009	-0.850	0.908
7	0.150	-0.518	0.000	1.491	0.671	-0.122	0.035	1.191	-0.826	0.909
8	0.175	-0.600	0.000	1.484	0.674	-0.121	0.041	1.362	-0.797	0.911
9	0.200	-0.681	0.000	1.477	0.677	-0.120	0.048	1.519	-0.766	0.914
10	0.225	-0.760	0.000	1.468	0.681	-0.119	0.054	1.665	-0.730	0.916
11	0.250	-0.837	0.000	1.459	0.685	-0.118	0.060	1.795	-0.694	0.919
12	0.275	-0.911	0.000	1.449	0.690	-0.116	0.066	1.911	-0.653	0.922
13	0.300	-0.983	0.000	1.438	0.696	-0.114	0.073	2.013	-0.611	0.925
14	0.325	-1.053	0.000	1.426	0.701	-0.112	0.079	2.096	-0.567	0.928
15	0.350	-1.120	0.000	1.413	0.706	-0.110	0.085	2.167	-0.523	0.931
16	0.375	-1.184	0.000	1.400	0.714	-0.108	0.091	2.219	-0.478	0.935
17	0.400	-1.246	0.000	1.386	0.721	-0.106	0.097	2.258	-0.431	0.938
18	0.425	-1.306	0.000	1.372	0.729	-0.103	0.103	2.281	-0.387	0.942
19	0.450	-1.360	0.000	1.357	0.737	-0.101	0.109	2.291	-0.342	0.945
20	0.475	-1.413	0.000	1.342	0.745	-0.098	0.115	2.287	-0.298	0.948
21	0.500	-1.463	0.000	1.326	0.754	-0.095	0.121	2.271	-0.255	0.952
22	0.525	-1.511	0.000	1.310	0.763	-0.092	0.127	2.244	-0.213	0.955
23	0.550	-1.555	0.000	1.294	0.773	-0.089	0.134	2.206	-0.174	0.959
24	0.575	-1.597	0.000	1.277	0.783	-0.085	0.140	2.158	-0.136	0.962
25	0.600	-1.636	0.000	1.261	0.793	-0.082	0.146	2.103	-0.099	0.965
26	0.625	-1.672	0.000	1.244	0.804	-0.078	0.152	2.041	-0.067	0.968
27	0.650	-1.706	0.000	1.227	0.815	-0.074	0.158	1.972	-0.034	0.971
28	0.675	-1.737	0.000	1.210	0.826	-0.070	0.165	1.898	-0.006	0.974
29	0.700	-1.766	0.000	1.194	0.838	-0.066	0.172	1.822	0.021	0.976
30	0.725	-1.793	0.000	1.177	0.850	-0.061	0.178	1.742	0.045	0.979
31	0.750	-1.818	0.000	1.160	0.862	-0.057	0.185	1.659	0.069	0.981
32	0.775	-1.840	0.000	1.143	0.875	-0.052	0.193	1.577	0.088	0.984
33	0.800	-1.861	0.000	1.127	0.888	-0.047	0.200	1.493	0.105	0.986
34	0.825	-1.879	0.000	1.110	0.901	-0.042	0.208	1.411	0.121	0.988
35	0.850	-1.896	0.000	1.094	0.914	-0.037	0.216	1.329	0.135	0.990
36	0.875	-1.911	0.000	1.078	0.928	-0.031	0.225	1.249	0.146	0.992
37	0.900	-1.925	0.000	1.062	0.942	-0.025	0.234	1.172	0.156	0.994
38	0.925	-1.937	0.000	1.046	0.956	-0.020	0.244	1.096	0.164	0.995
39	0.950	-1.948	0.000	1.030	0.970	-0.013	0.254	1.025	0.171	0.997
40	0.975	-1.958	0.000	1.015	0.985	-0.007	0.266	0.954	0.176	0.999
41	1.000	-1.966	0.000	1.000	1.000	0.000	0.272	0.954	0.176	1.000

Table 7

600-m-ALTITUDE NUMERICAL PREDICTIONS FOR PARAMETER CASE C
(DECREASED MAGNITUDE OF INLET VERTICAL VELOCITY)

FOR J = 20 (Y = 6.000):

I	Z	U	V	T	RHO	P	PX	NU*UXX	K*TXK	Q(T)
1	0.000	0.000	1.507	1.002	0.998	-0.960	0.000	0.000	0.000	0.000
2	0.025	0.000	1.505	1.002	0.998	-0.960	0.000	0.000	-0.004	0.000
3	0.050	0.000	1.500	1.002	0.998	-0.960	0.000	0.000	-0.003	0.000
4	0.075	0.000	1.493	1.002	0.998	-0.960	0.000	0.000	-0.004	0.000
5	0.100	0.000	1.484	1.002	0.998	-0.960	0.000	0.000	-0.005	0.000
6	0.125	0.000	1.472	1.002	0.998	-0.960	0.000	0.000	-0.002	0.000
7	0.150	0.000	1.457	1.002	0.998	-0.960	0.000	0.001	-0.005	0.000
8	0.175	0.000	1.441	1.002	0.998	-0.960	0.000	0.001	-0.002	0.000
9	0.200	0.000	1.422	1.002	0.998	-0.960	0.000	0.001	-0.003	0.000
10	0.225	0.000	1.401	1.002	0.998	-0.960	0.000	0.001	-0.004	0.000
11	0.250	0.000	1.378	1.002	0.998	-0.960	0.000	0.001	-0.002	0.000
12	0.275	0.000	1.354	1.002	0.998	-0.960	0.000	0.001	-0.003	0.000
13	0.300	0.000	1.328	1.002	0.998	-0.960	0.000	0.001	-0.005	0.000
14	0.325	-0.001	1.300	1.002	0.998	-0.960	0.000	0.001	-0.001	0.000
15	0.350	-0.001	1.271	1.002	0.998	-0.960	0.000	0.001	-0.002	0.000
16	0.375	-0.001	1.241	1.002	0.998	-0.960	0.000	0.001	-0.003	0.000
17	0.400	-0.001	1.210	1.002	0.998	-0.960	0.000	0.001	-0.003	0.000
18	0.425	-0.001	1.177	1.002	0.998	-0.960	0.000	0.001	-0.001	0.000
19	0.450	-0.001	1.145	1.002	0.998	-0.960	0.000	0.001	-0.003	0.000
20	0.475	-0.001	1.111	1.002	0.998	-0.960	0.000	0.001	-0.002	0.000
21	0.500	-0.001	1.078	1.002	0.998	-0.960	0.000	0.001	-0.002	0.000
22	0.525	-0.001	1.043	1.002	0.998	-0.960	0.000	0.001	-0.002	0.000
23	0.550	-0.001	1.009	1.002	0.998	-0.960	0.000	0.001	-0.002	0.000
24	0.575	-0.001	0.975	1.001	0.999	-0.960	0.000	0.001	0.000	0.000
25	0.600	-0.001	0.941	1.001	0.999	-0.960	0.000	0.001	-0.003	0.000
26	0.625	-0.001	0.907	1.001	0.999	-0.960	0.000	0.001	0.001	0.000
27	0.650	-0.001	0.873	1.001	0.999	-0.960	0.000	0.001	-0.002	0.000
28	0.675	-0.001	0.840	1.001	0.999	-0.960	0.000	0.001	-0.002	0.000
29	0.700	-0.001	0.807	1.001	0.999	-0.960	0.000	0.001	0.000	0.000
30	0.725	-0.001	0.775	1.001	0.999	-0.960	0.000	0.001	-0.002	0.000
31	0.750	-0.001	0.744	1.001	0.999	-0.960	0.000	0.001	0.000	0.000
32	0.775	-0.001	0.713	1.001	0.999	-0.960	0.000	0.001	-0.001	0.000
33	0.800	-0.001	0.683	1.001	0.999	-0.960	0.000	0.001	-0.001	0.000
34	0.825	-0.001	0.654	1.001	0.999	-0.960	0.000	0.001	0.000	0.000
35	0.850	-0.001	0.625	1.001	0.999	-0.960	0.000	0.001	0.000	0.000
36	0.875	-0.001	0.597	1.000	1.000	-0.960	0.000	0.001	0.000	0.000
37	0.900	-0.001	0.570	1.000	1.000	-0.960	0.000	0.001	-0.002	0.000
38	0.925	-0.001	0.544	1.000	1.000	-0.960	0.000	0.001	0.001	0.000
39	0.950	-0.001	0.518	1.000	1.000	-0.960	0.000	0.000	0.001	0.000
40	0.975	-0.001	0.494	1.000	1.000	-0.960	0.000	-0.004	-0.002	0.000
41	1.000	-0.001	0.481	1.000	1.000	-0.960	0.000	-0.004	-0.002	0.000

pressure profiles as well as similar horizontal velocity gradients. The pressure gradient is slightly higher near the outer boundary for the case of the lowest vertical velocity (case C, Table 6). In general, all parameters show remarkably similar behavior over this wide range of boundary velocity values. Interestingly, the ratio of center-line velocity to boundary velocity at the top of the combustion layer (a height of 600 m) is highest (Table 5) for the highest-boundary-velocity case B ($\hat{\alpha} = 1.5$). The ratio between the central and boundary velocities is nearly 4.4. For case A ($\hat{\alpha} = 1.0$), the ratio is 3.6 (Table 3); and for the lowest-boundary-velocity case C, the ratio is 3.1 (Table 7). In all cases, the pressure gradients are essentially zero at the "top" of the combustion layer; and the diffusion terms are negligible in the lowest-velocity case (Table 7).

Cases F and G explore the influence of radiation loss. Case F represents an increase in the radiation loss rate, and case G represents a decrease (in both cases, the change is about a factor of 2). No significant changes are evident, and the results resemble those for the baseline case. The only discernible change is in the center-line temperature at the bottom and top of the combustion zone, where changes of about 1 percent occur for both increased and decreased radiation loss rates.

The influence of the diffusion terms is evident in Fig. 13, which compares enhanced turbulent diffusion with the standard case. In case H, the coefficients M_{11} and K_1 are increased by a factor of 3 above those assumed in the baseline case. The velocity vector plot shows a similar turning of the flow in the lower region, but with a much more uniform velocity across the entire column above the combustion region.

Figure 14 compares pressure and temperature contours. The increased turbulence rapidly reduces the pressure and temperature gradients in the rising column.

The temperature and velocity profiles along the center line in Fig. 15 show again the rapid drop in temperature above the fire zone and the decrease in velocity above the burning region. Clearly, the enhanced diffusion substantially lowers both the temperature and the velocity on the center line (a factor of 4 in velocity).

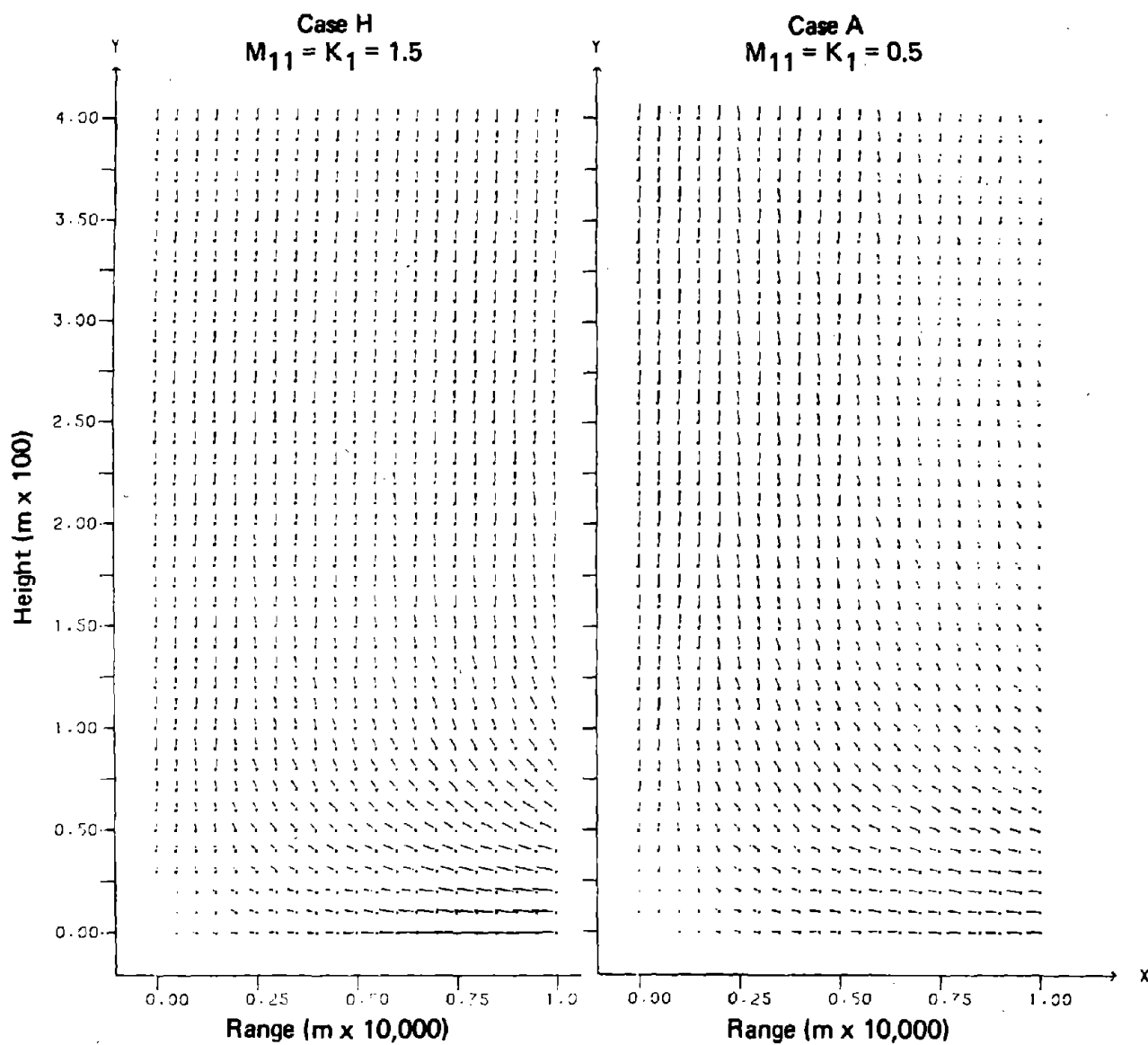


Fig. 13--Velocity fields generated for different values of common heat/momentum diffusion coefficients

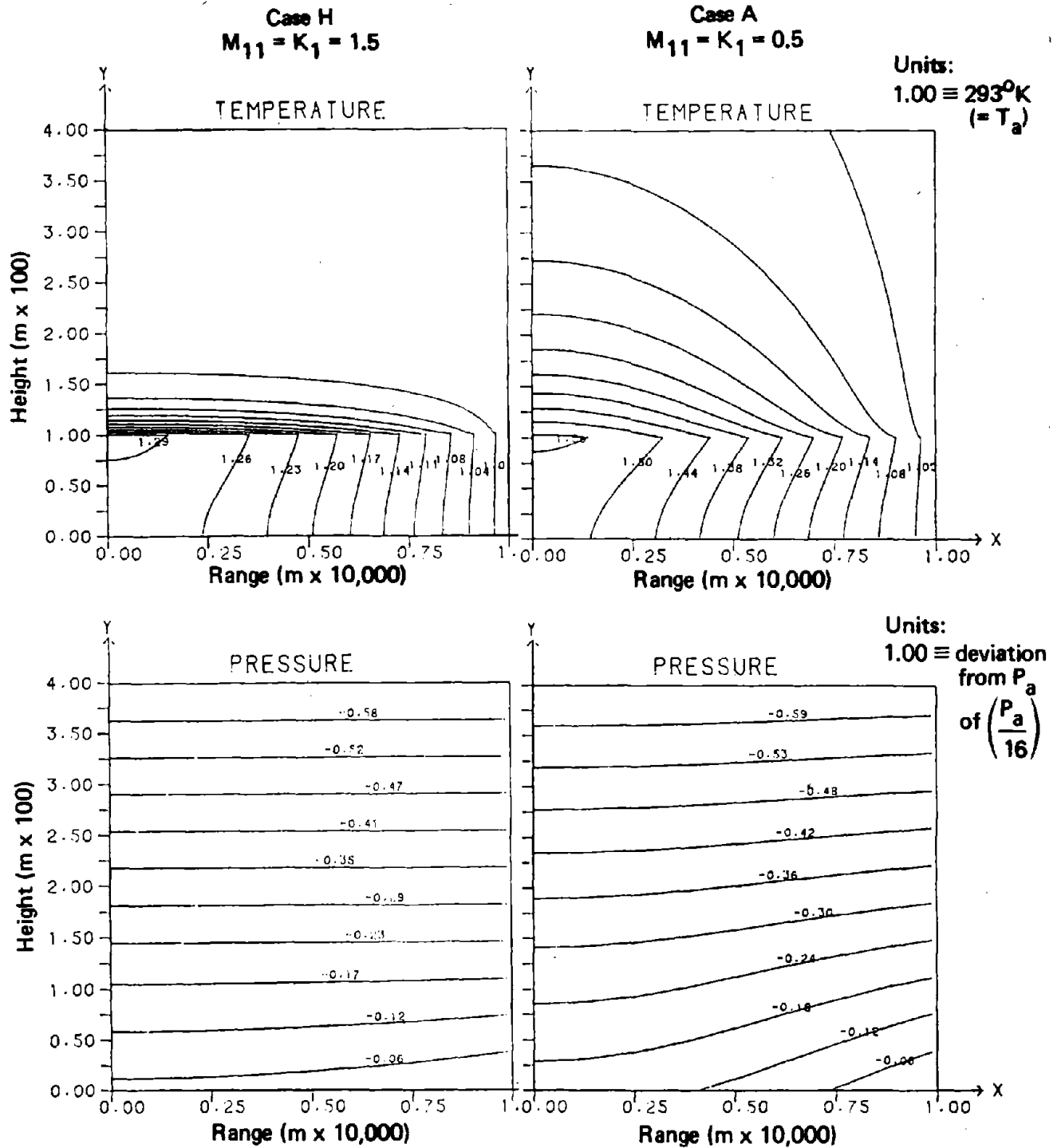


Fig. 14--Temperature and pressure contours generated for different values of common heat/momentum diffusion coefficients

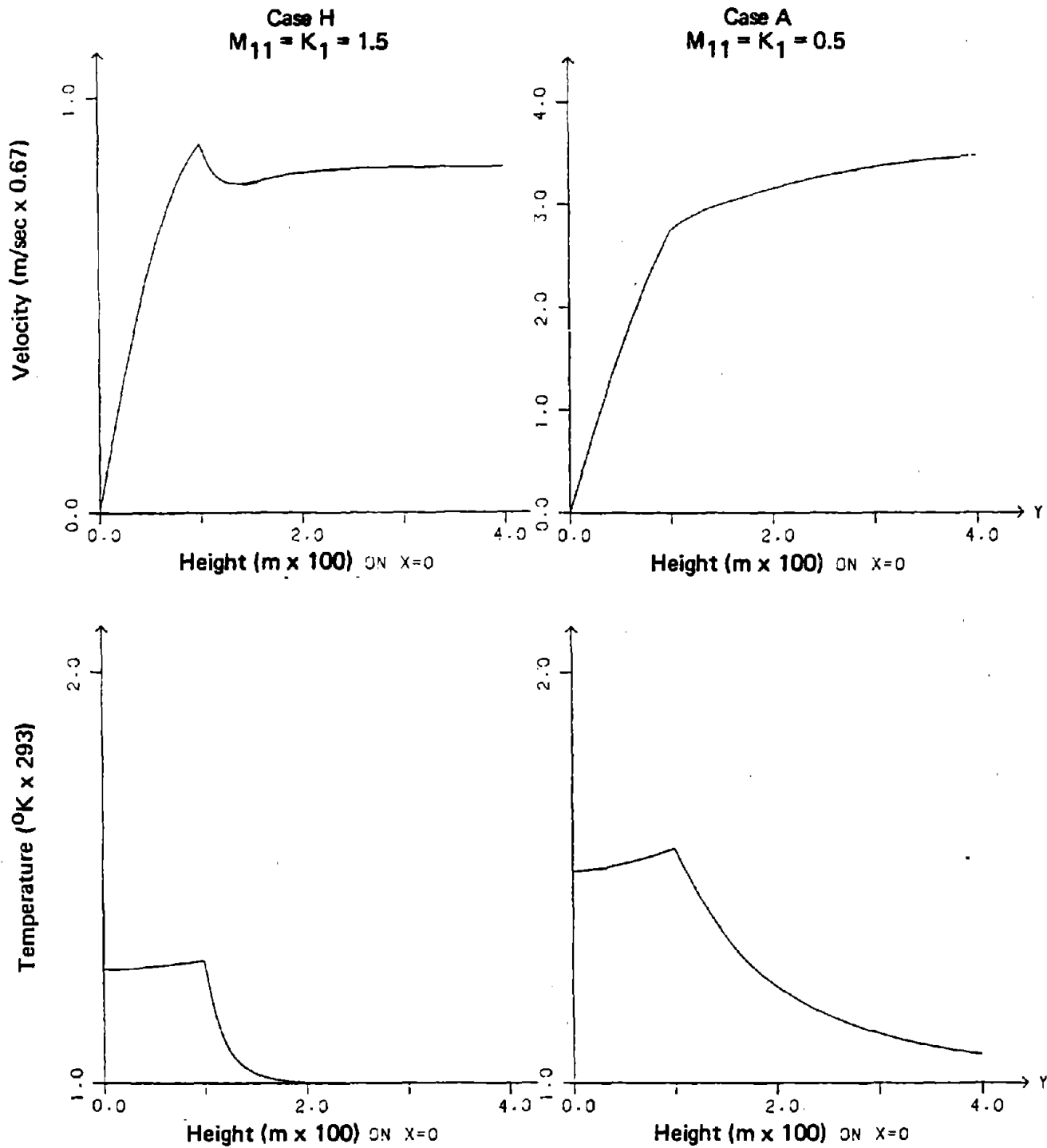


Fig. 15--Center-line velocities and temperatures generated for different values of common heat/momentum diffusion coefficients

Figure 16 shows the horizontal velocities to be of lower magnitude everywhere, and more rapidly suppressed above and even in the fire zone for the increased-turbulent-mixing case H.

Figure 17 shows for the enhanced diffusion case a very uniform velocity profile across the rising plume, i.e., virtually all the velocity is vertical and quite uniform, with approximately the value of the boundary velocity. It is slightly lower in the center of the plume owing to the dominant effect of the diffusive forces. In contrast, the baseline case A resembles a Gaussian plume distribution, as expected. It appears that the larger coefficients for diffusion may be unrealistic.

Case L displays an enhancement of the diffusion of momentum (larger M_{11}) along with a reduction in the heat diffusion coefficient K_1 . A comparison with the standard case A is made in Figs. 18 through 22, illustrating the importance of balancing boundary conditions and adopting realistic physical assumptions. In this case, the assumed outer-boundary vertical velocity appears to be incompatible with the enhanced diffusion of momentum and reduced diffusion of heat in the fire and the rising column. The fact that the vertical velocities are high at the boundary of the plume, becoming smaller toward the center of the plume as shown in Fig. 18, suggests that the combination of coefficients used in case L may be incorrect. It may be unrealistic to pair such a large diffusion of momentum with correspondingly little heat dissipation.

The effect of enhanced turbulence is illustrated in Fig. 19, which compares temperature and pressure contours. Though pressure gradients are suppressed in case L, both the temperature gradient above the fire and the peak temperature are much higher. The peak temperature is nearly 2.25 (at $y = 1$) and drops to near unity before $y = 2.5$. The baseline case A has a peak of 1.56 (at $y = 1$), but does not approach unity until $y > 4$.

Similarly, as shown in Fig. 20, the center-line temperature and velocity profiles with altitude show higher temperatures in the fire and a more rapid decrease in temperature above the heated region. In the velocity comparison, we see for case L a decrease in the magnitude of the vertical velocities even in the burning region.

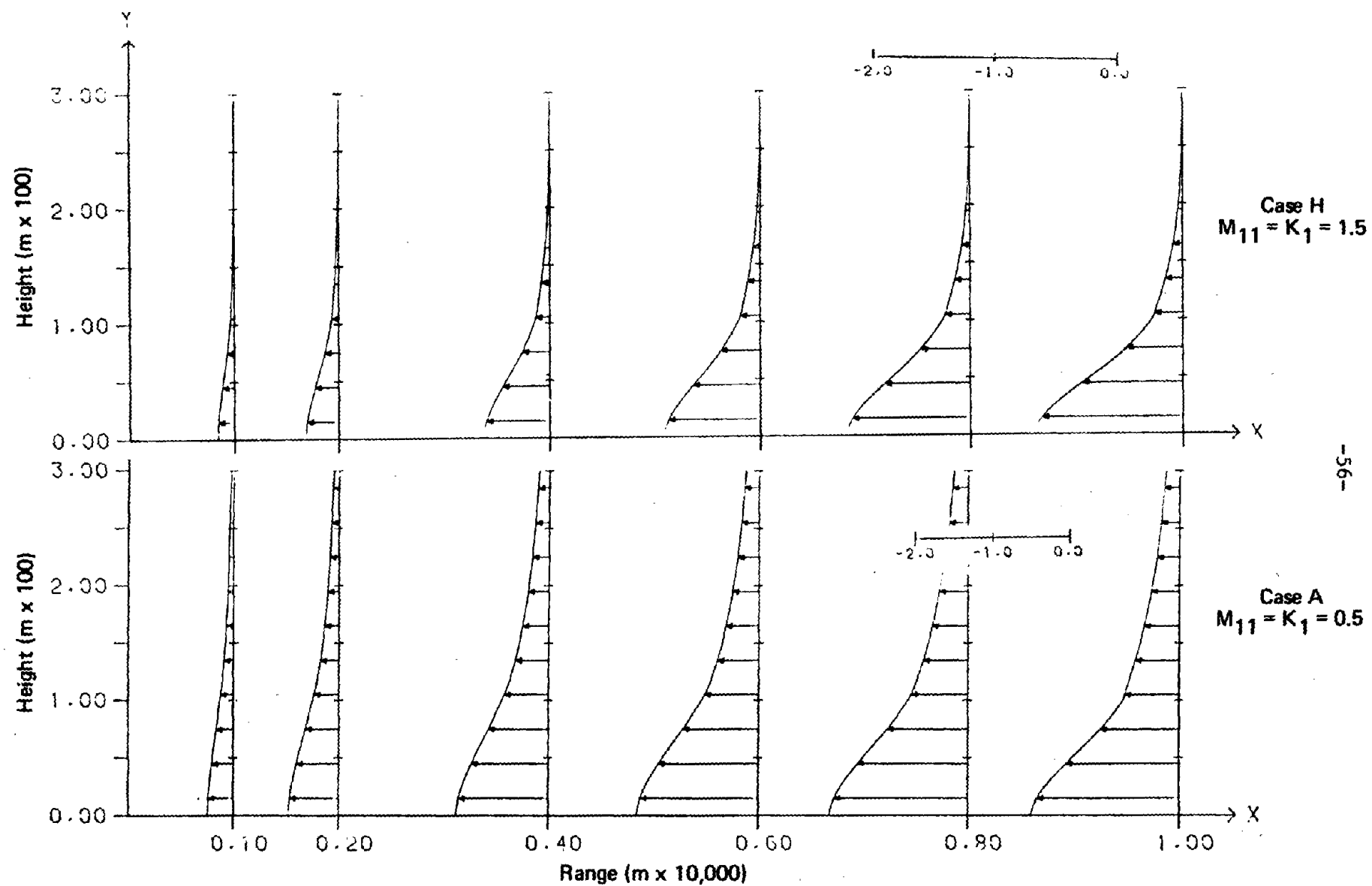


Fig. 16--Horizontal velocity profiles generated for different values of common heat/momentum diffusion coefficients

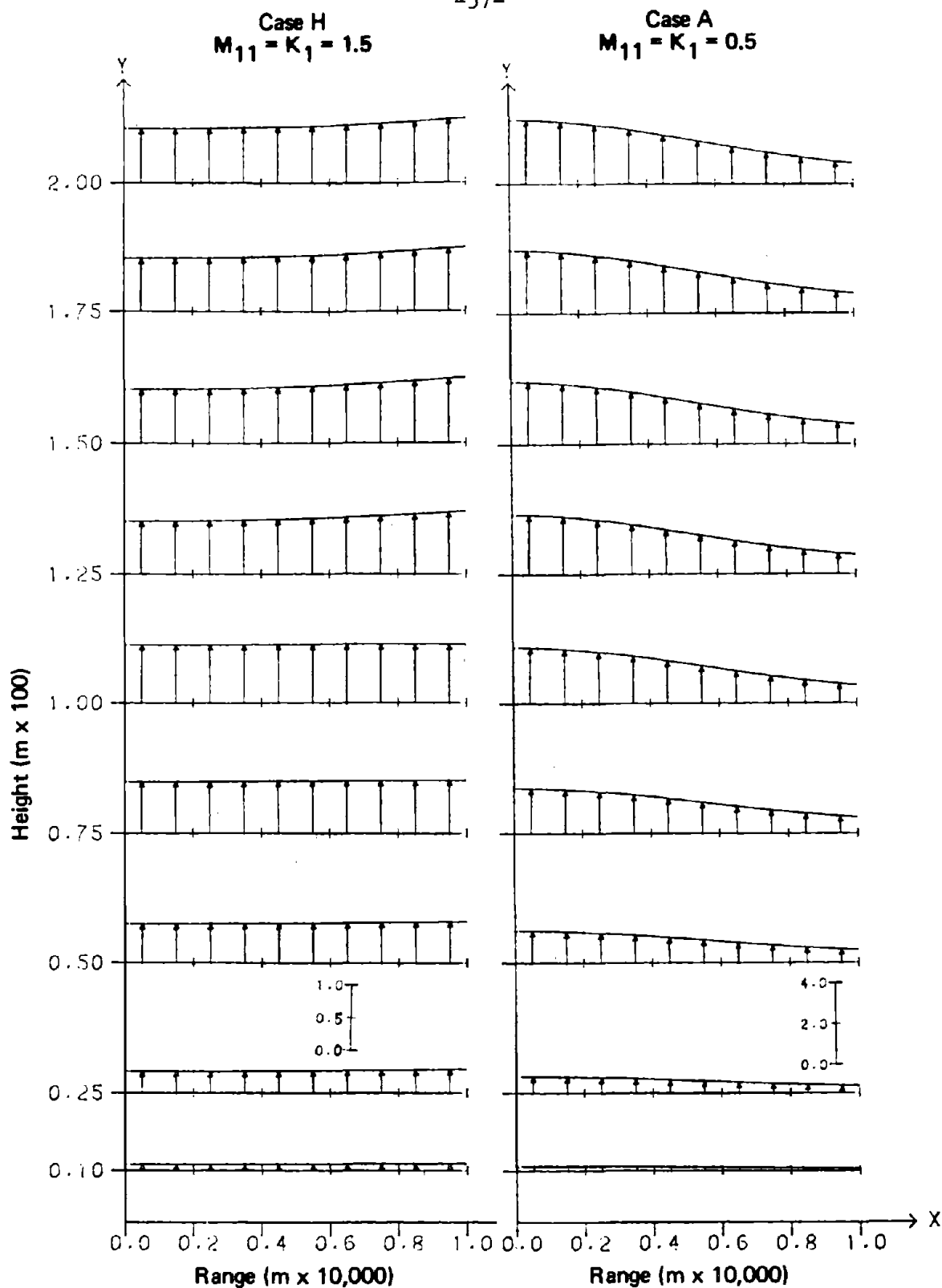


Fig. 17--Vertical velocity profiles generated for different values of common heat/momentum diffusion coefficients

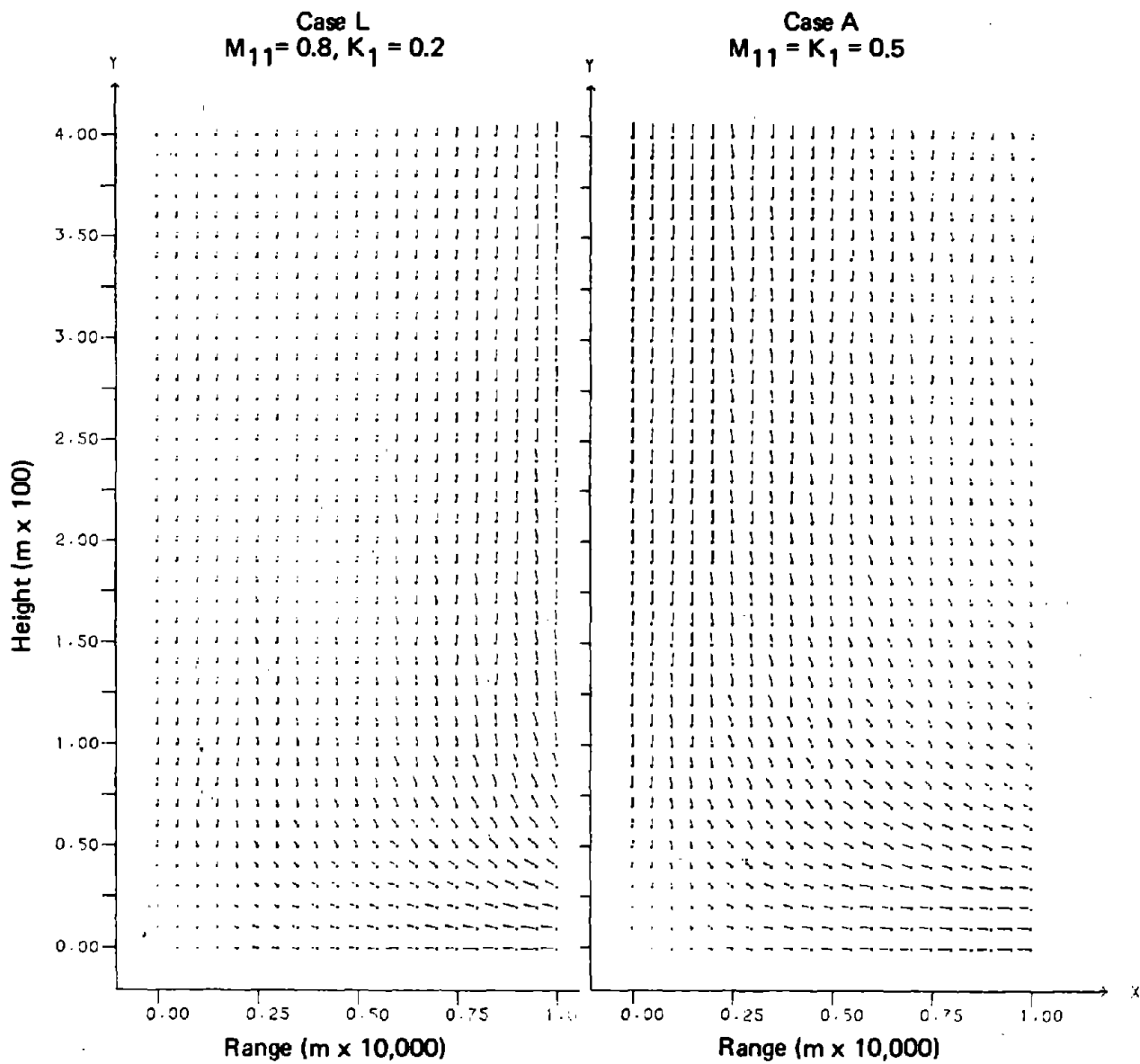


Fig. 18--Velocity fields generated for selected diffusion coefficient mixes

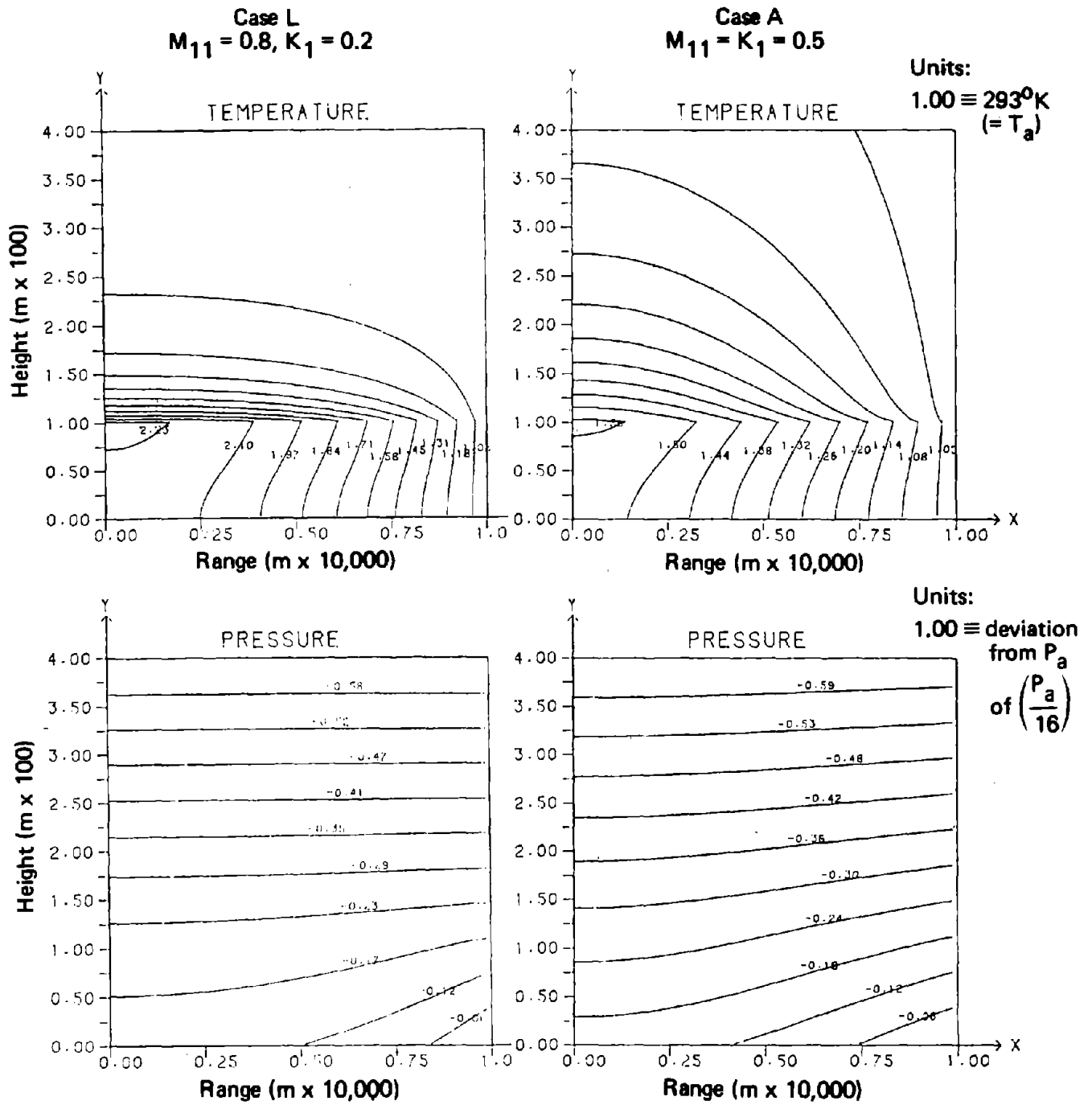


Fig. 19--Temperature and pressure contours generated for selected diffusion coefficient mixes

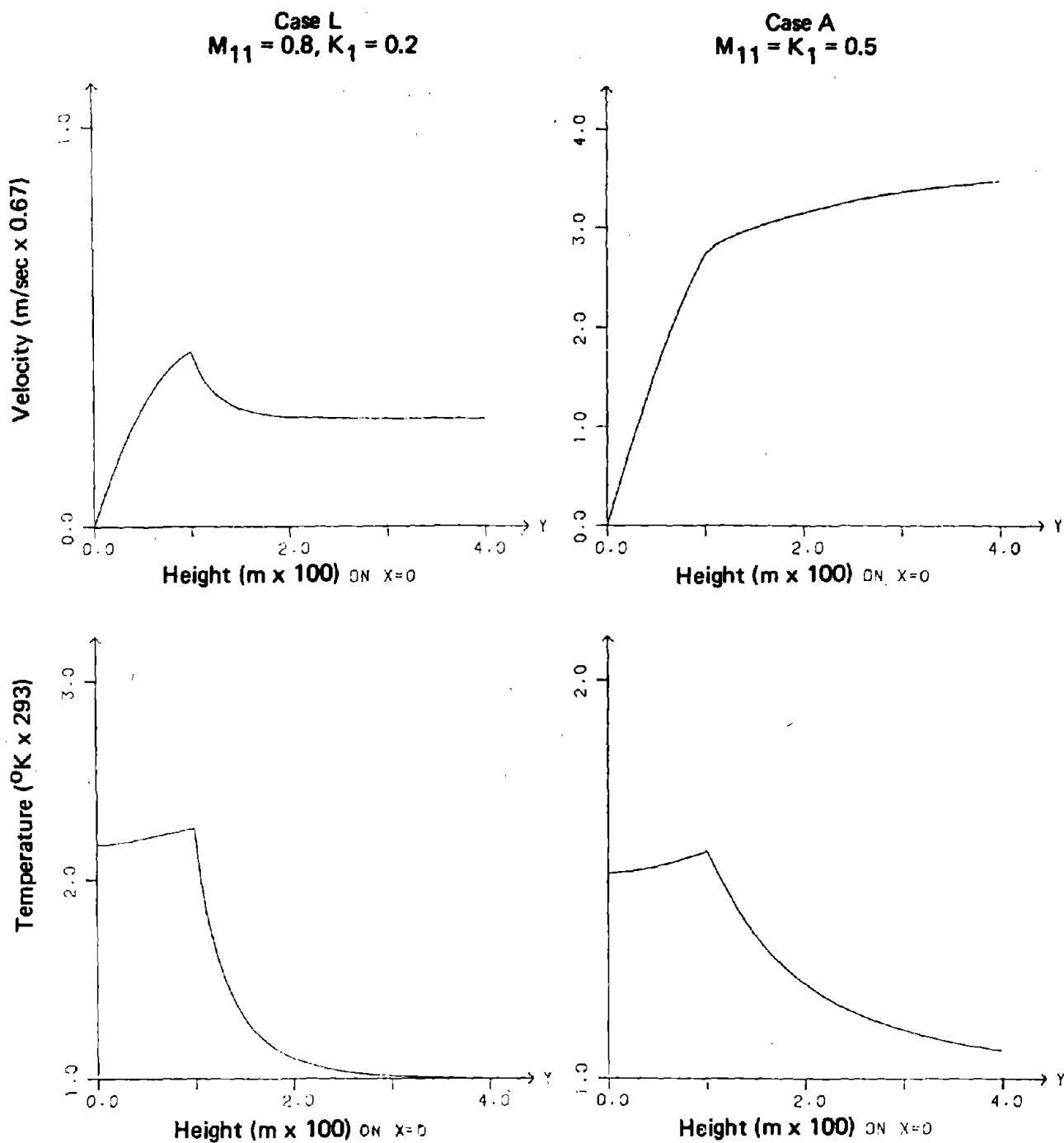
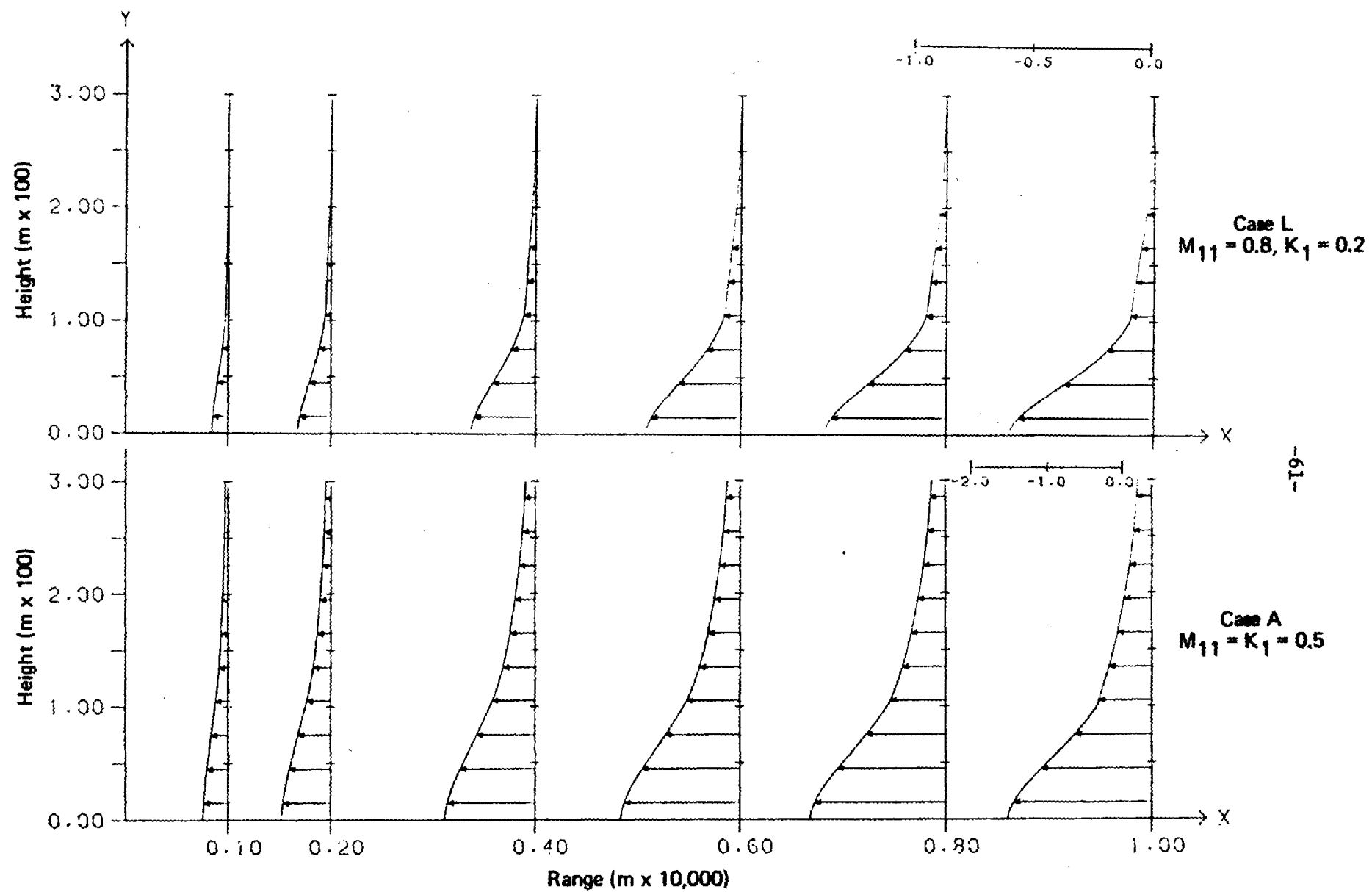


Fig. 20--Center-line velocities and temperatures generated for selected diffusion coefficient mixes



-61-

(m/sec x 67)

generated for selected diffusion coefficient mixes

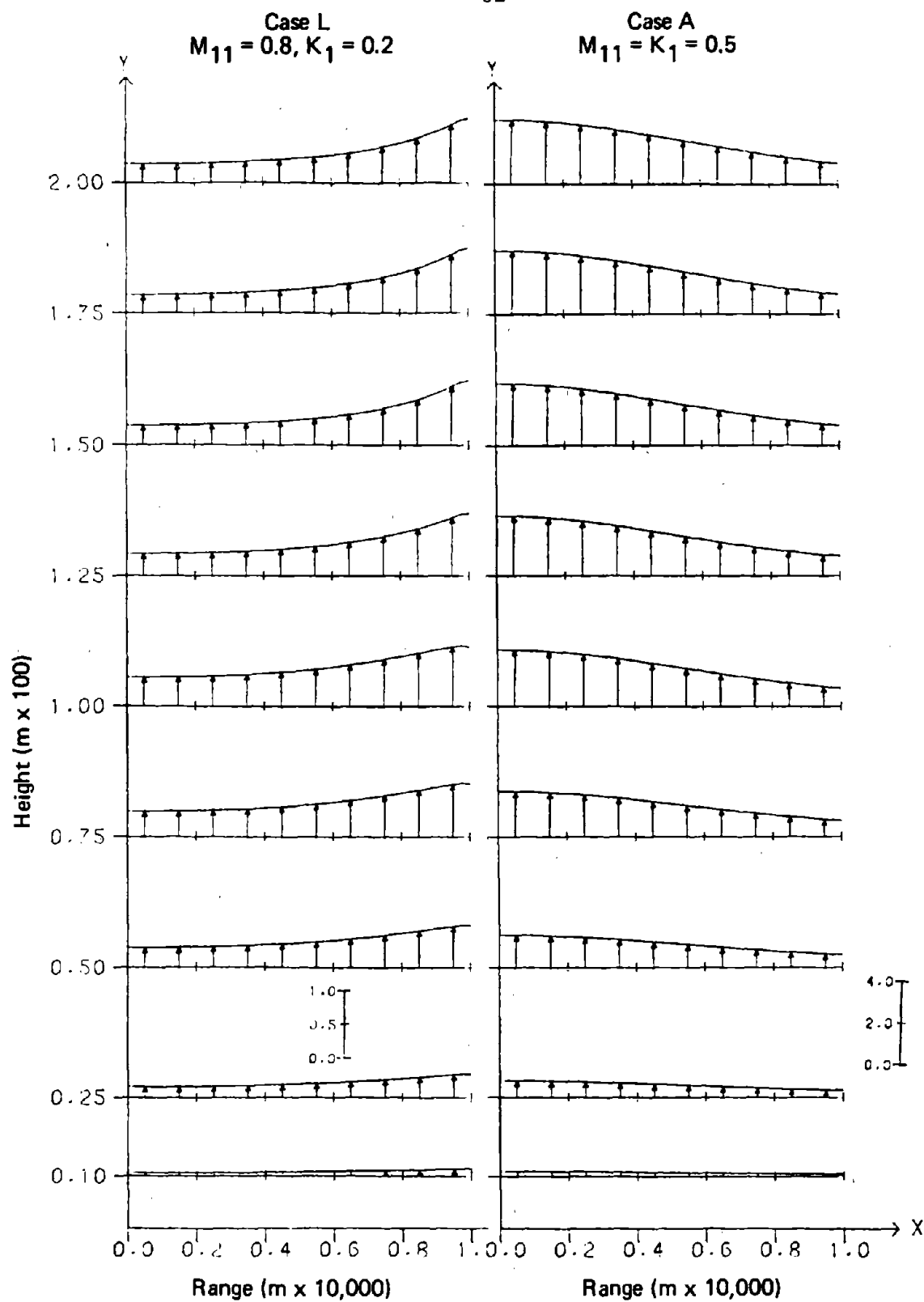


Fig. 22--Vertical velocity profiles generated for selected diffusion coefficient mixes

Figure 21 shows the effect on horizontal velocities to be not just rapid damping above the surface but also a dramatic reduction in the peak horizontal velocity as well. The peak-horizontal-velocity case L is only about a third of the corresponding peak horizontal velocity for the baseline case (note the difference in scales).

Figure 22 shows the effect of increased turbulent momentum transfer with a reversal of the vertical velocity profiles. The prescribed velocity at the outer boundary maintains the vertical flow at $x = 1$; however, the center-line velocity decreases with increasing altitude. In case A, the center-line velocity continues to increase with y .

A series of calculations were performed with variations in the combustive-heat addition rate $q(x, y)$. Figure 23 illustrates the distributions considered. Cases A through L correspond to a uniform rate of unity (in dimensionless units). Case M had double that rate, and case N had half. Cases O and P used sinusoidal distributions in horizontal range (but still uniform in height from the surface up to the top of the burning region, $y = 1$). Case O used two cycles from $x = 0$ to $x = 1$, whereas case P used ten.

Case M (Fig. 24), with double the burning rate, appears to have a velocity vector plot similar to that of case L (Fig. 18). In each case, the velocity field is suppressed along the center line with vertical velocities maintained by the boundary condition at the outer edge of the combustion region. Both cases contrast strikingly with the baseline case.

Figure 25 shows the similar suppression of the temperature and pressure contours (cf. Fig. 19). Likewise, Fig. 26 illustrates the rapid drop in temperature above the fire zone, and an even greater reduction of the velocities--again, not unlike that of case L (Fig. 20).

Figures 27 and 28 illustrate the changes in the horizontal and vertical velocities across the combustion layer, further showing the trend similar to that of the case with enhanced mixing and suppressed heat diffusion (Figs. 21 and 22). Both cases show rapidly decreasing horizontal velocities with altitude and decreasing vertical velocities along the axis. The similar behavior exhibited in cases L and M shows that either an increase in heat addition (case M: $Q = 2$, $K_1 = 0.5$)

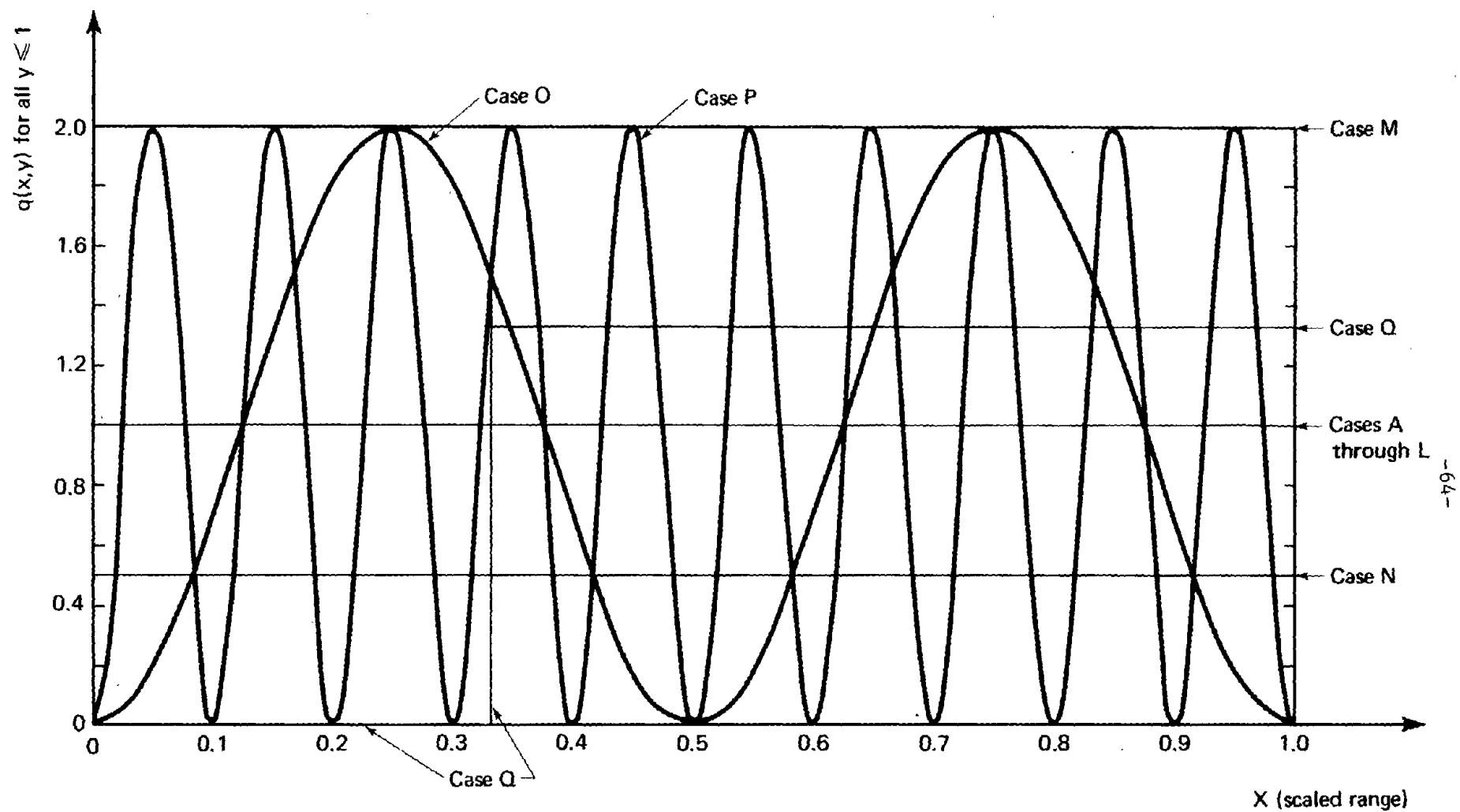


Fig. 23--Spatial distributions of heat-release-rate variations

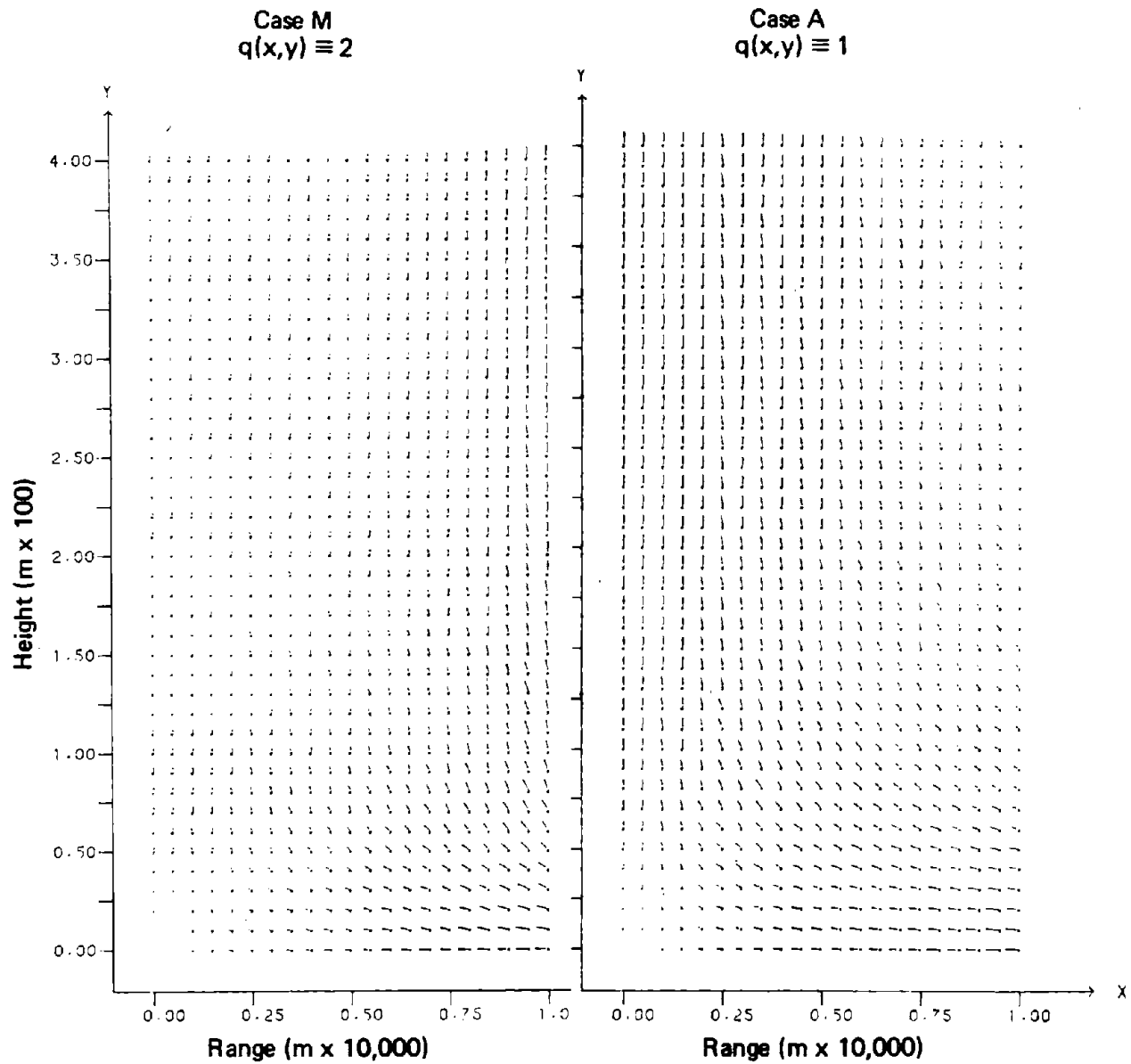


Fig. 24--Velocity fields generated for different spatially uniform heat release rates

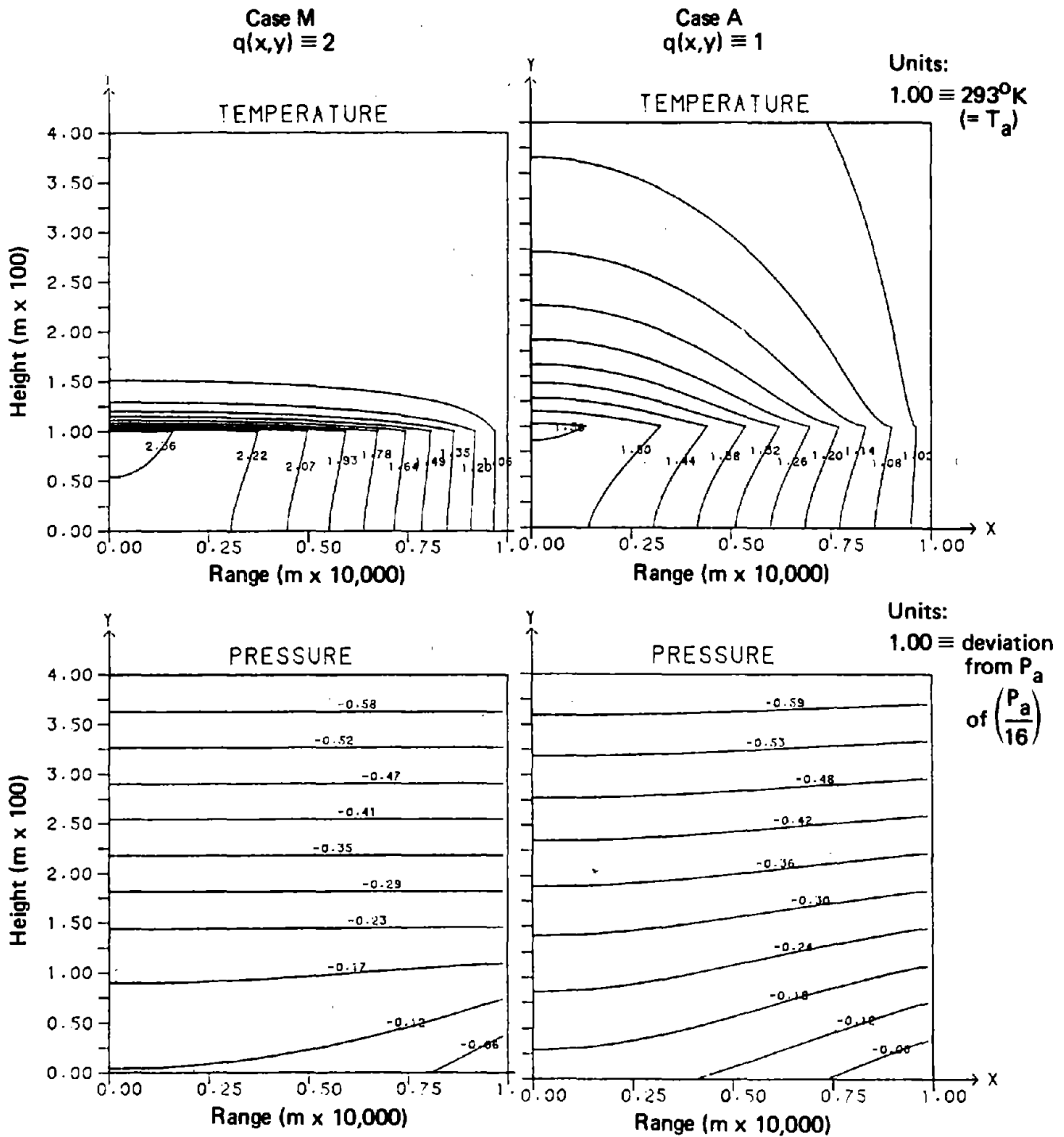


Fig. 25--Temperature and pressure contours generated for different spatially uniform heat release rates

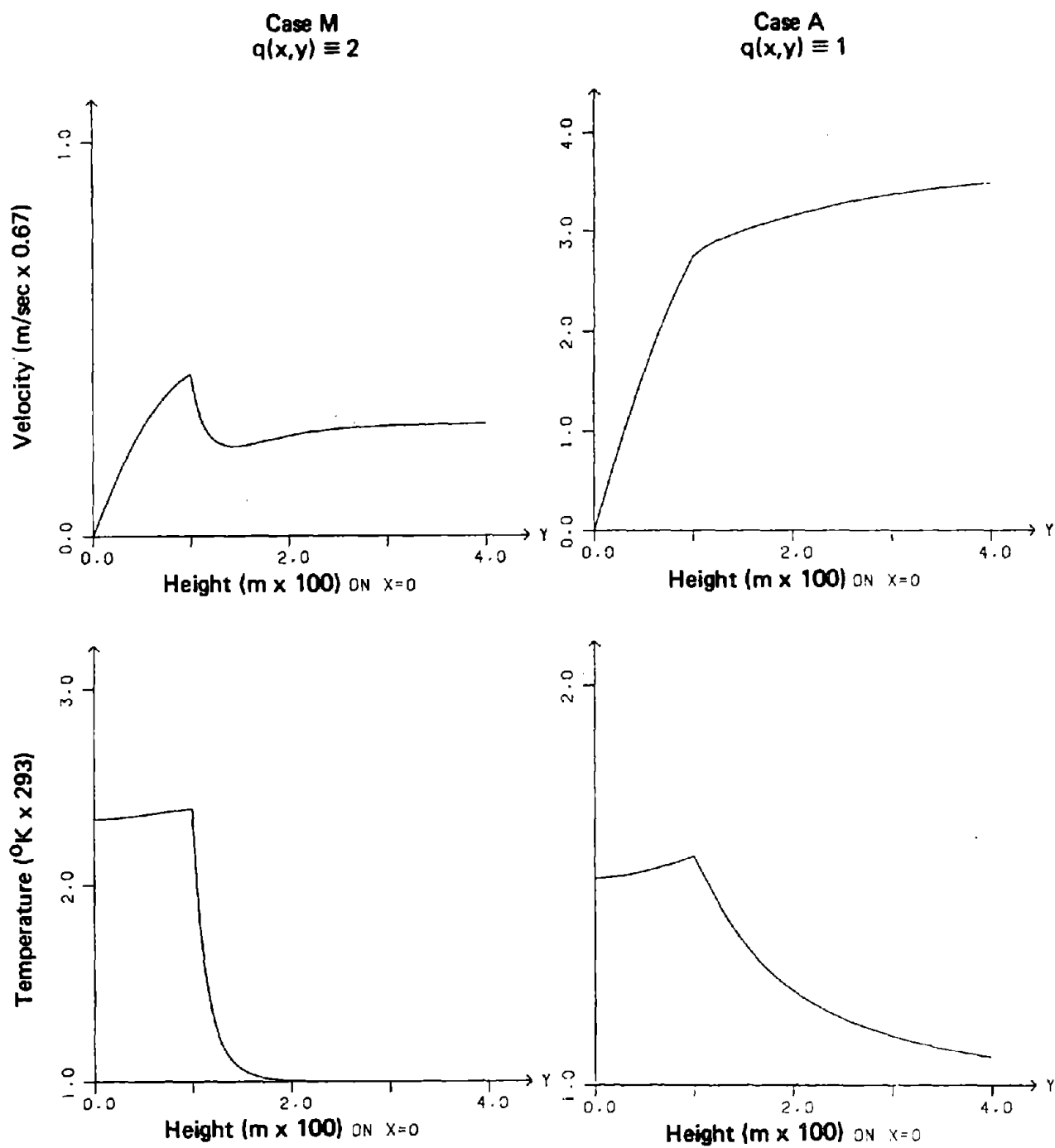


Fig. 26--Center-line velocities and temperatures generated for different spatially uniform heat release rates

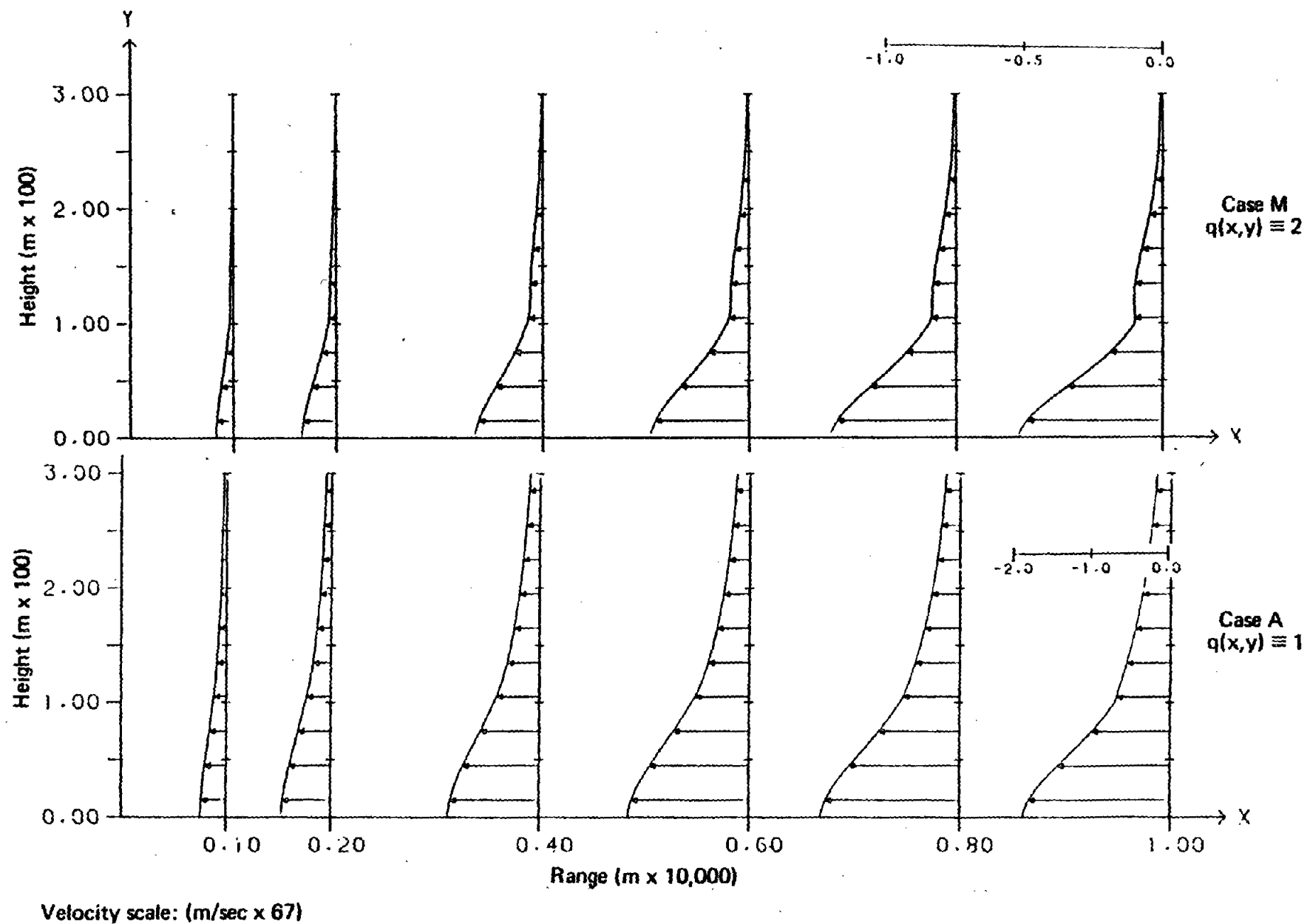


Fig. 27--Horizontal velocity profiles generated for different spatially uniform heat release rates

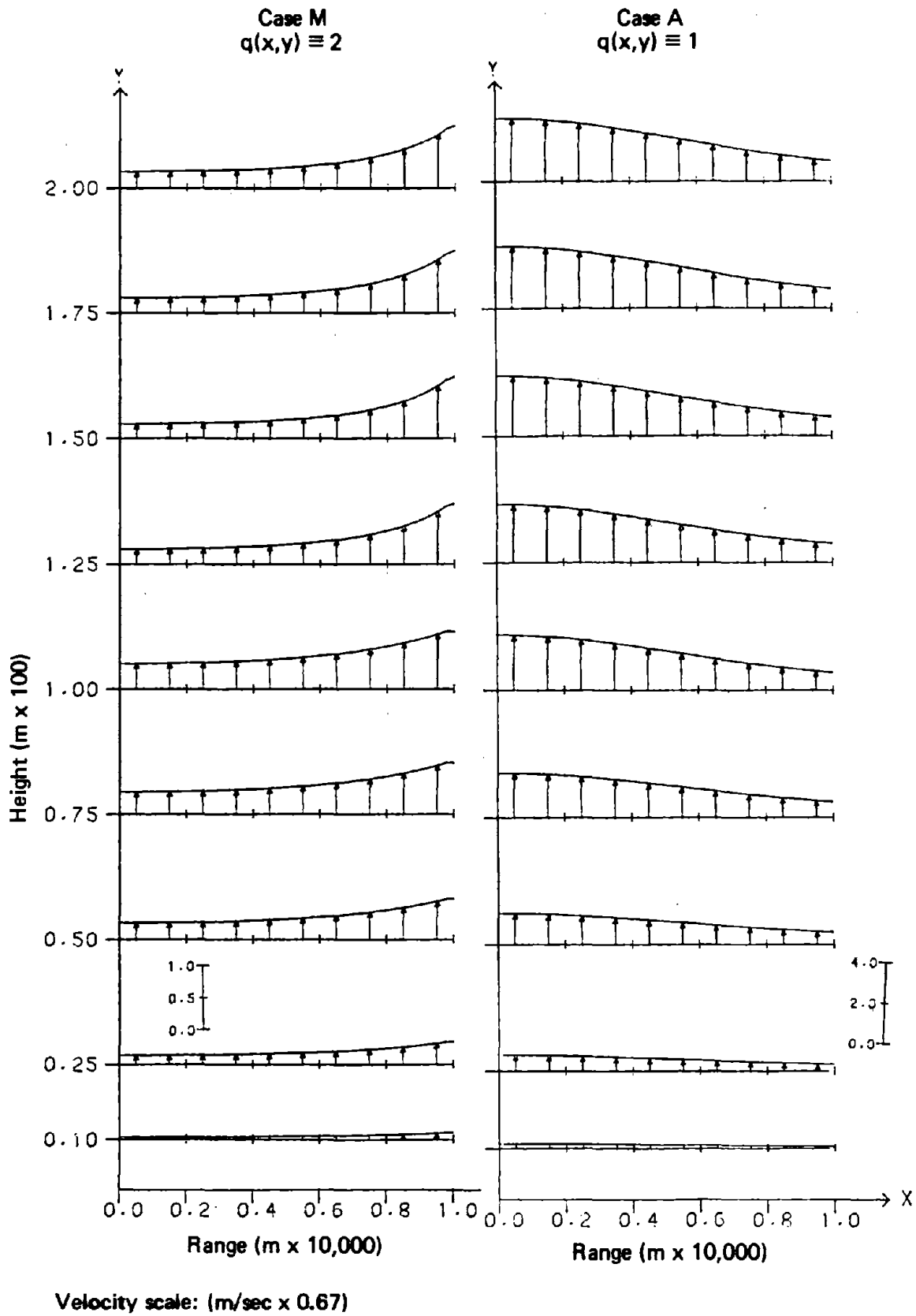


Fig. 28--Vertical velocity profiles generated for different spatially uniform heat release rates

or a decreased diffusion of heat (case L: $Q = 1$, $K_1 = 0.2$) engenders dynamically similar flows.

The vertical velocity profiles are fairly uniform for case H (Figs. 13 through 17), in which the coefficients for turbulent diffusion of heat and momentum were both increased three-fold above the baseline case. For cases L and M, the vertical velocities are greater at $x = 1$ than on the center line.

Further study is required to determine the most appropriate combinations of physically meaningful parameters such as diffusion coefficients, heating rates, and boundary velocities. However, these initial runs already suggest that a wider range of boundary velocities should be investigated.

A comparison of the ground-level and 600-m-altitude predictions for case M (Tables 8 and 9) with those for the baseline case A (Tables 2 and 3) shows that, as expected, the temperature at the ground rises significantly for the doubled-burning-rate case M. Comparison of the surface values (Tables 8 and 2) shows that the horizontal velocities are lower by a factor of more than 3 in the increased-burning-rate case--a result not immediately intuitive. With twice the heat addition rate (case M), the dominant effect is the diffusion of heat; in case A, however, the diffusion of momentum is greater than the diffusion of heat.

At 600 m (Tables 9 and 3), the horizontal velocities are negligible, and all vertical velocities except those at the outer boundary are a small fraction of the baseline velocities. The horizontal temperature and pressure gradients at 600 m are remarkably uniform.

Two calculations were made with periodic fires, i.e., with a sinusoidal variation in the burning rate such that the average was the same as in the baseline case. In case O, two burning rate peaks (cycles) were employed between the outer edge and the center line. In case P, a ten-peak fire was considered. Figures 29 through 33 compare the two-peak fire with the single uniform fire of case A. The flow fields (Fig. 29) show very little difference. Correspondingly, the pressure and temperature contours (Fig. 30) appear fairly similar. The center-line conditions (Fig. 31) are likewise quite similar. The horizontal

Table 8

GROUND-LEVEL NUMERICAL PREDICTIONS FOR PARAMETER CASE M
(INCREASED UNIFORM HEAT RELEASE RATE)

FIREX SOLUTION OF COMBUSTION LAYER BOUNDARY VALUE PROBLEM

SYSTEM PARAMETERS: A = 0.160 SIGMA = 0.023 NU = 0.500 K = 0.500

MESH: M = 40 DX = 0.025 N = 240 DY = 0.025

ITERATION PARAMETERS: ETLINE = 0.001000 MAXITL = 20 ETOLP = 0.005000 MAXITP = 20

INLET PARAMETERS: ALPHA = 1.000 BETA = 1.500 BLOSS = 0.000

FOR J = 1 (Y = 0.000):

I	X	U	V	T	RHO	P	PX	NU*UXX	K*TXX	Q(T)
1	0.000	0.000	0.000	2.336	0.428	-0.114	0.000	0.000	0.000	1.338
2	0.025	-0.016	0.000	2.336	0.428	-0.114	0.001	0.006	-1.337	1.338
3	0.050	-0.032	0.000	2.335	0.428	-0.114	0.004	0.013	-1.339	1.340
4	0.075	-0.047	0.000	2.331	0.429	-0.114	0.007	0.020	-1.340	1.344
5	0.100	-0.063	0.000	2.326	0.430	-0.114	0.009	0.027	-1.344	1.350
6	0.125	-0.079	0.000	2.319	0.431	-0.114	0.012	0.034	-1.347	1.357
7	0.150	-0.095	0.000	2.311	0.433	-0.113	0.015	0.041	-1.352	1.367
8	0.175	-0.110	0.000	2.301	0.435	-0.113	0.018	0.048	-1.357	1.378
9	0.200	-0.126	0.000	2.289	0.437	-0.112	0.021	0.055	-1.364	1.391
10	0.225	-0.141	0.000	2.276	0.439	-0.112	0.024	0.062	-1.370	1.406
11	0.250	-0.157	0.000	2.261	0.442	-0.111	0.028	0.070	-1.378	1.422
12	0.275	-0.172	0.000	2.244	0.446	-0.110	0.031	0.078	-1.385	1.440
13	0.300	-0.187	0.000	2.225	0.449	-0.110	0.034	0.085	-1.394	1.459
14	0.325	-0.202	0.000	2.205	0.454	-0.109	0.038	0.093	-1.402	1.480
15	0.350	-0.217	0.000	2.183	0.458	-0.108	0.042	0.101	-1.408	1.501
16	0.375	-0.232	0.000	2.159	0.463	-0.107	0.046	0.109	-1.418	1.524
17	0.400	-0.247	0.000	2.133	0.469	-0.106	0.050	0.118	-1.424	1.547
18	0.425	-0.262	0.000	2.105	0.475	-0.104	0.054	0.127	-1.431	1.571
19	0.450	-0.276	0.000	2.076	0.482	-0.103	0.059	0.136	-1.435	1.596
20	0.475	-0.290	0.000	2.045	0.489	-0.101	0.064	0.145	-1.440	1.621
21	0.500	-0.304	0.000	2.012	0.497	-0.100	0.070	0.155	-1.441	1.646
22	0.525	-0.318	0.000	1.978	0.506	-0.098	0.076	0.165	-1.443	1.671
23	0.550	-0.332	0.000	1.941	0.515	-0.096	0.082	0.175	-1.441	1.696
24	0.575	-0.345	0.000	1.903	0.525	-0.094	0.089	0.186	-1.437	1.721
25	0.600	-0.359	0.000	1.863	0.537	-0.091	0.097	0.198	-1.431	1.746
26	0.625	-0.372	0.000	1.821	0.549	-0.089	0.105	0.210	-1.421	1.770
27	0.650	-0.384	0.000	1.778	0.563	-0.086	0.115	0.223	-1.408	1.793
28	0.675	-0.397	0.000	1.732	0.577	-0.083	0.125	0.238	-1.392	1.816
29	0.700	-0.409	0.000	1.685	0.593	-0.080	0.136	0.253	-1.372	1.838
30	0.725	-0.421	0.000	1.636	0.611	-0.076	0.149	0.269	-1.348	1.858
31	0.750	-0.432	0.000	1.586	0.631	-0.072	0.163	0.286	-1.317	1.878
32	0.775	-0.443	0.000	1.534	0.652	-0.068	0.179	0.306	-1.284	1.896
33	0.800	-0.454	0.000	1.480	0.676	-0.063	0.197	0.327	-1.244	1.913
34	0.825	-0.465	0.000	1.425	0.702	-0.058	0.218	0.350	-1.196	1.928
35	0.850	-0.474	0.000	1.368	0.731	-0.052	0.242	0.376	-1.145	1.942
36	0.875	-0.484	0.000	1.310	0.764	-0.046	0.269	0.405	-1.084	1.955
37	0.900	-0.493	0.000	1.250	0.800	-0.039	0.302	0.438	-1.018	1.967
38	0.925	-0.501	0.000	1.189	0.841	-0.031	0.340	0.476	-0.941	1.977
39	0.950	-0.509	0.000	1.127	0.887	-0.022	0.385	0.520	-0.856	1.986
40	0.975	-0.516	0.000	1.064	0.940	-0.012	0.440	0.573	-0.759	1.994
41	1.000	-0.523	0.000	1.000	1.000	0.000	0.471	0.573	-0.759	2.000

Table 9

600-m-ALTITUDE NUMERICAL PREDICTIONS FOR PARAMETER CASE M
(INCREASED UNIFORM HEAT RELEASE RATE)

FOR J = 241 (Y = 6.000):

I	X	U	V	T	RHO	P	PX	NU*UXX	K*TXX	Q(T)
1	0.000	0.000	0.289	1.000	1.000	-0.961	0.000	0.000	0.000	0.000
2	0.025	0.000	0.289	1.000	1.000	-0.961	0.000	0.000	-0.001	0.000
3	0.050	0.000	0.289	1.000	1.000	-0.961	0.000	0.000	0.001	0.000
4	0.075	0.000	0.290	1.000	1.000	-0.961	0.000	0.000	-0.001	0.000
5	0.100	0.000	0.290	1.000	1.000	-0.961	0.000	0.000	0.001	0.000
6	0.125	0.000	0.291	1.000	1.000	-0.961	0.000	0.000	-0.001	0.000
7	0.150	0.000	0.292	1.000	1.000	-0.961	0.001	0.001	-0.001	0.000
8	0.175	0.000	0.294	1.000	1.000	-0.961	0.001	0.001	0.002	0.000
9	0.200	0.000	0.295	1.000	1.000	-0.961	0.001	0.001	-0.003	0.000
10	0.225	0.000	0.297	1.000	1.000	-0.961	0.001	0.001	0.005	0.000
11	0.250	0.000	0.299	1.000	1.000	-0.961	0.001	0.001	-0.004	0.000
12	0.275	0.000	0.302	1.000	1.000	-0.961	0.001	0.001	0.002	0.000
13	0.300	0.000	0.305	1.000	1.000	-0.961	0.001	0.001	0.001	0.000
14	0.325	0.000	0.308	1.000	1.000	-0.961	0.001	0.001	-0.001	0.000
15	0.350	0.000	0.312	1.000	1.000	-0.961	0.001	0.001	0.001	0.000
16	0.375	-0.001	0.316	1.000	1.000	-0.961	0.001	0.001	-0.001	0.000
17	0.400	-0.001	0.320	1.000	1.000	-0.960	0.001	0.001	-0.001	0.000
18	0.425	-0.001	0.326	1.000	1.000	-0.960	0.001	0.001	0.001	0.000
19	0.450	-0.001	0.331	1.000	1.000	-0.960	0.002	0.002	0.002	0.000
20	0.475	-0.001	0.339	1.000	1.000	-0.960	0.001	0.001	-0.002	0.000
21	0.500	-0.001	0.345	1.000	1.000	-0.960	0.001	0.001	0.001	0.000
22	0.525	-0.001	0.353	1.000	1.000	-0.960	0.002	0.002	0.000	0.000
23	0.550	-0.001	0.362	1.000	1.000	-0.960	0.001	0.001	-0.002	0.000
24	0.575	-0.001	0.372	1.000	1.000	-0.960	0.001	0.001	0.002	0.000
25	0.600	-0.001	0.384	1.000	1.000	-0.960	0.002	0.002	0.000	0.000
26	0.625	-0.001	0.396	1.000	1.000	-0.960	0.001	0.001	-0.001	0.000
27	0.650	-0.001	0.411	1.000	1.000	-0.960	0.001	0.001	0.000	0.000
28	0.675	-0.001	0.427	1.000	1.000	-0.960	0.001	0.001	-0.002	0.000
29	0.700	-0.001	0.445	1.000	1.000	-0.960	0.001	0.001	0.002	0.000
30	0.725	-0.001	0.465	1.000	1.000	-0.960	0.001	0.001	0.000	0.000
31	0.750	-0.001	0.488	1.000	1.000	-0.960	0.001	0.001	-0.001	0.000
32	0.775	-0.001	0.514	1.000	1.000	-0.960	0.001	0.001	0.000	0.000
33	0.800	-0.001	0.544	1.000	1.000	-0.960	0.001	0.001	0.000	0.000
34	0.825	-0.001	0.578	1.000	1.000	-0.960	0.001	0.001	0.000	0.000
35	0.850	-0.001	0.617	1.000	1.000	-0.960	0.000	0.001	-0.002	0.000
36	0.875	-0.001	0.662	1.000	1.000	-0.960	0.000	0.000	0.002	0.000
37	0.900	-0.001	0.715	1.000	1.000	-0.960	0.000	0.000	-0.001	0.000
38	0.925	-0.001	0.776	1.000	1.000	-0.960	-0.001	-0.001	0.000	0.000
39	0.950	-0.001	0.849	1.000	1.000	-0.960	-0.001	-0.001	0.000	0.000
40	0.975	-0.001	0.935	1.000	1.000	-0.960	-0.002	-0.002	0.000	0.000
41	1.000	-0.001	0.981	1.000	1.000	-0.960	-0.002	-0.002	0.000	0.000

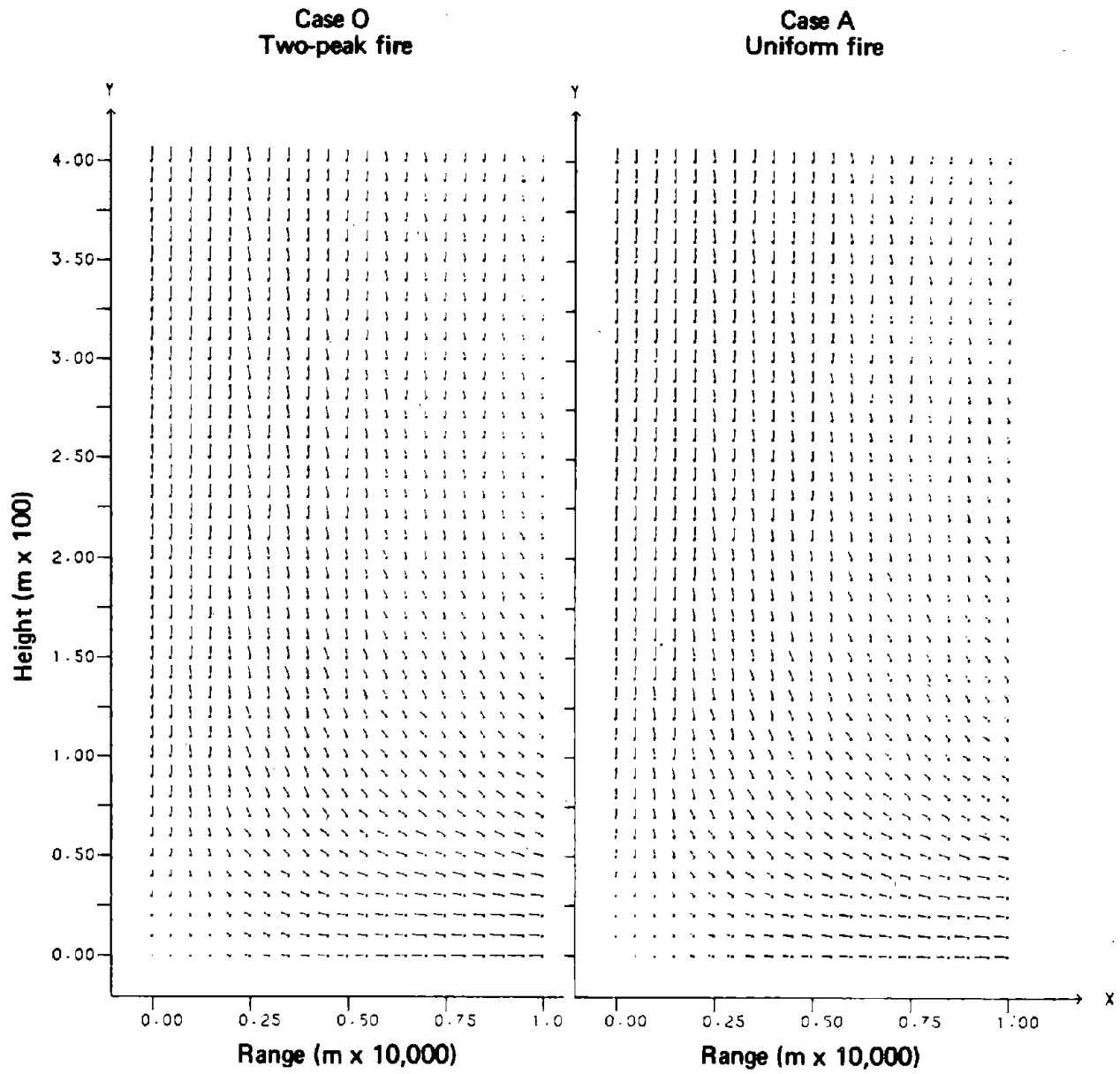


Fig. 29--Velocity fields generated for uniform and two-cycle oscillatory heat release rates

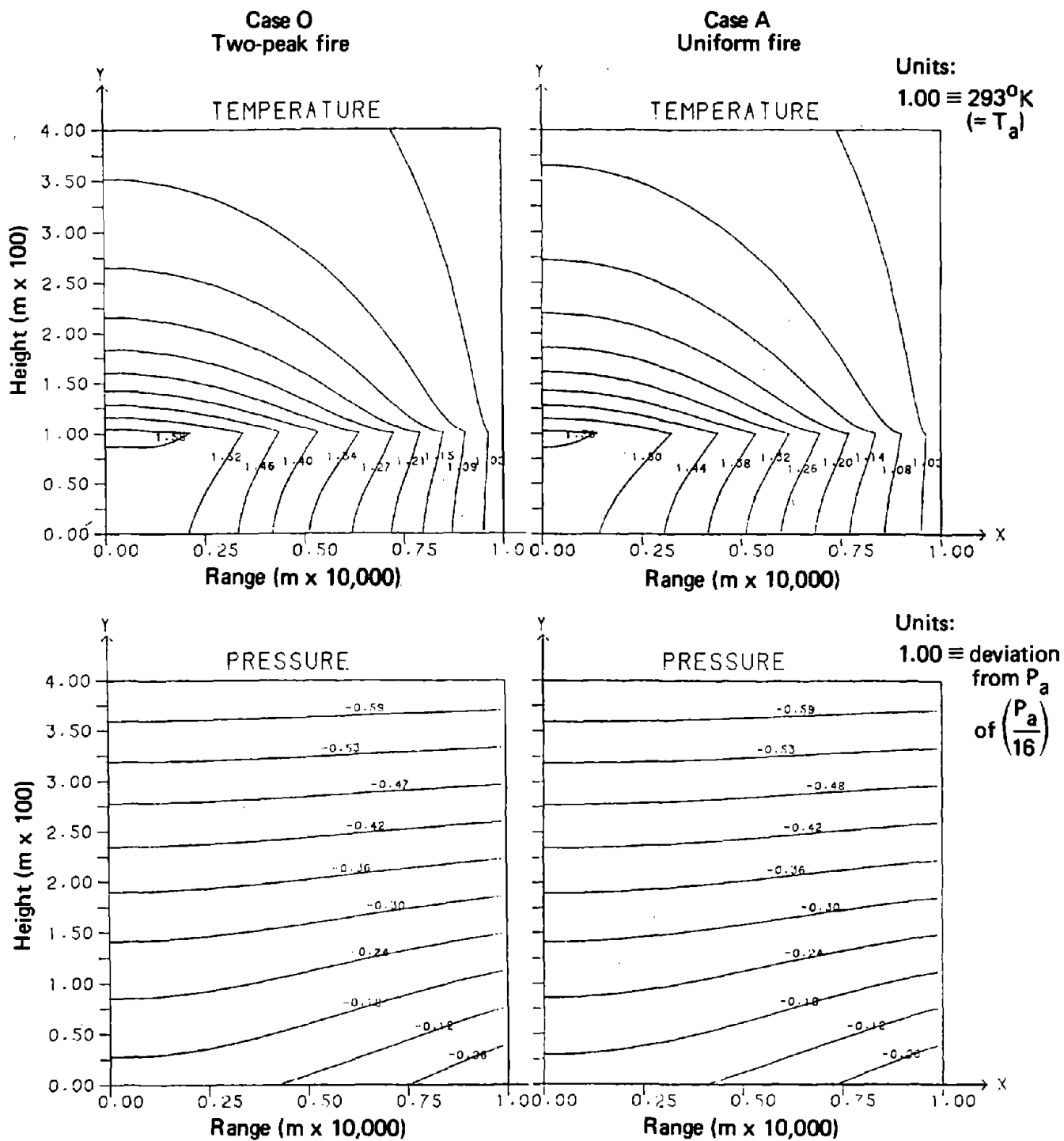


Fig. 30--Temperature and pressure contours generated for uniform and two-cycle oscillatory heat release rates

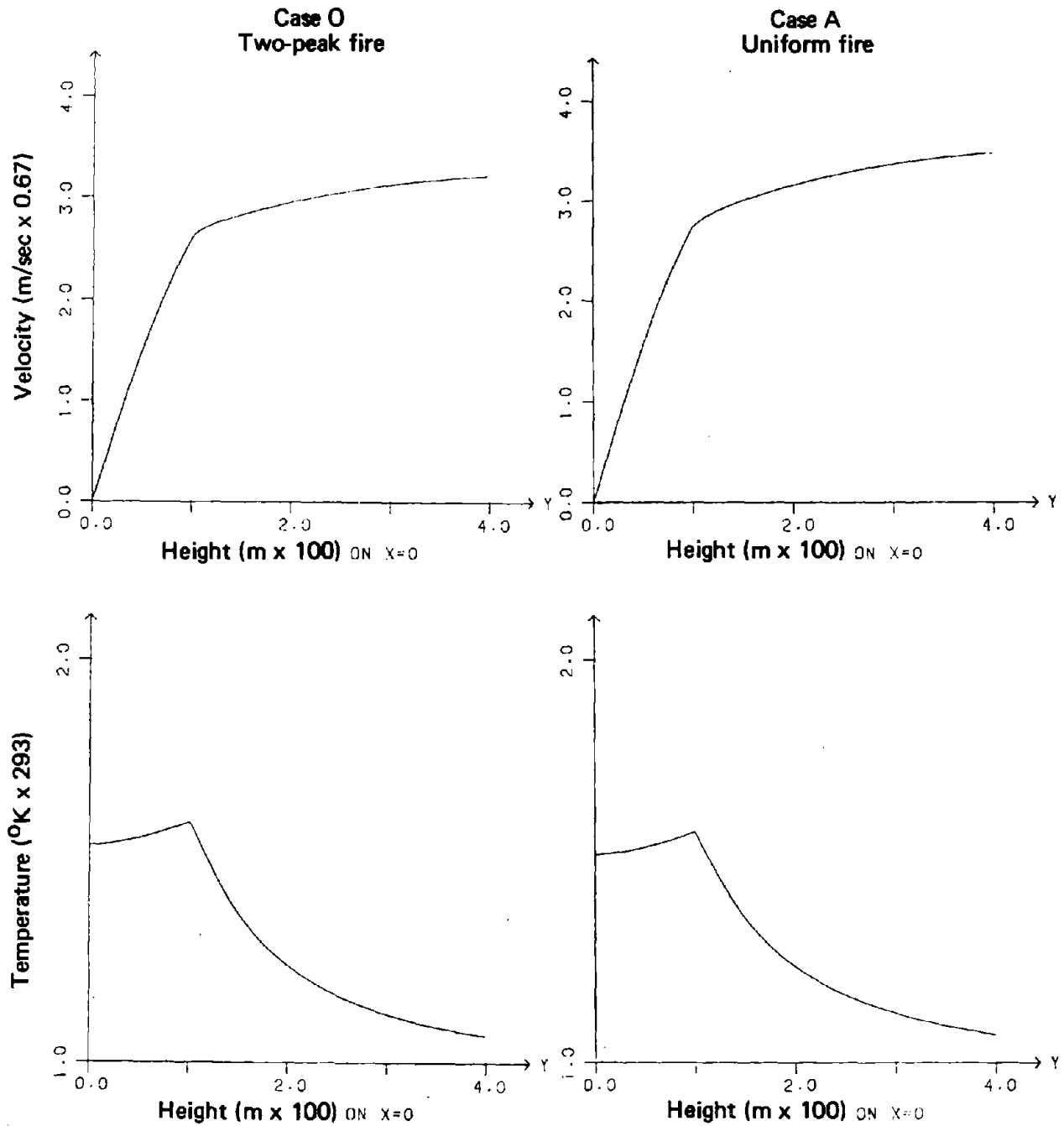
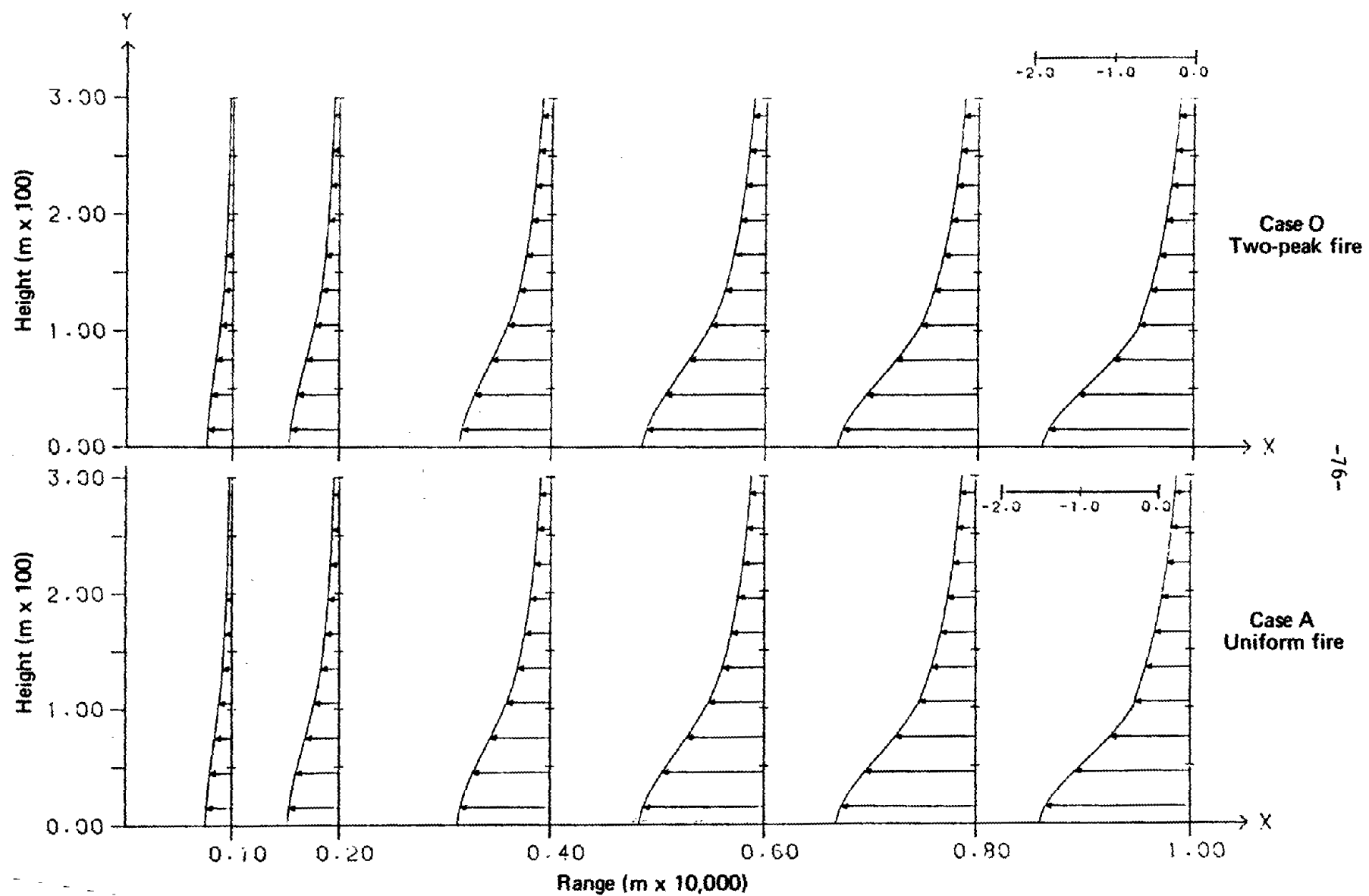


Fig. 31--Center-line velocities and temperatures generated for uniform and two-cycle oscillatory heat release rates



-76-

generated for uniform and two-cycle oscillatory

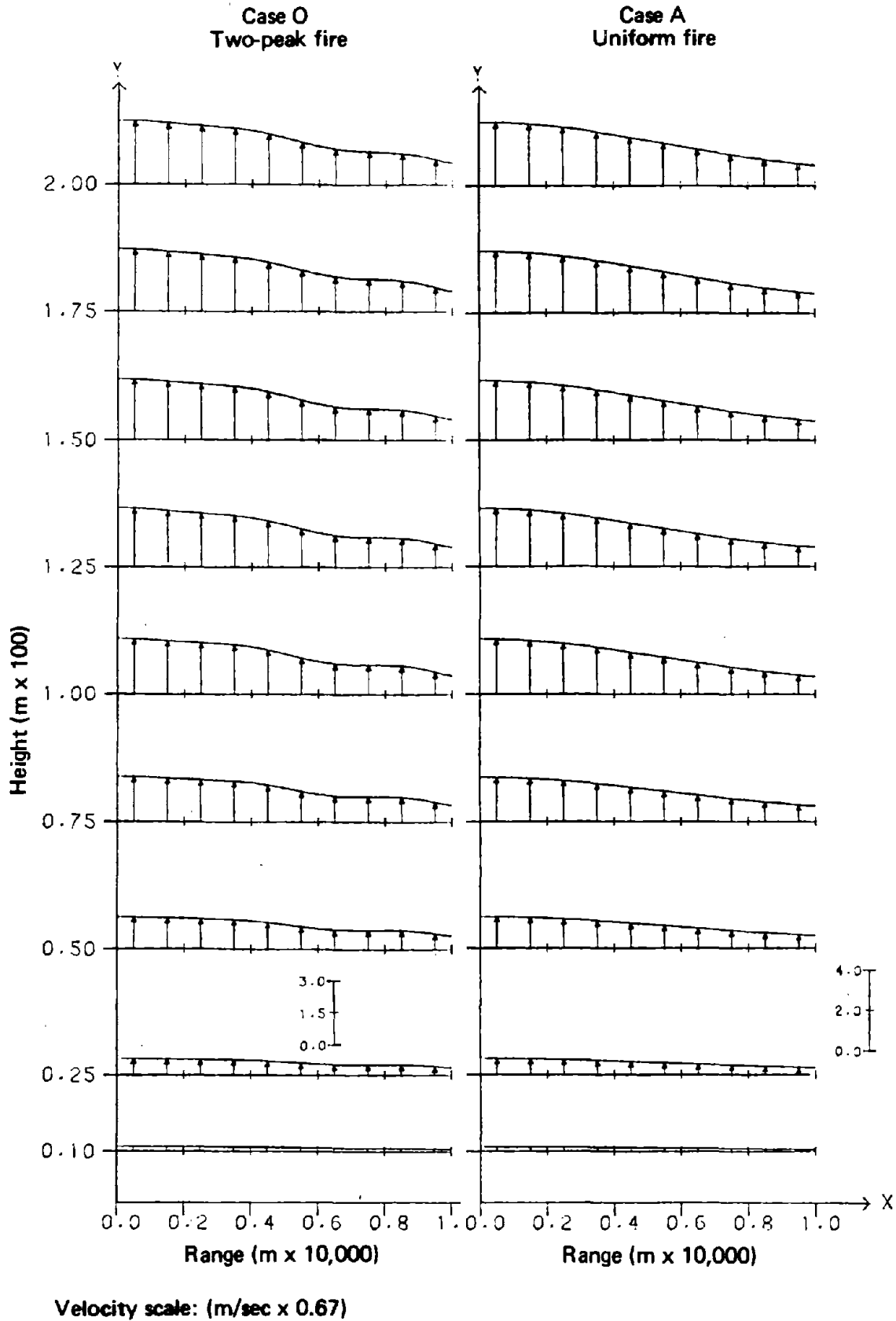


Fig. 33--Vertical velocity profiles generated for uniform and two-cycle oscillatory heat release rates

velocities (Fig. 32) show almost no difference. However, some difference in the vertical velocities (Fig. 33) does persist above the fire.

For the ten-peak fire of case P, very little difference from the baseline case is discernible in Figs. 34 through 38. Dispersive mechanisms are sufficient to make the individual fires unrecognizable beyond the burning region, or even in the burning region.

Case Q considers a fire with no combustion ($Q = 0$, $x < 1/3$, $y \leq 1$) in the inner third of the burning region. For comparison, the outer two-thirds of the combustion zone is assumed to burn with an increase such that the total amount of heat added is the same as in the baseline case. Figures 39 through 43 make the comparison. The velocity fields in Fig. 39 show relatively more motion up the plume for the "inner dead zone" fire. The differences are less obvious in the plots because of the differences in vector scaling. In fact, for the dead-zone fire, a much stronger central column velocity occurs, so that the inflow at the base and the rest of the column updraft appears to be smaller.

The temperature and pressure contours in Fig. 40 show that the highest temperatures occur at the inner edge of the burning region ($x = 1/3$) rather than at the center line--a result that is compatible with the competition between the heating source and the dissipative mechanisms. The center-line velocity and temperature contours in Fig. 41 show a much depressed temperature along the center line for the dead-zone case, but a much higher velocity. The dead zone appears to act as a flue or focusing chimney for the rising column.

Figure 42, which compares the horizontal velocities, shows some to be higher for case Q (again the cases are plotted with different scales). The vertical velocity profiles in Fig. 43 show a much larger velocity gradient near the center line for the dead-zone case (again, different scales). Both cases exhibit identical vertical velocities at $x = 1$ --but the dead-zone case has a center-line velocity that, at the top of the plume, is 11 times greater than the boundary velocity, whereas the baseline case has a velocity ratio of approximately 3.5:1.

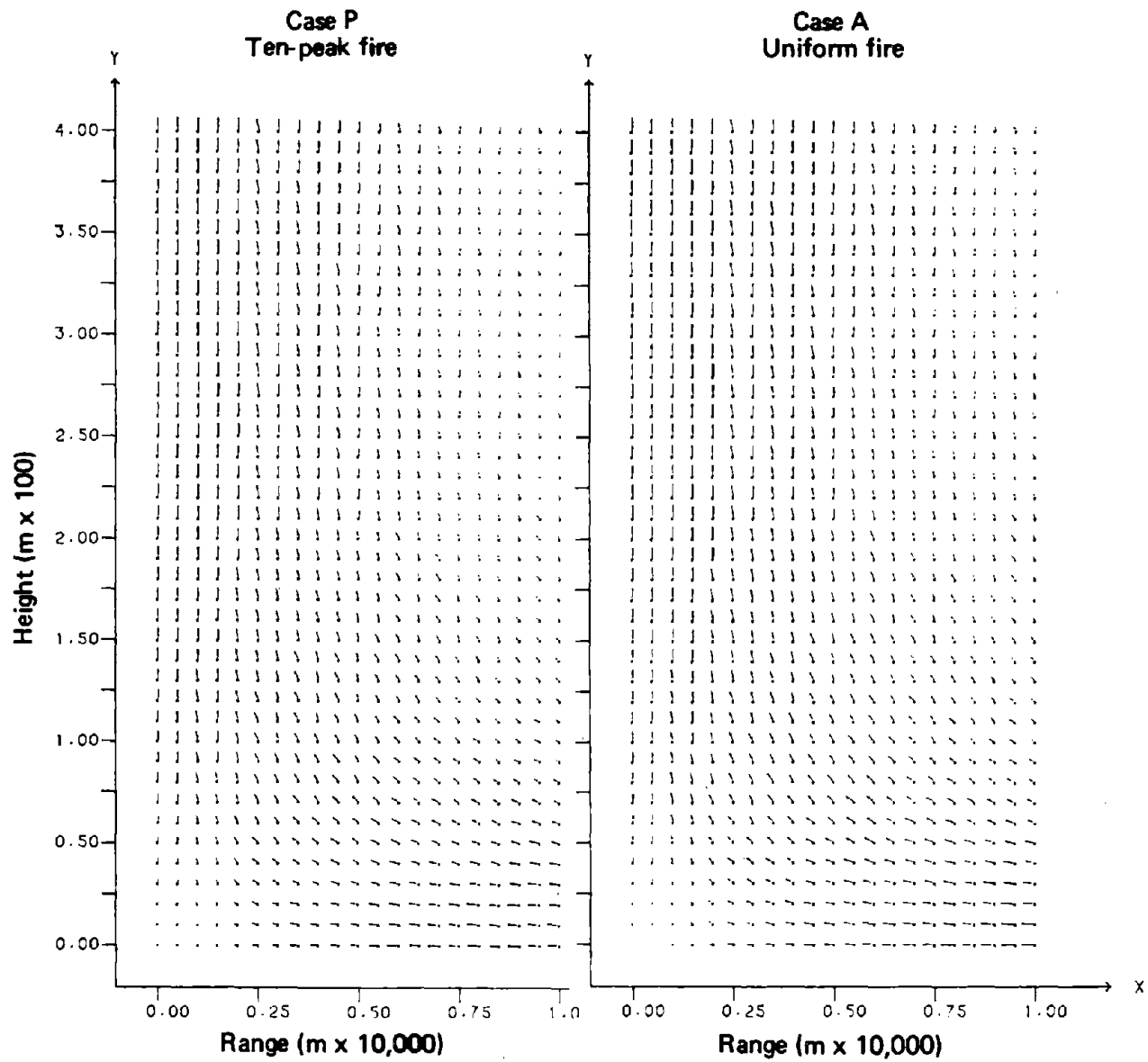
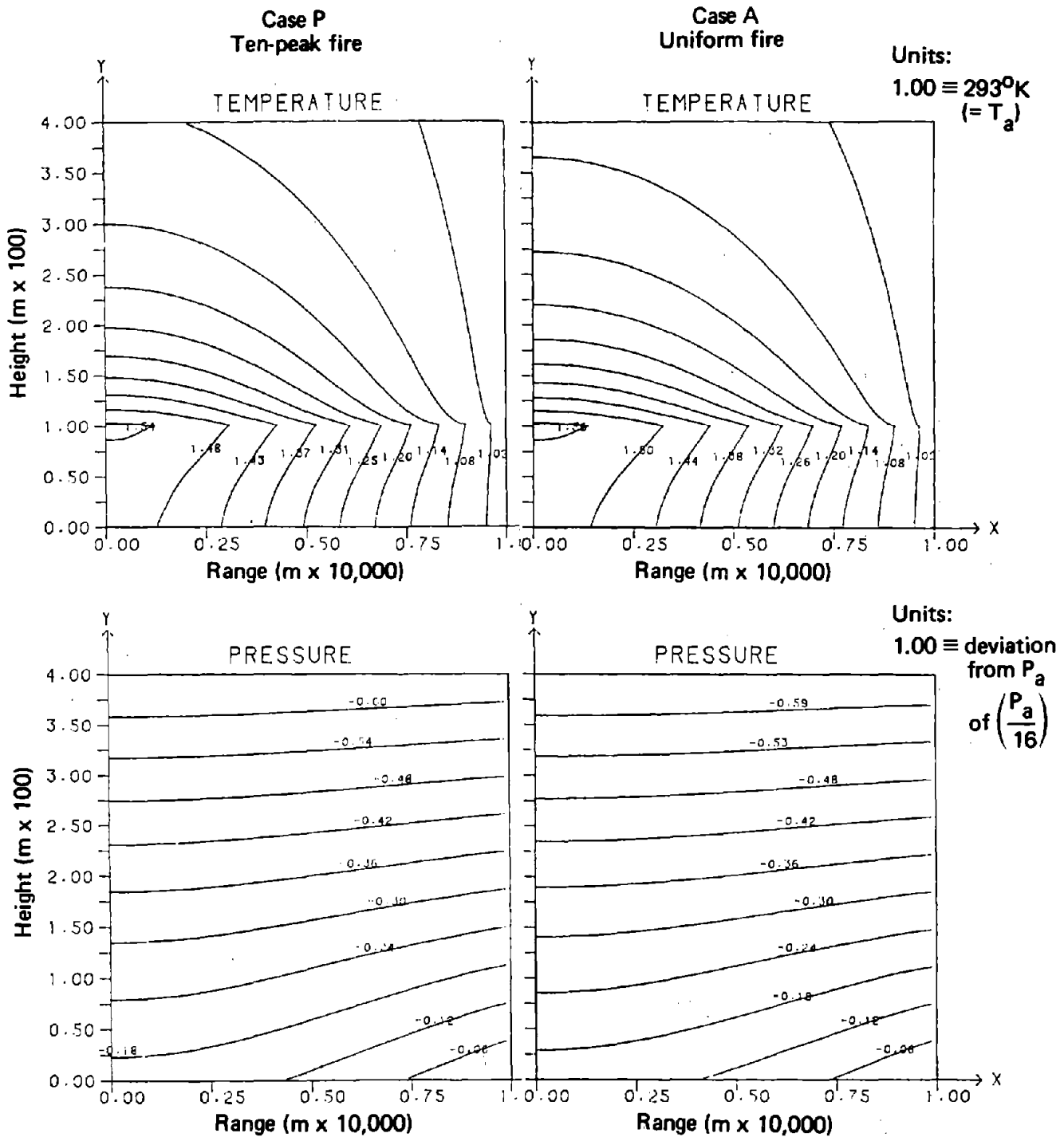


Fig. 34--Velocity fields generated for uniform and ten-cycle oscillatory heat release rates



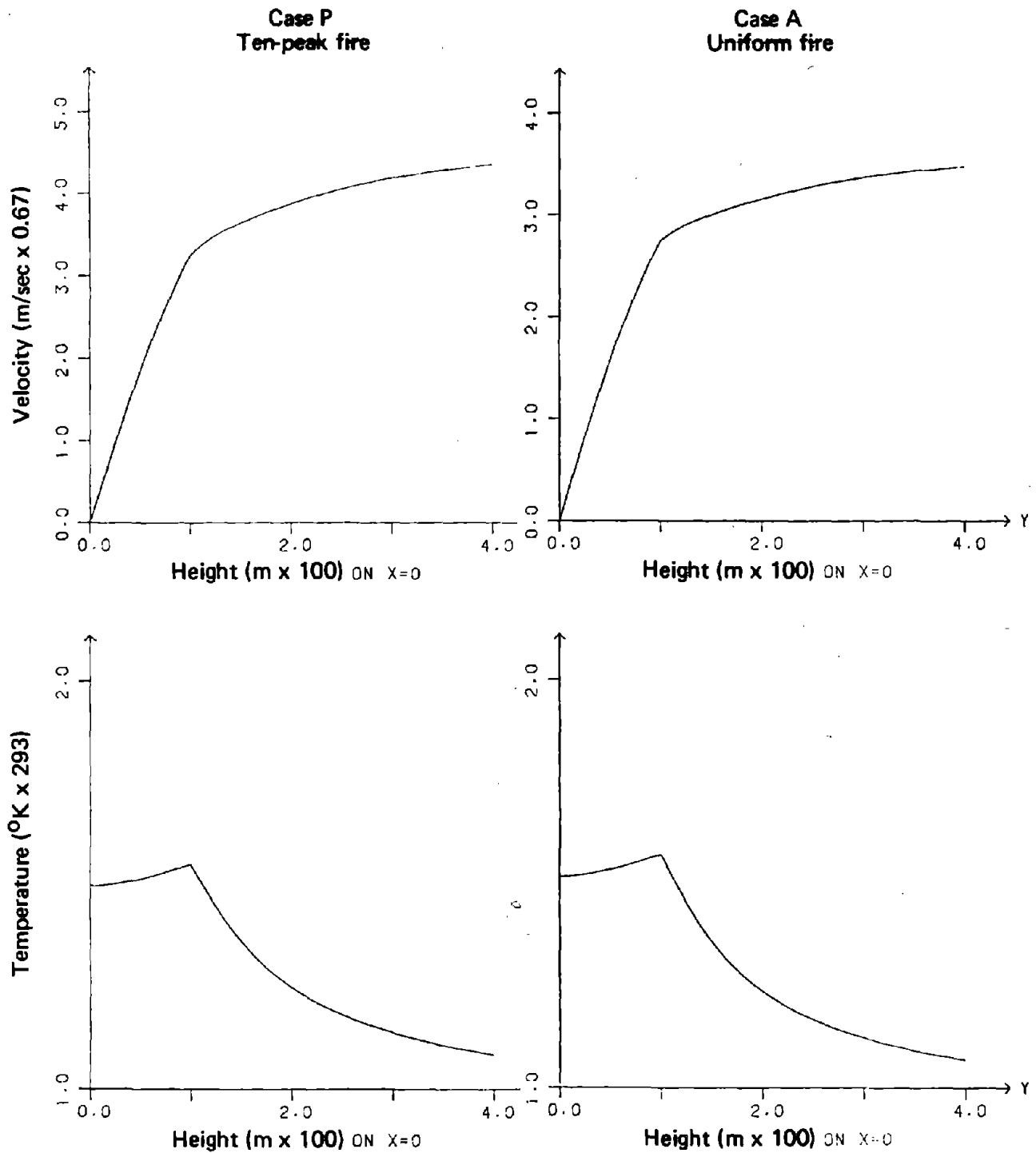
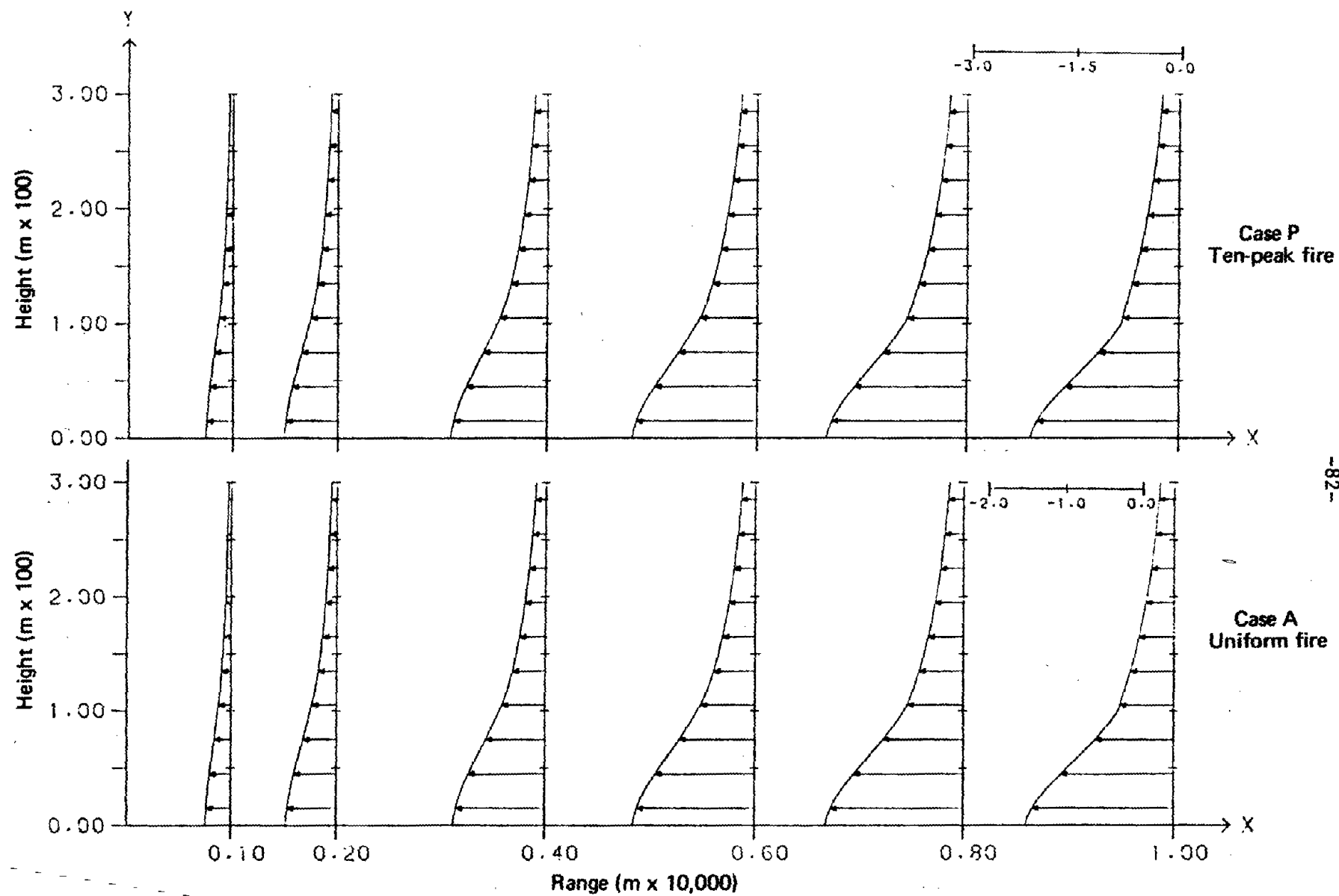


Fig. 36--Center-line velocities and temperatures generated for uniform and ten-cycle oscillatory heat release rates



-82-

...ed for uniform and ten-cycle oscillatory

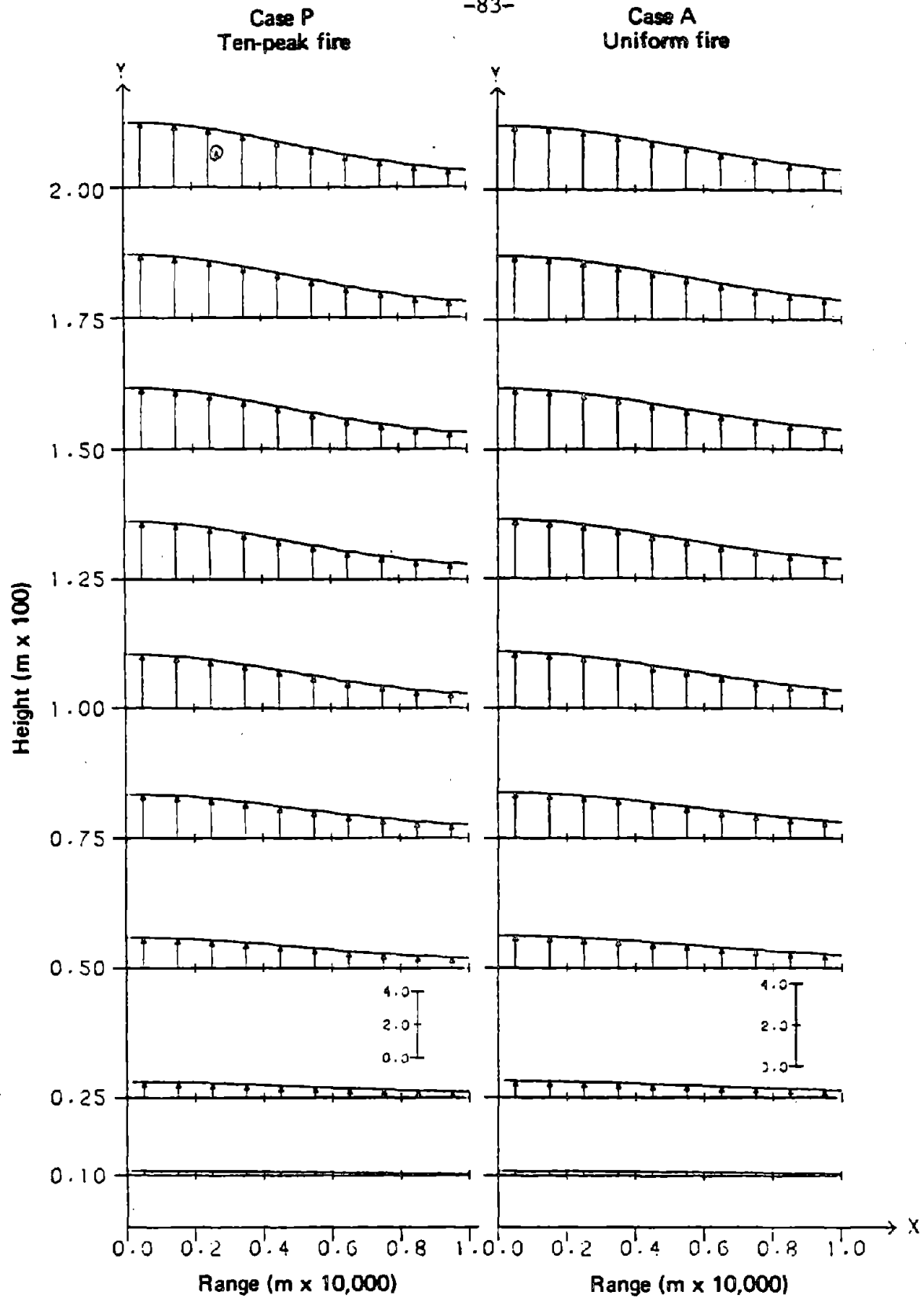


Fig. 38--Vertical velocity profiles generated for uniform and ten-cycle oscillatory heat release rates

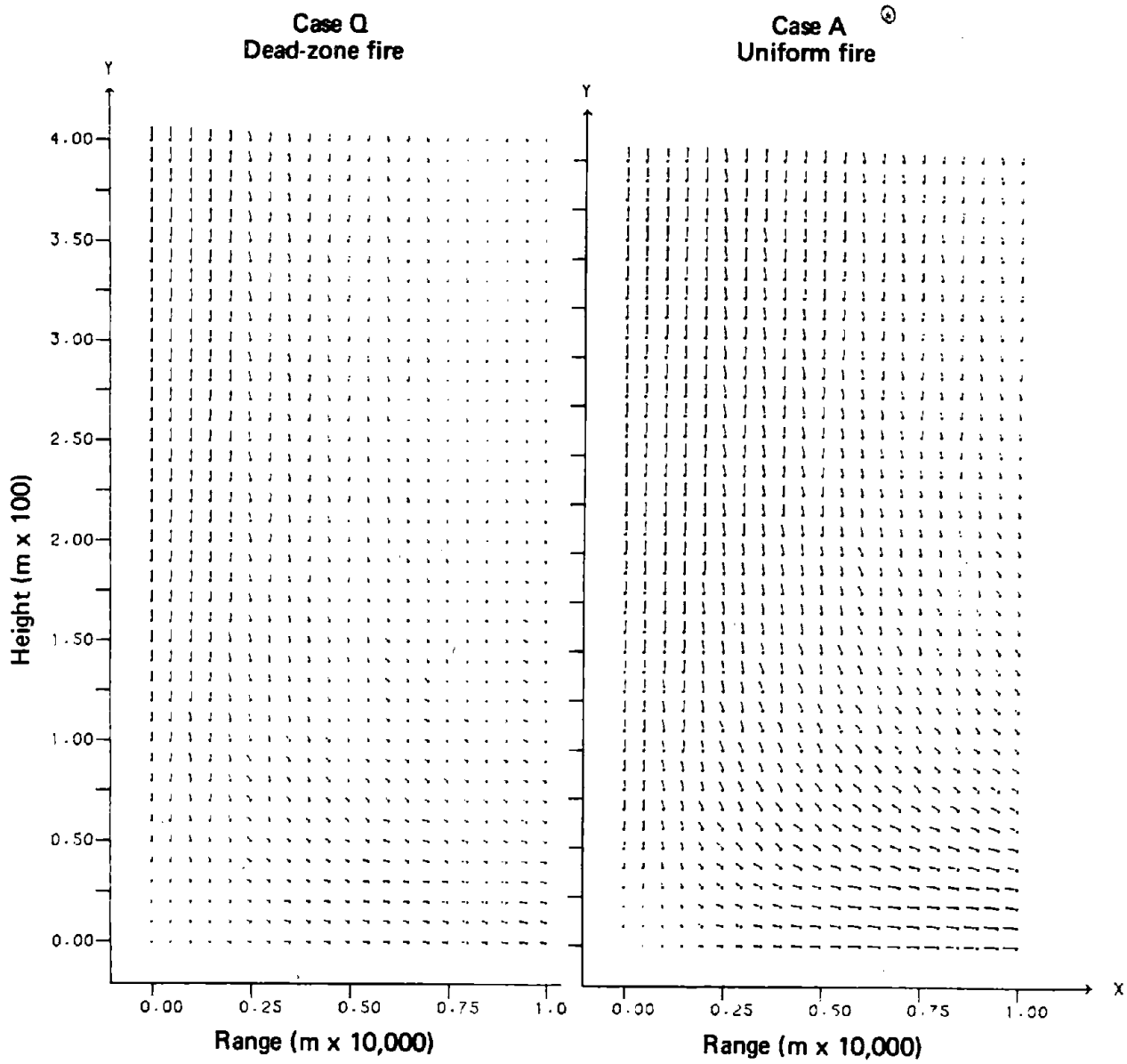


Fig. 39--Velocity fields generated for uniform and dead-zone heat release rates

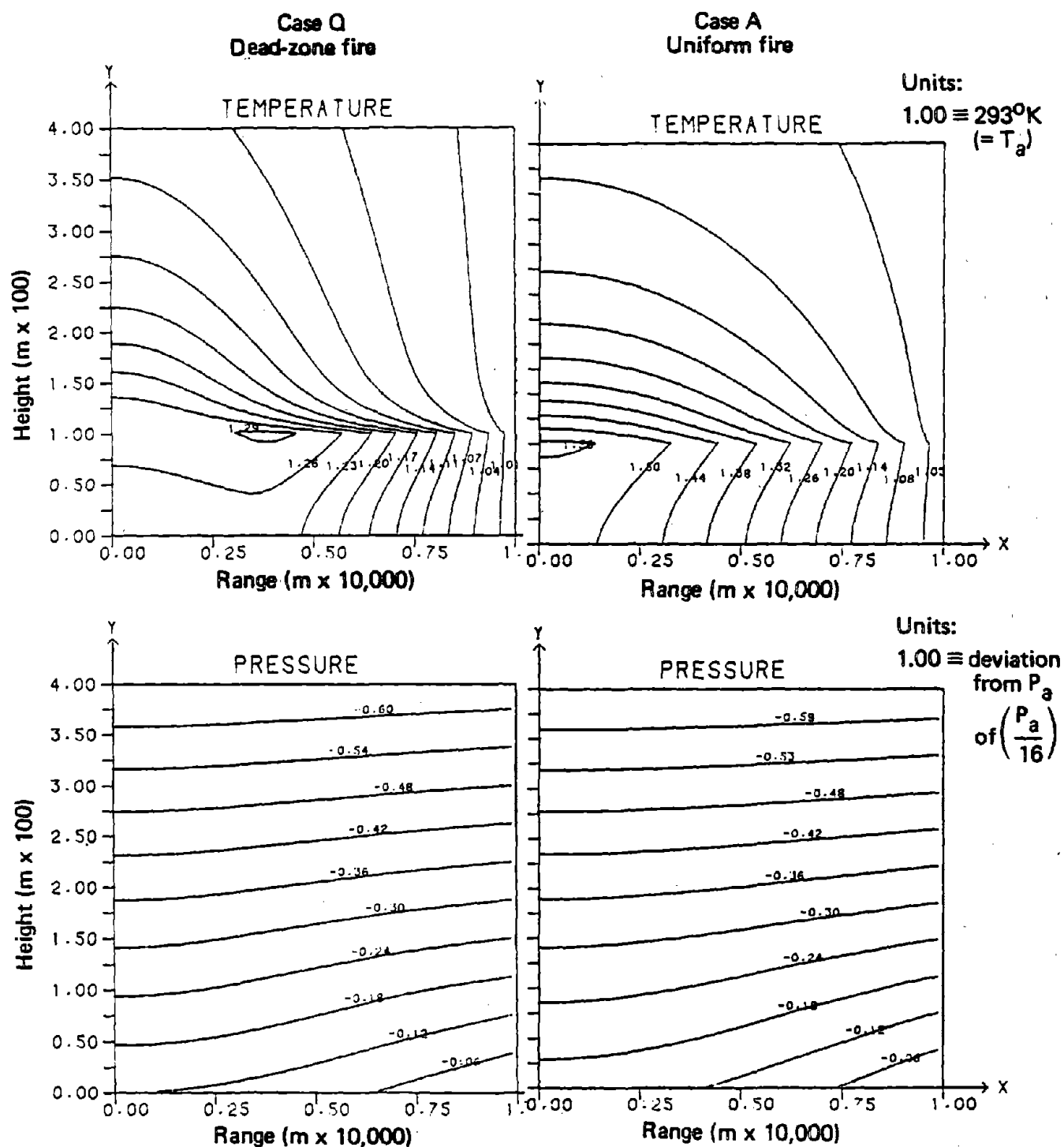


Fig. 40--Temperature and pressure contours generated for uniform and dead-zone heat release rates

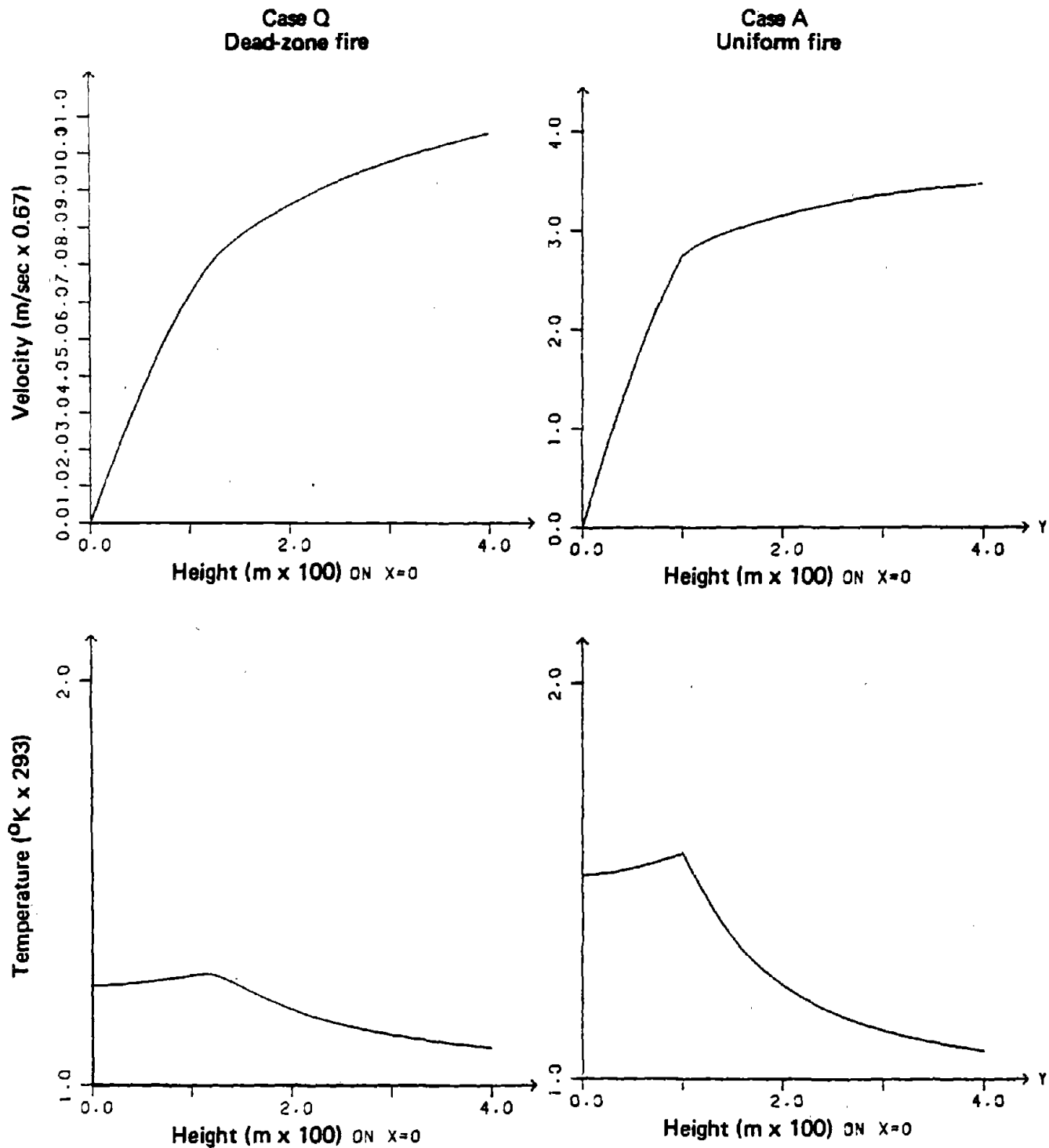
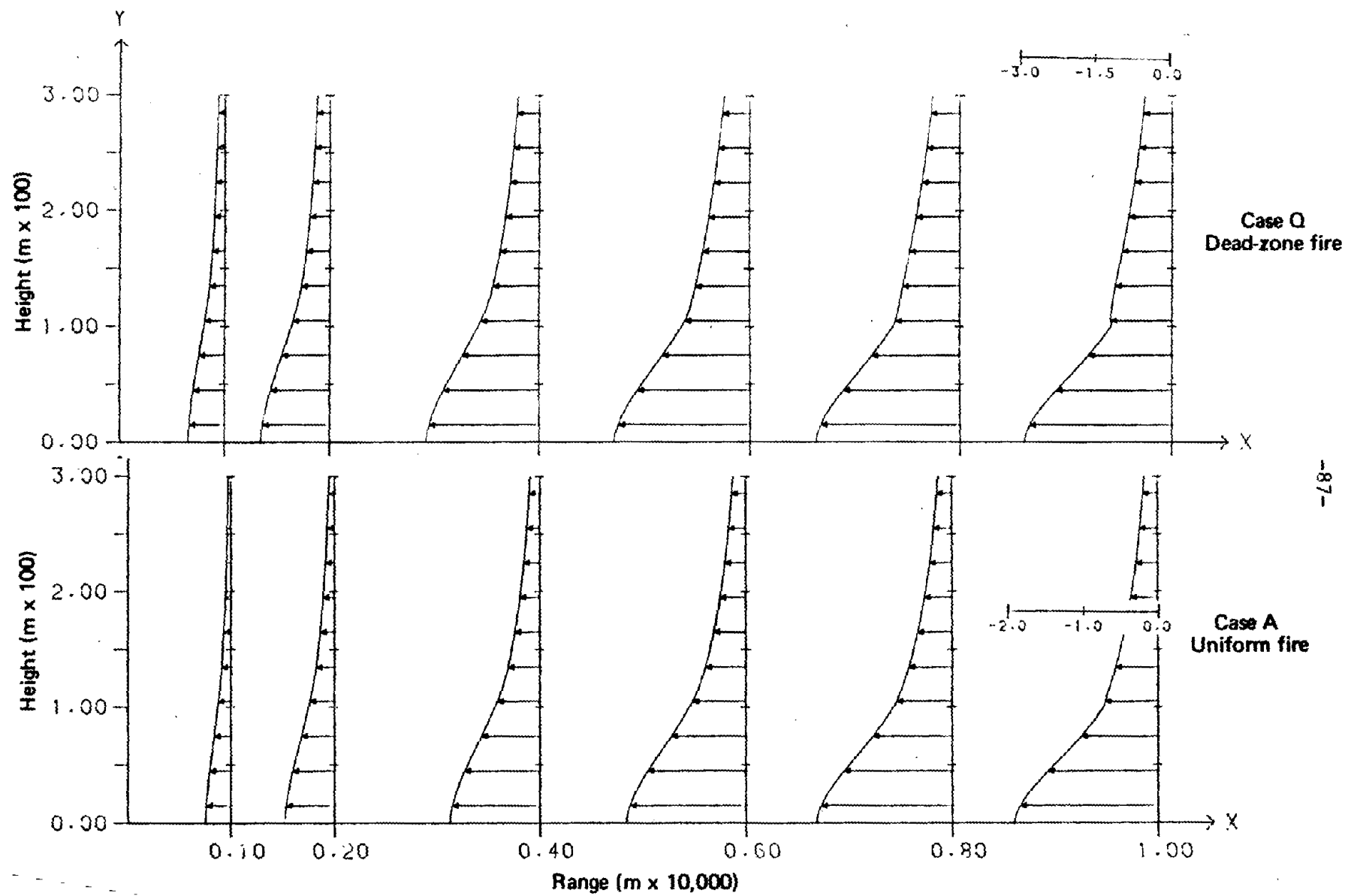


Fig. 41--Center-line velocities and temperatures generated for uniform and dead-zone heat release rates



-87-

(m x 67)

for uniform and dead-zone heat release rates

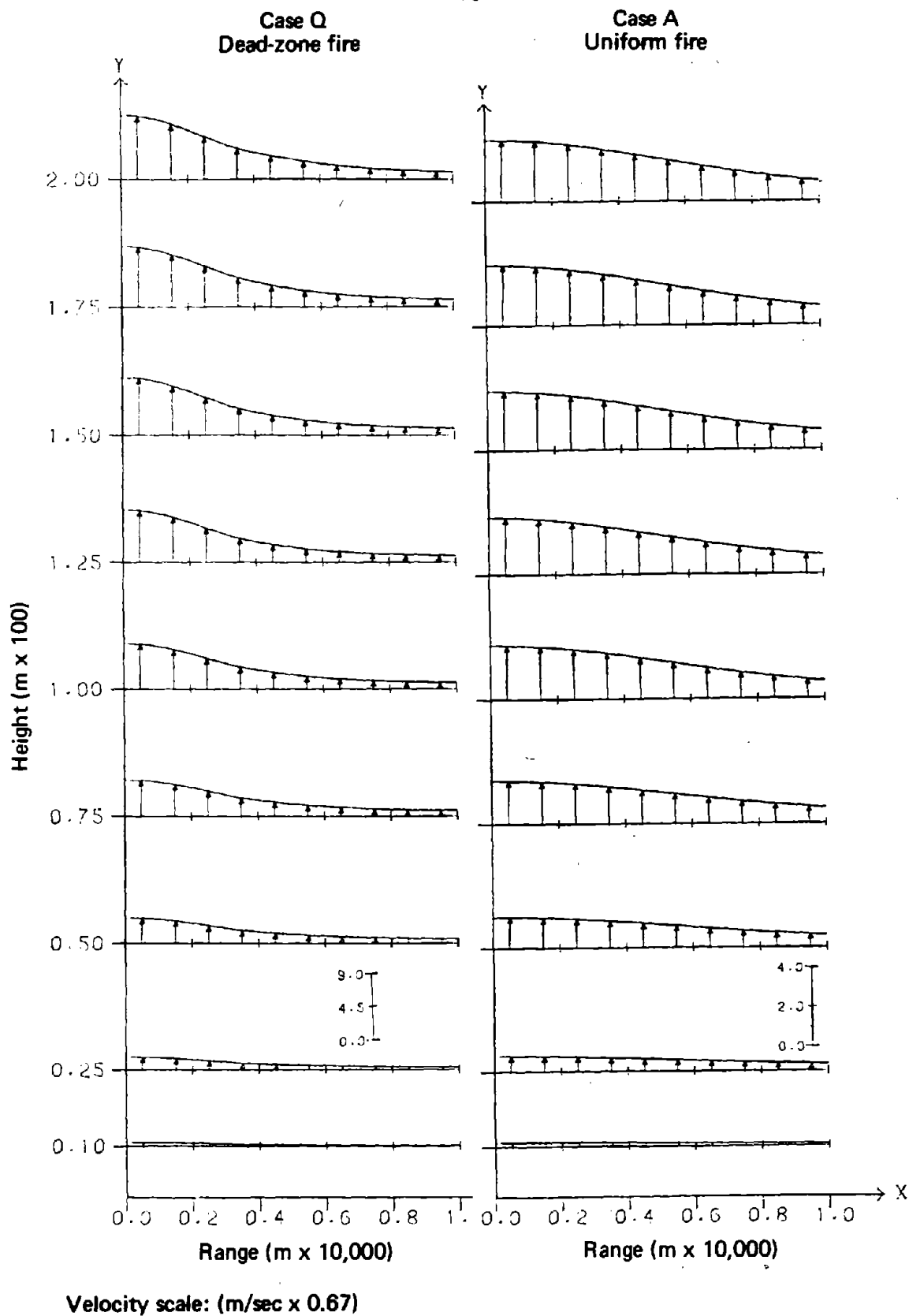


Fig. 43--Vertical velocity profiles generated for uniform and dead-zone heat release rates

Case Q is further elucidated in Tables 10 and 11. Ground-level velocities (Table 10) are appreciably higher than those in the baseline case (Table 2). The temperature at the center is lower, but the turbulent forces are more than three times higher than in the dead-zone fire case, with a peak just inside the inner edge of the fire. At 600 m (Table 11); horizontal velocities are much higher for case Q than for case A--nearly five times, in fact--though still small compared with the vertical velocities. Even here, turbulent stresses are nearly an order of magnitude higher than in the baseline case.

The Flambeau fire experiments were intended as models of large urban fires, with ricks of forest cuttings and brush separated by "streets." The tests resulted in fires approximately the size shown in Fig. 4 (p. 22). Application of our large-area-fire model to this configuration led to the results depicted in Figs. 44 through 48.

The velocity vectors of Fig. 44 are reassuringly similar to those of the baseline calculation (case A). The temperature and pressure contours of Fig. 45 also resemble those of the baseline calculation, but with somewhat different temperature profiles within the fire zone itself. The center-line temperature and velocity plots of Fig. 46 show the same general features as those of the baseline case. The horizontal velocity profiles in Fig. 47 show a persistence of the boundary velocities uniformly throughout the fire, with an exponential decay above $y = 1$. The vertical velocity profiles shown in Fig. 48 result in the plume formed over the fire having a fairly conventional velocity distribution, with a maximum along the center line and a decrease with distance toward $x = 1$. These results not only parallel those of many of the urban-fire parametric cases discussed above, but are satisfyingly close to actual observations of the Flambeau experiments. The similarity of the results to the observations/experiments is very encouraging.

Table 10

GROUND-LEVEL NUMERICAL PREDICTIONS FOR PARAMETER CASE Q
(DEAD-ZONE FIRE)

FIRE: SOLUTION OF COMBUSTION LAYER BOUNDARY VALUE PROBLEM

SYSTEM PARAMETERS: A = 0.160 SIGMA = 0.023 NU = 0.500 K = 0.500

MESH: M = 40 DX = 0.025 N = 240 DY = 0.025

ITERATION PARAMETERS: ETLINE = 0.001000 MAXITL = 20 ETOLP = 0.005000 MAXITP = 20

INLET PARAMETERS: ALPHA = 1.000 BETA = 1.500 BLOSS = 0.000

FOR J = 1 (Y = 0.000):

I	X	U	V	T	RHO	P	PX	NU*UXX	K*TXX	Q(T)
1	0.000	0.000	0.000	1.246	0.802	-0.122	0.000	0.000	0.000	-0.032
2	0.025	-0.187	0.000	1.246	0.802	-0.122	0.005	1.126	0.032	-0.032
3	0.050	-0.373	0.000	1.246	0.802	-0.122	0.014	2.222	0.032	-0.032
4	0.075	-0.556	0.000	1.246	0.802	-0.121	0.023	3.254	0.031	-0.032
5	0.100	-0.735	0.000	1.246	0.802	-0.121	0.031	4.192	0.024	-0.033
6	0.125	-0.909	0.000	1.247	0.802	-0.120	0.040	5.016	0.028	-0.033
7	0.150	-1.076	0.000	1.247	0.802	-0.119	0.048	5.707	0.025	-0.033
8	0.175	-1.237	0.000	1.247	0.802	-0.117	0.055	6.261	0.024	-0.033
9	0.200	-1.389	0.000	1.247	0.802	-0.116	0.063	6.670	0.021	-0.033
10	0.225	-1.533	0.000	1.248	0.802	-0.114	0.069	6.945	0.018	-0.033
11	0.250	-1.669	0.000	1.248	0.801	-0.112	0.075	7.086	0.017	-0.033
12	0.275	-1.795	0.000	1.248	0.801	-0.110	0.081	7.112	0.014	-0.033
13	0.300	-1.913	0.000	1.248	0.801	-0.108	0.086	7.034	0.011	-0.033
14	0.325	-2.022	0.000	1.249	0.801	-0.106	0.090	6.870	0.010	-0.033
15	0.350	-2.123	0.000	1.249	0.801	-0.104	0.097	6.637	-1.268	1.297
16	0.375	-2.215	0.000	1.248	0.801	-0.101	0.107	6.359	-1.159	1.297
17	0.400	-2.299	0.000	1.245	0.803	-0.099	0.115	6.048	-1.053	1.298
18	0.425	-2.375	0.000	1.241	0.806	-0.096	0.123	5.710	-0.947	1.298
19	0.450	-2.445	0.000	1.236	0.809	-0.092	0.130	5.357	-0.849	1.299
20	0.475	-2.507	0.000	1.230	0.813	-0.089	0.136	4.997	-0.754	1.300
21	0.500	-2.564	0.000	1.223	0.818	-0.086	0.142	4.636	-0.665	1.302
22	0.525	-2.615	0.000	1.215	0.823	-0.082	0.147	4.280	-0.582	1.303
23	0.550	-2.660	0.000	1.206	0.829	-0.078	0.151	3.934	-0.506	1.304
24	0.575	-2.700	0.000	1.197	0.836	-0.074	0.156	3.600	-0.436	1.306
25	0.600	-2.736	0.000	1.187	0.843	-0.070	0.159	3.284	-0.372	1.307
26	0.625	-2.768	0.000	1.176	0.850	-0.066	0.162	2.980	-0.314	1.309
27	0.650	-2.796	0.000	1.166	0.858	-0.062	0.165	2.699	-0.262	1.311
28	0.675	-2.821	0.000	1.155	0.866	-0.058	0.164	2.435	-0.214	1.312
29	0.700	-2.843	0.000	1.143	0.875	-0.054	0.170	2.189	-0.173	1.314
30	0.725	-2.861	0.000	1.132	0.884	-0.050	0.172	1.964	-0.136	1.315
31	0.750	-2.878	0.000	1.120	0.893	-0.045	0.174	1.755	-0.102	1.317
32	0.775	-2.892	0.000	1.108	0.903	-0.041	0.176	1.566	-0.073	1.318
33	0.800	-2.905	0.000	1.096	0.912	-0.037	0.177	1.392	-0.048	1.320
34	0.825	-2.915	0.000	1.084	0.923	-0.032	0.179	1.235	-0.026	1.321
35	0.850	-2.924	0.000	1.072	0.933	-0.028	0.180	1.093	-0.006	1.323
36	0.875	-2.932	0.000	1.060	0.944	-0.023	0.181	0.964	0.011	1.324
37	0.900	-2.938	0.000	1.048	0.954	-0.019	0.183	0.849	0.025	1.325
38	0.925	-2.944	0.000	1.036	0.965	-0.014	0.184	0.746	0.038	1.327
39	0.950	-2.948	0.000	1.024	0.977	-0.009	0.185	0.655	0.048	1.328
40	0.975	-2.952	0.000	1.012	0.988	-0.005	0.186	0.571	0.057	1.329

Table 11

600-m-ALTITUDE NUMERICAL PREDICTIONS FOR PARAMETER CASE Q
(DEAD-ZONE FIRE)

FOR J = 241 (Y = 6.000):

I	X	U	V	T	RHO	P	PX	NU*UXX	K*TXX	Q(T)
1	0.000	0.000	11.315	1.057	0.946	-0.960	0.000	0.000	0.000	-0.006
2	0.025	-0.009	11.273	1.057	0.946	-0.960	0.000	0.045	-0.125	-0.006
3	0.050	-0.018	11.149	1.057	0.946	-0.960	0.000	0.088	-0.123	-0.006
4	0.075	-0.027	10.947	1.056	0.947	-0.960	0.000	0.129	-0.120	-0.006
5	0.100	-0.035	10.674	1.056	0.947	-0.960	0.000	0.167	-0.115	-0.006
6	0.125	-0.044	10.337	1.055	0.948	-0.960	0.000	0.201	-0.109	-0.006
7	0.150	-0.052	9.945	1.055	0.948	-0.960	0.000	0.230	-0.103	-0.005
8	0.175	-0.060	9.510	1.054	0.949	-0.960	0.000	0.253	-0.096	-0.005
9	0.200	-0.067	9.042	1.053	0.950	-0.960	0.000	0.272	-0.087	-0.005
10	0.225	-0.075	8.552	1.052	0.951	-0.960	0.000	0.285	-0.082	-0.005
11	0.250	-0.081	8.048	1.050	0.952	-0.960	0.000	0.294	-0.071	-0.005
12	0.275	-0.088	7.541	1.049	0.953	-0.960	0.000	0.298	-0.066	-0.005
13	0.300	-0.094	7.037	1.048	0.954	-0.960	0.000	0.298	-0.056	-0.005
14	0.325	-0.100	6.544	1.046	0.956	-0.960	0.000	0.295	-0.051	-0.005
15	0.350	-0.105	6.101	1.045	0.957	-0.960	0.000	0.291	-0.042	-0.004
16	0.375	-0.110	5.713	1.043	0.959	-0.960	0.000	0.285	-0.037	-0.004
17	0.400	-0.115	5.343	1.042	0.960	-0.960	0.000	0.279	-0.032	-0.004
18	0.425	-0.119	4.991	1.040	0.962	-0.960	0.000	0.271	-0.027	-0.004
19	0.450	-0.123	4.658	1.038	0.963	-0.960	0.000	0.261	-0.021	-0.004
20	0.475	-0.127	4.343	1.037	0.965	-0.960	0.000	0.251	-0.020	-0.004
21	0.500	-0.130	4.047	1.035	0.966	-0.960	0.000	0.240	-0.014	-0.003
22	0.525	-0.133	3.768	1.033	0.968	-0.960	0.000	0.229	-0.011	-0.003
23	0.550	-0.136	3.506	1.031	0.970	-0.960	0.000	0.218	-0.010	-0.003
24	0.575	-0.139	3.260	1.030	0.971	-0.960	0.000	0.206	-0.005	-0.003
25	0.600	-0.141	3.031	1.028	0.973	-0.960	0.000	0.195	-0.002	-0.003
26	0.625	-0.143	2.816	1.026	0.975	-0.960	0.000	0.184	-0.002	-0.002
27	0.650	-0.144	2.616	1.024	0.976	-0.960	0.000	0.173	0.001	-0.002
28	0.675	-0.146	2.429	1.022	0.978	-0.960	0.001	0.162	0.004	-0.002
29	0.700	-0.147	2.256	1.021	0.980	-0.960	0.001	0.152	0.002	-0.002
30	0.725	-0.148	2.095	1.019	0.981	-0.960	0.001	0.142	0.006	-0.002
31	0.750	-0.149	1.945	1.017	0.983	-0.960	0.001	0.132	0.006	-0.002
32	0.775	-0.150	1.807	1.015	0.985	-0.960	0.001	0.123	0.006	-0.001
33	0.800	-0.151	1.679	1.014	0.987	-0.960	0.001	0.115	0.008	-0.001
34	0.825	-0.151	1.560	1.012	0.988	-0.960	0.001	0.107	0.008	-0.001
35	0.850	-0.152	1.450	1.010	0.990	-0.960	0.001	0.099	0.011	-0.001
36	0.875	-0.152	1.349	1.008	0.992	-0.960	0.001	0.092	0.006	-0.001
37	0.900	-0.152	1.255	1.007	0.993	-0.960	0.001	0.086	0.013	-0.001
38	0.925	-0.152	1.169	1.005	0.995	-0.960	0.001	0.079	0.006	0.000
39	0.950	-0.152	1.090	1.003	0.997	-0.960	0.001	0.074	0.012	0.000
40	0.975	-0.152	1.017	1.002	0.998	-0.960	0.001	0.067	0.010	0.000
41	1.000	-0.152	0.981	1.000	1.000	-0.960	0.002	0.067	0.010	0.000

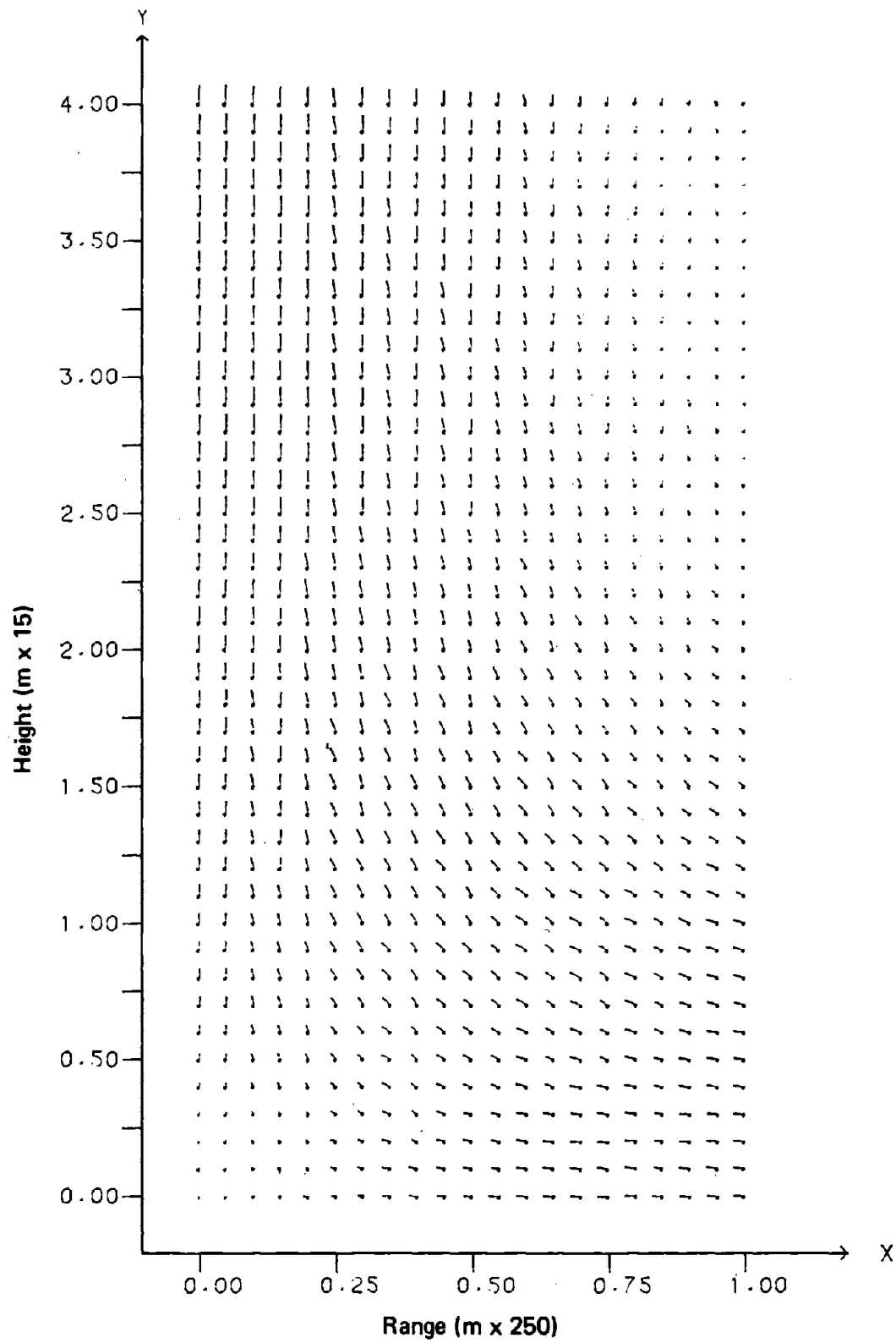


Fig. 44--Velocity field predicted for typical multiple-fuel-bed Flambeau fire
(cf. Fig. 4)

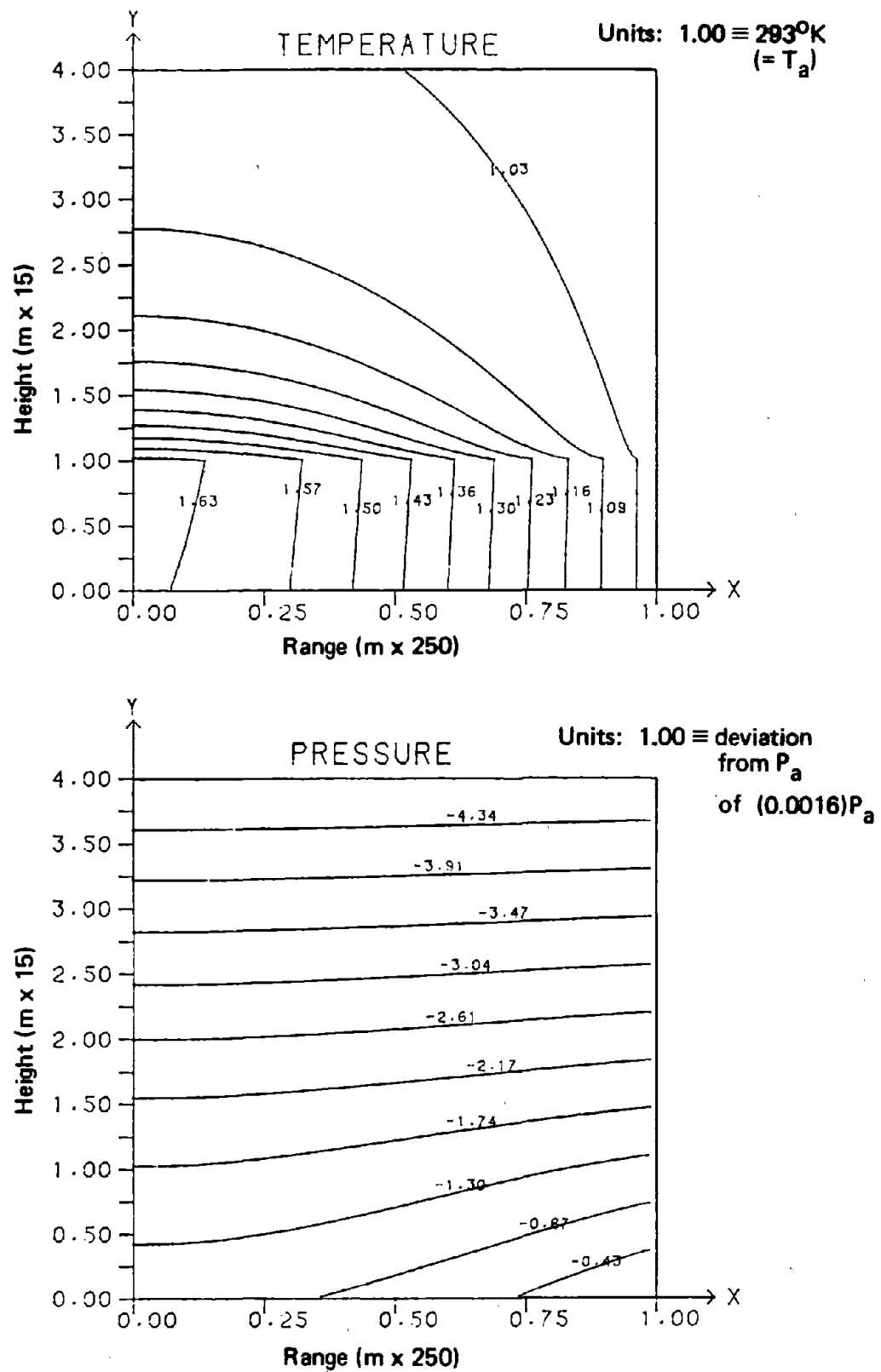


Fig. 45--Temperature and pressure contours predicted for typical multiple-fuel-bed Flambeau fire

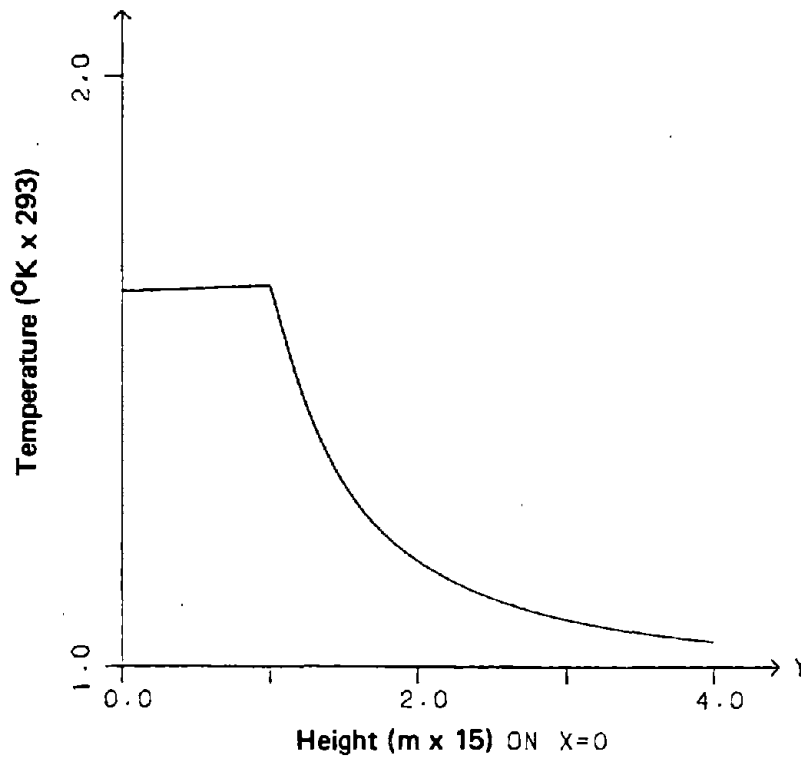
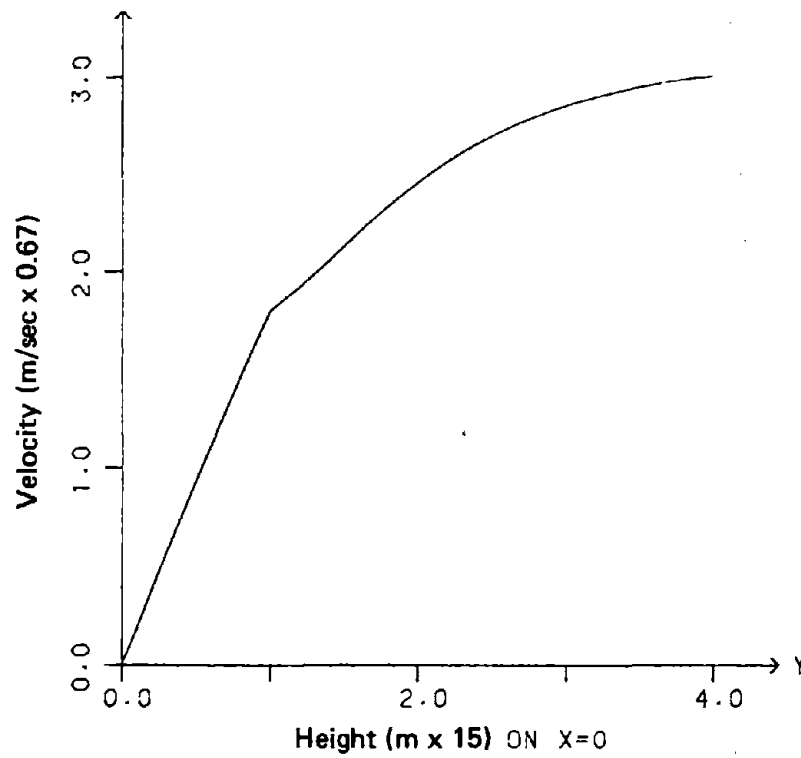
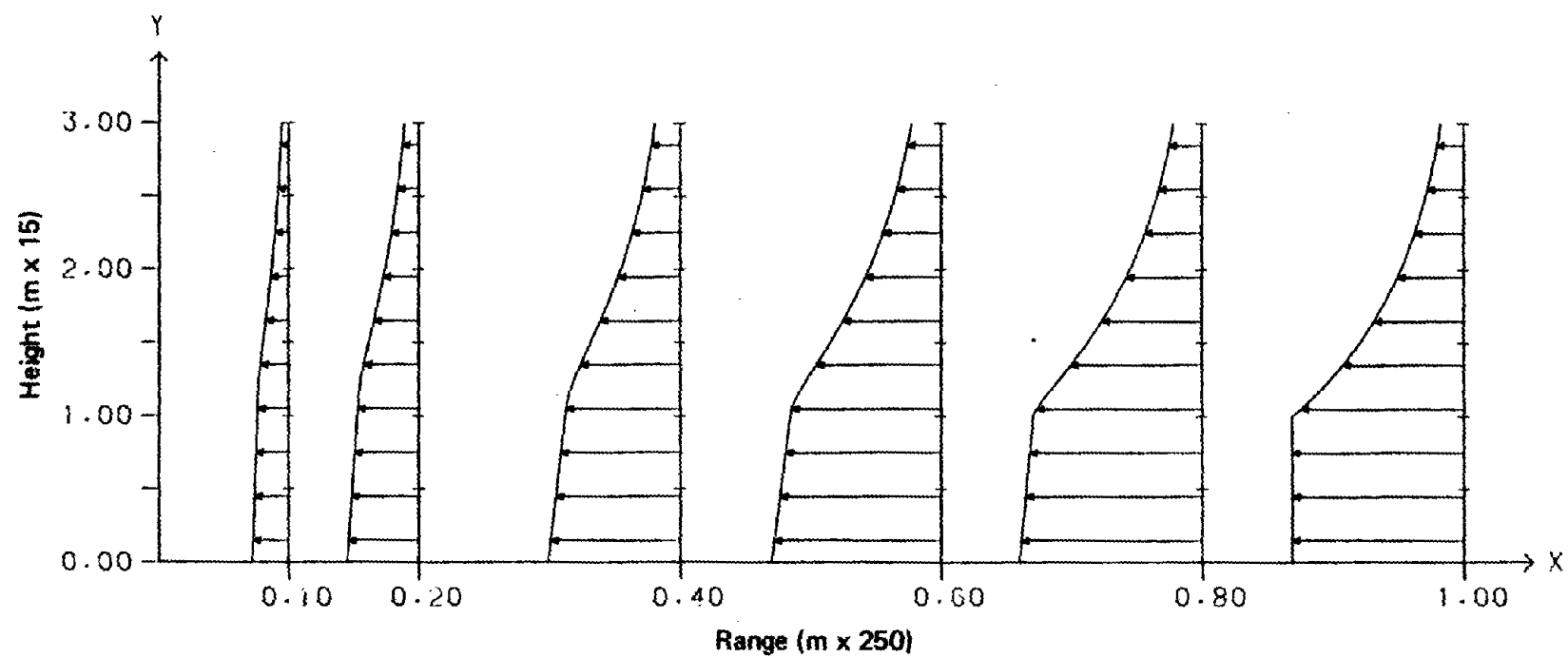


Fig. 46--Center-line velocities and temperatures predicted for typical multiple-fuel-bed Flambeau fire



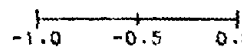

 Velocity scale: (m/sec x 11.2)

Fig. 47--Horizontal velocity profiles predicted for typical multiple-fuel-bed Flambeau fire

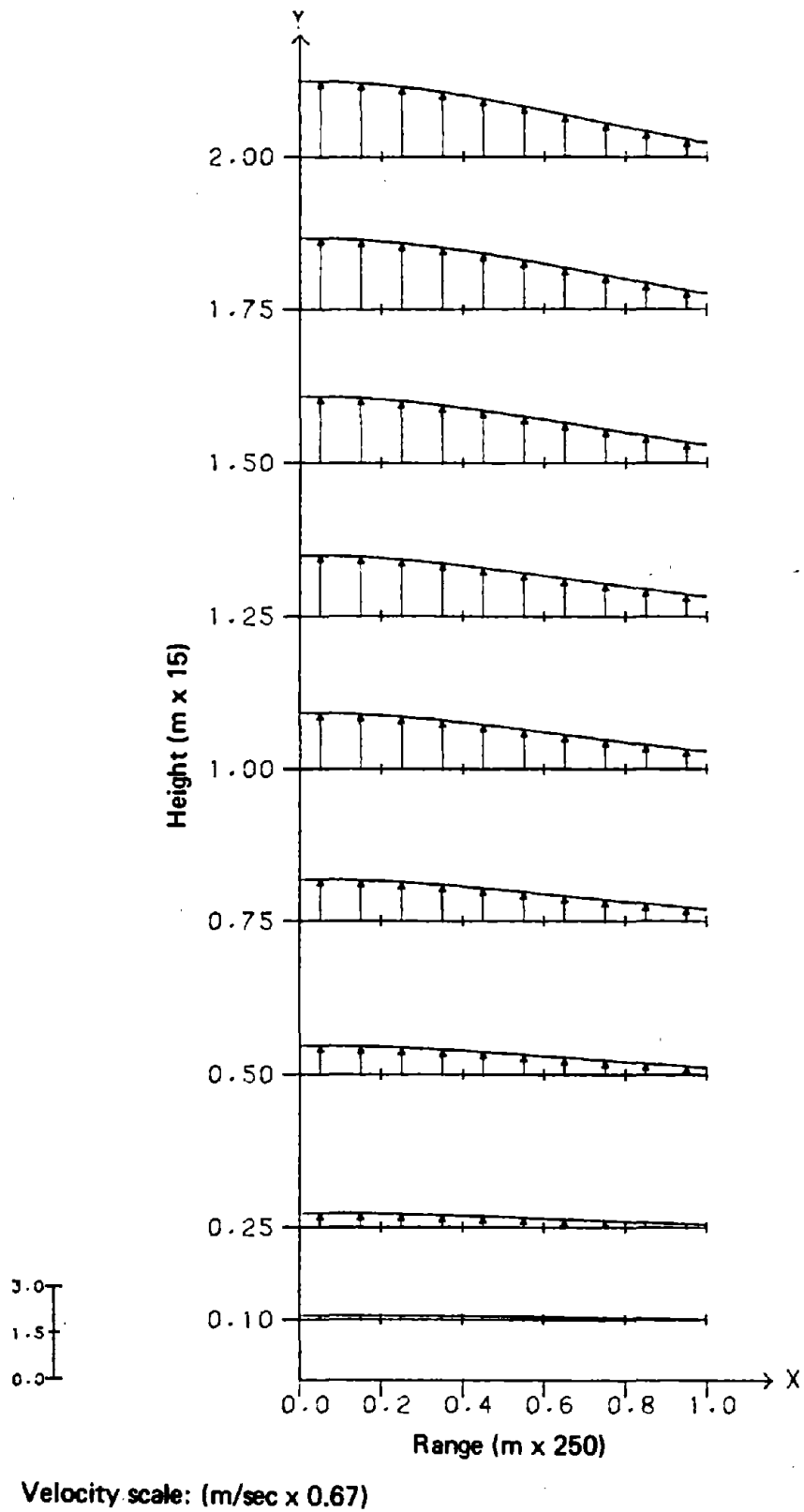


Fig. 48--Vertical velocity profiles predicted for typical multiple-fuel-bed Flambeau fire

IV. DISCUSSION

The use of a "component" model to describe large urban fires allows for detailed resolution of the dynamics of the combustion layer region without ignoring the influence of the rising plume or atmospheric recirculation. Ultimately, an even finer resolution of the combustion layer may be desired--for example, with a horizontal-length scale on the order of a city block, or even the width of a building. For such cases, the combustion layer model described here provides the ambient background against which the local flow (e.g., around buildings) and thermodynamic perturbations can be calculated. Our model thus represents a basic characterization of the environment in the fire zone.

The combustion layer model does have certain limitations. The combustive-heat release rate $Q = q(x, y)$ must be prescribed independent of the dynamics; heat losses due to hot gas radiation are only qualitatively modeled, as if they were grey body or nearly "transparent" [Murgai, 1962]; and Reynolds stresses are only crudely approximated by diffusion terms with constant eddy diffusivities. In addition, as discussed in Sec. III, the proper velocity boundary condition along the outer edge of the fire and plume must still be determined.

More detailed modeling of the basic combustion processes, the resultant hot-gas radiation, and turbulence should, however, greatly reduce all limitations but the last. In general, those tasks are left for future investigations. Nevertheless, we note that Sec. III indicates the manner in which the combustion kinetics could approximately be coupled with the air flow. Our current simulation indicates that the sensitivity of the results to variations in the level of radiative cooling is relatively small and possibly negligible. Additionally, we anticipate that a more accurate description of the Reynolds stresses will show them to be much larger near the ground and near the symmetry axis than elsewhere, except possibly at the fire periphery.

More important, a refined combustion layer model can be used to answer major practical questions concerning the fire environment. One basic question concerns the dependence of the maximum fire-generated

winds on fire intensity [or, quantitatively, $\iint_{\mathcal{D}} Q \cdot q(x, y) dx dy$, with \mathcal{D} denoting the fire zone]. Simple scaling provides a partial answer to this question: from Eq. (2.6), U is proportional to both Q and D . Such scaling provides order-of-magnitude estimates, but more detailed analysis is required for reliable quantitative predictions. For example, civil defense professionals should know whether the maximum wind speeds associated with the nominal scale in Eq. (2.7) of $U \sim 150$ mph are actually only 50 mph ($U/3$) or 450 mph ($3U$). A model like ours will provide such information, as well as predictions of corresponding temperature, concentrations of carbon monoxide and carbon dioxide, smoke maxima, and oxygen minima.

A second major practical question that can be resolved with model analysis concerns the horizontal extent of the induced fire winds and the corresponding range of wind damage. The solution entails the description of the fire-generated flow pattern near the bottom of the recirculation region (i.e., especially in subregions IA and IB of Fig. 3). One possibility is that the flow into the inlet region (IA) from regions III and IB is basically radial (i.e., sink-like), its magnitude falling off like $1/\hat{R}$, with

$$\hat{R} = \sqrt{\hat{x}^2 + y^2}, \quad \hat{x} = \frac{x - 1}{\epsilon^\alpha}. \quad (4.1)$$

In this case, the high fire winds would extend only slightly beyond the fire's periphery (i.e., only a horizontal distance on the order of $\epsilon^\alpha D$). On the other hand, in the fully developed large-fire environment, the flow through regions IA and IB may well be nearly parallel. In that case, the fire winds would extend far past the fire periphery (and could be on the order of tens of kilometers for $D \sim 10$ km). The true situation can be determined only through further research. In fact, the answer to this question is probably coupled to the determination of the proper velocity boundary condition along the outer edge of the combustion layer--the nature of the flow in region IA (Fig. 3) being the key to both answers.

Even the current combustion layer model demonstrates one major physical observation: the width of the convection column can be comparable to that of the fire zone only if turbulence plays a dominant role in combustion layer dynamics. Otherwise, the column must be considerably thinner than the fire zone, with the air that passes through the fire converging toward the column center line and remaining near as it rises.

The two types of columns, which we refer to as thick and thin plumes, respectively, are illustrated in Fig. 49. The nature of the plume is a principal feature of any fire, and one that has been considered throughout the present investigation. Small free-burning fires exhibit a thin-plume structure in which the plume height is much greater than the cross-section dimension. Thin-plume fires have also been created in laboratory or table-top models with a closely spaced matrix of burners. In general, thin plumes can result from rotational or wind-shear effects, where centrifugal forces combined with a buoyant rise cause a fast-rising, rotating, thin column. Fuel storage fires for which the availability of the fuel for burning is dominated by the turbulent mixing of vapors with the external air often exhibit a thick plume.

All the Flambeau fires exhibited a thick plume, as did many of the large urban fires of World War II. For this reason, it is expected that the plumes over future urban fires will have horizontal dimensions comparable to the burning-fuel-bed dimension. That expectation is further supported by a more detailed analysis of the combustion in such fires. Blocks or houses will be burning furiously, with non-combustible streets or open areas in between. Such irregular local burning encourages a kind of localized turbulent action, which could then generate a thick-plume flow.

Additional numerical results not reported here confirm that the fire plume must be thin unless turbulence significantly affects the combustion layer dynamics. In those runs, the thickness of the plume tends toward zero as the diffusion coefficients are reduced, all other parameters (and boundary conditions) being held fixed.

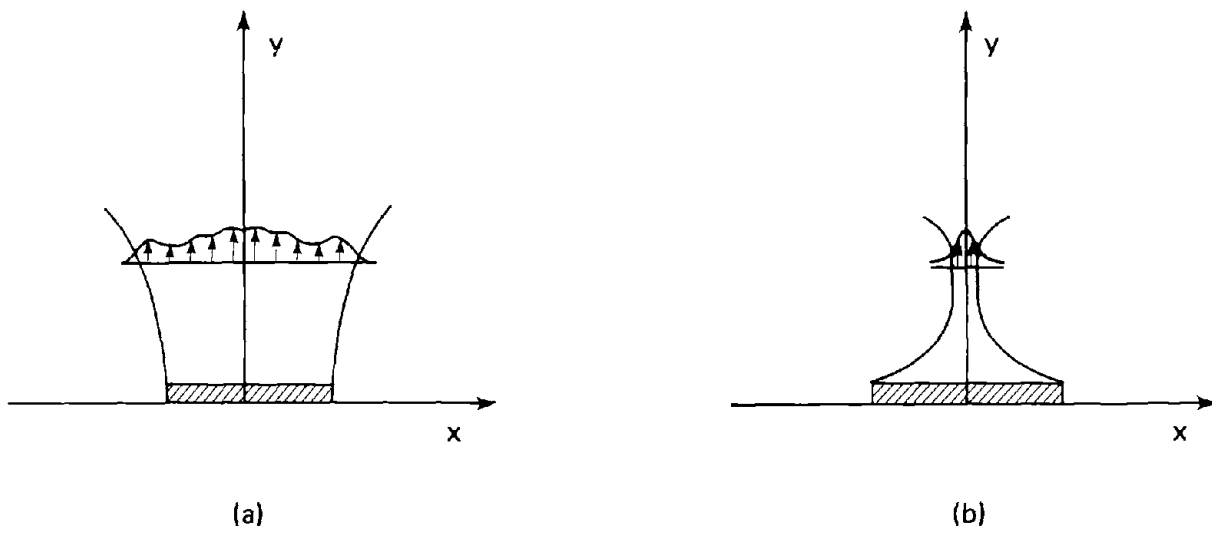


Fig. 49--Classification of possible convection plumes

Physically, this conclusion is explained as follows. In the combustion layer, the fire-generated buoyancy creates an updraft and a low pressure, so that air is sucked in from the far field. Those phenomena create large horizontal velocities, which must be decelerated if the flow is to be turned upward to form a thick plume. As demonstrated in the numerical runs, only in the region near the fire's center are the pressure gradients large enough to provide such a decelerating force. In fact, pressure gradients act over most of the combustion layer to accelerate the flow in toward the center. Other stresses--in particular, turbulent stresses--are thus required to provide deceleration and hence establish an upward thick-plume flow.

It is of major significance that our research provides the first description of the formation near the ground of a thick plume. A careful study of related work by other authors [Nielsen and Tao, 1965; Smith, Morton, and Leslie, 1975; Delage and Taylor, 1970 (for "heat island flows"--not fires)] shows that, in all cases, their results apply to thin plumes. Thus, though many more details of the gas dynamics of large burning regions can reasonably be incorporated into the calculational method, the current model reveals for the first time the nature of the thick plume and its relation to turbulent forces in and near the burning region.

In the modeling of both the combustion layer and the convection column flows, the effects of rotation (i.e., angular velocity) were for two reasons considered secondary and ignored. First, films of the multiple-fuel-bed Flambeau fires^{*} showed no significant angular motion (swirl). Some slight rotation was observed in the initial build-up to a maximum heat release, and also in the final decay of the fires (in the form of small fire whirls), but neither transient situation pertains to the current modeling. Second, as shown in this report, a viable theory for a large area fire can be developed without including rotational phenomena.

Finally, research must be undertaken to determine the nature of the flow in the outflow region (IV) on top of the convection column

^{*}From the U.S. Forest Service Laboratory, Riverside, California.

and the recirculation region. The modeling of that flow probably will involve additional meteorological physics (e.g., condensation, presence of inversion layers) not considered in the present analysis.

Large urban areas burning simultaneously are an expected result of nuclear warfare. The current modeling is intended to assist in understanding the nature of the velocity and temperature fields associated with such unprecedentedly large fires. If we succeed in modeling such fires, what have we learned? Of what value is the knowledge to civil defense? Effective efforts to limit damage under such extreme conditions must deal realistically with the actual environment that firefighting or rescue operations will face. Thus they would stand to profit from an improved understanding of the effects.

The possibility of additional damage due to large fire-associated or collateral winds can better be evaluated using the range of velocities predicted here. Concentrations of poisonous fumes, carbon monoxide, carbon dioxide, soot, and smoke can be calculated using the same mathematical model, and could be of great help in planning for adequate shelters and protection for key installations in an anticipated urban fire region. In short, the adequacy of any protective structures or actions against such large fires can better be evaluated using the calculations reported here.

Appendix A

SYMBOLS

MATHEMATICAL SYMBOLS

A, B = dimensionless constants

C_p = specific heat capacity at constant pressure

D = half-width of combustion zone

\mathcal{D} = two-dimensional domain representing combustion zone

D_{1m}, D_{2m} = diffusion coefficients for species m , which represents oxygen, carbon monoxide, carbon dioxide, or smoke (particulates)

$\mathcal{E}_{11}, \mathcal{E}_{12}, \mathcal{E}_{21}, \mathcal{E}_{22}$ = effective kinematic viscosities (including turbulence effects)

\mathfrak{F} = functional form for inlet velocity boundary condition

g = gravitational acceleration

\hat{g} = dimensionless horizontal velocity inlet profile

H = scale height of atmosphere

\mathcal{W} = functional form for inlet velocity boundary condition

k^* = reciprocal of grey-body radiation mean free path

k_1, k_2 = effective thermal conductivities (including turbulence effects)

K_1, K_2 = dimensionless heat diffusion coefficients

\tilde{K}_1 = rescaling of K_1

ℓ = mixing length

L = mean height of combustion zone

$M_{11}, M_{12}, M_{21}, M_{22}$ = dimensionless momentum diffusion coefficients

$\tilde{M}_{11}, \tilde{M}_{21}$ = rescalings of M_{11} and M_{21}

- P = pressure
- P_a = ground-level atmospheric pressure in far field
- P_0 = leading-order pressure in $\epsilon \rightarrow 0$ limit
- P_i = correction pressure in $\epsilon \rightarrow 0$ limit (integer i)
- \tilde{P} = sum of pressures through five orders in ϵ
($\epsilon \rightarrow 0$ limit)
- q = dimensionless volumetric heat-addition-rate
distribution in combustion zone
- Q = volume heat source scale
- r = dimensionless radial coordinate
- R = universal gas constant
- \hat{R} = dimensionless radial coordinate in the (\hat{x}, y)
plane
- \mathcal{R}_m = dimensionless volumetric depletion/addition rate
distribution for species m , which represents
oxygen, carbon monoxide, carbon dioxide, or
smoke (particulates)
- g_m = scales for volume depletion/addition during combus-
tion of species m , which represents oxygen, carbon
monoxide, carbon dioxide, or smoke (particulates)
- T = temperature
- T_a = ground-level atmospheric temperature in far field
- T_0 = leading-order temperature in $\epsilon \rightarrow 0$ limit
- T_i = correction temperature in $\epsilon \rightarrow 0$ limit (integer i)
- T_∞, \hat{T}_∞ = far-field ambient temperature in radiation law
(dimensionless, dimensional)
- $T_3^{(II)}$ = T_3 solution in region II
- u = horizontal velocity
- \tilde{u} = rescaled horizontal velocity
- u_0 = leading-order horizontal velocity in $\epsilon \rightarrow 0$ limit
- u_i = correction horizontal velocity in $\epsilon \rightarrow 0$ limit
(integer i)

$u_1^{(II)}$ = u_1 solution for region II

$u_{3/2}$ = correction horizontal velocity in $\epsilon \rightarrow 0$ limit

$\hat{u}_{3/2}$ = relative horizontal velocity in side-mixing-layer region (IIA)

U_I = maximum inlet horizontal velocity in Flambeau fire of Fig. 4

U = horizontal velocity scale

v = vertical velocity

v_0 = leading-order vertical velocity in $\epsilon \rightarrow 0$ limit

$v_0^{(II)}$ = v_0 solution in region II

v_i = correction vertical velocity in $\epsilon \rightarrow 0$ limit (integer i)

v_∞ = vertical velocity versus x profile at top of combustion zone

$v_{1/2}$ = correction vertical velocity in $\epsilon \rightarrow 0$ limit

x = horizontal position coordinate

\tilde{x} = rescaled horizontal coordinate

\hat{x} = rescaled horizontal coordinate

\bar{x} = rescaled horizontal coordinate

y = vertical position coordinate

\tilde{y} = rescaled vertical coordinate

y_∞ = maximum y value considered in numerical solution of leading-order combustion-layer problem

α = exponent such that the side-mixing-layer thickness is ϵ^α

$\hat{\alpha}$ = dimensionless parameter

β = dimensionless constant

$\hat{\beta}, \beta_0$ = dimensionless parameters

γ = specific heat ratio

Γ = dimensionless specific weight
 Γ_{∞} = dimensionless far-field ambient specific weight
 δ_1, δ_2 = dimensionless constants
 ϵ = combustion-zone aspect ratio
 η = horizontal coordinate of the side of the convection column (as a function of height)
 ρ = density
 ρ_a = ground-level atmospheric density in far field
 ρ_0 = leading-order density in $\epsilon \rightarrow 0$ limit
 ρ_i = correction density in $\epsilon \rightarrow 0$ limit (integer i)
 ρ_{∞} = total far-field ambient density through five orders in ϵ ($\epsilon \rightarrow 0$ limit)
 σ = Stefan's constant
 $\hat{\sigma}$ = dimensionless constant
 ϕ_m = mass fraction of species m in air, where m represents oxygen, carbon monoxide, carbon dioxide, or smoke (particulates)
 $\hat{\phi}$ = derivative with respect to y of the dimensionless inlet vertical velocity
 ω = relaxation factor in overall FIRE/FIRE2 code iteration

SYMBOLS* USED IN DOCUMENTATION OF THE COMBUSTION LAYER ALGORITHM

\hat{A} = product of A and B
 $\vec{F}, \vec{G}, \vec{H}$ = vectors of functions that are to be driven to zero (by the proper choice of \vec{x}) in Newton iterations, and that represent discretized model equations on individual lines of constant y

*Mathematical variables only--not FORTRAN labels.

$G_i, H_i = i\text{th}$ components of \vec{G} and \vec{H}

$i = \text{horizontal position index } (1 \leq i \leq M + 1)$

$j = \text{vertical position index } (1 \leq j \leq N + 1)$

$J = \frac{\partial \vec{F}}{\partial \vec{x}}$ Jacobian matrix

$M, N = \text{number of finite-difference cells in the horizontal and vertical directions}$

$\bar{M} = (M + 1)$ for condition in Eq. (C.3), and M for Eq. (C.4)

$\hat{P}_1 = \text{rescaling of } P_1$

$P_{1,j} = \hat{P}_1(x_i, y_j)$

$R_i = \text{sum of all terms in } G_i \text{ for any line } y = y_j, j \text{ fixed, that depend only on } y = y_{j-1} \text{ data}$

$\vec{T} = \text{vector of discrete } T_0 \text{ values for a line of constant } y$

$T_{i,j} = T_0(x_i, y_j)$

$\vec{u} = \text{vector of discrete } u_0 \text{ values for a line of constant } y$

$u_{i,j} = u_0(x_i, y_j)$

$v_{i,j} = v_0(x_i, y_j)$

$w_{1,j} = \text{generic finite-difference variable (for all } i, j)$

$\vec{x} = \text{vector of discrete } u_0 \text{ and } T_0 \text{ values for a line of constant } y$

$\tilde{x}_i = i\text{th component of } \vec{x}$

$x_i = (i - 1)(\Delta x)$

$y_j = (j - 1)(\Delta y)$

$\alpha_{i,j} = \text{nonzero element in the } \frac{\partial \vec{G}}{\partial \vec{u}} \text{ Jacobian } (0 \leq i \leq 2, 1 \leq j \leq \bar{M} - 1)$

$\beta_{i,j} = \text{nonzero element in the } \frac{\partial \vec{G}}{\partial \vec{T}} \text{ Jacobian } (0 \leq i \leq 2, 1 \leq j \leq M - 1)$

$\gamma_{i,j}$ = nonzero element in the $\frac{\partial \vec{H}}{\partial \vec{u}}$ Jacobian ($0 \leq i \leq 2$,
 $1 \leq j \leq \bar{M} - 1$)

$\delta_{i,j}$ = nonzero element in the $\frac{\partial \vec{H}}{\partial T}$ Jacobian ($0 \leq i \leq 2$,
 $1 \leq j \leq M - 1$)

$\vec{\delta}$ = vector difference between successive values of \vec{x}
in Newton iterations

$\Delta x, \Delta y$ = horizontal and vertical mesh widths

II_i = sum of all terms in H_i for any line $y = y_j$, j
fixed, that depend only on $y = y_{j-1}$ data

Appendix B

ANALYTIC DEVELOPMENT FOR CONVECTION COLUMN MODEL

The order estimates in Eq. (2.18) result directly from using the conventional mixing-length approximation

$$\frac{\mathcal{E}_{11}}{\rho_a}, \frac{\mathcal{E}_{12}}{\rho_a}, \frac{K_1}{\rho_a} \sim \ell^2 \left(\frac{\partial v}{\partial x} \right), \quad (\text{B.1})$$

where ℓ is the mixing length. Subject to the parameter definitions in Eq. (2.4) and the scalings in Eq. (2.2), then (for $j = 1, 2$) in nondimensional variables

$$\frac{M_{1j}}{\epsilon}, \frac{K_1}{\epsilon} \sim \left(\frac{1}{U\epsilon D} \right) \left[\ell^2 \left(\frac{\epsilon U}{D} \right) \left(\frac{\partial v}{\partial x} \right) \right] \sim \left(\frac{\ell}{D} \right)^2. \quad (\text{B.2})$$

Recalling that $D \sim 10^4$ m and assuming a mixing length $\ell \lesssim 10^3$ m, we obtain the first part of Eq. (2.18). The second part then follows from the fact that the horizontal turbulence effects must dominate for the basically upward column flow.

The leading-order equations in Eq. (2.28) for the side mixing layer are derived as follows. Subject to Eq. (2.18) and the rescaling in Eq. (2.27), Eq. (2.17) becomes

$$\begin{aligned} & \left(\frac{1}{\sqrt{\epsilon}} \right) \left[\frac{\partial}{\partial \tilde{x}} (\rho \tilde{u}) - \left(\frac{d\eta}{d\tilde{y}} \right) \frac{\partial}{\partial \tilde{x}} (\rho v) \right] + \frac{\partial}{\partial \tilde{y}} (\rho v) = 0 ; \\ & \rho \left\{ \left(\frac{1}{\sqrt{\epsilon}} \right) \left[\tilde{u} \frac{\partial \tilde{u}}{\partial \tilde{x}} - \left(\frac{d\eta}{d\tilde{y}} \right) v \frac{\partial u}{\partial \tilde{x}} \right] + v \frac{\partial \tilde{u}}{\partial \tilde{y}} \right\} = - \frac{B}{\epsilon^{7/2}} \frac{\partial P}{\partial \tilde{x}} + \left(\frac{M_{11}}{\epsilon^2} \right) \left[\frac{\partial^2 \tilde{u}}{\partial \tilde{x}^2} + o(1) \right] ; \\ & \rho \left\{ \left(\frac{1}{\sqrt{\epsilon}} \right) \left[\tilde{u} \frac{\partial v}{\partial \tilde{x}} - \left(\frac{d\eta}{d\tilde{y}} \right) v \frac{\partial v}{\partial \tilde{x}} \right] + v \frac{\partial v}{\partial \tilde{y}} \right\} = - \frac{B}{\epsilon^3} \left(\frac{\partial P}{\partial \tilde{y}} + A\rho \right) + \left(\frac{M_{21}}{\epsilon^2} \right) \left[\frac{\partial^2 \tilde{v}}{\partial \tilde{x}^2} + o(1) \right] ; \end{aligned}$$

$$\rho \left\{ \left(\frac{1}{\sqrt{\epsilon}} \right) \left[\tilde{u} \frac{\partial T}{\partial \tilde{x}} - \left(\frac{d\eta}{d\tilde{y}} \right) v \frac{\partial T}{\partial \tilde{x}} \right] + v \frac{\partial T}{\partial \tilde{y}} \right\} = \left(\frac{\gamma - 1}{\gamma} \right) \left\{ \left(\frac{1}{\sqrt{\epsilon}} \right) \left[\tilde{u} \frac{\partial P}{\partial \tilde{x}} - \left(\frac{d\eta}{d\tilde{y}} \right) v \frac{\partial P}{\partial \tilde{x}} \right] + v \frac{\partial P}{\partial \tilde{y}} \right\} + \left(\frac{K_1}{\epsilon^2} \right) \left[\frac{\partial^2 T}{\partial \tilde{x}^2} + o(1) \right] ;$$

$$P = \rho T . \quad (B.3)$$

Substituting the expansions for \tilde{u} and v in Eq. (2.29) and those for P , ρ , and T in Eq. (2.10) into Eq. (B.3), it is found that ρ_0 , T_0 , P_0 , ρ_1 , T_1 , P_1 , ρ_2 , T_2 , and P_2 are all functions of \tilde{y} alone, and hence (from the continuity equation)

$$\rho_0(\tilde{y}) \frac{\partial}{\partial \tilde{x}} \left[u_1 - \left(\frac{d\eta}{d\tilde{y}} \right) v_0 \right] = 0 . \quad (B.4)$$

The quantity $[u_1 - \left(\frac{d\eta}{d\tilde{y}} \right) v_0]$ is thus also a function of \tilde{y} alone and, in particular, must (for a matching of region II and IIA solutions) be

$$\lim_{x \rightarrow \eta(\tilde{y})} \left[u_1 - \left(\frac{d\eta}{d\tilde{y}} \right) v_0 \right]_{\text{region II}} .$$

But this limit must actually be zero for all \tilde{y} , since the $x = \eta(\tilde{y})$ streamline is defined by

$$\frac{d\eta}{d\tilde{y}} = \lim_{x \rightarrow \eta(\tilde{y})} \left[\left(\frac{u_1}{v_0} \right) \right]_{\text{region II}} .$$

Thus

$$u_1 = \left(\frac{d\eta}{d\tilde{y}} \right) v_0 , \quad (B.5)$$

and the other leading-order equations in region II become [using Eqs. (2.10) and (2.29) in Eq. (B.3)]

$$\frac{\partial P_3}{\partial \tilde{x}} = 0 ;$$

$$\begin{aligned} \rho_0 \left\{ \left[u_{3/2} - \left(\frac{d\eta}{d\tilde{y}} \right) v_{1/2} \right] \frac{\partial v_0}{\partial \tilde{x}} + v_0 \frac{\partial v_0}{\partial \tilde{y}} \right\} &= -B \left(\frac{\partial P_3}{\partial \tilde{y}} + A\rho \right) + \tilde{M}_{21} \frac{\partial^2 v_0}{\partial \tilde{x}^2} ; \\ \rho_0 \left\{ \left[u_{3/2} - \left(\frac{d\eta}{d\tilde{y}} \right) v_{1/2} \right] \frac{\partial T_3}{\partial \tilde{x}} + v_0 \frac{\partial T_3}{\partial \tilde{y}} \right\} &= \left(\frac{\gamma - 1}{\gamma} \right) \left\{ \left[u_{3/2} - \left(\frac{d\eta}{d\tilde{y}} \right) v_{1/2} \right] \frac{\partial P_3}{\partial \tilde{x}} + v_0 \frac{\partial P_3}{\partial \tilde{y}} \right\} \\ &\quad + \tilde{K}_1 \frac{\partial^2 T_3}{\partial \tilde{x}^2} - v_0 \left(\rho_1 \frac{dT_2}{d\tilde{y}} + \rho_2 \frac{dT_1}{d\tilde{y}} + \rho_3 \frac{dT_0}{d\tilde{y}} \right) ; \end{aligned}$$

$$P_3 = \rho_0 T_3 + \rho_1 T_2 + \rho_2 T_1 + \rho_3 T_0 , \quad (B.6)$$

with \tilde{M}_{21} and \tilde{K}_1 as defined in Eq. (2.31). Finally, the first correction to the leading-order continuity equation [Eq. (B.4)] is then

$$\frac{\partial}{\partial \tilde{x}} \left\{ \rho_0 \left[u_{3/2} - \left(\frac{d\eta}{d\tilde{y}} \right) v_{1/2} \right] \right\} + \frac{\partial}{\partial \tilde{y}} (\rho_0 v_0) = 0 . \quad (B.7)$$

Equations (B.4) and (B.7) and the final three equations in Eq. (B.6) [with $(\partial P_3 / \partial \tilde{x}) = 0$] are equivalent to Eq. (2.28) once the definition of Eq. (2.30) is made.

Appendix C

ALGORITHM DOCUMENTATION

The construction of the solution algorithm for the combustion-layer boundary-value problem depends on the form of the inlet boundary condition [cf. Eqs. (3.5) and (3.6)]. In the general case [Eq. (3.5)], an additional difference equation is required on each line of constant y , necessitating an expanded variable matrix. For convenience, separate codes were written to account for the slight differences in logic. Both algorithms provide numerical solutions to

$$\frac{\partial}{\partial x} (\rho_0 u_0) + \frac{\partial}{\partial y} (\rho_0 v_0) = 0 ;$$

$$\rho_0 \left(u_0 \frac{\partial u_0}{\partial x} + v_0 \frac{\partial u_0}{\partial y} \right) = - \frac{\partial \hat{P}_1}{\partial x} + M_{11} \frac{\partial^2 u_0}{\partial x^2} ;$$

$$\frac{\partial \hat{P}_1}{\partial y} + \hat{A} \rho_0 = 0 ;$$

$$\rho_0 \left(u_0 \frac{\partial T_0}{\partial x} + v_0 \frac{\partial T_0}{\partial y} \right) = q(x, y) - \sigma(T_0^4 - 1) + K_1 \frac{\partial^2 T_0}{\partial x^2} ;$$

$$\rho_0 T_0 = 1 , \tag{C.1}$$

subject to

- a. along $y = 0$, $v_0 = 0$,
- b. along $x = 0$, $u_0 = \frac{\partial T_0}{\partial x} = 0$,
- c. as $y \rightarrow \infty$, $\frac{\partial \hat{P}_1}{\partial x} \rightarrow 0$,
- d. along $x = 1$, $T_0 = 1$, (C.2)

with different versions for

$$\text{i. along } x = 1, \quad \frac{\partial}{\partial x} (\rho_0 u_0) = \hat{\phi}(y) + \beta_0 u, \quad (\text{C.3})$$

$$\text{ii. along } x = 1, \quad u_0 = \hat{g}(y). \quad (\text{C.4})$$

For convenience, $P_1(x, y)$ and A have been rescaled as

$$\hat{P}_1 = BP_1; \quad \hat{A} = BA. \quad (\text{C.5})$$

As shown in the flowchart in Fig. 6 (p. 35), the codes use an iterative "shooting" method [Keller, 1968] to solve the overall boundary value problem, each "shoot" employing a nonlinear Crank-Nicolson finite-difference scheme.

INPUTS AND OUTPUTS

The following is an ordered list of the (FORTRAN) inputs for the code corresponding to Eq. (C.3):

a. System parameters:

A	\hat{A} [in Eq. (C.5)]
SIGMA	σ
XNUIN	M_{11}
XKIN	K_1

b. Mesh descriptors:

YMAX	y_∞
M	Number of finite difference cells in horizontal direction.*
N	Number of finite difference cells in vertical direction.*

c. Iteration parameters:

ETLINE	Maximum absolute error allowed in solving discretized (Crank-Nicolson) equations on any line of constant y .
ETOLP	Maximum absolute error allowed in $\partial \hat{P}_1 / \partial x$ on $y = y_\infty$.

* Mesh widths and heights are individual constants.

MAXITL Maximum number of (Newton) iterations allowed in solving discretized equations on any line of constant y .
 MAXITP Maximum number of (complete shoot) iterations allowed in solving the complete boundary value problem.

d. Boundary condition parameters:

ALPHA/BETA $\hat{\alpha}$ and $\hat{\beta}$, parameters that define $\hat{\phi}(y)$ as

$$\hat{\phi}(y) = -\hat{\beta} \operatorname{sech}^2\left(\frac{\hat{\beta}}{\hat{\alpha}}\right) y \quad (\text{C.6})$$

for the case $\beta_0 = 0$ and $v_0(1, y)$ as specified in Eq. (3.4) [cf. Eq. (3.6)].

BLOSS β_0

IGUESS Parameter that controls the specification of the (first shoot, $y = 0$) initial guesses for I GUESS = 1, 2, or 3:

1. Discretized versions of $\hat{P}_1(x, 0)$, $T_0(x, 0)$, and $u_0(x, 0)$ must also be supplied as inputs.
2. A discretized version of $\hat{P}_1(x, 0)$ must also be supplied, but "standard" specifications of $T_0(x, 0)$ and $u_0(x, 0)$ are automatically made. ("Standard" specifications may of course be modified by reprogramming.)
3. "Standard" initial guesses are made for all variables.

Additionally, the functional form of $q(x, y)$ must be prescribed. Currently, this is given by

$$q(x, y) = \begin{cases} 1 & \text{for } 0 \leq x \leq 1, \quad 0 \leq y \leq 1 \\ 0 & \text{otherwise} \end{cases} \quad (\text{C.7})$$

Changes require reprogramming (in subroutine BCFUNC). Finally, as an added option, the dissipation coefficients M_{11} and K_1 may also be made to depend on x and y via reprogramming (also in BCFUNC). Currently, those coefficients are simply taken as constants.

A sample input data stream is

A = 0.16 , SIGMA = 0.023 , XNUIN = XKIN = 0.5 ;
 YMAX = 6 , M = 40 , N = 400 ;
 ETLINE = 0.001 , ETOLP = 0.005 , MAXITL = MAXITP = 20 ;
 ALPHA = 1.0 , BETA = 1.5 , BLOSS = 0.0 , IGUESS = 2 ;

with $\hat{\phi}(y)$ as in Eq. (C.6). The corresponding output is listed in Table C.1. With IGUESS = 2, $\hat{P}_1(x, 0)$, data similar to those in the J = 1 (y = 0.0) printout were used to generate the output. The other, "standard" initial function guesses were

$$T_0(x, 0) = 1.76 - 0.6x, \quad u_0(x, 0) = 1.9 \tanh(1.6x) .$$

Additionally, all output data are automatically dumped onto a disk file from which are made the vector, contour, and profile plots displayed in Sec. III.

Inputs and corresponding outputs for both codes are almost identical. The only change is that the functional form of $u(1, y)$ must be prescribed (in subroutine BCFUNC) when Eq. (C.4) is used, whereas ALPHA, BETA, and BLOSS are used to describe $\frac{\partial}{\partial x} (\rho_0 u_0)$ when Eq. (C.3) is used.

PROGRAM FLOW

A macro flowchart for both codes is given in Fig. 6 (p. 35). A flowchart for the main program is presented in Fig. C.1. Inputs/outputs and the overall shooting iteration are controlled by the main program. In subroutine BCFUNC, functional forms that may be varied [e.g., $q(x, y)$] are specified; and in subroutine SPRINT, final output data are printed. In subroutine MSWEEP, most of the computations--those providing a (one shoot) finite difference solution to Eq. (3.1) for given data along $y = 0$, $x = 0$, and $x = 1$ (only)--are carried out. The flow of that subroutine is shown in Figs. C.3 and C.4 below (pp. 124-125) and details of the underlying numerical analysis presented in the accompanying text. Complete FORTRAN listings of all subroutines and main programs are presented at the end of this appendix.

Table C.1
SAMPLE FIRE CODE OUTPUT

FIRE: SOLUTION OF COMBUSTION LAYER BOUNDARY VALUE PROBLEM

SYSTEM PARAMETERS: A = 0.160 SIGMA = 0.023 NU = 0.500 K = 0.500
 MESH: M = 40 DX = 0.025 N = 400 DY = 0.025
 ITERATION PARAMETERS: ETLINE = 0.001000 MAXITL = 20 ETOLP = 0.005000 MAXITP = 20
 INLET PARAMETERS: ALPHA = 1.000 BETA = 1.500 BLOSS = 0.000

FOR J = 1 (Y = 0.000):

I	X	U	V	T	RHO	P	PX	NU*UXX	K*TXK	Q(T)
1	0.000	0.000	0.000	1.519	0.658	-0.155	0.000	0.000	0.000	0.900
2	0.025	-0.083	0.000	1.519	0.658	-0.155	0.004	0.185	-0.899	0.900
3	0.050	-0.165	0.000	1.518	0.659	-0.155	0.015	0.374	-0.894	0.901
4	0.075	-0.248	0.000	1.516	0.660	-0.155	0.024	0.558	-0.883	0.901
5	0.100	-0.329	0.000	1.513	0.661	-0.154	0.033	0.737	-0.869	0.903
6	0.125	-0.410	0.000	1.508	0.663	-0.153	0.043	0.912	-0.851	0.904
7	0.150	-0.489	0.000	1.503	0.665	-0.152	0.054	1.079	-0.826	0.906
8	0.175	-0.567	0.000	1.496	0.668	-0.150	0.062	1.233	-0.802	0.908
9	0.200	-0.643	0.000	1.489	0.672	-0.149	0.071	1.378	-0.771	0.910
10	0.225	-0.718	0.000	1.480	0.676	-0.147	0.081	1.515	-0.739	0.913
11	0.250	-0.791	0.000	1.471	0.680	-0.145	0.089	1.635	-0.703	0.915
12	0.275	-0.862	0.000	1.461	0.685	-0.142	0.097	1.743	-0.666	0.918
13	0.300	-0.931	0.000	1.449	0.690	-0.140	0.107	1.841	-0.625	0.921
14	0.325	-0.997	0.000	1.437	0.696	-0.137	0.117	1.925	-0.584	0.925
15	0.350	-1.061	0.000	1.425	0.702	-0.134	0.124	1.991	-0.542	0.928
16	0.375	-1.122	0.000	1.412	0.708	-0.131	0.131	2.045	-0.497	0.932
17	0.400	-1.181	0.000	1.398	0.716	-0.127	0.139	2.097	-0.455	0.935
18	0.425	-1.238	0.000	1.383	0.723	-0.124	0.147	2.114	-0.410	0.939
19	0.450	-1.291	0.000	1.368	0.731	-0.120	0.154	2.129	-0.366	0.942
20	0.475	-1.342	0.000	1.353	0.739	-0.116	0.160	2.131	-0.323	0.946
21	0.500	-1.391	0.000	1.337	0.748	-0.112	0.169	2.126	-0.282	0.950
22	0.525	-1.436	0.000	1.320	0.757	-0.108	0.175	2.103	-0.240	0.953
23	0.550	-1.479	0.000	1.304	0.767	-0.103	0.182	2.077	-0.201	0.957
24	0.575	-1.520	0.000	1.287	0.777	-0.099	0.188	2.038	-0.162	0.960
25	0.600	-1.558	0.000	1.270	0.787	-0.094	0.194	1.991	-0.127	0.963
26	0.625	-1.593	0.000	1.253	0.798	-0.089	0.201	1.940	-0.091	0.966
27	0.650	-1.626	0.000	1.236	0.809	-0.084	0.204	1.979	-0.059	0.969
28	0.675	-1.657	0.000	1.218	0.821	-0.079	0.211	1.814	-0.029	0.972
29	0.700	-1.685	0.000	1.201	0.833	-0.073	0.219	1.749	-0.001	0.975
30	0.725	-1.711	0.000	1.184	0.845	-0.068	0.220	1.675	0.024	0.978
31	0.750	-1.735	0.000	1.166	0.857	-0.062	0.225	1.599	0.050	0.980
32	0.775	-1.757	0.000	1.149	0.870	-0.057	0.231	1.525	0.070	0.983
33	0.800	-1.779	0.000	1.132	0.883	-0.051	0.239	1.449	0.092	0.985
34	0.825	-1.796	0.000	1.115	0.897	-0.045	0.240	1.368	0.109	0.987
35	0.850	-1.813	0.000	1.098	0.911	-0.039	0.244	1.292	0.124	0.990
36	0.875	-1.828	0.000	1.081	0.925	-0.033	0.252	1.217	0.138	0.992
37	0.900	-1.841	0.000	1.064	0.939	-0.026	0.255	1.143	0.149	0.993
38	0.925	-1.853	0.000	1.048	0.954	-0.020	0.258	1.066	0.160	0.995
39	0.950	-1.864	0.000	1.032	0.969	-0.013	0.261	0.994	0.167	0.997
40	0.975	-1.874	0.000	1.016	0.984	-0.007	0.267	0.927	0.175	0.999
41	1.000	-1.882	0.000	1.000	1.000	0.000	0.270	0.927	0.175	1.000

Table C.1--Continued

FOR J = 2 (Y = 0.025):

I	X	U	V	T	RHO	P	PX	NU*UXX	K*TX	Q(T)
1	0.000	0.000	0.083	1.520	0.658	-0.158	0.000	0.000	0.000	0.900
2	0.025	-0.082	0.083	1.520	0.658	-0.158	0.004	0.183	-0.896	0.900
3	0.050	-0.165	0.082	1.519	0.659	-0.158	0.015	0.371	-0.890	0.901
4	0.075	-0.246	0.082	1.516	0.660	-0.157	0.024	0.553	-0.880	0.901
5	0.100	-0.327	0.082	1.513	0.661	-0.157	0.032	0.731	-0.867	0.903
6	0.125	-0.407	0.081	1.509	0.663	-0.156	0.043	0.903	-0.846	0.904
7	0.150	-0.486	0.080	1.503	0.665	-0.155	0.054	1.069	-0.828	0.906
8	0.175	-0.564	0.080	1.497	0.668	-0.153	0.062	1.222	-0.798	0.908
9	0.200	-0.640	0.079	1.489	0.672	-0.151	0.070	1.366	-0.770	0.910
10	0.225	-0.714	0.078	1.481	0.675	-0.150	0.080	1.501	-0.738	0.913
11	0.250	-0.787	0.077	1.471	0.680	-0.147	0.088	1.621	-0.703	0.915
12	0.275	-0.857	0.076	1.461	0.685	-0.145	0.096	1.729	-0.664	0.918
13	0.300	-0.926	0.075	1.450	0.690	-0.143	0.106	1.825	-0.627	0.921
14	0.325	-0.992	0.073	1.438	0.695	-0.140	0.116	1.908	-0.584	0.925
15	0.350	-1.055	0.072	1.425	0.702	-0.137	0.123	1.978	-0.542	0.929
16	0.375	-1.116	0.071	1.412	0.708	-0.134	0.130	2.029	-0.500	0.932
17	0.400	-1.175	0.069	1.398	0.715	-0.130	0.137	2.071	-0.455	0.935
18	0.425	-1.231	0.068	1.384	0.723	-0.127	0.146	2.100	-0.413	0.939
19	0.450	-1.284	0.067	1.369	0.731	-0.123	0.152	2.116	-0.368	0.942
20	0.475	-1.335	0.065	1.353	0.739	-0.119	0.159	2.119	-0.327	0.946
21	0.500	-1.383	0.064	1.337	0.748	-0.115	0.167	2.110	-0.284	0.950
22	0.525	-1.429	0.062	1.321	0.757	-0.111	0.173	2.094	-0.243	0.953
23	0.550	-1.472	0.061	1.305	0.767	-0.106	0.181	2.065	-0.203	0.956
24	0.575	-1.512	0.059	1.288	0.777	-0.102	0.187	2.028	-0.166	0.960
25	0.600	-1.550	0.057	1.271	0.787	-0.097	0.192	1.983	-0.128	0.963
26	0.625	-1.585	0.056	1.254	0.798	-0.092	0.199	1.931	-0.095	0.966
27	0.650	-1.618	0.054	1.236	0.809	-0.087	0.202	1.870	-0.063	0.969
28	0.675	-1.648	0.053	1.219	0.820	-0.082	0.209	1.810	-0.031	0.972
29	0.700	-1.677	0.052	1.202	0.832	-0.077	0.216	1.743	-0.003	0.975
30	0.725	-1.703	0.050	1.184	0.844	-0.071	0.218	1.668	0.021	0.978
31	0.750	-1.727	0.049	1.167	0.857	-0.066	0.223	1.597	0.047	0.980
32	0.775	-1.749	0.047	1.150	0.870	-0.060	0.229	1.520	0.068	0.983
33	0.800	-1.769	0.046	1.132	0.883	-0.054	0.235	1.447	0.088	0.985
34	0.825	-1.787	0.045	1.115	0.897	-0.048	0.237	1.366	0.105	0.987
35	0.850	-1.804	0.044	1.098	0.911	-0.042	0.241	1.289	0.122	0.990
36	0.875	-1.819	0.042	1.081	0.925	-0.036	0.249	1.218	0.134	0.992
37	0.900	-1.832	0.041	1.065	0.939	-0.030	0.253	1.141	0.148	0.993
38	0.925	-1.844	0.040	1.048	0.954	-0.024	0.255	1.067	0.156	0.995
39	0.950	-1.855	0.039	1.032	0.969	-0.017	0.259	0.996	0.166	0.997
40	0.975	-1.864	0.038	1.016	0.984	-0.011	0.264	0.926	0.173	0.999
41	1.000	-1.873	0.037	1.000	1.000	-0.004	0.267	0.926	0.173	1.000

Table C.1--Continued

•
•
•

FOR J = 401 (Y = 10.000):

I	X	U	V	Y	RHO	P	PX	NU*UXX	K*TX	Q(T)
1	0.000	0.000	3.525	1.004	0.996	-1.600	0.000	0.000	0.000	0.000
2	0.025	0.000	3.521	1.004	0.996	-1.600	0.000	0.000	-0.006	0.000
3	0.050	0.000	3.511	1.004	0.996	-1.600	0.001	0.002	-0.005	0.000
4	0.075	-0.001	3.495	1.004	0.996	-1.600	0.000	0.001	-0.006	0.000
5	0.100	-0.001	3.473	1.004	0.996	-1.600	-0.001	0.001	-0.004	0.000
6	0.125	-0.001	3.446	1.004	0.996	-1.600	0.000	0.002	-0.005	0.000
7	0.150	-0.001	3.413	1.004	0.996	-1.600	0.002	0.004	-0.005	0.000
8	0.175	-0.001	3.375	1.004	0.996	-1.600	0.001	0.003	-0.006	0.000
9	0.200	-0.001	3.331	1.004	0.996	-1.600	0.000	0.003	-0.005	0.000
10	0.225	-0.002	3.283	1.004	0.996	-1.600	0.001	0.004	-0.005	0.000
11	0.250	-0.002	3.230	1.004	0.996	-1.600	0.000	0.004	-0.005	0.000
12	0.275	-0.002	3.174	1.004	0.996	-1.600	-0.001	0.003	-0.005	0.000
13	0.300	-0.002	3.113	1.003	0.997	-1.600	0.001	0.005	-0.005	0.000
14	0.325	-0.002	3.047	1.003	0.997	-1.600	0.002	0.006	-0.004	0.000
15	0.350	-0.002	2.978	1.003	0.997	-1.600	0.001	0.005	-0.005	0.000
16	0.375	-0.002	2.906	1.003	0.997	-1.600	0.000	0.005	-0.005	0.000
17	0.400	-0.003	2.832	1.003	0.997	-1.600	0.000	0.004	-0.003	0.000
18	0.425	-0.003	2.755	1.003	0.997	-1.600	0.001	0.006	-0.003	0.000
19	0.450	-0.003	2.676	1.003	0.997	-1.600	0.000	0.005	-0.004	0.000
20	0.475	-0.003	2.595	1.003	0.997	-1.600	0.000	0.004	-0.002	0.000
21	0.500	-0.003	2.512	1.003	0.997	-1.600	0.001	0.006	-0.004	0.000
22	0.525	-0.003	2.428	1.003	0.997	-1.600	0.000	0.005	-0.002	0.000
23	0.550	-0.003	2.343	1.002	0.998	-1.600	0.001	0.006	-0.002	0.000
24	0.575	-0.003	2.258	1.002	0.998	-1.600	0.001	0.005	-0.002	0.000
25	0.600	-0.003	2.172	1.002	0.998	-1.600	0.000	0.005	-0.002	0.000
26	0.625	-0.003	2.086	1.002	0.998	-1.600	0.002	0.006	-0.002	0.000
27	0.650	-0.003	2.000	1.002	0.998	-1.600	-0.001	0.003	-0.002	0.000
28	0.675	-0.003	1.916	1.002	0.998	-1.600	0.000	0.005	-0.000	0.000
29	0.700	-0.004	1.831	1.002	0.998	-1.600	0.002	0.006	-0.002	0.000
30	0.725	-0.004	1.748	1.002	0.998	-1.600	-0.001	0.003	-0.002	0.000
31	0.750	-0.004	1.667	1.001	0.999	-1.600	-0.001	0.003	-0.001	0.000
32	0.775	-0.004	1.587	1.001	0.999	-1.600	0.000	0.004	-0.001	0.000
33	0.800	-0.004	1.508	1.001	0.999	-1.600	0.001	0.005	-0.002	0.000
34	0.825	-0.004	1.431	1.001	0.999	-1.600	-0.001	0.002	-0.001	0.000
35	0.850	-0.004	1.356	1.001	0.999	-1.600	-0.002	0.002	-0.003	0.000
36	0.875	-0.004	1.283	1.001	0.999	-1.600	0.002	0.005	0.002	0.000
37	0.900	-0.004	1.211	1.001	0.999	-1.600	0.001	0.004	-0.002	0.000
38	0.925	-0.004	1.142	1.000	1.000	-1.600	-0.002	0.001	-0.002	0.000
39	0.950	-0.004	1.076	1.000	1.000	-1.600	-0.002	0.000	-0.004	0.000
40	0.975	-0.004	1.013	1.000	1.000	-1.600	-0.001	0.001	-0.004	0.000
41	1.000	-0.004	0.961	1.000	1.000	-1.600	0.001	0.001	0.004	0.000

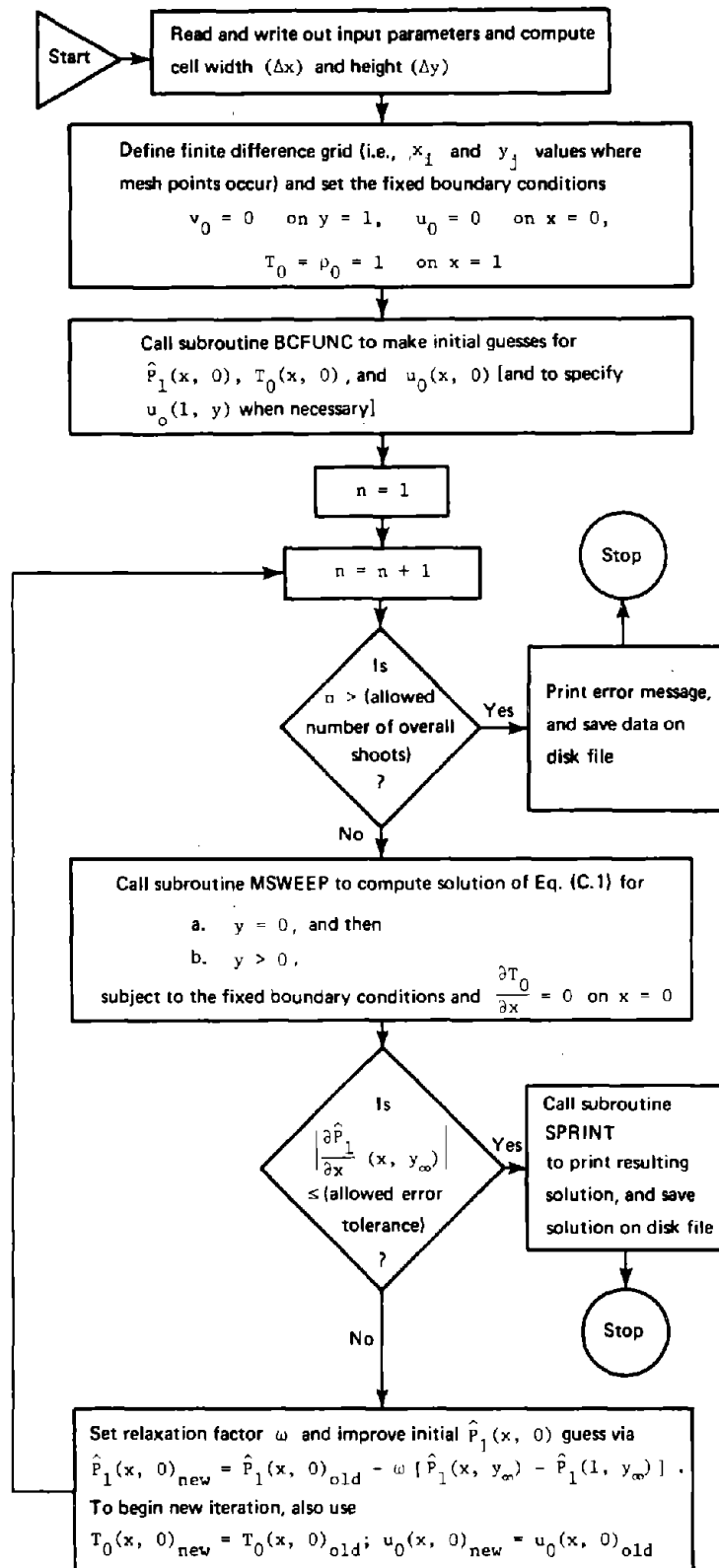


Fig. C.1--Flowchart of main program

FINITE DIFFERENCE ANALYSIS AND SUBROUTINE MSWEEP

The finite difference scheme underlying both codes is based on the rectangular grid (covering the combustion layer region) and "stencils" in Fig. C.2. The grid has uniform mesh widths ($\Delta x = 1/M$) and heights ($\Delta y = y_\infty/N$). Mesh points are thus located at (x_i, y_i) points with

$$\begin{aligned} x_i &= (i - 1)(\Delta x) , & \text{for } 1 \leq i \leq M + 1 , \\ y_i &= (j - 1)(\Delta y) , & \text{for } 1 \leq j \leq N + 1 , \end{aligned} \tag{C.8}$$

and dependent variables evaluated at those points are given corresponding (i, j) suffices. For example, then, $x_1 = 0$ (and not one), $y_{N+1} = y_\infty$, $u_{1,N+1} = u_0(0, y_\infty)$. The accurate approximation of $(u_{i,j}; v_{i,j}; P_{i,j}; T_{i,j}; \rho_{i,j})_{1 \leq i \leq M+1, 1 \leq j \leq N+1}$ constitutes a numerical solution of the problem posed by Eqs. (C.1) and (C.2) together with (C.3) or (C.4). The stencils in Fig. C.2, explained below, are indicative of the types of differencing used in the codes.

Along the $y = 0$ line (where $j = 1$), $v_0 \equiv 0$. As shown in Fig. C.1, a guess at \hat{P}_1 along this line [actually, the $\{P_{i1}\}_{i=1}^{M+1}$ values] is also made prior to the calling of the MSWEEP subroutine. As noted in the first large block of Fig. 6 (p. 35), Eqs. (C.1) and (C.2) then reduce along this line to the following (ordinary differential equation) boundary value problem for u_0 and T_0 alone (with $\rho_0 = 1/T_0$):

$$\begin{aligned} \left(\frac{u_0}{T_0}\right) \frac{\partial u_0}{\partial x} &= - \frac{\partial \hat{P}_1}{\partial x} + M_{11} \frac{\partial^2 u_0}{\partial x^2} ; \\ \left(\frac{u_0}{T_0}\right) \frac{\partial T_0}{\partial x} &= q(x, 0) - \sigma(T_0^4 - 1) + K_1 \frac{\partial^2 T_0}{\partial x^2} ; \\ u_0 = \frac{\partial T_0}{\partial x} &= 0 \quad \text{on} \quad x = 0 ; \end{aligned}$$

$T_0 = 1$ and either

$$\frac{\partial}{\partial x} \left(\frac{u_0}{T_0} \right) = \hat{\phi}(y) + \beta_0 u_0$$

$$\text{or } u_0 = \hat{g}(y)$$

(C.9)

on $x = 1$.

The standard finite-difference solution for this problem involves the solution of

$$\vec{F}(\vec{x}) = \vec{0}, \quad (C.10)$$

where

$$\vec{x} \equiv \begin{pmatrix} \tilde{x}_1 \\ \tilde{x}_2 \\ \tilde{x}_3 \\ \tilde{x}_4 \\ \vdots \\ \tilde{x}_{2M-3} \\ \tilde{x}_{2M-2} \\ \tilde{x}_{2M-1} \end{pmatrix} = \begin{pmatrix} u_{2,1} \\ T_{2,1} \\ u_{3,1} \\ T_{3,1} \\ \vdots \\ \vdots \\ u_{M,1} \\ T_{M,1} \\ u_{M+1,1} \end{pmatrix} \quad (C.11)$$

and the components of \vec{F} are the finite difference equations obtained from the discretization of Eq. (C.9). The Crank-Nicolson solution of Eq. (C.1)--subject to the solution of (C.9) [for given $\hat{P}_1(x, 0)$] and the $x = 0$ and $x = 1$ (only) boundary conditions in Eqs. (C.2) together with (C.3) or (C.4)--also involves the solution of Eq. (C.10) for successive j , $j = 2, 3, 4, \dots, N, N + 1$. For this, the components of \vec{F} are slightly different from those of $j = 1$; and for each fixed $j (\geq 2)$, \vec{x} is redefined [cf. Eq. (C.11)] as

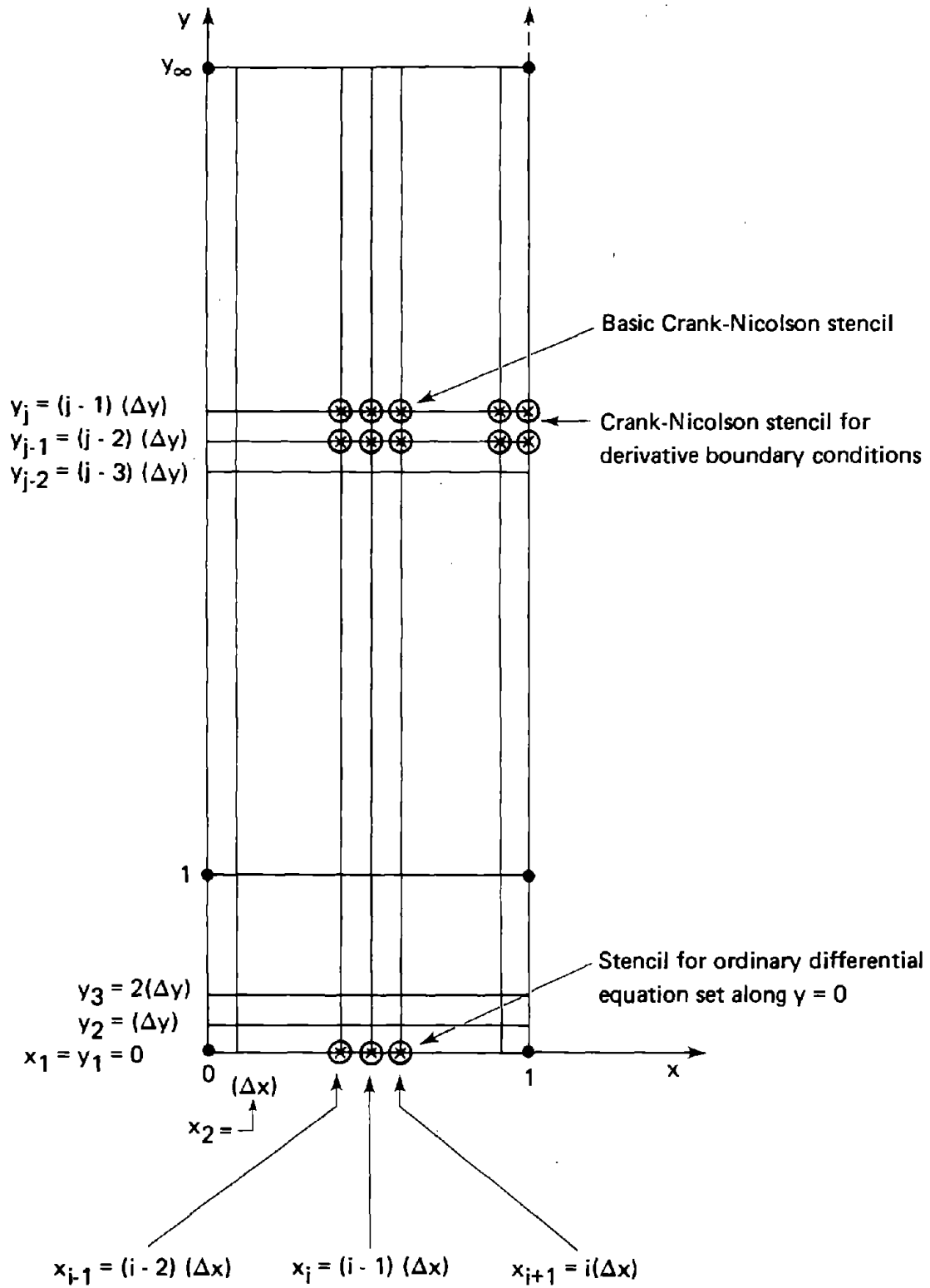


Fig. C.2--Finite difference grid and stencils for numerical solution of leading-order combustion-layer problem

$$\vec{x} \equiv \begin{pmatrix} \tilde{x}_1 \\ \tilde{x}_2 \\ \tilde{x}_3 \\ \tilde{x}_4 \\ \vdots \\ \vdots \\ \tilde{x}_{2M-3} \\ \tilde{x}_{2M-2} \\ \tilde{x}_{2M-1} \end{pmatrix} = \begin{pmatrix} u_{2,j} \\ T_{2,j} \\ u_{3,j} \\ T_{3,j} \\ \vdots \\ \vdots \\ u_{M,j} \\ T_{M,j} \\ u_{M+1,j} \end{pmatrix} \quad (C.12)$$

The overall flow in subroutine MSWEEP is thus as outlined in Fig. C.3, Newton's method (Fig. C.4) being used in all cases to solve the equations represented by Eq. (C.10) because they are nonlinear.

To fully describe subroutine MSWEEP, we must define the following processes:

1. The specific finite-difference reduction of Eqs. (C.9) and (C.2) through (C.10).
2. The corresponding specifications of $J (= \frac{\partial \vec{F}}{\partial \vec{x}})$.
3. The specific Gaussian elimination scheme used to compute $\vec{\delta}$ (as $-J^{-1}\vec{F}$).

For $j = 1$ (i.e., $y = 0$), the usual discretization for second-order ordinary differential equations is used to reduce Eq. (C.9) to Eq. (C.10). That is, for any dependent variable w , interior derivatives are replaced by the centered difference approximations

$$\begin{aligned} \left(\frac{\partial^2 w}{\partial x^2} \right)_{i,1} &\rightarrow \frac{w_{i+1,1} - 2w_{i,1} + w_{i-1,1}}{(\Delta x)^2} ; \\ \left(\frac{\partial w}{\partial x} \right)_{i,1} &\rightarrow \frac{w_{i+1,1} - w_{i-1,1}}{2(\Delta x)} ; \end{aligned} \quad (C.13)$$

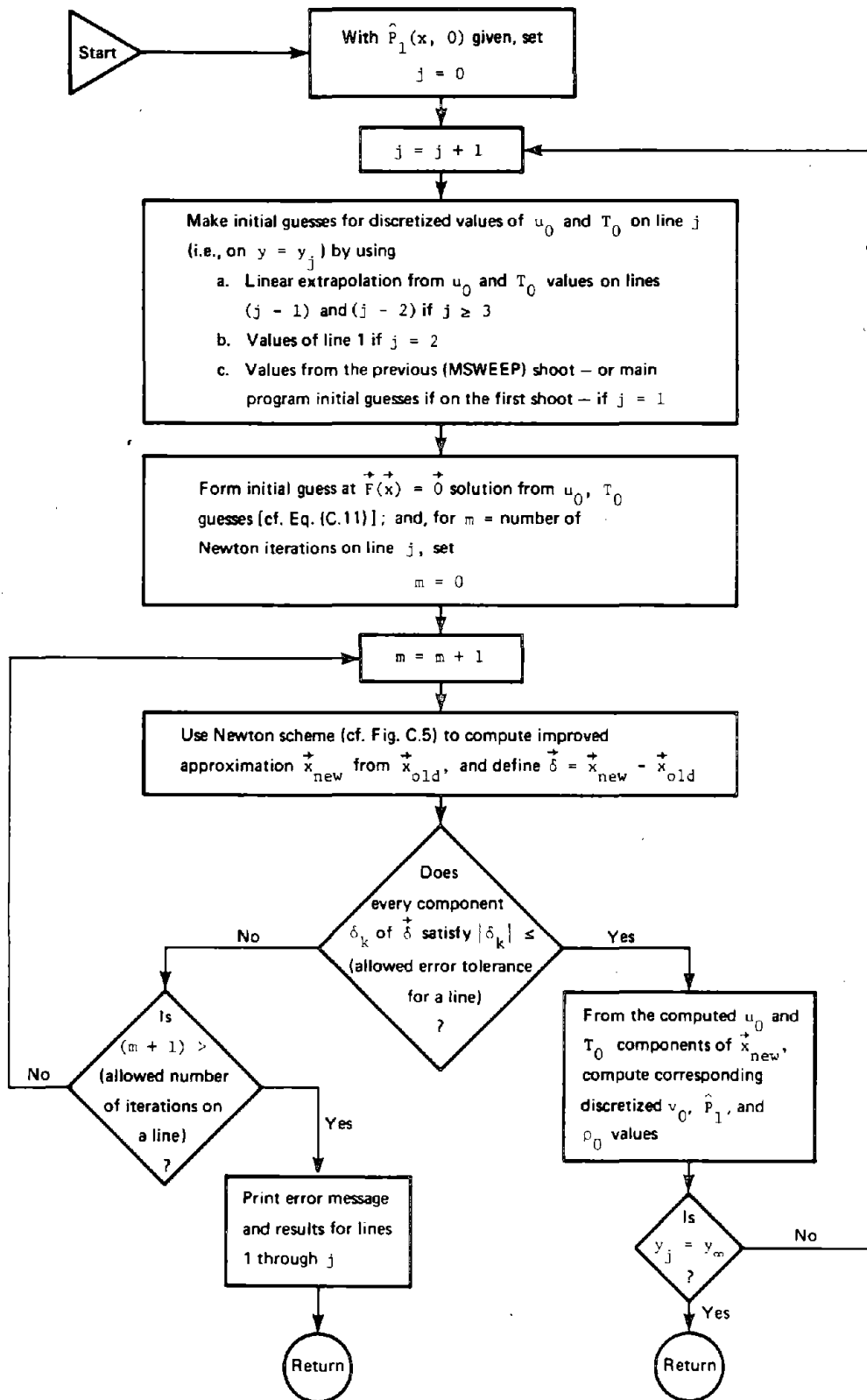


Fig. C.3--Macro flowchart of subroutine MSWEEP

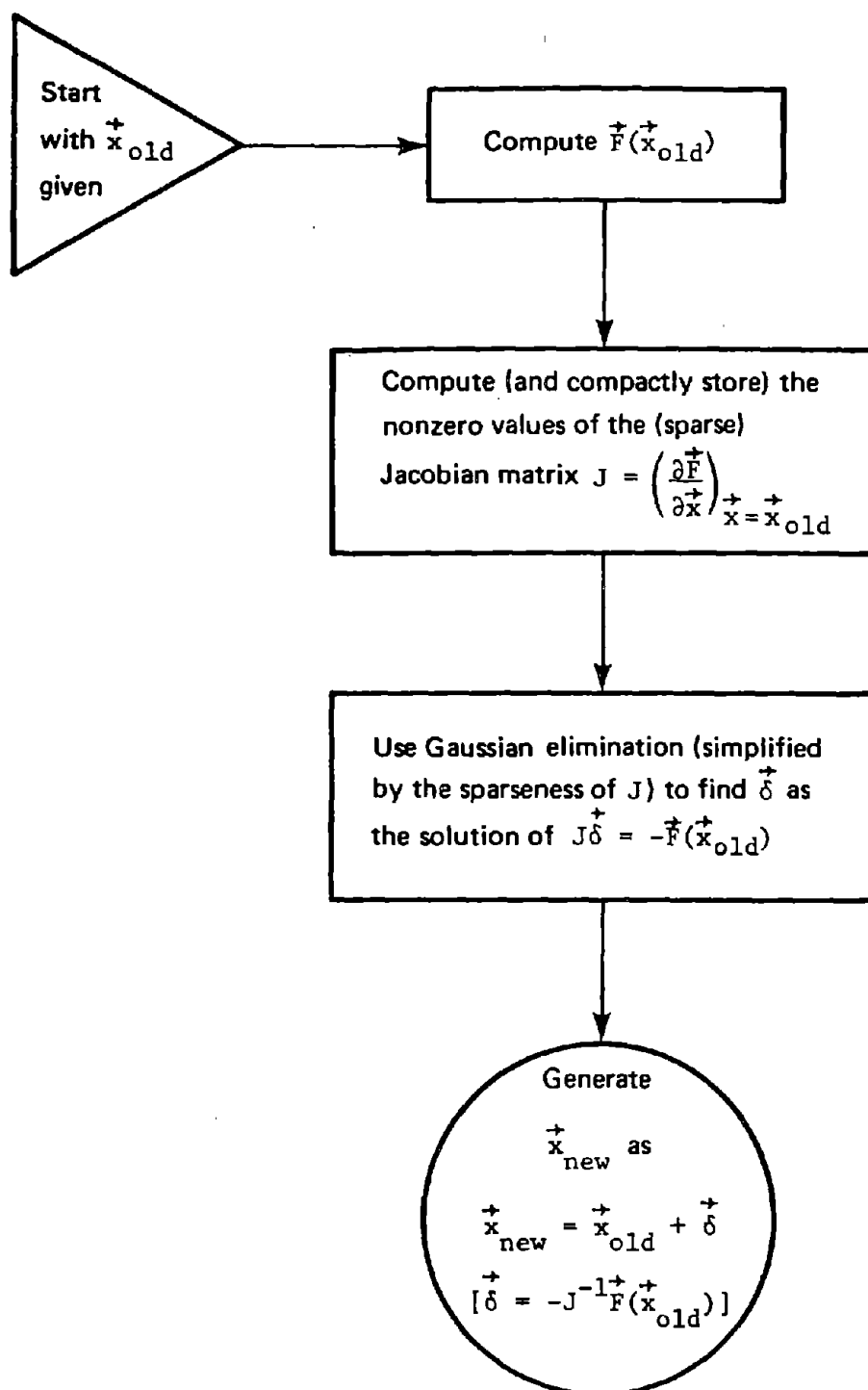


Fig. C.4--Flow diagram of basic Newton step used in subroutine MSWEEP

and boundary derivatives are taken as, for example,

$$\left(\frac{\partial w}{\partial x}\right)_{1,1} \rightarrow \frac{w_{2,1} - w_{1,1}}{(\Delta x)}. \quad (C.14)$$

As indicated by the corresponding discretization stencil at the bottom of Fig. C.2, no more than three values of u_0 and T_0 are thus involved in each component equation in Eq. (C.10) [cf. Eq. (C.11)]--and these values are at successive x_i . For each $j \geq 2$, the Crank-Nicolson scheme to be defined by Eqs. (C.15) and (C.16) is used to reduce Eqs. (C.1) and (C.2) together with (C.3) or (C.4), to Eq. (C.10). Centered differences are also used, with interior and boundary approximation stencils as shown in Fig. C.2, interior approximations being

$$\begin{aligned} \left(\frac{\partial^2 w}{\partial x^2}\right)_{i,j} &\rightarrow \frac{1}{2} \left[\frac{w_{i+1,j} - 2w_{i,j} + w_{i-1,j}}{(\Delta x)^2} + \frac{w_{i+1,j-1} - 2w_{i,j-1} + w_{i-1,j-1}}{(\Delta x)^2} \right]; \\ \left(\frac{\partial w}{\partial x}\right)_{i,j} &\rightarrow \frac{1}{2} \left[\frac{w_{i+1,j} - w_{i-1,j}}{2(\Delta x)} + \frac{w_{i+1,j-1} - w_{i-1,j-1}}{2(\Delta x)} \right]; \\ \left(\frac{\partial w}{\partial y}\right)_{i,j} &\rightarrow \left(\frac{w_{i,j} - w_{i,j-1}}{\Delta y} \right); \\ (w)_{i,j} &\rightarrow \frac{1}{2} (w_{i,j} + w_{i,j-1}); \end{aligned} \quad (C.15)$$

and the boundary formulas being of the form

$$\begin{aligned} \left(\frac{\partial w}{\partial x}\right)_{1,j} &\rightarrow \frac{1}{2} \left[\frac{w_{2,j} - w_{1,j}}{(\Delta x)} + \frac{w_{2,j-1} - w_{1,j-1}}{(\Delta x)} \right]; \\ (w)_{1,j} &\rightarrow \frac{1}{2} (w_{1,j} + w_{1,j-1}). \end{aligned} \quad (C.16)$$

As in linear problems [Isaacson and Keller, 1966], the scheme has proven to be convergent, stable, and accurate for both nonlinear formulations of the combustion-layer boundary-value problem.

In effecting the reduction of Eqs. (C.9), and (C.1) and (C.2) together with (C.3) or (C.4), to Eq. (C.10) by means of Eqs. (C.13) through (C.16), it proves convenient--both notationally and computationally--to begin by decomposing \vec{x} (for all j) into

$$\vec{u} = \begin{pmatrix} u_{2,j} \\ u_{3,j} \\ \vdots \\ \vdots \\ u_{M,j} \\ \text{---} \\ u_{M+1,j} \end{pmatrix} ; \quad \vec{T} = \begin{pmatrix} T_{2,j} \\ T_{3,j} \\ \vdots \\ \vdots \\ T_{M,j} \end{pmatrix} \quad (C.17)$$

and arranging the corresponding $\vec{F}(\vec{x})$ as

$$\vec{F} = \begin{pmatrix} G_2 \\ H_2 \\ G_3 \\ H_3 \\ \vdots \\ \vdots \\ G_M \\ H_M \\ \text{---} \\ G_{M+1} \end{pmatrix} , \quad (C.18)$$

where (for all relevant i) G_i and H_i represent the components that arise (as is shown below) basically from the discretization of the horizontal momentum and energy equations, respectively, about the

grid point (x_i, y_j) . As mentioned above, centered differencing results in each G_i and H_i involving at most six of the various $(2M - 2)$ $u_{i,j}$ and $T_{i,j}$. Hence, the Jacobian matrix derivatives of

$$\vec{G}(\vec{u}, \vec{T}) = \begin{pmatrix} G_2 \\ G_3 \\ \vdots \\ G_M \\ \text{---} \\ G_{M+1} \end{pmatrix} ; \quad \vec{H}(\vec{u}, \vec{T}) = \begin{pmatrix} H_2 \\ H_3 \\ \vdots \\ H_M \end{pmatrix} \quad (C.19)$$

with respect to \vec{u} and \vec{T} have the following sparse, banded forms:

$$\frac{\partial \vec{G}}{\partial \vec{u}} = \begin{pmatrix} \alpha_{11} & \alpha_{12} & & & 0 & | & 0 \\ \alpha_{20} & \alpha_{21} & \alpha_{22} & & & & \\ & \alpha_{30} & \alpha_{31} & \alpha_{32} & & & \\ & & & & \alpha_{M-2,0} & \alpha_{M-2,1} & \alpha_{M-2,2} \\ 0 & & & & & \alpha_{M-1,0} & \alpha_{M-1,1} & \alpha_{M-1,2} \\ \text{---} & & & & & & & \\ 0 & & & & & & \alpha_{M,0} & \alpha_{M,1} \end{pmatrix} ;$$

$$\frac{\partial \vec{G}}{\partial \vec{T}} = \begin{bmatrix} \beta_{11} & \beta_{12} & & & & 0 \\ \beta_{20} & \beta_{21} & \beta_{22} & & & \\ & \beta_{30} & \beta_{31} & \beta_{32} & & \\ & & & & \beta_{M-2,0} & \beta_{M-2,1} & \beta_{M-2,2} \\ & & & & & \beta_{M-1,0} & \beta_{M-1,1} \\ 0 & & & & & & \\ \hline 0 & & & & & & \beta_{M,0} \end{bmatrix} ;$$

$$\frac{\partial \vec{H}}{\partial \vec{u}} = \begin{bmatrix} \gamma_{11} & \gamma_{12} & & & & 0 & | & 0 \\ \gamma_{20} & \gamma_{21} & \gamma_{22} & & & & & & \\ & \gamma_{30} & \gamma_{31} & \gamma_{32} & & & & & \\ & & & & \gamma_{M-2,0} & \gamma_{M-2,1} & \gamma_{M-2,2} & & \\ & & & & & \gamma_{M-1,0} & \gamma_{M-1,1} & | & \gamma_{M-1,2} \\ 0 & & & & & & & & \end{bmatrix} ;$$

[illegible]

From Eqs. (C.12) and (C.17) through (C.20), the $J = \partial \vec{F} / \partial \vec{x}$ Jacobian is then easily computed from the nonzero elements in these [Eq. (C.20)] Jacobians as

[illegible]

DIFFERENCE EQUATIONS AND JACOBIAN ELEMENTS

Specific forms for \vec{G} and \vec{H} , and hence for \vec{F} and the various α , β , γ , and δ coefficients in Eqs. (C.20) and (C.21), are derived as follows. Subject to Eq. (C.13), the first two lines of Eq. (C.9) are approximated at $x = x_i$, $2 \leq i \leq M$, by

$$\begin{aligned} \left(\frac{u_{i,1}}{T_{i,1}} \right) \left[\frac{u_{i+1,1} - u_{i-1,1}}{2(\Delta x)} \right] &= - \left[\frac{P_{i+1,1} - P_{i-1,1}}{2(\Delta x)} \right] \\ &+ M_{11} \left[\frac{u_{i+1,1} - 2u_{i,1} + u_{i-1,1}}{(\Delta x)^2} \right], \\ \left(\frac{u_{i,1}}{T_{i,1}} \right) \left[\frac{T_{i+1,1} - T_{i-1,1}}{2(\Delta x)} \right] &= q(x_i, 0) - \sigma(T_{i,1}^4 - 1) \\ &+ K_1 \left[\frac{T_{i+1,1} - 2T_{i,1} + T_{i-1,1}}{(\Delta x)^2} \right]. \quad (C.22) \end{aligned}$$

From the third and fourth lines in Eq. (C.9) and from Eq. (C.14), we then also have

$$u_{1,1} = 0 ; \quad T_{1,1} = T_{2,1} ; \quad T_{M+1,1} = 1 ; \quad (C.23)$$

and

$$\left(\frac{1}{\Delta x} \right) \left(\frac{u_{M+1,1}}{T_{M+1,1}} - \frac{u_{M,1}}{T_{M,1}} \right) = \hat{\phi}(0) + \beta_0 u_{M+1,1}$$

or

$$u_{M+1,1} = \hat{g}(0) . \quad (C.24)$$

For $j = 1$, we thus have for both codes

$$\begin{aligned}
 G_2 &= \left(\frac{M_{11}}{\Delta x} \right) (u_{3,1} - 2u_{2,1}) - \left(\frac{1}{2} \right) \left(\frac{u_{2,1}}{T_{2,1}} \right) u_{3,1} - \left(\frac{1}{2} \right) (P_{3,1} - P_{1,1}) ; \\
 H_2 &= \left(\frac{K_1}{\Delta x} \right) (T_{3,1} - T_{2,1}) - \left(\frac{1}{2} \right) \left(\frac{u_{2,1}}{T_{2,1}} \right) (T_{3,1} - T_{2,1}) \\
 &\quad + \left[q(x_2, 0) - \sigma(T_{2,1}^4 - 1) \right] (\Delta x) ; \tag{C.25}
 \end{aligned}$$

and, for $3 \leq i \leq M$,

$$\begin{aligned}
 G_i &= \left(\frac{M_{11}}{\Delta x} \right) (u_{i+1,1} - 2u_{i,1} + u_{i-1,1}) - \left(\frac{1}{2} \right) \left(\frac{u_{i,1}}{T_{i,1}} \right) (u_{i+1,1} - u_{i-1,1}) \\
 &\quad - \left(\frac{1}{2} \right) (P_{i+1,1} - P_{i-1,1}) ; \\
 H_i &= \left(\frac{K_1}{\Delta x} \right) (T_{i+1,1} - 2T_{i,1} + T_{i-1,1}) - \left(\frac{1}{2} \right) \left(\frac{u_{i,1}}{T_{i,1}} \right) (T_{i+1,1} - T_{i-1,1}) \\
 &\quad + \left[q(x_i, 0) - \sigma(T_{i,1}^4 - 1) \right] (\Delta x) . \tag{C.26}
 \end{aligned}$$

In this case, we also have [from Eq. (C.24)]

$$G_{M+1} = \left(\frac{1}{\Delta x} \right) \left[u_{M+1,1} - \left(\frac{u_{M,1}}{T_{M,1}} \right) \right] - \beta_0 u_{M+1,1} - \phi(0) , \tag{C.27}$$

but G_{M+1} is not defined when $u_0 = \hat{g}(y)$ is prescribed on $x = 1$.

From Eqs. (C.25) and (C.26), the following Jacobian elements of Eq. (C.20) are then found to be the same for both codes for $j = 1$:

$$\begin{aligned}
 \alpha_{11} &= -2 \left(\frac{M_{11}}{\Delta x} \right) - \left(\frac{1}{2} \right) \left(\frac{u_{3,1}}{T_{2,1}} \right) , \\
 \alpha_{12} &= \left(\frac{M_{11}}{\Delta x} \right) - \left(\frac{1}{2} \right) \left(\frac{u_{2,1}}{T_{2,1}} \right) ;
 \end{aligned}$$

$$\beta_{11} = \left(\frac{1}{2}\right) \left(\frac{u_{2,1} u_{3,1}}{T_{2,1}^2} \right) ,$$

$$\beta_{12} = 0 ;$$

$$\gamma_{11} = - \left(\frac{1}{2}\right) \left(\frac{T_{3,1}}{T_{2,1}} - 1 \right) ,$$

$$\gamma_{12} = 0 ;$$

$$\delta_{11} = - \left(\frac{K_1}{\Delta x} \right) + \left(\frac{1}{2} \right) \left(\frac{u_{2,1} T_{3,1}}{T_{2,1}^2} \right) - 4\sigma T_{2,1}^3 (\Delta x) ,$$

$$\delta_{12} = \left(\frac{K_1}{\Delta x} \right) - \left(\frac{1}{2} \right) \left(\frac{u_{2,1}}{T_{2,1}} \right) ; \quad (C.28)$$

and, for $3 \leq i \leq M$,

$$\alpha_{i-1,0} = \left(\frac{M_{11}}{\Delta x} \right) + \left(\frac{1}{2} \right) \left(\frac{u_{i,1}}{T_{i,1}} \right) ,$$

$$\alpha_{i-1,1} = -2 \left(\frac{M_{11}}{\Delta x} \right) - \left(\frac{1}{2} \right) \left(\frac{u_{i+1,1} - u_{i-1,1}}{T_{i,1}} \right) ,$$

$$\alpha_{i-1,2} = \left(\frac{M_{11}}{\Delta x} \right) - \left(\frac{1}{2} \right) \left(\frac{u_{i,1}}{T_{i,1}} \right) ;$$

$$\beta_{i-1,0} = 0 ,$$

$$\beta_{i-1,1} = \left(\frac{1}{2} \right) \left(\frac{u_{i,1}}{T_{i,1}^2} \right) (u_{i+1,1} - u_{i-1,1}) ,$$

$$\beta_{i-1,2} = 0 ;$$

$$\gamma_{i-1,0} = 0 ,$$

$$\gamma_{i-1,1} = - \left(\frac{1}{2} \right) \left(\frac{T_{i+1,1} - T_{i-1,1}}{T_{i,1}} \right) ,$$

$$\gamma_{i-1,2} = 0 ;$$

$$\delta_{i-1,0} = \left(\frac{K_1}{\Delta x} \right) + \left(\frac{1}{2} \right) \left(\frac{u_{i,1}}{T_{i,1}} \right) ,$$

$$\delta_{i-1,1} = -2 \left(\frac{K_1}{\Delta x} \right) + \left(\frac{1}{2} \right) \left(\frac{u_{i,1}}{T_{i,1}^2} \right) (T_{i+1,1} - T_{i-1,1})$$

$$-4\sigma T_{i,1}^3 (\Delta x) ,$$

$$\delta_{i-1,2} = \left(\frac{K_1}{\Delta x} \right) - \left(\frac{1}{2} \right) \left(\frac{u_{i,1}}{T_{i,1}} \right) ; \quad (C.29)$$

except that $\beta_{M-1,2}$ and $\delta_{M-1,2}$ are undefined if Eq. (C.3) is specified and $\alpha_{M-1,2}$, $\beta_{M-1,2}$, $\gamma_{M-1,2}$, and $\delta_{M-1,2}$ are all undefined if Eq. (C.4) is used. If Eq. (C.3) is specified, the remaining Jacobian elements are [from Eq. (C.27)]

$$\alpha_{M,0} = - \left(\frac{1}{\Delta x} \right) \left(\frac{1}{T_{M,1}} \right) ,$$

$$\alpha_{M,1} = \left(\frac{1}{\Delta x} \right) - \beta_0 ,$$

$$\beta_{M,0} = \left(\frac{1}{\Delta x} \right) \left(\frac{u_{M,1}}{T_{M,1}^2} \right) . \quad (C.30)$$

For $j \geq 2$, the derivation of relevant forms for \vec{G} and \vec{H} begins with a preliminary rewriting of Eq. (C.1) in the following, equivalent "conservation" form:

$$\frac{\partial}{\partial x} (\rho_0 u_0) + \frac{\partial}{\partial y} (\rho_0 v_0) = 0 ;$$

$$\frac{\partial}{\partial x} (\rho_0 u_0^2 + \hat{P}_1) + \frac{\partial}{\partial y} (\rho_0 u_0 v_0) = M_{11} \frac{\partial^2 u_0}{\partial x^2} ;$$

$$\frac{\partial \hat{P}_1}{\partial y} + \hat{A} \rho_0 = 0 ;$$

$$\begin{aligned} \frac{\partial u_0}{\partial x} + \frac{\partial v_0}{\partial y} &\equiv \frac{\partial}{\partial x} (\rho_0 u_0 T_0) + \frac{\partial}{\partial y} (\rho_0 v_0 T_0) = K_{11} \frac{\partial^2 T_0}{\partial x^2} \\ &+ \left[q(x, y) - \sigma(T_0^4 - 1) \right] ; \end{aligned}$$

$$\rho_0 T_0 = 1 . \quad (C.31)$$

Subject to Eq. (C.15), this set is approximated at each interior grid point (x_i, y_j) , $2 \leq i \leq M$, of line j , $2 \leq j \leq N+1$, by the finite difference system

$$\begin{aligned} &\left(\frac{1}{4\Delta x} \right) \left[\left(\frac{u}{T} \right)_{i+1,j} + \left(\frac{u}{T} \right)_{i+1,j-1} - \left(\frac{u}{T} \right)_{i-1,j} - \left(\frac{u}{T} \right)_{i-1,j-1} \right] \\ &+ \left(\frac{1}{\Delta y} \right) \left[\left(\frac{v}{T} \right)_{i,j} - \left(\frac{v}{T} \right)_{i,j-1} \right] = 0 ; \\ &\left(\frac{1}{4\Delta x} \right) \left[\left(\frac{u^2}{T} + P \right)_{i+1,j} + \left(\frac{u^2}{T} + P \right)_{i+1,j-1} - \left(\frac{u^2}{T} + P \right)_{i-1,j} - \left(\frac{u^2}{T} + P \right)_{i-1,j-1} \right] \\ &+ \left(\frac{1}{\Delta y} \right) \left[\left(\frac{uv}{T} \right)_{i,j} - \left(\frac{uv}{T} \right)_{i,j-1} \right] = \left[\frac{M_{11}}{2(\Delta x)^2} \right] \\ &\times \left(u_{i+1,j} - 2u_{i,j} + u_{i-1,j} + u_{i+1,j-1} - 2u_{i,j-1} + u_{i-1,j-1} \right) ; \\ &\left(\frac{1}{\Delta y} \right) (P_{i,j} - P_{i,j-1}) + \left(\frac{\hat{A}}{2} \right) \left[\left(\frac{1}{T} \right)_{i,j} + \left(\frac{1}{T} \right)_{i,j-1} \right] ; \end{aligned}$$

$$\begin{aligned}
 & \left(\frac{1}{4\Delta x} \right) (u_{i+1,j} + u_{i+1,j-1} - u_{i-1,j} - u_{i-1,j-1}) + \left(\frac{1}{\Delta y} \right) (v_{i,j} - v_{i,j-1}) \\
 & = \left[\frac{K_{11}}{2(\Delta x)^2} \right] (T_{i+1,j} - 2T_{i,j} + T_{i-1,j} + T_{i+1,j-1} - 2T_{i,j-1} + T_{i-1,j-1}) \\
 & + \left(\frac{1}{2} \right) \left[q(x_i, y_j) + q(x_i, y_{j-1}) \right] + \sigma \left[\left(\frac{T_{i,j} + T_{i,j-1}}{2} \right)^4 - 1 \right] ; \\
 & \hspace{25em} (C.32)
 \end{aligned}$$

ρ_0 having been eliminated for simplicity. This system is further simplified by solving the first and third equations [in Eq. (C.32)] for $v_{i,j}$ and $P_{i,j}$ in terms of the various u and T on line j and variables on line $j - 1$ as

$$\begin{aligned}
 v_{i,j} &= \left(\frac{v}{T} \right)_{i,j-1} T_{i,j} - \left(\frac{1}{4} \right) \left(\frac{\Delta y}{\Delta x} \right) \left[\left(\frac{u}{T} \right)_{i+1,j} + \left(\frac{u}{T} \right)_{i+1,j-1} \right. \\
 & \quad \left. - \left(\frac{u}{T} \right)_{i-1,j} - \left(\frac{u}{T} \right)_{i-1,j-1} \right] T_{i,j} ; \\
 P_{i,j} &= P_{i,j-1} - \left(\frac{\hat{A}}{2} \right) \left[\left(\frac{1}{T} \right)_{i,j} + \left(\frac{1}{T} \right)_{i,j-1} \right] (\Delta y) ; \hspace{2em} (C.33)
 \end{aligned}$$

and substituting these results into the second and fourth lines to generate (for $2 \leq i \leq M$)

$$\begin{aligned}
 G_i &\equiv \left[\frac{M_{11}}{2(\Delta x)} \right] (u_{i+1,j} - 2u_{i,j} + u_{i-1,j}) - \left(\frac{1}{4} \right) \left\{ \left(\frac{u^2}{T} \right)_{i+1,j} \right. \\
 & \quad \left. - \left(\frac{u^2}{T} \right)_{i-1,j} - \hat{A} \left(\frac{\Delta y}{2} \right) \left[\left(\frac{1}{T_{i+1,j}} \right) - \left(\frac{1}{T_{i-1,j}} \right) \right] \right\} - \left(\frac{\Delta x}{\Delta y} \right) u_{i,j} \\
 & \times \left\{ \left(\frac{v}{T} \right)_{i,j-1} - \left(\frac{\Delta y}{4\Delta x} \right) \left[\left(\frac{u}{T} \right)_{i+1,j} - \left(\frac{u}{T} \right)_{i-1,j} + \left(\frac{u}{T} \right)_{i+1,j-1} \right. \right. \\
 & \quad \left. \left. - \left(\frac{u}{T} \right)_{i-1,j-1} \right] \right\} - R_i = 0 ;
 \end{aligned}$$

$$\begin{aligned}
 H_i \equiv & \left[\frac{K_1}{2(\Delta x)} \right] \left(T_{i+1,j} - 2T_{i,j} + T_{i-1,j} \right) - \left(\frac{1}{4} \right) \left(u_{i+1,j} - u_{i-1,j} \right) \\
 & - \left(\frac{\Delta x}{\Delta y} \right) T_{i,j} \left\{ \left(\frac{v}{T} \right)_{i,j-1} - \left(\frac{\Delta y}{4\Delta x} \right) \left[\left(\frac{u}{T} \right)_{i+1,j} - \left(\frac{u}{T} \right)_{i-1,j} \right. \right. \\
 & \left. \left. + \left(\frac{u}{T} \right)_{i+1,j-1} - \left(\frac{u}{T} \right)_{i-1,j-1} \right] \right\} + \sigma \left[\left(\frac{T_{i,j} + T_{i,j-1}}{2} \right)^4 - 1 \right] (\Delta x) \\
 & - \Pi_i = 0 ; \tag{C.34}
 \end{aligned}$$

where

$$\begin{aligned}
 R_i = & - \left[\frac{M_{11}}{2(\Delta x)} \right] \left(u_{i+1,j-1} - 2u_{i,j-1} + u_{i-1,j-1} \right) - \left(\frac{1}{4} \right) \left\{ \left(\frac{u^2}{T} \right)_{i+1,j-1} - \left(\frac{u^2}{T} \right)_{i-1,j-1} \right. \\
 & \left. + 2 \left(p_{i+1,j-1} - p_{i-1,j-1} \right) - \hat{A} \left(\frac{\Delta y}{2} \right) \left[\left(\frac{1}{T_{i+1,j-1}} \right) + \left(\frac{1}{T_{i-1,j-1}} \right) \right] \right\} \\
 & + \left(\frac{\Delta x}{\Delta y} \right) \left[\left(\frac{uv}{T} \right)_{i,j-1} \right] ; \\
 \Pi_i = & - \left\{ \left[\frac{K_1}{2(\Delta x)} \right] \left(T_{i+1,j-1} - 2T_{i,j-1} + T_{i-1,j-1} \right) - \left(\frac{1}{4} \right) \left(u_{i+1,j-1} \right. \right. \\
 & \left. \left. - u_{i-1,j-1} \right) + \left(\frac{\Delta x}{\Delta y} \right) v_{i,j-1} + \left(\frac{1}{2} \right) \left[q(x_i, y_j) + q(x_i, y_{j-1}) \right] (\Delta x) \right\} . \tag{C.35}
 \end{aligned}$$

As outlined in Fig. C.3, a recursive Crank-Nicolson scheme is employed in subroutine MSWEEP to generate a numerical solution for Eq. (C.1) subject to a given $\hat{P}_1(x, 0)$. For $j = 2, 3, \dots, N+1$, the solution on line j is found using solution data on line $(j-1)$, the solution just described for $j=1$ being used to start the recursion. For each $j \geq 2$ in both codes, the relevant forms of G_i and H_i (as components of \vec{F}), $2 \leq i \leq M$, are therefore exactly those in Eq. (C.34) [cf. Eqs. (C.25) and (C.26)], variables with $j-1$ suffices being known. Also known are the discretized boundary conditions

$$u_{1,j} = 0 ; \quad T_{1,j} = T_{2,j} ; \quad T_{M+1,j} = 1 ; \quad (C.36)$$

and

$$u_{M+1,j} = \hat{g}(y_j) , \quad \text{if } u_0 = \hat{g}(y) \text{ is given on } x = 1 \quad (C.37)$$

[cf. Eqs. (C.23) and (C.24)]. With specification of the boundary condition in Eq. (C.3), Eq. (C.37) is replaced [using Eq. (C.16) in Eq. (C.3)] by

$$\begin{aligned} G_{M+1} = & \left[\frac{1}{2(\Delta x)} \right] \left[u_{M+1,j} - \left(\frac{u}{T} \right)_{M,j} + u_{M+1,j-1} - \left(\frac{u}{T} \right)_{M,j-1} \right] \\ & - \left(\frac{1}{2} \right) \left[\beta_0 \left(u_{M+1,j} + u_{M+1,j-1} \right) + \hat{\phi}(y_j) + \hat{\phi}(y_{j-1}) \right] = 0 . \quad (C.38) \end{aligned}$$

This defines the last component of \vec{G} .

In both codes, the following Jacobian elements are then found [from Eq. (C.34)] to be the same for each fixed choice of $j \geq 2$:

$$\alpha_{11} = -2 \left[\frac{M_{11}}{2(\Delta x)} \right] - \left\{ \left(\frac{\Delta x}{\Delta y} \right) \left(\frac{v}{T} \right)_{2,j-1} - \left(\frac{1}{4} \right) \left[\left(\frac{u}{T} \right)_{3,j} + \left(\frac{u}{T} \right)_{3,j-1} \right] \right\} ,$$

$$\alpha_{12} = \left[\frac{M_{11}}{2(\Delta x)} \right] - \left(\frac{1}{4} \right) \left[2 \left(\frac{u}{T} \right)_{3,j} - \left(\frac{u_{2,j}}{T_{3,j}} \right) \right] ;$$

$$\beta_{11} = \left(\frac{1}{4} \right) \left[\hat{A} \left(\frac{\Delta y}{2} \right) \left(\frac{1}{T_{2,j}} \right)^2 \right] ,$$

$$\beta_{12} = \left(\frac{1}{4} \right) \left[\left(\frac{u}{T} \right)_{3,j}^2 - \hat{A} \left(\frac{\Delta y}{2} \right) \left(\frac{1}{T_{3,j}} \right)^2 - u_{2,j} \left(\frac{u}{T^2} \right)_{3,j} \right]$$

since $T_{1,j} = T_{2,j}$ [cf. Eq. (C.36)];

$$\gamma_{11} = 0 ,$$

$$\gamma_{12} = - \left(\frac{1}{4} \right) \left(1 - \frac{T_{2,j}}{T_{3,j}} \right) ;$$

$$\begin{aligned} \delta_{11} = & - \left[\frac{K_1}{2(\Delta x)} \right] - \left\{ \left(\frac{\Delta x}{\Delta y} \right) \left(\frac{v}{T} \right)_{2,j-1} - \left(\frac{1}{4} \right) \left[\left(\frac{u}{T} \right)_{3,j} + \left(\frac{u}{T} \right)_{3,j-1} \right] \right\} \\ & + 2\sigma \left(\frac{T_{2,j} + T_{2,j-1}}{2} \right)^3 (\Delta x) , \end{aligned}$$

$$\delta_{12} = \left[\frac{K_1}{2(\Delta x)} \right] - \left(\frac{1}{4} \right) \left[T_{2,j} \left(\frac{u}{T^2} \right)_{3,j} \right] ; \quad (C.39)$$

and, for $3 \leq i \leq M$,

$$\alpha_{i-1,0} = \left[\frac{M_{11}}{2(\Delta x)} \right] + \left(\frac{1}{4} \right) \left[2 \left(\frac{u}{T} \right)_{i-1,j} - \left(\frac{u_{i,j}}{T_{i-1,j}} \right) \right] ,$$

$$\begin{aligned} \alpha_{i-1,1} = & -2 \left[\frac{M_{11}}{2(\Delta x)} \right] - \left\{ \left(\frac{\Delta x}{\Delta y} \right) \left(\frac{v}{T} \right)_{i,j-1} - \left(\frac{1}{4} \right) \left[\left(\frac{u}{T} \right)_{i+1,j} + \left(\frac{u}{T} \right)_{i+1,j-1} \right. \right. \\ & \left. \left. - \left(\frac{u}{T} \right)_{i-1,j} - \left(\frac{u}{T} \right)_{i-1,j-1} \right] \right\} , \end{aligned}$$

$$\alpha_{i-1,2} = \left[\frac{M_{11}}{2(\Delta x)} \right] - \left(\frac{1}{4} \right) \left[2 \left(\frac{u}{T} \right)_{i+1,j} - \left(\frac{u_{i,j}}{T_{i+1,j}} \right) \right] ;$$

$$\beta_{i-1,0} = - \left(\frac{1}{4} \right) \left[\left(\frac{u}{T} \right)_{i-1,j}^2 - \hat{A} \left(\frac{\Delta y}{2} \right) \left(\frac{1}{T_{i-1,j}} \right)^2 - u_{i,j} \left(\frac{u}{T^2} \right)_{i-1,j} \right] ,$$

$$\beta_{i-1,1} = 0 ,$$

$$\beta_{i-1,2} = \left(\frac{1}{4} \right) \left[\left(\frac{u}{T} \right)_{i+1,j}^2 - \hat{A} \left(\frac{\Delta y}{2} \right) \left(\frac{1}{T_{i+1,j}} \right)^2 - u_{i,j} \left(\frac{u}{T^2} \right)_{i+1,j} \right] ;$$

$$\gamma_{i-1,0} = \left(\frac{1}{4}\right) \left[1 - \left(\frac{T_{i,j}}{T_{i-1,j}} \right) \right] ,$$

$$\gamma_{i-1,1} = 0 ,$$

$$\gamma_{i-1,2} = - \left(\frac{1}{4}\right) \left[1 - \left(\frac{T_{i,j}}{T_{i+1,j}} \right) \right] ;$$

$$\delta_{i-1,0} = \left[\frac{K_1}{2(\Delta x)} \right] + \left(\frac{1}{4}\right) \left[T_{i,j} \left(\frac{u}{T^2} \right)_{i-1,j} \right] ,$$

$$\begin{aligned} \delta_{i-1,1} = & -2 \left[\frac{K_1}{2(\Delta x)} \right] - \left\{ \left(\frac{\Delta x}{\Delta y} \right) \left(\frac{v}{T} \right)_{i,j-1} - \left(\frac{1}{4}\right) \left[\left(\frac{u}{T} \right)_{i+1,j} + \left(\frac{u}{T} \right)_{i+1,j-1} \right. \right. \\ & \left. \left. - \left(\frac{u}{T} \right)_{i-1,j} - \left(\frac{u}{T} \right)_{i-1,j-1} \right] \right\} + 2\sigma \left(\frac{T_{i,j} + T_{i,j-1}}{2} \right)^3 (\Delta x) , \end{aligned}$$

$$\delta_{i-1,2} = \left[\frac{K_1}{2(\Delta x)} \right] - \left(\frac{1}{4}\right) \left[T_{i,j} \left(\frac{u}{T^2} \right)_{i+1,j} \right] . \quad (C.40)$$

However, we do not define $\beta_{M-1,2}$ and $\delta_{M-1,2}$ in both versions or $\alpha_{M-1,2}$ and $\gamma_{M-1,2}$ in the version where $u_0(1, y)$ is given. In the general version (FIRE), which uses Eq. (C.3), the remaining Jacobian elements are [from Eq. (C.38)];

$$\alpha_{M,0} = - \left[\frac{1}{2(\Delta x)} \right] \left(\frac{1}{T_{M,j}} \right) .$$

$$\alpha_{M,1} = \left(\frac{1}{2}\right) \left[\frac{1}{(\Delta x)} - \beta_0 \right] ;$$

$$\beta_{M,0} = \left[\frac{1}{2(\Delta x)} \right] \left(\frac{u_{M,j}}{T_{M,j}^2} \right) . \quad (C.41)$$

The detailed specification of \vec{G} , \vec{H} , and $J (= \partial \vec{F} / \partial \vec{x})$ is now complete for all cases. $J\vec{\delta} = -\vec{F}$ is solved for $\vec{\delta}$ using (cf. Fig. C.4) Gaussian elimination [Isaacson and Keller, 1966]. For efficiency, standard sparse-matrix methods are employed: only nonzero elements of J [cf. Eq. (C.21)] are stored, and operations involving zero elements are automatically omitted.

PROGRAM LISTING

FORTRAN listings of both codes are now presented. Table C.2 is the FIRE code listing; Table C.3 is the FIRE2 code listing.

Table C.2

LISTING OF FIRE CODE

FORTRAN-VIID:RD4000SED RESTRICTED RIGHTS AS STATED IN LICENSE L-0336 *** SEE DOCUMENTATION FOR A000004-000099.0/ 1 V

```

1      %BATCH
2      C
3      C
4      000000I      PROGRAM FIRE
5      C
6      C
7      000006I      COMMON U(41,241),V(41,241),P(41,241),T(41,241),RHO(41,241),
8      1      X(41),Y(241),
9      2      A,SIGMA,XNUIN,XKIN,YMAX,M,N,
10     3      MP,NP,DX,DY,DYDX,DXDY,NNN,
11     4      ETLINE,MAXITL,ETOLP,MAXITP,
12     5      QVAL,XNU,XK,QPRIM,
13     6      ALPHA,BETA,BLOSS,IGUESS,
14     7      IPRINT,ITTY,KOUT
15     C
16     C
17     C      READ AND WRITE OUT INPUTS
18     C
19     C
20     000006I      ITTY=1
21     000006I      IPRINT=2
22
23     000016I      READ (ITTY,1) A, SIGMA, XNUIN, XKIN
24     000040I      READ (ITTY,3) YMAX, M, N
25     000068I      READ (ITTY,2) ETLINE, ETOLP, MAXITL, MAXITP
26     000094I      READ (ITTY,4) ALPHA, BETA, BLOSS, IGUIESS
27     0000C0I      1      FORMAT (4F10.0)
28     0000CEI      2      FORMAT (2F10.0, 2I10)
29     0000E0I      3      FORMAT (F10.0, 2I10)
30     0000F0I      4      FORMAT (3F10.0, I10)
31
32     000100I      DX=1./FLOAT(M)
33     000126I      DY=YMAX/FLOAT(N)
34
35     000144I      WRITE(IPRINT,10)
36     000164I      10     FORMAT (//// 2X 'FIRE: SOLUTION OF COMBUSTION LAYER ',
37     1      'BOUNDARY VALUE PROBLEM' ///)
38     000182I      WRITE(IPRINT,12)A,SIGMA,XNUIN,XKIN
39     00010CI      12     FORMAT(' SYSTEM PARAMETERS: A = ' F8.3 ' SIGMA = ' F8.3
40     1      ' M = ' F8.3 ' N = ' F8.3 ')
41     000226I      WRITE(IPRINT,14)M,DX,N,DY
42     000250I      14     FORMAT(/ ' MESH: M = ' I5 ' DX = ' F8.3 ' N = ' I5
43     1      ' DY = ' F8.3 ')
44     000284I      WRITE(IPRINT,16)ETLINE,MAXITL,ETOLP,MAXITP
45     000284I      16     FORMAT(/ ' ITERATION PARAMETERS: ETLINE = ' F8.6
46     1      ' MAXITL = ' I5 ' ETOLP = ' F8.6 ' MAXITP = ' I5)
47     000312I      WRITE (IPRINT,18) ALPHA, BETA, BLOSS
48     000338I      18     FORMAT (/ ' INLET PARAMETERS: ALPHA = ' F8.3 ' BETA = '
49     1      F8.3 ' BLOSS = ' F8.3)
50     C
51     C
52     C      INITIALIZATION
53     C
54     C
55     00037EI      DYDX=DY/DX
56     000390I      DXDY=DX/DY
57     0003A2I      MP=M+1

```


Table C.2--Continued

FORTRAN-VIID:R04600SED RESTRICTED RIGHTS AS STATED IN LICENSE L-0335

***, SEE DOCUMENTATION PAPER A08-004-205R99.2/

2 V

```

58 000380I      NP=N+1
59
60 00038E1      X(1)=0.0
61 0003CAI      Y(1)=0.0
62 0003D6I      DO 30 I=2,M
63 0003EAI      X(I)=DX*(FLOAT(I)-1.)
64 000414I      30  CONTINUE
65 000432I      DO 32 J=2,N
66 000446I      Y(J)=DY*(FLOAT(J)-1.)
67 000476I      32  CONTINUE
68 00048EI      X(MP)=1.0
69 0004A2I      Y(NP)=YMAX
70
71 0004B6I      DO 35 I=1,MP
72 0004CAI      V(I,1)=0.0
73 0004DEI      35  CONTINUE
74
75 0004F6I      DO 40 J=1,NP
76 00050AI      U(1,J)=0.0
77 000524I      T(MP,J)=1.0
78 000544I      RHO(MP,J)=1.0
79 000564I      40  CONTINUE
80      C
81      C      MAKE INITIAL GUESSES ALONG Y = 0.0
82      C
83 00057CI      IZERO=0
84 000584I      KK=1
85 00058CI      CALL BCFUNC(KK,IZERO,IZERO)
86 0005ACI      KOUT = 0
87      C
88      C
89      C
90      C      OVERALL ITERATION: MARCHING FROM Y=0.0 TO
91      C      Y=YMAX, RECURSIVELY FINDING
92      C      SOLN. ON Y=Y(J+1) FROM SOLN.
93      C      ON Y=Y(J), AND REPEATING UNTIL
94      C      PX=0 ON Y=YMAX
95      C
96      C
97
98
99 0005B4I      NNN=0
100 0005BCI      50  CONTINUE
101 0005RCI      NNN=NNN+1
102 0005CAI      IF(NNN.GE.MAXITP) GO TO 950
103
104
105 0005E2I      CALL MSWEEP
106 0005EAI      IF (KOUT.EQ. 1) GO TO 980
107      C
108      C      OVERALL CONVERGENCE CHECK PLUS
109      C      NEWTON MODIFICATIONS
110      C
111 000600I      DO 110 I=1,M
112 000614I      IP=I+1
113 000622I      IF (ABS(P(I,NP)-P(IP,NP)).GE.(DX*FTOLP)) GO TO 115
114 0006BEI      110  CONTINUE

```

```

58
59
60
61
62
63
64
65
66
67
68
69
70
71
72
73
74
75
76
77
78
79
80
81
82
83
84
85
86
87
88
89
90
91
92
93
94
95
96
97
98
99
100
101
102
103
104
105
106
107
108
109
110
111
112
113
114

```

Table C.2--Continued

FORTRAN-VIID:ROSEBNSED RESTRICTED RIGHTS AS STATED IN LICENSE L-0336

***, SEE DOCUMENTATION PAGE 004-90699.9/

3 v

115	0006A6I		GO TO 900	115
116				116
117	0006ACI	115	CONTINUE	117
118	0006ACI		XOMEGA=0.9	118
119	0006B8I		DO 120 I=1,M	119
120	0006CCI		P(I,1)=P(I,1)*XOMEGA*(P(MP,NP)-P(I,NP))	120
121	000722I	120	CONTINUE	121
122	00073AI		GO TO 50	122
123		C		123
124		C		124
125		C	STANDARD PRINTOUT	125
126		C		126
127		C		127
128	00073EI	900	CONTINUE	128
129	00073EI		DO 920 J=1,NP	129
130	000752I		CALL SPRINT(J)	130
131	000768I	920	CONTINUE	131
132	000780I		GO TO 980	132
133		C		133
134		C		134
135		C	ERROR PRINTOUT	135
136		C		136
137		C		137
138	000786I	950	CONTINUE	138
139	000786I		WRITE(IPRINT,960) MAXITP	139
140	0007A4I	960	FORMAT(////, ' NO CONVERGENCE IN '.I6, ' OVERALL 1 ITERATIONS ON P', ///)	140
141				141
142				142
143	000806I		CALL SPRINT(NP)	143
144	00081CI		STOP 0	144
145	000840I	980	CONTINUE	145
146				146
147	000840I		WRITE (8) A, SIGMA, XNUIN, XKIN, YMAX, ETLINE, ETOLP, DX, DY	147
148	00087CI		WRITE (8) M, N, MAXITL, MAXITP, KOUT, IGUESS	148
149	0008ACI		DO 990 J = 1, NP	149
150	0008C0I		WRITE (8) (U(I,J), I = 1, MP)	150
151	00094CI	990	CONTINUE	151
152	000964I		DO 991 J = 1, NP	152
153	000978I		WRITE (8) (V(I,J), I = 1, MP)	153
154	000A00I	991	CONTINUE	154
155	000A18I		WRITE (9) A, SIGMA, XNUIN, XKIN, YMAX, ETLINE, ETOLP, DX, DY	155
156	000A54I		WRITE (9) M, N, MAXITL, MAXITP, KOUT, IGUESS	156
157	000A84I		DO 992 J = 1, NP	157
158	000A98I		WRITE (9) (T(I,J), I = 1, MP)	158
159	000B20I	992	CONTINUE	159
160	000B38I		DO 993 J = 1, NP	160
161	000B4CI		WRITE (9) (P(I,J), I = 1, MP)	161
162	000B04I	993	CONTINUE	162
163		C	WRITE (7) A, SIGMA, XNUIN, XKIN, YMAX, ETLINE, ETOLP, DX, DY	163
164		C	WRITE (7) M, N, MAXITL, MAXITP, KOUT, IGUESS	164
165		C	DO 994 J = 1, NP	165
166		C	WRITE (7) (RHO(I,J), I = 1, MP)	166
167		C994	CONTINUE	167
168	000BECI		STOP	168
169	000BF4I		END	169

NO ERRORS:F7D R04-00 MAINPROG FIRE 07/17/81 10:20:06 TABLE SPACE: 5 KB

Table C.2--Continued

FORTRAN-VIIO:RQ\$E88SED RESTRICTED RIGHTS AS STATED IN LICENSE L-0336

***, SEE DOCUMENTATION PAGE 88-004-P88899.7/

5 V

1	000000I	SUBROUTINE BCFUNC(KEY,II,JJ)	170
2			171
3			172
4	000004I	COMMON U(41,241),V(41,241),P(41,241),T(41,241),RHO(41,241),	173
5		1 X(41),Y(241),	174
6		2 A,SIGMA,XNUIN,XKIN,YMAX,M,N,	175
7		3 MP,NP,DX,DY,DYDX,DXDY,NNN,	176
8		4 ETLINE,MAXITL,ETOLP,MAXITP,	177
9		5 QVAL,XNU,XK,QPRIM,	178
10		6 ALPHA,BETA,BLOSS,IGUESS,	179
11		7 IPRINT,ITTY,<OUT	180
12			181
13			182
14	000004I	GO TO (100, 200, 300, 400, 500) KEY	183
15		C	184
16		C	185
17		C INITIAL GUESSES FOR Y=0.0 - CAN BE CHANGED	186
18		C	187
19		C	188
20	000036I	100 GO TO (125, 150, 175) I GUESS	189
21			190
22	00005EI	125 DO 126 I = 1, MP	191
23	000072I	READ (ITTY, 127) U(I,1), T(I,1), P(I,1)	192
24	000100I	126 CONTINUE	193
25	000118I	127 FORMAT (3F10.0)	194
26	000126I	GO TO 900	195
27			196
28	00012CI	150 CONTINUE	197
29	00012CI	DO 150 I = 1, MP	198
30	000140I	READ (ITTY,161) P(I,1)	199
31	000174I	160 CONTINUE	200
32	00018CI	161 FORMAT (F10.0)	201
33			202
34	000198I	175 CONTINUE	203
35	000198I	DO 180 I = 1, MP	204
36	0001ACI	IF (IGUESS .EQ. 3) P(I,1) = 0.	205
37	000100I	T(I,1) = 1.76-0.76*X(I)	206
38	0001FAI	CC = 1.6	207
39	000206I	CCC=1.9	208
40	000212I	EP = EXP(CC*X(I))	209
41	00024AI	EM = EXP(-CC*X(I))	210
42	00028AI	U(I,1) = -CCC*(EP-EM)/(EP+EM)	211
43	0002C0I	180 CONTINUE	212
44	000208I	GO TO 900	213
45		C	214
46		C	215
47		C Q(X,Y) PRESCRIPTION - CAN BE CHANGED	216
48		C	217
49		C	218
50	0002DEI	200 CONTINUE	219
51	00020EI	IF (JJ.EQ.1) TAVG=T(II,JJ)	220
52	00030EI	JJM=JJ-1	221
53	00031CI	IF (JJ.GE.2) TAVG=0.5*(T(II,JJ)+T(II,JJM))	222
54			223
55	00036CI	QVAL=1.0-SIGMA*(TAVG**4-1.0)	224
56			225
57	000394I	IF (Y(JJ).GT.1.0) QVAL=QVAL-1.0	226

Table C.2--Continued

FORTRAN-VIIO:R0400SED RESTRICTED RIGHTS AS STATED IN LICENSE L-0336

***, SEE DOCUMENT AT T081PACBABB1004-R03M99.2/

6 V

58	C		227
59	C		228
60	C	NU(X,Y) PRESCRIPTION - CAN BE CHANGED	229
61	C		230
62	C		231
63	0003C0I	300 CONTINUE	232
64	0003C0I	XNU = XNUIN	233
65	0003CCI	CNU=0.0	234
66	0003D8I	XNU=XNU*EXP(-CNU*X(II))	235
67	00041CI	IF(X(II).GT.1.0)XNU=0.0	236
68	000442I	GO TO 900	237
59	C		238
70	C		239
71	C	K(X,Y) PRESCRIPTION - CAN BE CHANGED	240
72	C		241
73	C		242
74	000448I	400 CONTINUE	243
75	000448I	XK = XKIN	244
76	000454I	CK=0.0	245
77	000460I	XK=XK*EXP(-CK*X(II))	246
78	0004A4I	IF(X(II).GT.1.0)XK=0.0	247
79	0004CAI	GO TO 900	248
80	C		249
81	C	QPRIME COMPUTATION - CAN BE CHANGED	250
82	C		251
83	0004D0I	500 CONTINUE	252
84	0004D0I	IF(JJ.EQ.1)TAVG=T(II,JJ)	253
85	000500I	JJM=JJ-1	254
86	00050EI	IF(JJ.GE.2)TAVG=(T(II-JJ)+T(II,JJM))/2.	255
87			256
88	00055EI	QPRIM=-4.*SIGMA*(TAVG**3)	257
89			258
90	000588I	900 CONTINUE	259
91	000588I	RETURN	260
92	00058EI	END	261

NO ERRORS:F7D R04-00 SUBROUTINE BCFUNC 07/17/81 10:20:09 TABLE SPACE: 4 KB
 STATEMENT BUFFER: 20 LINES/1321 BYTES STACK SPACE: 174 WORDS
 SINGLE PRECISION FLOATING PT SUPPORT REQUIRED FOR EXECUTION

Table C.2--Continued

FORTRAN-VIID:RQ46B05E RESTRICTED RIGHTS AS STATED IN LICENSE L-0336

***, SEE DOCUMENTATIONIPACHA004-004-005099.V/

7 V

```

1 000000I      SUBROUTINE SPRINT(JJ)
2
3
4 000004I      COMMON U(41,241),V(41,241),P(41,241),T(41,241),RHO(41,241),
5
6      1      X(41),Y(241),
7      2      A,SIGMA,XNUIN,XKIN,YMAX,M,N,
8      3      MP,NP,DX,DY,DYDX,DXDY,NNN,
9      4      ETLINE,MAXITL,ETOLP,MAXITP,
10     5      QVAL,XNU,XK,QPRIM,
11     6      ALPHA,BETA,BLOSS,IGUESS,
12     7      IPRINT,ITTY,XOUT
13 000004I      DIMENSION PX(41), VISC(41), DIFF(41), HEAT(41)
14
15 C
16 C      COMPUTE PX, UXX, TXX AND Q(T) TERMS
17 C
18 C
19 000004I      DO 50 I = 1, MP
20 0002H0I      IP = I + 1
21 0002B0I      IM = I - 1
22 0002C0I      DO 10 KK = 2, 4
23 0002D4I      CALL RCFUNC (KK, I, JJ)
24 0002F4I      10 CONTINUE
25 00030AI      IF (I .EQ. 1) GO TO 20
26 000320I      IF (I .EQ. MP) GO TO 30
27
28 000338I      PX(I) = (P(IP,JJ)-P(IM,JJ))/(2.*DX)
29 000386I      VISC(I) = (U(IP,JJ)-2.*U(I,JJ)+U(IM,JJ))*XNU/(DX*DX)
30 0003FCI      DIFF(I) = (T(IP,JJ)-2.*T(I,JJ)+T(IM,JJ))*XK/(DX*DX)
31 000472I      HEAT(I) = QVAL
32 000484I      GO TO 50
33
34 00048AI      20 PX(I) = 0.
35 00049CI      VISC(I) = 0.
36 0004AEI      DIFF(I) = 2.*(T(IP,JJ)-T(IM,JJ))*XK/(DX*DX)
37 00050HI      HEAT(I) = QVAL
38 00051AI      GO TO 50
39
40 000520I      30 PX(I) = (P(I,JJ)-P(IM,JJ))/DX
41 000566I      VISC(I) = VISC(IM)
42 00057EI      DIFF(I) = DIFF(IM)
43 000596I      HEAT(I) = QVAL
44
45 0005A8I      50 CONTINUE
46 C
47 C
48 C      STANDARD PRINTOUT
49 C
50 C
51 0005C0I      WRITE(IPRINT,100)JJ,Y(JJ)
52 0005F8I      100 FORMAT(////, ' FOR J =', I5, ' (Y =', F8.3, ') :')
53 000620I      WRITE(IPRINT,120)
54 00063CI      120 FORMAT(//, '
55 I      , RHO      P, 21X, PX      U      V      T,
56      DO 150 I=1,MP
57 000696I      WRITE(IPRINT,140)I,X(I),U(I,JJ),V(I,JJ),T(I,JJ),RHO(I,JJ),

```

Table C.2--Continued

```

FORTRAN-VIID:RQ4600SED RESTRICTED RIGHTS AS STATED IN LICENSE L-0336      *** SEE DOCUMENTATION:IPAC0408:004-043899.2/      8 V
58          1          P(I,JJ), PX(I), VISC(I), DIFF(I), HEAT(I)          319
59 000804I    140  FORMAT(3X,16,6F8.3, 15X, 4F8.3)          320
60 00081CI    160  CONTINUE          321
61 000834I          RETURN          322
52 000834I          END          323

NO ERRORS:F7D R04-00      SUBROUTINE SPRINT      07/17/81 10:20:12 TABLE SPACE:      3 KB
STATEMENT BUFFER:      20 LINES/1321 BYTES      STACK SPACE: 171 WORDS
SINGLE PRECISION FLOATING PT SUPPORT REQUIRED FOR EXECUTION

```

Table C.2--Continued

FORTRAN-VIID:R04E00SED RESTRICTED RIGHTS AS STATED IN LICENSE L-0336

***, SEE DOCUMENT AT 7081 PAGE 4081004-P05899.V/

9 V

```

1 0000001      SUBROUTINE MSWEEP
2
3
4 0000041      COMMON U(41,241),V(41,241),P(41,241),T(41,241),RHO(41,241),
5 1          X(41),Y(241),
6 2          A,SIGMA,XNUIN,XKIN,YMAX,M,N,
7 3          MP,NP,DX,DY,DYDX,DYDY,NNN,
8 4          ETLINE,MAXITL,ETOLP,MAXITP,
9 5          QVAL,XNU,XK,QPRIM,
10 6          ALPHA,BETA,BLOSS,IGUESS,
11 7          IPRINT,ITTY,KOUT
12
13 0000041      DIMENSION XX(200),FF(200),AZ(100),A1(100),
14 1          A2(100),BZ(100),B1(100),B2(100),
15 2          CZ(100),C1(100),C2(100),DZ(100),
16 3          D1(100),D2(100),XMAT(7,200),
17 4          DNEW(200)
18
19
20 0000041      MM=M-1
21 00321A1      MR=2*(M-1)+1
22 0032301      MRM = MR - 1
23 00323E1      MRM2 = MR - 2
24 00324C1      MRM3 = MR - 3
25
26 0032541      DO 800 J=1,NP
27 00326E1      JM=J-1
28 00327C1      JM2=J-2
29
30 C
31 C      INITIAL GUESSES FOR U AND T ON LINE J
32 C
33 C
34 00328A1      DO 20 I=2,MP
35 00329E1      IU=2*(I-1)-1
36 0032841      IT=2*(I-1)
37 0032C81      IF(J.EQ.1) GO TO 14
38 0032DE1      IF(J.EQ. 2) GO TO 12
39
40 C
41 C      LINEAR EXTRAPOLATION USED FOR J .GE. 3
42
43 0032F41      U(I,J)=2.*U(I,JM)-U(I,JM2)
44 0033481      T(I,J)=2.*T(I,JM)-T(I,JM2)
45 00339C1      GO TO 14
46
47 C
48 C      PREVIOUS VALUES (=INITIAL GUESSES FOR NNN=1) USED FOR J = 1 OR J = 2
49
50 0033A21 12 U(I,J)=U(I,JM)
51 0033D61 12 T(I,J)=T(I,JM)
52 00340A1 14 CONTINUE
53 00340A1 14 XX(I,J)=U(I,J)
54 0034301 14 XX(IT)=T(I,J)
55 0034561 14 IF(I.EQ.2)T(1,J)=T(I,J)
56 0034941 20 CONTINUE
57
58 C
59 C
60 C

```

Table C.2--Continued

FORTRAN-VIIO:ROSEBUSED RESTRICTED RIGHTS AS STATED IN LICENSE L-0336

***, SEE DOCUMENTATION PAID 0488:004-285899.2/

10 V

58	C	OVERALL VECTOR NEWTON ITERATION	381
59	C	USING GAUSS ELIMINATION ON LINEAR EQNS.	382
60	C		383
61	C		384
62	C		385
63	0034ACI	NUMITL = 0	386
64	003484I	100 NUMITL=NUMITL+1	387
65	0034C2I	IF(NUMITL.GT.MAXITL)GO TO 900	388
66			389
67			390
68	0034DAI	DO 200 I=2,MP	391
69	0034EEI	IM=I-1	392
70	0034FCI	IP=I-1	393
71	00350AI	IU=2*(I-1)-1	394
72	00352OI	IT=2*(I-1)	395
73	003534I	IF(J.EQ.1) JM=1	396
74			397
75	00354CI	KK=2	398
76	003554I	CALL BCFUNC(KK,I,J)	399
77	003574I	KK=3	400
78	00357CI	CALL BCFUNC(KK,I,JM)	401
79	00359CI	XNUM=XNU	402
80	0035AB I	KK=3	403
81	00358OI	CALL BCFUNC(KK,I,J)	404
82	0035DOI	KK=4	405
83	0035DOB I	CALL BCFUNC(KK,I,JM)	406
84	0035FBI	XKM=XK	407
85	003604I	KK=4	408
86	00360CI	CALL BCFUNC(KK,I,J)	409
87	00362CI	KK=5	410
88	003634I	CALL BCFUNC(KK,I,J)	411
89			412
90	003654I	IF(J.GE.2) GO TO 110	413
91			414
92	C		415
93	C	NEWTON SET-UP FOR J = 1	416
94	C		417
95	C		418
96	003664I	IF(I.GE.MP) GO TO 112	419
97	003682I	RR=0.5*(P(IP,1)-P(IM,1))	420
98	0036AAI	PI=0.	421
99			422
100	003686I	FF(IU)=(U(IP,1)-2.*U(I,1)+U(IM,1))*XNU/DX	423
101		1 -0.5*(U(IP,1)-U(IM,1))*U(I,1)/T(I,1)-RR	424
102			425
103	003746I	FF(IT)=(T(IP,1)-2.*T(I,1)+T(IM,1))*XK/DX	426
104		1 -0.5*(T(IP,1)-T(IM,1))*U(I,1)/T(I,1)+DX*QVAL	427
105			428
106	0037DEI	IF(IM.GE.2) GO TO 108	429
107	0037F4I	AZ(1)=0.0	430
108	0037FEI	A1(1)=-2.*XNU/DX-0.5*U(3,1)/T(2,1)	431
109	00383OI	A2(1)=XNU/DX-0.5*U(2,1)/T(2,1)	432
110	003854I	BZ(1)=0.0	433
111	00385EI	B1(1)=0.5*U(3,1)*U(2,1)/(T(2,1)**2)	434
112	003884I	B2(1)=0.0	435
113	00388EI	CZ(1)=0.0	436
114	00389BI	C1(1)=-0.5*(T(3,1)/T(2,1)-1.0)	437

Table C.2--Continued

FORTTRAN-VIIO:RQ4EBWSED RESTRICTED RIGHTS AS STATED IN LICENSE L-0336

***, SEE DOCUMENTATIONIPAC20001004-P06099.0/

11 V

115	00388CI	C2(I)=0.0	438
116	0038C6I	DZ(I)=0.0	439
117	0038D0I	D1(I)=-XK/DX+0.5*T(3,I)*U(2,I)/(T(2,I)**2)	440
118		1 DX*QPRIM	441
119	00391AI	D2(I)=XK/DX-0.5*U(2,I)/T(2,I)	442
120	00393EI	GO TO 200	443
121			444
122	003944I	108 AZ(IM)=XNU/DX+0.5*U(I,I)/T(I,I)	445
123	003980I	A1(IM)=-2.*XNU/DX-0.5*(U(IP,I)-U(IM,I))/T(I,I)	446
124	0039D8I	A2(IM)=XNU/DX-0.5*U(I,I)/T(I,I)	447
125	003A14I	BZ(IM)=0.0	448
126	003A26I	B1(IM)=0.5*(U(IP,I)-U(IM,I))*U(I,I)/(T(I,I)**2)	449
127	003A86I	B2(IM)=0.0	450
128	003A98I	CZ(IM)=0.0	451
129	003AAA I	C1(IM)=-0.5*(T(IP,I)-T(IM,I))/T(I,I)	452
130	003AEEI	C2(IM)=0.0	453
131	003B00I	DZ(IM)=XK/DX+0.5*U(I,I)/T(I,I)	454
132	003B3CI	D1(IM)=-2.*XK/DX+0.5*(T(IP,I)-T(IM,I))*U(I,I)	455
133		1 / (T(I,I)**2) * DX * QPRIM	456
134	003BC6I	D2(IM)=XK/DX-0.5*U(I,I)/T(I,I)	457
135			458
136	003C02I	IF(I.LT.M) GO TO 200	459
137			460
138	003C1AI	D2(IM)=0.0	461
139			462
140	003C2CI	GO TO 200	463
141		C	464
142		C	465
143		C	466
144		C	467
145		C	468
146	003C32I	110 CONTINUE	469
147	003C32I	IF(I.GE.MP) GO TO 112	470
148	003C4AI	RR=(U(IP,JM)-2.*U(I,JM)+U(IM,JM))*XNUM	471
149		1 / (2.*DX) - ((U(IP,JM)**2)/T(IP,JM)	472
150		1 - (U(IM,JM)**2)/T(IM,JM) + 2.*(P(IP,JM)	473
151		3 - P(IM,JM)) - 0.5*A*DY*(1./T(IP,JM)	474
152		4 - 1./T(IM,JM))/4.	475
153	003DDCI	RR=-RR-U(I,JM)*V(I,JM)/T(I,JM)*DXDY	476
154	003E44I	PI=-((T(IP,JM)-2.*T(I,JM)+T(IM,JM))*XKM	477
155		1 / (2.*DX) - (U(IP,JM)-U(IM,JM))/4.*V(I,JM)*DXDY)	478
156			479
157	003F1AI	FF(IU)=(U(IP,J)-2.*U(I,J)+U(IM,J))*XNU	480
158		1 / (2.*DX) - 0.25*(U(IP,J)**2)/T(IP,J)	481
159		2 - (U(IM,J)**2)/T(IM,J) - 0.5*A*DY	482
160		3 * (1./T(IP,J) - 1./T(IM,J)) - U(I,J)*	483
161		4 (DXDY*V(I,JM)/T(I,JM) - 0.25*(U(IP,J)	484
162		5 /T(IP,J)+U(IP,JM)/T(IP,JM)-U(IM,J)	485
163		6 /T(IM,J)-U(IM,JM)/T(IM,JM))-RR	486
164			487
165	0041BCI	FF(IT)=(T(IP,J)-2.*T(I,J)+T(IM,J))*XK	488
166		1 / (2.*DX) - 0.25*(U(IP,J)-U(IM,J))	489
167		2 - T(I,J)*(DXDY*V(I,JM)/T(I,JM) - 0.25	490
168		3 * (U(IP,J)/T(IP,J)+U(IP,JM)/T(IP,JM)	491
169		4 - U(IM,J)/T(IM,J)-U(IM,JM)/T(IM,JM))	492
170		5 *DX*QVAL-P	493
171			494

Table C.2--Continued

FORTRAN-VI:RD4680SED RESTRICTED RIGHTS AS STATED IN LICENSE L-0336			***. SEE DOCUMENTATION: PAC8A088:004-R03899.V/	12 V
172	004388I	GO TO 114		495
173		C		496
174		C		497
175		C	PRESCRIPTION OF INLET VELOCITY BC - CAN BE CHANGED	498
176		C		499
177		C	$-(DV)/(DY) = D(RHO*U)/(DX)$	500
178		C	$= BLOSS*U*BIN$	501
179		C		502
180		C	NOMINAL V CASE:	503
181		C	$BLOSS = 0.0, V = ALPHA*TANH((BETA/ALPHA)*Y)$	504
182		C		505
183		C		506
184	00438EI	112	CONTINUE	507
185	00438EI		$BYA = BETA*Y(J)/ALPHA$	508
186	0043DEI		$SECH = 2./(EXP(BYA)+EXP(-BYA))$	509
187	004438I		$BIN = -BETA*(SECH**2)$	510
188				511
189		C	ALTERNATIVE V CASE:	512
190		C	$BLOSS=0.0, V = ALPHA*Y*EXP(-BETA*Y)$	513
191		C		514
192		C	$BIN=-ALPHA*(1.0-BETA*Y(J))*EXP(-BETA*Y(J))$	515
193		C		516
194				517
195	00445AI		$FF(IJ)=(1.0-0.5*DX*BLOSS)*U(MP,J)-U(M,J)$	518
196		1	$*(1.0/T(M,J)+0.5*DX*BLOSS)-BIN*DX$	519
197	0044FAI		$IF(J,GE,2) FF(IU)=FF(IU)-((1.0/T(M,JM)+0.5*DX*BLOSS$	520
198		1	$)*U(M,JM)-(1.0-0.5*DX*BLOSS)*U(MP,JM))$	521
199		2	$-BIN*DX$	522
200	0045BAI		$FF(IJ)=FF(IU)/DX$	523
201	0045DCI		GO TO 130	524
202				525
203	0045E2I	114	CONTINUE	526
204	0045E2I		$IF(IM,GE,2) GO TO 120$	527
205	0045F8I		$AZ(1)=0.0$	528
206	004602I		$A1(1)=-2.*XNU/(2.*DX)-(DX*DY*V(2,JM)/T(2,JM)$	529
207		1	$-0.25*(U(3,J)/T(3,J)+U(3,JM)/T(3,JM))$	530
208	0046B2I		$A2(1)=XNU/(2.*DX)-0.25*(2.*U(3,J)-U(2,J))/T(3,J)$	531
209	004714I		$BZ(1)=0.0$	532
210	00471EI		$B1(1)=0.25*(0.5*A*DY/(T(2,J)**2))$	533
211	004758I		$B2(1)=0.25*((U(3,J)**2-U(2,J)*U(3,J))/T(3,J)$	534
212		1	$**2)-0.5*A*DY/(T(3,J)**2))$	535
213	004804I		$CZ(1)=0.0$	536
214	00480EI		$C1(1)=0.0$	537
215	004818I		$C2(1)=-0.25*(1.-T(2,J)/T(3,J))$	538
216	004854I		$DZ(1)=0.0$	539
217	004864I		$D1(1)=-XK/(2.*DX)-(DX*DY*V(2,JM)/T(2,JM)$	540
218		1	$-0.25*(U(3,J)/T(3,J)+U(3,JM)/T(3,JM))$	541
219		2	$+0.5*DX*OPRIM$	542
220	004922I		$D2(1)=XK/(2.*DX)-0.25*T(2,J)*U(3,J)/T(3,J)**2)$	543
221	004988I		GO TO 200	544
222				545
223	00498EI	120	$AZ(IM)=XNU/(2.*DX)+0.25*(2.*U(IM,J)-U(I,J))/T(IM,J)$	546
224	004A0CI		$A1(IM)=-2.*XNU/(2.*DX)-(DX*DY*V(I,JM)/T(I,JM)$	547
225		1	$-0.25*(U(IP,J)/T(IP,J)+U(IP,JM)/T(IP,JM)$	548
226		2	$-U(IM,J)/T(IM,J)-U(IM,JM)/T(IM,JM))$	549
227	004956I		$A2(IM)=XNU/(2.*DX)-0.25*(2.*U(IP,J)-U(I,J))/T(IP,J)$	550
228	0049D4I		$BZ(IM)=-0.25*((U(IM,J)-U(I,J))*U(IM,J)/T(IM,J)$	551

Table C.2--Continued

FORTRAN-VIIIO:R04688SED RESTRICTED RIGHTS AS STATED IN LICENSE L-0336

***. SEE DOCUMENTATIONIPACRA00:004-R06899.9/

13 V

229		1	$0.5 * A * DY / (T(I, J) ** 2)$	552
230	004CA6I		B1(I, J) = 0.0	553
231	004CBAI		B2(I, J) = 0.25 * ((U(IP, J) - U(I, J)) * U(IP, J) / (T(IP, J)	554
232		1	$0.5 * A * DY / (T(IP, J) ** 2)$	555
233	004D82I		C2(I, J) = 0.25 * (1. - T(I, J) / T(IP, J))	556
234	004DD0I		C1(I, J) = 0.0	557
235	004DE2I		C2(I, J) = -0.25 * (1. - T(I, J) / T(IP, J))	559
236	004E38I		DZ(I, J) = XK / (2. * DX) * 0.25 * T(I, J) * U(IM, J) / (T(IM, J) ** 2)	559
237	004EC4I		D1(I, J) = -2. * XK / (2. * DX) - (DX * DY * V(I, JM) / T(I, JM)	560
238		1	-0.25 * (U(IP, J) / T(IP, J) + U(IP, JM) / T(IP, JM)	561
239		2	-U(IM, J) / T(IM, J) - U(IM, JM) / T(IM, JM))	562
240		3	+0.5 * DX * QPRIM	563
241	005020I		D2(I, J) = XK / (2. * DX) - 0.25 * T(I, J) * U(IP, J) / (T(IP, J) ** 2)	564
242				565
243	0050ACI		IF(I, LT, M) GO TO 200	566
244	0050C4I		B2(I, J) = 0.0	567
245	0050D8I		D2(I, J) = 0.0	568
246	0050EAI		GO TO 200	569
247				570
248	0050F0I	130	CONTINUE	571
249	0050F0I		AZ(I, J) = -(1.0 / T(M, J) + 0.5 * DX * BLOSS) / DX	572
250	005140I		A1(I, J) = (1.0 - 0.5 * DX * BLOSS) / DX	573
251	00516EI		A2(I, J) = 0.0	574
252	005182I		BZ(I, J) = U(M, J) / (T(M, J) ** 2) / DX	575
253	0051E0I		B1(I, J) = 0.0	576
254	0051F4I		B2(I, J) = 0.0	577
255	005208I		C2(I, J) = 0.0	578
256	00521CI		C1(I, J) = 0.0	579
257	005230I		C2(I, J) = 0.0	580
258	005242I		DZ(I, J) = 0.0	581
259	005254I		D1(I, J) = 0.0	582
260	005266I		D2(I, J) = 0.0	583
261				584
262	005278I	200	CONTINUE	585
263		C		586
264		C		587
265		C	SPARSE (JACOBIAN) MATRIX COMPACTIFICATION	588
266		C		589
267		C		590
268	005290I		DO 250 IM=1, M	591
269	0052A4I		IU=2 * IM-1	592
270	0052B4I		IT=2 * IM	593
271	0052C2I		XMAT(1, IU) = 0.0	594
272	0052DAI		XMAT(2, IU) = AZ(IM)	595
273	0052FAI		XMAT(3, IU) = BZ(IM)	596
274	00531AI		XMAT(4, IU) = A1(IM)	597
275	00533AI		XMAT(5, IU) = B1(IM)	598
276	00535AI		XMAT(6, IU) = A2(IM)	599
277	00537AI		XMAT(7, IU) = B2(IM)	600
278	00539AI		IF(I, SE, M) GO TO 250	601
279	0053B2I		XMAT(1, IT) = C2(IM)	602
280	0053D2I		XMAT(2, IT) = DZ(IM)	603
281	0053F0I		XMAT(3, IT) = C1(IM)	604
282	005410I		XMAT(4, IT) = D1(IM)	605
283	00542EI		XMAT(5, IT) = C2(IM)	606
284	00544EI		XMAT(6, IT) = D2(IM)	607
285	00546CI		XMAT(7, IT) = 0.0	608

Table C.2--Continued

FORTRAN-VIIO:R04688SED RESTRICTED RIGHTS AS STATED IN LICENSE L-0336

***, SEE DOCUMENTATIONIPAC18A881004-P03899.0/

14 V

286	005484I	250	CONTINUE	609
287		C		610
288		C		611
289		C	GAUSS ELIMINATION TO SOLVE JD=-F	612
290		C		613
291		C		614
292	005490I		DO 500 I=1,MRM	615
293	005480I		KMAX=3	616
294	005488I		IF(I.EQ.MBM2) KMAX=2	617
295	005402I		IF(I.EQ.MBM) KMAX=1	618
296				619
297	0054ECI		DO 490 K=1,KMAX	620
298	005500I		IK=I+K	621
299	005512I		M4K=4-K	622
300	005520I		PIVOT=XMAT(M4K,IK)/XMAT(4,I)	623
301				624
302	005550I		DO 490 LL=4.7	625
303	005558I		ML=LL-K	626
304	00556AI		XMAT(ML,IK)=XMAT(ML,IK)-PIVOT*XMAT(LL,I)	627
305	00558AI	480	CONTINUE	628
306				629
307	005500I		FF(IK)=FF(IK)-PIVOT*FF(I)	630
308	005502I	490	CONTINUE	631
309	00561AI	500	CONTINUE	632
310				633
311	005632I		DNEW(MB)=-FF(MB)/XMAT(4,MB)	634
312	005666I		DNEW(MBM)=- (FF(MBM)*XMAT(5,MBM)+DNEW(MB))/XMAT(4,MBM)	635
313	005688I		DNEW(MBM2)=- (FF(MBM2)*XMAT(5,MBM2)+DNEW(MBM)	636
314		1	+XMAT(6,MBM2)*DNEW(MB))/XMAT(4,MBM2)	637
315				638
316	00572AI		DO 550 I=1,MRM3	639
317	00573FI		IR=MRM2-I	640
318	005750I		XXX=FF(IR)	641
319	005764I		DO 540 K=5.7	642
320	00576CI		IRP=IR-K-4	643
321	005780I		XXX=XXX+XMAT(K,IR)*DNEW(IRP)	644
322	005740I	540	CONTINUE	645
323	0057C6I		DNEW(IR)=-XXX/XMAT(4,IR)	646
324	0057F2I	550	CONTINUE	647
325		C		648
326		C		649
327		C	CHECK FOR NEWTON CONVERGENCE	650
328		C		651
329		C		652
330	00580AI		IFLAG=0	653
331	005812I		DO 420 IB=1,MR	654
332	005826I		XX(IB)=XX(IB)+DNEW(IR)	655
333	00584FI		IF(ABS(DNEW(IB)).GT.ETLINE) IFLAG=1	656
334	00588CI	420	CONTINUE	657
335				658
336	0058A4I		DO 450 I=2,MP	659
337	005888I		IJ=2*(I-1)-1	660
338	0058CFI		IT=2*(I-1)	661
339	0058E2I		U(I,J)=XX(IJ)	662
340	00590AI		IF(I.GE.MP) GO TO 450	663
341	005922I		T(I,J)=XX(IT)	664
342	00594AI		IF(I.EQ.2) T(I,J)=T(I,J)	665

Table C.2--Continued

FORTRAN-VI:R040805D RESTRICTED RIGHTS AS STATED IN LICENSE L-0336

***, SEE DOCUMENT AT 1001 PAC 0488:004-205B99.9/

15 V

343	005988I	450	CONTINUE	666
344				667
345	0059A0I		IF (IFLAG.EQ.0) GO TO 700	668
346	0059B6I		GO TO 100	669
347		C		670
348		C		671
349		C	SUCCESSFUL LINE SWEEP TERMINATION	672
350		C		673
351		C		674
352	0059BAI	700	CONTINUE	675
353				676
354	0059BAI		DO 750 I=1,MP	677
355				678
356	0059CEI		IF (J.EQ. 1) GO TO 740	679
357				680
358	0059E4I		IP=1+1	681
359	0059F2I		IF (I.EQ.MP) IP=I	682
360	005A10I		IM=I-1	683
361	005A1EI		IF (I.EQ.1) IM=I	684
362	005A3AI		FRAC=0.25	685
363	005A45I		IF (I.EQ.1) FRAC=0.5	686
364	005A62I		IF (I.EQ.MP) FRAC=0.5	687
365				688
366	005A80I		V(I,J)=V(I,JM)*T(I,J)/T(I,JM)-FRAC*DYDX	689
367		1	*T(I,J)*(U(IP,J)/T(IP,J)+U(IP,JM)	690
368		2	/T(IP,JM)-U(IM,J)/T(IM,J)-U(IM,JM)	691
369		3	/T(IM,JM))	692
370				693
371	0059E8I		P(I,J)=P(I,JM)-0.5*A*DY*(1./T(I,J)+1./T(I,JM))	694
372	005C74I	740	RHO(I,J)=1./T(I,J)	695
373				696
374	005CAEI	750	CONTINUE	697
375	005CC6I	800	CONTINUE	698
376	005CDEI		GO TO 980	699
377		C		700
378		C		701
379		C	ERROR PRINTOUT - NO CONVERGENCE	702
380		C		703
381		C		704
382	005CE4I	900	CONTINUE	705
383	005CE4I		WRITE(IPRINT,905) J, NNN, MAXITL	706
384	005D0CI	905	FORMAT(///,' NO NEWTON CONVERGENCE ON LINE',	707
385		1	16 ' OF OVERALL SWEEP' 16 ' IN' 16 ' ITERATIONS')	708
386	005D64I		KOUT=1	709
387	005D6CI		DO 920 JA=1,J	710
388	005D80I		CALL SPRINT(JA)	711
389	005D98I	920	CONTINUE	712
390	005D80I		STOP 1	713
391				714
392	005D04I	980	CONTINUE	715
393	005D04I		RETURN	716
394	005D0CI		END	717

NO ERRORS: F7D R04-00 SUBROUTINE MSWEEP 07/17/81 10:20:37 TABLE SPACE: 6 KB
 STATEMENT BUFFER: 20 LINES/1321 BYTES STACK SPACE: 228 WORDS
 SINGLE PRECISION FLOATING PT SUPPORT REQUIRED FOR EXECUTION

Table C.3

LISTING OF FIRE2 CODE

FORTRAN-VII: RELEASED RESTRICTED RIGHTS AS STATED IN LICENSE L-0336

***. SEE DOCUMENTATION PAGE 009:204-805899.V/

1 V

```

1      $BATCH
2      C
3      C
4      0000001      PROGRAM FIRE2
5      C
6      C
7      0000061      COMMON U(41,241),V(41,241),P(41,241),T(41,241),RHO(41,241),
8          1          X(41),Y(241),
9          2          A,SIGMA,XNUIN,XKIN,YMAX,M,N,
10         3          MP,NP,DX,DY,DYDX,DXDY,NNN,
11         4          ETLINE,MAXITL,ETOLP,MAXITP,
12         5          QVAL,XNU,XK,QPRIM,
13         6          KOUT,IGUESS,
14         7          IPRINT,ITTY
15      C
16      C
17      C      READ AND WRITE OUT INPUTS
18      C
19      C
20      0000061      ITTY=1
21      0000061      IPRINT=2
22
23      0000161      READ (ITTY,1) A, SIGMA, XNUIN, XKIN
24      0000401      READ (ITTY,1) YMAX, ETLINE, ETOLP
25      0000681      READ (ITTY,2) M, N, MAXITL, MAXITP
26      0000941      READ (ITTY,2) KOUT, I GUESS
27      0000881      1      FORMAT (4F10.0)
28      0000C51      2      FORMAT (4I10)
29
30      0000D21      DX=1./FLOAT(M)
31      0000F61      DY=YMAX/FLOAT(N)
32
33      0001141      WRITE(IPRINT,10)
34      0001341      10      FORMAT (10X 'FIRE: SOLUTION OF COMBUSTION LAYER ',
35          1          'BOUNDARY VALUE PROBLEM' ///)
36      0001A21      WRITE(IPRINT,12)A,SIGMA,XNUIN,XKIN,YMAX
37      0001B01      12      FORMAT(' SYSTEM PARAMETERS: A = F8.3 ' SIGMA = F8.3
38          1          ' NU = F8.3 ' K = F8.3 ' YMAX = F8.3)
39      00020A1      WRITE(IPRINT,14)M,DX,N,DY
40      0002341      14      FORMAT(/ ' MESH: M = I5 ' DX = F8.3 ' N = I5
41          1          ' DY = F8.3)
42      00026F1      WRITE(IPRINT,16)ETLINE,MAXITL,ETOLP,MAXITP,IGUESS
43      00029C1      16      FORMAT(/ ' ITERATION PARAMETERS: ETLINE = F8.6
44          1          ' MAXITL = I5 ' ETOLP = F8.6 ' MAXITP = I5
45          2          ' I GUESS = I2)
46      C
47      C
48      C      INITIALIZATION
49      C
50      C
51      00030A1      DYDX=DY/DX
52      00031C1      DXDY=DX/DY
53      00032E1      MP=M+1
54      00033C1      NP=N+1
55
56      00034A1      X(1)=0.0
57      0003561      Y(1)=0.0

```

Table C.3--Continued

FORTRAN-VIIID:R04E00SED RESTRICTED RIGHTS AS STATED IN LICENSE L-0336

***, SEE DOCUMENTATION PAGE 1204-PAGE 99.2/

2 V

58	000362I		DO 30 I=2,M	58
59	000376I		X(I)=DX*(FLOAT(I)-1.)	59
60	0003A6I	30	CONTINUE	60
61	0003BEI		DO 32 J=2,N	61
62	0003D2I		Y(J)=DY*(FLOAT(J)-1.)	62
63	000402I	32	CONTINUE	63
64	00041AI		X(MP)=1.0	64
65	00042EI		Y(NP)=YMAX	65
66				66
67	000442I		DO 35 I=1,MP	67
68	000456I		V(I,1)=0.0	68
69	00046AI	35	CONTINUE	69
70				70
71	000482I		DO 40 J=1,NP	71
72	000496I		U(I,J)=0.0	72
73	0004B0I		T(MP,J)=1.0	73
74	0004D0I		RHO(MP,J)=1.0	74
75	0004F0I	40	CONTINUE	75
76		C		76
77		C	PRESCRIBE U ALONG X = 1.0 AND MAKE INITIAL GUESSES ALONG Y = 0.0	77
78		C		78
79	000508I		IZERO=0	79
80	000510I		KK=1	80
81	000518I		CALL BCFUNC(KK,IZERO,IZERO)	81
82		C		82
83		C		83
84		C		84
85		C	OVERALL ITERATION: MARCHING FROM Y=0.0 TO	85
86		C	Y=YMAX,RECURSIVELY FINDING	86
87		C	SOLN. ON Y=Y(J+1) FROM SOLN.	87
88		C	ON Y=Y(I), AND REPEATING UNTIL	88
89		C	PX=0 ON Y=YMAX	89
90		C		90
91		C		91
92				92
93				93
94	000538I		NNN=0	94
95	000540I	50	CONTINUE	95
96	000540I		NNN=NNN+1	96
97	00054EI		IF(NNN.GE.MAXITP) GO TO 950	97
98				98
99				99
100	000566I		CALL MSWEEP	100
101	00056EI		IF (KOUT.EQ. 0) GO TO 980	101
102		C		102
103		C	CALL SPRINT(NNN)	103
104		C	IF(NNN.EQ.1) GOTO 993	104
105		C		105
106				106
107		C		107
108		C	OVERALL CONVERGENCE CHECK PLUS	108
109		C	NEWTON MODIFICATIONS	109
110		C		110
111	000584I		DO 110 I=1,M	111
112	000598I		IP=1+1	112
113	0005A6I		IF (ABS(P(I,NP)-P(IP,NP)).GE.(DX*ETOLP)) GO TO 115	113
114	000612I	110	CONTINUE	114

Table C.3--Continued

FORTRAN-VIID:R04688SED RESTRICTED RIGHTS AS STATED IN LICENSE L-0336

***. SEE DOCUMENTATION PAPER 1204-001M99.2/

3 V

```

115 00062A1      GO TO 900
116
117 0006301      115  CONTINUE
118 0006301      XOMEGA=0.9
119 0006301      DO 120 I=1,M
120 0006501      P(I,1)=P(I,1)+XOMEGA*(P(MP,NP)-P(I,NP))
121 0006A61      120  CONTINUE
122 00068E1      GO TO 50
123
124      C
125      C      STANDARD PRINTOUT
126      C
127      C
128 0006C21      900  CONTINUE
129 0006C21      DO 920 J=1,NP
130 0006D61      CALL SPRINT(J)
131 0006EC1      920  CONTINUE
132 0007041      GO TO 980
133
134      C
135      C      ERROR PRINTOUT
136      C
137      C
138 0007041      950  CONTINUE
139 0007041      WRITE(1,PRINT,960) MAXITP
140 0007281      960  FORMAT(//////,' NO CONVERGENCE IN',I6,' OVERALL
141      1          ITERATIONS ON P',////)
142
143 0007841      CALL SPRINT(NP)
144 0007A01      980  CONTINUE
145
146 0007A01      WRITE (8)  A, SIGMA, XNUIN, XKIN, YMAX, ETLINE, ETOLP, DX, DY
147 0007DC1      WRITE (8)  M, N, MAXITL, MAXITP, KOUT, IGVFSS
148 00090C1      DO 990 J = 1, NP
149 0009201      WRITE (8)  (U(I,J), I = 1, MP)
150 0009AC1      990  CONTINUE
151 0009AC1      DO 991 J = 1, NP
152 0009DB1      WRITE (8)  (V(I,J), I = 1, MP)
153 0009601      991  CONTINUE
154 0009781      WRITE (9)  A, SIGMA, XNUIN, XKIN, YMAX, ETLINE, ETOLP, DX, DY
155 0009841      WRITE (9)  M, N, MAXITL, MAXITP, KOUT, IGVFSS
156 0009E41      DO 992 J = 1, NP
157 0009F81      WRITE (9)  (T(I,J), I = 1, MP)
158 000A801      992  CONTINUE
159 000A981      DO 993 J = 1, NP
160 000AAC1      WRITE (9)  (P(I,J), I = 1, MP)
161 000A341      993  CONTINUE
162 000B4C1      WRITE (7)  A, SIGMA, XNUIN, XKIN, YMAX, ETLINE, ETOLP, DX, DY
163 000B881      WRITE (7)  M, N, MAXITL, MAXITP, KOUT, IGVFSS
164 000B881      DO 994 J = 1, NP
165 0009CC1      WRITE (7)  (WH0(I,J), I = 1, MP)
166 000C541      994  CONTINUE
167 000C6C1      STOP
168 000C741      END

```

NO ERRORS: FTD R04-00 MAINPR0G FIRE2 07/17/81 10:17:32 TABLE SPACE: 4 KB
 STATEMENT BUFFER: 20 LINES/1321 BYTES STACK SPACE: 175 WORDS

Table C.3--Continued

FORTRAN-VIIO:RD4GBNSD RESTRICTED RIGHTS AS STATED IN LICENSE L-0336

*** SEE DOCUMENTATION 01PAC (MAG 264-203899.V)

5 V

1	000000I	SUBROUTINE HCFUNC(KEY,II,JJ)	169
2			170
3			171
4	000004I	COMMON U(41,241),V(41,241),P(41,241),T(41,241),PHO(41,241),	172
5		1 X(41),Y(241),	173
6		2 A,SIGMA,XNUIN,XKIN,YMAX,M,N,	174
7		3 MP,NP,DX,DY,DYDX,DYDY,NNN,	175
8		4 ETLNE,MAXITL,ETOLP,MAXITP,	176
9		5 QVAL,XNU,XK,DPRIM,	177
10		6 KOUT, IGUESS,	178
11		7 IPRINT,ITTY	179
12			180
13			181
14	000004I	GOTO(100,200,300,400,500)KEY	182
15		C	183
16		C	184
17		C U INLET PRESCRIPTION - CAN BE CHANGED	185
18		C	186
19		C	187
20	000036I	100 CONTINUE	188
21	000036I	READ(ITTY,90) CCCIN	189
22	000054I	90 FORMAT(F10.0)	190
23		C	191
24	000060I	CONTINUE	192
25	000060I	DO 150 J=1,NP	193
26	000074I	CC=1.0	194
27	000080I	CCC=CCCIN	195
28	000080I	CFAC=(EXP(CC)-EXP(-CC))/(EXP(CC)+EXP(-CC))	196
29	000132I	U(MP,J)=-CCC*CFAC*EXP(-CCC*Y(J))	197
30	000190I	U(MP,J)=-CCC	198
31	000102I	IF(Y(J).GT.1.0) U(MP,J)=-CCC*EXP(-(Y(J)-1.0))	199
32	000230I	150 CONTINUE	200
33		C	201
34		C	202
35		C INITIAL GUESSES FOR Y=0.0 - CAN BE CHANGED	203
36		C	204
37		C	205
38	000254I	IF (IGUESS.EQ. 0) GO TO 170	206
39	000264I	DO 160 I = 1, MP	207
40	000270I	READ (ITTY,161) P(I,1)	208
41	000280I	160 CONTINUE	209
42	000208I	161 FORMAT (F10.0)	210
43	000204I	GO TO 170	211
44			212
45	000204I	170 CONTINUE	213
46	000204I	DO 180 I = 1, MP	214
47	000200I	P(I,1) = 0.67-4.0+4.0*x(I)**2-0.67*x(I)**3+1.0	215
48	000356I	P(I,1)=X(I)*X(I)-1.0	216
49	000386I	T(I,1) = 1.6-0.6*x(I)	217
50	000380I	CC = 1.	218
51	000380I	CCC=CCCIN	219
52	000308I	EP = EXP(CC*x(I))	220
53	000300I	EM = EXP(-CC*x(I))	221
54	000430I	U(I,1) = -CCC*(EP-EM)/(EP+EM)	222
55	000474I	U(I,1)=U(I,1)/CFAC	223
56			224
57	000496I	180 CONTINUE	225

Table C.3--Continued

FORTRAN-VIIID:RQ4E88SED RESTRICTED RIGHTS AS STATED IN LICENSE L-0336

***. SEE DOCUMENTATION PACKAGE 1264-R05899.0/

6 V

58	0004AEI	GOTO 900	226
59		C	227
60		C	228
61		C Q(X,Y) PRESCRIPTION - CAN BE CHANGED	229
62		C	230
63		C	231
64	0004B4I	200 CONTINUE	232
65	0004H4I	IF(JJ.EQ.1)TAVG=T(II,JJ)	233
66	0004E4I	JJM=JJ-1	234
67	0004F2I	IF(JJ.GE.2)TAVG=0.5*(T(II,JJ)+T(II,JJM))	235
68			236
69	000542I	QVAL=1.0-SIGMA*(TAVG**4-1.0)	237
70			238
71	00056AI	IF(Y(JJ).GT.1.0) QVAL=QVAL-1.0	239
72		C	240
73		C	241
74		C NU(X,Y) PRESCRIPTION - CAN BE CHANGED	242
75		C	243
76		C	244
77	000596I	300 CONTINUE	245
78	000596I	XNU = XNUIN	246
79	0005A2I	CNU=0.0	247
80	0005AEI	XNU=XNU**EXP(-CNU**X(II))	248
81	0005F4I	IF(X(II).GT.1.0)XNU=0.0	249
82	000614I	GOTO 900	250
83		C	251
84		C	252
85		C K(X,Y) PRESCRIPTION - CAN BE CHANGED	253
86		C	254
87		C	255
88	000520I	400 CONTINUE	256
89	000520I	XK = XKIN	257
90	00052CI	CK=0.0	258
91	000538I	XK=XK**EXP(-CK*X(II))	259
92	00057CI	IF(X(II).GT.1.0)XK=0.0	260
93	0006A2I	GOTO 900	261
94		C	262
95		C QPRIME COMPUTATION - CAN BE CHANGED	263
96		C	264
97	0006A8I	500 CONTINUE	265
98	0006A8I	IF(JJ.EQ.1)TAVG=T(II,JJ)	266
99	0006D8I	JJM=JJ-1	267
100	0006E6I	IF(JJ.GE.2)TAVG=(T(II,JJ)+T(II,JJM))/2.	268
101			269
102	000736I	QPRIM=-4.*SIGMA*(TAVG**3)	270
103			271
104	000760I	900 CONTINUE	272
105	000760I	RETURN	273
106	000766I	END	274

NO ERRORS:F7D R04-00 SUBROUTINE RCFUNC 07/17/81 10:17:36 TABLE SPACE: 4 KB
 STATEMENT BUFFER: 20 LINES/1321 BYTES STACK SPACE: 213 WORDS
 SINGLE PRECISION FLOATING PT SUPPORT REQUIRED FOR EXECUTION

Table C.3--Continued

FORTRAN-VIID:RQ4688SED RESTRICTED RIGHTS AS STATED IN LICENSE L-0336

***, SEE DOCUMENTATION PAPER 284-PA899.Y/

7 V

```

1 000000I      SUBROUTINE SPRINT(JJ)
2
3
4 000004I      COMMON U(41,241),V(41,241),P(41,241),T(41,241),PHO(41,241),
5                1 X(41),Y(241),
6                2 A,SIGMA,XNUIN,XKIN,YMAX,M,N,
7                3 MP,NP,DX,DY,DYDX,DXDY,NNN,
8                4 ETLIN,MAXITL,ETOLP,MAXITP,
9                5 QVAL,XNU,XK,3PRIM,
10               6 KOUT,IGUESS,
11               7 IPRINT,ITTY
12
13 000004I      DIMENSION PX(41),VISC(41),DIFF(41),HEAT(41)
14
15 C
16 C      COMPUTE PX, UXX, TXX AND Q(T) TERMS
17 C
18 C
19 000004I      DO 50 I = 1, MP
20 000280I      IP = I + 1
21 000280I      IM = I - 1
22 000200I      DO 10 KK = 2, 4
23 000204I      CALL BCFUNC (KK, I, JJ)
24 0002F4I      10 CONTINUE
25 000304I      IF (I .EQ. 1) GO TO 20
26 000320I      IF (I .EQ. MP) GO TO 30
27
28 000338I      PX(I) = (P(IP,JJ)-P(IM,JJ))/(2.*DX)
29 000386I      VISC(I) = (U(IP,JJ)-2.*U(I,JJ)+U(IM,JJ))*XNU/(DX*DX)
30 0003FCI      DIFF(I) = (T(IP,JJ)-2.*T(I,JJ)+T(IM,JJ))*XK/(DX*DX)
31 000472I      HEAT(I) = QVAL
32 000484I      GO TO 50
33
34 000484I      20 PX(I) = 0.
35 000490I      VISC(I) = 0.
36 0004AEI      DIFF(I) = 2.*(T(IP,JJ)-T(I,JJ))*XK/(DX*DX)
37 000508I      HEAT(I) = QVAL
38 00051AI      GO TO 50
39
40 000520I      30 PX(I) = (P(I,JJ)-P(IM,JJ))/DX
41 000566I      VISC(I) = VISC(IM)
42 00057EI      DIFF(I) = DIFF(IM)
43 000596I      HEAT(I) = QVAL
44
45 0005ARI      50 CONTINUE
46 C
47 C
48 C      STANDARD PRINTOUT
49 C
50 C
51 0005C0I      WRITE(IPRINT,100)JJ,Y(JJ)
52 0005F8I      100 FORMAT(//// ' FOR J = ' I5 ' (Y = ' F8.3 '):')
53 000520I      WRITE(IPRINT,120)
54 00053CI      120 FORMAT(//, '      I      X      U      V      T,
55                1 PHO      P' 21X 'PX      NU*UXX      K*TXX      Q(T)' /)
56 0006A2I      DO 150 I=1,MP
57 0006H5I      WRITE(IPRINT,140)I,X(I),U(I,JJ),V(I,JJ),T(I,JJ),PHO(I,JJ),

```

275
276
277
278
279
280
281
282
283
284
285
286
287
288
289
290
291
292
293
294
295
296
297
298
299
300
301
302
303
304
305
306
307
308
309
310
311
312
313
314
315
316
317
318
319
320
321
322
323
324
325
326
327
328
329
330
331

Table C.3--Continued

```

FORTRAN-VIID:RQ4E88SED RESTRICTED RIGHTS AS STATED IN LICENSE L-0336      ***. SEE DOCUMENTATION 001PAC08A68:204-805899.0/      8 V
58      1      P(I,JJ), PX(I), VISC(I), DIFF(I), HEAT(I)      332
59 000804I 140  FORMAT(3X,16.6F8.3, 15X. 4F8.3)      333
60 00081CI 160  CONTINUE      334
61 000834I      RETURN      335
62 000834I      END      336

NO ERRORS:F70 R04-00      SUBROUTINE SPRINT      07/17/81 10:17:39 TABLE SPACE: 3 KB
STATEMENT BUFFER: 20 LINES/1321 BYTES      STACK SPACE: 171 WORDS
SINGLE PRECISION FLOATING PT SUPPORT REQUIRED FOR EXECUTION

```

Table C.3--Continued

FORTRAN-VIID:R0468850 RESTRICTED RIGHTS AS STATED IN LICENSE L-0336

***, SEE DOCUMENTATION PAGES 264-265-266-267-268-269-270-271-272-273-274-275-276-277-278-279-280-281-282-283-284-285-286-287-288-289-290-291-292-293-294-295-296-297-298-299-300-301-302-303-304-305-306-307-308-309-310-311-312-313-314-315-316-317-318-319-320-321-322-323-324-325-326-327-328-329-330-331-332-333-334-335-336-337-338-339-340-341-342-343-344-345-346-347-348-349-350-351-352-353-354-355-356-357-358-359-360-361-362-363-364-365-366-367-368-369-370-371-372-373-374-375-376-377-378-379-380-381-382-383-384-385-386-387-388-389-390-391-392-393-394-395-396-397-398-399-400-401-402-403-404-405-406-407-408-409-410-411-412-413-414-415-416-417-418-419-420-421-422-423-424-425-426-427-428-429-430-431-432-433-434-435-436-437-438-439-440-441-442-443-444-445-446-447-448-449-450-451-452-453-454-455-456-457-458-459-460-461-462-463-464-465-466-467-468-469-470-471-472-473-474-475-476-477-478-479-480-481-482-483-484-485-486-487-488-489-490-491-492-493-494-495-496-497-498-499-500-501-502-503-504-505-506-507-508-509-510-511-512-513-514-515-516-517-518-519-520-521-522-523-524-525-526-527-528-529-530-531-532-533-534-535-536-537-538-539-540-541-542-543-544-545-546-547-548-549-550-551-552-553-554-555-556-557-558-559-560-561-562-563-564-565-566-567-568-569-570-571-572-573-574-575-576-577-578-579-580-581-582-583-584-585-586-587-588-589-590-591-592-593-594-595-596-597-598-599-600-601-602-603-604-605-606-607-608-609-610-611-612-613-614-615-616-617-618-619-620-621-622-623-624-625-626-627-628-629-630-631-632-633-634-635-636-637-638-639-640-641-642-643-644-645-646-647-648-649-650-651-652-653-654-655-656-657-658-659-660-661-662-663-664-665-666-667-668-669-670-671-672-673-674-675-676-677-678-679-680-681-682-683-684-685-686-687-688-689-690-691-692-693-694-695-696-697-698-699-700-701-702-703-704-705-706-707-708-709-710-711-712-713-714-715-716-717-718-719-720-721-722-723-724-725-726-727-728-729-730-731-732-733-734-735-736-737-738-739-740-741-742-743-744-745-746-747-748-749-750-751-752-753-754-755-756-757-758-759-760-761-762-763-764-765-766-767-768-769-770-771-772-773-774-775-776-777-778-779-780-781-782-783-784-785-786-787-788-789-790-791-792-793-794-795-796-797-798-799-800-801-802-803-804-805-806-807-808-809-810-811-812-813-814-815-816-817-818-819-820-821-822-823-824-825-826-827-828-829-830-831-832-833-834-835-836-837-838-839-840-841-842-843-844-845-846-847-848-849-850-851-852-853-854-855-856-857-858-859-860-861-862-863-864-865-866-867-868-869-870-871-872-873-874-875-876-877-878-879-880-881-882-883-884-885-886-887-888-889-890-891-892-893-894-895-896-897-898-899-900-901-902-903-904-905-906-907-908-909-910-911-912-913-914-915-916-917-918-919-920-921-922-923-924-925-926-927-928-929-930-931-932-933-934-935-936-937-938-939-940-941-942-943-944-945-946-947-948-949-950-951-952-953-954-955-956-957-958-959-960-961-962-963-964-965-966-967-968-969-970-971-972-973-974-975-976-977-978-979-980-981-982-983-984-985-986-987-988-989-990-991-992-993-994-995-996-997-998-999-1000

9 V

```

1 0000001 SUBROUTINE MSWEEP 337
2 338
3 339
4 0000041 COMMON U(41,241),V(41,241),P(41,241),T(41,241),RHO(41,241), 340
5 1 X(41),Y(241), 341
6 2 A,SIGMA,XNUIN,XKIN,YMAX,M,N, 342
7 3 MP,NP,DX,DY,DYDX,DXDY,NNN, 343
8 4 ETLIN,MAXITL,ETOLP,MAXITP, 344
9 5 QVAL,XNU,XK,QPRIM, 345
10 6 KOUT,IGUESS, 346
11 7 IPRINT,ITTY 347
12 348
13 0000041 DIMENSION XX(200),FF(200),AZ(100),A1(100), 349
14 1 A2(100),B2(100),B1(100),B2(100), 350
15 2 C2(100),C1(100),C2(100),DZ(100), 351
16 3 D1(100),D2(100),XMAT(7,200), 352
17 4 DNEW(200) 353
18 354
19 355
20 0000041 MM=M-1 356
21 00321A1 MB=2*(M-1) 357
22 00322E1 MBM = MB - 1 358
23 00323C1 MBM2 = MB - 2 359
24 00324A1 MBM3 = MB - 3 360
25 361
26 362
27 00325B1 DO 800 J=1,NP 363
28 00326C1 JM=J-1 364
29 00327A1 JM2=J-2 365
30 C 366
31 C 367
32 C INITIAL GUESSES FOR U AND T ON LINE J 368
33 C 369
34 C 370
35 00328B1 DO 20 I=2,M 371
36 00329C1 IU=2*(I-1)-1 372
37 00328B1 IT=2*(I-1) 373
38 0032C6I IF(J.EQ.1) GO TO 14 374
39 00320C1 IF(J.EQ.2) GO TO 12 375
40 C 376
41 C LINEAR EXTRAPOLATION USED FOR J .GE. 3 377
42 C 378
43 0032F2I U(I,J)=2.*U(I,JM)-U(I,JM2) 379
44 003346I T(I,J)=2.*T(I,JM)-T(I,JM2) 380
45 00339A1 GO TO 14 381
46 C 382
47 C PREVIOUS VALUES (=INITIAL GUESSES FOR NNN=1) USED FOR J = 1 OR J = 2 383
48 C 384
49 0033A0I 12 U(I,J)=U(I,JM) 385
50 003304I T(I,J)=T(I,JM) 386
51 003408I 14 CONTINUE 387
52 003408I XX(I,J)=U(I,J) 388
53 00342FI XX(IT)=T(I,J) 389
54 003454I IF(I.EQ.2) T(I,J)=T(I,J) 390
55 003492I 20 CONTINUE 391
56 C 392
57 C 393

```

Table C.3--Continued

FORTRAN-VIID:R04688SED RESTRICTED RIGHTS AS STATED IN LICENSE L-0336

***. SEE DOCUMENT AIT081PAC0462:264-P03899.R/

10 V

58	C		394
59	C	OVERALL VECTOR NEWTON ITERATION	395
60	C	USING GAUSS ELIMINATION ON LINEAR EQNS.	396
61	C		397
62	C		398
63	C		399
64	0034A4I	NUMITL = 0	400
65	0034B2I	100 NUMITL=NUMITL+1	401
66	0034C0I	IF (NUMITL.GT.MAXITL) GOTO 900	402
67			403
68			404
69	0034D8I	DO 200 I=2,M	405
70	0034ECI	IM=I-1	406
71	0034FAI	IP=I+1	407
72	003508I	IU=2*(I-1)-1	408
73	00351EI	IT=2*(I-1)	409
74	003532I	IF (J.EQ.1) JM=1	410
75			411
76	00354AI	KK=2	412
77	003552I	CALL BCFUNC(KK,I,J)	413
78	003570I	KK=3	414
79	003578I	CALL BCFUNC(KK,I,JM)	415
80	003598I	XNUM=XNI	416
81	0035A4I	KK=3	417
82	0035ACI	CALL BCFUNC(KK,I,J)	418
83	0035CCI	KK=4	419
84	0035D4I	CALL BCFUNC(KK,I,JM)	420
85	0035F4I	XKM=XK	421
86	003500I	KK=4	422
87	003608I	CALL BCFUNC(KK,I,J)	423
88	003628I	KK=5	424
89	003630I	CALL BCFUNC(KK,I,J)	425
90			426
91	003450I	IF (J.GE.2) GO TO 110	427
92			428
93	C		429
94	C	NEWTON SET-UP FOR J = 1	430
95	C		431
96	C		432
97	003666I	RR=0.5*(P(IP,1)-P(IM,1))	433
98	0036AEI	PI=0.	434
99			435
100	00369AI	FF(IJ)=(U(IP,1)-2.*U(I,1)+U(IM,1))*XNU/DX	436
101		1 -0.5*(U(IP,1)-U(IM,1))*U(I,1)/T(I,1)-RR	437
102			438
103	00372AI	FF(IT)=(T(IP,1)-2.*T(I,1)+T(IM,1))*XK/DX	439
104		1 -0.5*(T(IP,1)-T(IM,1))*U(I,1)/T(I,1)*DX*QVAL	440
105			441
106	0037C2I	IF (IM.GE.2) GO TO 108	442
107	0037D8I	A7(1)=0.0	443
108	0037F2I	A1(1)=-2.*XNU/DX-0.5*U(3,1)/T(2,1)	444
109	003814I	A2(1)=XNU/DX-0.5*U(2,1)/T(2,1)	445
110	003838I	B7(1)=0.0	446
111	003842I	H1(1)=0.5*U(3,1)*U(2,1)/(T(2,1)*2)	447
112	003864I	H2(1)=0.0	448
113	003872I	C7(1)=0.0	449
114	00387CI	C1(1)=-0.5*(T(3,1)/T(2,1)-1.0)	450

Table C.3--Continued

FORTRAN-VIIO:R0468850 RESTRICTED RIGHTS AS STATED IN LICENSE L-0336

***, SEE DOCUMENTATION PAM4671264-P03899.8/

11 V

```

115 0039A0I      C2(I)=0.0                      451
116 0038AAI      DZ(I)=0.0                      452
117 0038B4I      D1(I)=-XK/DX+0.5*T(3,1)*U(2,1)/(T(2,1)**2) 453
118              1      +DX*QPRIM                454
119 0038FEI      D2(I)=XK/DX-0.5*U(2,1)/T(2,1)      455
120 003922I      GO TO 200                        456
121              457
122 003928I      108  AZ(IM)=XNU/DX+0.5*U(I,1)/T(I,1) 458
123 003964I      A1(IM)=-2.*XNU/DX-0.5*(U(IP,1)-U(IM,1))/T(I,1) 459
124 00398CI      A2(IM)=XNU/DX-0.5*U(I,1)/T(I,1)      460
125 0039F8I      BZ(IM)=0.0                      461
126 003A0AI      B1(IM)=0.5*(U(IP,1)-U(IM,1))*U(I,1)/(T(I,1)**2) 462
127 003A6AI      B2(IM)=0.0                      463
128 003A7CI      CZ(IM)=0.0                      464
129 003A8EI      C1(IM)=-0.5*(T(IP,1)-T(IM,1))/T(I,1) 465
130 003AD2I      C2(IM)=0.0                      466
131 003AE4I      DZ(IM)=XK/DX+0.5*U(I,1)/T(I,1)      467
132 003920I      D1(IM)=-2.*XK/DX+0.5*(T(IP,1)-T(IM,1))*U(I,1) 468
133              1      / (T(I,1)**2) +DX*QPRIM      469
134 0038AAI      D2(IM)=XK/DX-0.5*U(I,1)/T(I,1)      470
135              471
136 0039E6I      IF(I,LT,M) GO TO 200              472
137 0038FEI      A2(IM)=0.0                      473
138 003C10I      D2(IM)=0.0                      474
139              475
140 003C22I      GO TO 200                        476
141              C      477
142              C      478
143              C      NEWTON SET-UP FOR J .GE. 2 479
144              C      480
145              C      481
146 003C28I      110  CONTINUE                    482
147 003C28I      RR=(J(IP,JM)-2.*U(I,JM)+U(IM,JM))*XNUM 483
148              1      / (2.*DX) - ((U(IP,JM)**2)/T(IP,JM) 484
149              1      - (U(IM,JM)**2)/T(IM,JM) + 2.*(P(IP,JM) 485
150              3      - P(IM,JM)) - 0.5*A*DY*(1./T(IP,JM) 486
151              4      - 1./T(IM,JM)))/4.          487
152 003DBAI      RR=-RR-U(I,JM)*V(I,JM)/T(I,JM)*DXDY 488
153 003F22I      P1=-((T(IP,JM)-2.*T(I,JM)+T(IM,JM))*XKM 489
154              1      / (2.*DX) - (U(IP,JM)-U(IM,JM))/4.*V(I,JM)*DXDY) 490
155              491
156 003EF8I      FF(IJ)=(U(IP,J)-2.*U(I,J)+U(IM,J))*XNU 492
157              1      / (2.*DX) - 0.25*(U(IP,J)**2)/T(IP,J) 493
158              2      - (U(IM,J)**2)/T(IM,J) - 0.5*A*DY 494
159              3      *(1./T(IP,J)-1./T(IM,J))-U(I,J)* 495
160              4      (DXDY*V(I,JM)/T(I,JM)-0.25*(U(IP,J) 496
161              5      /T(IP,J)+U(IP,JM)/T(IP,JM)-U(IM,J) 497
162              6      /T(IM,J)-U(IM,JM)/T(IM,JM))-RR 498
163              499
164 00419AI      FF(IT)=(T(IP,J)-2.*T(I,J)+T(IM,J))*XK 500
165              1      / (2.*DX) - 0.25*(U(IP,J)-U(IM,J)) 501
166              2      - T(I,J)*(DXDY*V(I,JM)/T(I,JM)-0.25 502
167              3      *(U(IP,J)/T(IP,J)+U(IP,JM)/T(IP,JM) 503
168              4      -U(IM,J)/T(IM,J)-U(IM,JM)/T(IM,JM)) 504
169              5      +DX*QVAL-P1                505
170              506
171 004396I      IF(IM,GE,2)GO TO 120              507

```

Table C.3--Continued

FORTRAN-VIID:R01600SED RESTRICTED RIGHTS AS STATED IN LICENSE L-0336

***, SEE DOCUMENTATION PACBAGZ+264-203899.V/

12 V

```

172 0043ACI      A2(I)=0.0
173 004386I      A1(I)=-2.*XNU/(2.*DX)-(DXDY*V(2,JM)/T(2,JM)
174              1      -0.25*(U(3,J)/T(3,J)+U(3,JM)/T(3,JM))
175 004466I      A2(I)=XNU/(2.*DX)-0.25*(2.*U(3,J)-U(2,J))/T(3,J)
176 0044C8I      B7(I)=0.0
177 0044D2I      B1(I)=0.25*(0.5*A*DY/(T(2,J)**2))
178 00450CI      B2(I)=0.25*(U(3,J)**2-U(2,J)*U(3,J))/T(3,J)
179              1      **2)-0.5*A*DY/(T(3,J)**2))
180 004588I      CZ(I)=0.0
181 0045C2I      C1(I)=0.0
182 0045CCI      C2(I)=-0.25*(1.-T(2,J)/T(3,J))
183 00460EI      DZ(I)=0.0
184 004618I      D1(I)=-XK/(2.*DX)-(DXDY*V(2,JM)/T(2,JM)
185              1      -0.25*(U(3,J)/T(3,J)+U(3,JM)/T(3,JM))
186              2      +0.5*DX*OPRIM
187 0046D6I      D2(I)=XK/(2.*DX)-0.25*T(2,J)*U(3,J)/T(3,J)**2)
188 00473CI      GOTO 200
189
190 004742I      120  A2(IM)=XNU/(2.*DX)+0.25*(2.*U(IM,J)-U(I,J))/T(IM,J)
191 0047C0I      A1(IM)=-2.*XNU/(2.*DX)-(DXDY*V(I,JM)/T(I,JM)
192              1      -0.25*(U(IP,J)/T(IP,J)+U(IP,JM)/T(IP,JM)
193              2      -U(IM,J)/T(IM,J)-U(IM,JM)/T(IM,JM))
194 00490AI      A2(IM)=XNU/(2.*DX)-0.25*(2.*U(IP,J)-U(I,J))/T(IP,J)
195 004988I      B2(IM)=-0.25*(U(IM,J)-U(I,J))*U(IM,J)/T(IM,J)
196              1      **2)-0.5*A*DY/(T(IM,J)**2))
197 004A58I      B1(IM)=0.0
198 004A6AI      B2(IM)=0.25*(U(IP,J)-U(I,J))*U(IP,J)/T(IP,J)
199              1      **2)-0.5*A*DY/(T(IP,J)**2))
200 004B32I      CZ(IM)=0.25*(1.-T(I,J)/T(IM,J))
201 004B80I      C1(IM)=0.0
202 004B92I      C2(IM)=-0.25*(1.-T(I,J)/T(IP,J))
203 0049E9I      DZ(IM)=XK/(2.*DX)+0.25*T(I,J)*U(IM,J)/T(IM,J)**2)
204 004C74I      D1(IM)=-2.*XK/(2.*DX)-(DXDY*V(I,JM)/T(I,JM)
205              1      -0.25*(U(IP,J)/T(IP,J)+U(IP,JM)/T(IP,JM)
206              2      -U(IM,J)/T(IM,J)-U(IM,JM)/T(IM,JM))
207              3      +0.5*DX*OPRIM
208 004DD0I      D2(IM)=XK/(2.*DX)-0.25*T(I,J)*U(IP,J)/T(IP,J)**2)
209
210 004E5CI      IF(I.LT.M)GOTO 200
211 004F74I      A2(IM)=0.0
212 004E88I      B2(IM)=0.0
213 004E9CI      C2(IM)=0.0
214 004EAEI      D2(IM)=0.0
215
216 004EC0I      200  CONTINUE
217              C
218              C
219              C      SPARSE (JACOBIAN) MATRIX COMPACTIFICATION
220              C
221              C
222 004ED8I      DO 250 IM=1,MM
223 004EECI      IU=2*IM-1
224 004EFCI      IT=2*IM
225 004F0AI      XMAT(I,IU)=0.0
226 004F22I      XMAT(2,IU)=A7(IM)
227 004F42I      XMAT(3,IU)=B7(IM)
228 004F62I      XMAT(4,IU)=A1(IM)

```

508

509

510

511

512

513

514

515

516

517

518

519

520

521

522

523

524

525

526

527

528

529

530

531

532

533

534

535

536

537

538

539

540

541

542

543

544

545

546

547

548

549

550

551

552

553

554

555

556

557

558

559

560

561

562

563

564

Table C.3--Continued

FORTRAN-VIID:R046B05ED RESTRICTED RIGHTS AS STATED IN LICENSE L-0336

***, SEE DOCUMENTATION PAC8062, 204-805899.8/

13 V

229	004F82I		XMAT(5,IU)=B1(IM)	565
230	004FA2I		XMAT(6,IU)=A2(IM)	566
231	004FC2I		XMAT(7,IU)=B2(IM)	567
232	004FE2I		XMAT(1,IT)=C2(IM)	568
233	005002I		XMAT(2,IT)=D2(IM)	569
234	005020I		XMAT(3,IT)=C1(IM)	570
235	00503FI		XMAT(4,IT)=D1(IM)	571
236	00505CI		XMAT(5,IT)=C2(IM)	572
237	00507AI		XMAT(6,IT)=D2(IM)	573
238	00509AI		XMAT(7,IT)=0.0	574
239	005080I	250	CONTINUE	575
240		C		576
241		C		577
242		C	GAUSS ELIMINATION TO SOLVE JD=-F	578
243		C		579
244		C		580
245	0050C8I		DO 500 I=1,MBM	581
246	0050DCI		KMAX=3	582
247	0050E4I		IF(I.EQ.MBM2) KMAX=2	583
248	0050FEI		IF(I.EQ.MBM) KMAX=1	584
249				585
250	005118I		DO 490 K=1,KMAX	586
251	00512CI		IK=I+K	587
252	00513EI		M4K=4-K	588
253	00514CI		PIVOT=XMAT(M4K,IK)/XMAT(4,I)	589
254				590
255	00517CI		DO 480 LL=4,7	591
256	005184I		ML=LL-K	592
257	005196I		XMAT(ML,IK)=XMAT(ML,IK)-PIVOT*XMAT(LL,I)	593
258	0051E6I	480	CONTINUE	594
259				595
260	0051FCI		FF(IK)=FF(IK)-PIVOT*FF(I)	596
261	00522EI	490	CONTINUE	597
262	005246I	500	CONTINUE	598
263				599
264	00525EI		DNEW(MB)=-FF(MB)/XMAT(4,MB)	600
265	005292I		DNEW(MBM)=- (FF(MBM)+XMAT(5,MBM)*DNEW(MB))/XMAT(4,MBM)	601
266	0052E4I		DNEW(MBM2)=- (FF(MBM2)+XMAT(5,MBM2)*DNEW(MBM)	602
267		1	+XMAT(6,MBM2)*DNEW(MB))/XMAT(4,MBM2)	603
268				604
269	005356I		DO 550 I=1,MBM3	605
270	00536AI		IB=MBM2-I	606
271	00537CI		XXX=FF(IB)	607
272	005390I		DO 540 K=5,7	608
273	005398I		IBP=IB+K-4	609
274	0053ACI		XXX=XXX+XMAT(K,IB)*DNEW(IBP)	610
275	0053DCI	540	CONTINUE	611
276	0053F2I		DNEW(IB)=-XXX/XMAT(4,IB)	612
277	00541EI	550	CONTINUE	613
278		C		614
279		C		615
280		C	CHECK FOR NEWTON CONVERGENCE	616
281		C		617
282		C		618
283	005436I		IFLAG=0	619
284	00543EI		DO 420 IB=1,MB	620
285	005452I		XX(IB)=XX(IB)+DNEW(IB)	621

Table E.3--Continued

FORTRAN-VLID:RQ4EBBSED RESTRICTED RIGHTS AS STATED IN LICENSE L-0336
 ***. SEE DOCUMENT 7 AT 001 PACMAG 2:264-203899.0/ 14 V

286	00547AI		IF (ABS(DNEW(IB)).GT.ETLINE) IFLAG=1	622
287	00548BI	420	CONTINUE	623
288				624
289	0054D0I		DO 450 I=2,M	625
290	0054E4I		IU=2*(I-1)-1	626
291	0054FAI		IT=2*(I-1)	627
292	00550FI		U(I,J)=XX(IU)	628
293	005536I		T(I,J)=XX(IT)	629
294	00555EI		IF (I.EQ.2) T(I,J)=T(I,J)	630
295	00559CI	450	CONTINUE	631
296				632
297	0055B4I		IF (IFLAG.EQ.0) GOTO 700	633
298	0055CAI		GOTO 100	634
299		C		635
300		C		636
301		C	SUCCESSFUL LINE SWEEP TERMINATION	637
302		C		638
303		C		639
304	0055CEI	700	CONTINUE	640
305				641
306	0055CEI		DO 750 I=1,MP	642
307				643
308	0055E2I		IF (J.EQ.1) GO TO 740	644
309				645
310	0055FAI		IP=I+1	646
311	005606I		IF (I.EQ.MP) IP=I	647
312	005624I		IM=I-1	648
313	005632I		IF (I.EQ.1) IM=I	649
314	00564EI		FRAC=0.25	650
315	00565AI		IF (I.EQ.1) FRAC=0.5	651
316	005676I		IF (I.EQ.MP) FRAC=0.5	652
317				653
318	005694I		V(I,J)=V(I,JM)*T(I,J)/T(I,JM)-FRAC*DYDX	654
319		1	*T(I,J)*(U(IP,J)/T(IP,J)+U(IP,JM)	655
320		2	/T(IP,JM)-U(IM,J)/T(IM,J)-U(IM,JM)	656
321		3	/T(IM,JM))	657
322				658
323	0057FCI		P(I,J)=P(I,JM)-0.5*A*DY*(1./T(I,J)+1./T(I,JM))	659
324	00588BI	740	RHO(I,J)=1./T(I,J)	660
325				661
326	0058C2I	750	CONTINUE	662
327		C		663
328		C		664
329		C	IF (J.EQ.1) GOTO 980	665
330		C		666
331		C		667
332	0058DAI	800	CONTINUE	668
333	0054F2I		GOTO 980	669
334		C		670
335		C		671
336		C	ERROR PRINTOUT - NO CONVERGENCE	672
337		C		673
338		C		674
339	0058FAI	900	CONTINUE	675
340	0058FAI		WRITE(IPRINT,905) J, NNN, MAXITL	676
341	005920I	905	FORMAT(///, ' NO NEWTON CONVERGENCE ON LINE',	677
342		1	16 ' OF OVERALL SWEEP' 16 ' IN' 16 ' ITERATIONS')	678

Table C.3--Continued

FORTRAN-VI:RD46885ED RESTRICTED RIGHTS AS STATED IN LICENSE L-0335			***, SEE DOCUMENTATION PAGE 1284-203899.V/	15 V
343	005978I	KOUT=0	679	
344	005980I	DO 920 JA=1,J	680	
345	005994I	CALL SPRINT(JA)	681	
346	0059ACI	920 CONTINUE	682	
347			683	
348	0059C4I	980 CONTINUE	684	
349	0059C4I	RETURN	685	
350	0059CCI	END	686	

NO ERRORS:F7D R04-00 SUBROUTINE MSWEEP 07/17/81 10:18:01 TABLE SPACE: 6 KB
 STATEMENT BUFFER: 20 LINES/1321 BYTES STACK SPACE: 228 WORDS
 SINGLE PRECISION FLOATING PT SUPPORT REQUIRED FOR EXECUTION

REFERENCES

- Bond, H. (ed.), *Fire and the Air War*, 1st ed., National Fire Protection Association, Boston, Mass., 1951.
- Brode, H. L., *Large-Scale Urban Fires*, Pacific-Sierra Research Corporation, Note 348, December 1980.
- Byram, G. M., "Scaling Laws for Modeling Mass Fires," *Pyrodynamics*, Vol. 4, 1966, pp. 271-284.
- Countryman, C. M., *PROJECT FLAMBEAU . . . An Investigation of Mass Fire (1964-1967)*, Vol. 1, U.S. Department of Agriculture, U.S. Forest Service, Berkeley, California, 1969.
- Cox, G., and R. Chitty, "A Study of the Deterministic Properties of Unbounded Fire Plumes," *Comb. Flame*, Vol. 39, 1980, pp. 191-209.
- D CPA Attack Environment Manual*, Chap. 3, "What the Planner Needs To Know about Fire Ignition and Spread," U.S. Defense Civil Preparedness Agency and U.S. Department of Defense, Washington, D.C., June 1973.
- Delage, Y., and P. A. Taylor, "Numerical Studies of Heat Island Circulation," *Boundary-Layer Meteorology*, Vol. 1, 1970, pp. 201-226.
- Emmons, H. W., "Fire in the Forest," *Fire Res. Abstr. Rev.*, Vol. 5, 1963, pp. 163-178.
- (ed.), *Fire*, Proceedings of the 8th U.S. Applied Mechanics Meeting, University of California, Los Angeles, June 1978.
- Glasstone, S., and S. J. Dolan (eds.), *The Effects of Nuclear Weapons*, 3rd ed., U.S. Department of Defense and U.S. Department of Energy (USGPO), Washington, D.C., 1977.
- Irving, D., *Destruction of Dresden*, Kimber, London, 1963.
- Isaacson, E., and H. B. Keller, *Analysis of Numerical Methods*, Wiley, New York, 1966.
- Keller, H. B., *Numerical Methods for Two-Point Boundary-Value Problems*, Blaisdell, Waltham, Mass., 1968.
- Larson, D. A., and R. D. Small, *Large Area Fire--An Analytic Model*, Pacific-Sierra Research Corporation, Note 360, December 1980.
- Lee, S. L., "Fire Research," *Appl. Mech. Rev.*, Vol. 25, 1972, pp. 503-509.

Preceding page blank

Lowe, D., *The Great Chicago Fire in Eyewitness Accounts and 70 Contemporary Photographs and Illustrations*, Dover, New York, 1979.

McCaffrey, B. J., *Purely Buoyant Diffusion Flames: Some Experimental Results*, National Bureau of Standards, Washington, D.C., Report NBSIR79-1910, October 1979.

Morton, B. R., "Forced Plumes," *J. Fluid Mech.*, Vol. 5, 1959, pp. 151-163.

-----, C. Taylor, and J. S. Turner, "Turbulent Gravitational Convection from Maintained and Instantaneous Sources," *Proc. Roy. Soc. A.*, Vol. 24, 1956, pp. 1-23.

Murgai, M. P., "Radiative Transfer Effects in Natural Convections above Fires," *J. Fluid Mech.*, Vol. 12, 1962, pp. 441-448.

-----, and H. W. Emmons, "Natural Convection above Fires," *J. Fluid Mech.*, Vol. 8, 1960, pp. 611-624.

Nielsen, H. J., and L. N. Tao, "The Fire Plume above a Large Free-Burning Fire," *Tenth Symposium (International) on Combustion*, The Combustion Institute, Pittsburgh, 1965, pp. 965-972.

Small, R. D., and H. L. Brode, *Physics of Large Urban Fires*, Pacific-Sierra Research Corporation, Report 1010, March 1980.

Smith, R. K., "Radiation Effects on Large Fire Plumes," *Eleventh Symposium on Combustion*, The Combustion Institute, Pittsburgh, 1967, pp. 507-515.

-----, B. R. Morton, and L. M. Leslie, "The Role of Dynamic Pressure in Generating Fire Wind," *J. Fluid Mech.*, Vol. 68, 1975, pp. 1-19.

Yokoi, S., *Study on the Prevention of Fire-Spread Caused by Hot Upward Current*, Japanese Ministry of Construction, Building Research Institute, Report 34, November 1960.

EXECUTIVE SUMMARY

Large urban fires have resulted from natural disasters, explosions, and wartime actions. In many cases, entire urban areas were totally destroyed despite firefighters' efforts to contain the flames. The World War II firebombing raids on European and Japanese population centers caused immense damage and hundreds of thousands of casualties. Several ignited firestorms, with hurricane-force winds, high street-level temperatures, high concentrations of carbon monoxide, and complete burning of all combustible materials within the firestorm boundaries. Firestorms also produced a high number of casualties, seldom ameliorated even by concerted rescue efforts.

Large urban fires are a much greater threat in the age of nuclear weapons than ever before. Hundreds of square kilometers of an urban (or wildland) area can be ignited simultaneously by a single-megaton nuclear weapon. Indeed, superfires of unprecedented size could dwarf the tremendous fires of World War II.

After the firestorm in Hamburg, civil defense leaders in Germany addressed the problem of protecting the cities and the civilian population from such fierce fires. On the basis of the meager technical information then available, guidelines for rescue operations were outlined. However, the physical characteristics of the firestorm environment had not yet been defined--e.g., winds, temperatures, gas concentrations, sizes of combustible areas, and populations at risk. Such information is essential if planners are to design procedures for fire suppression/containment and population protection/rescue.

Today, years later, we are still without a complete and accurate picture of the superfire environment. No analysis has ever focused on the nature of the flow in and around the fire itself--which is the most vital information. Most studies have simply attempted to extrapolate results from classical plume theories, known to be valid only well above a small free-burning fire.

This report uses a new analytical approach to analyze the superfire environment. Our approach is based on a "component" model in

which different sets of equations are employed to represent the fundamentally different physics in separate parts of the fire-generated flow. Asymptotic analysis is used to derive the individual equation sets from standard conservation laws.

The "component" approach allows us to consider in detail the nature of the superfire environment in the critical region in and around the fire itself. Our analysis of that "combustion" region constitutes the first--and most interesting--model component.

The intensity and extent of the fires in the combustion region largely determine the characteristics of the entire flow field. Cold air is drawn into the burning zone and heated by the ongoing combustion processes. The heated air rises buoyantly, establishing a natural convection column. The buoyant air in the column cools and expands until a local equilibrium is established either in the upper atmosphere or at an inversion layer (of sufficient magnitude). Finally, a mesoscale recirculation pattern is established similar to a nocturnal urban heat island flow. Analyses of the convection column and recirculation flows produce the other basic model components.

We focus on the combustion region. Our analysis is valid in the upper limit for large urban fires with horizontal dimensions on the order of tens of kilometers and in the lower limit for fires the size of the multiple-fuel-bed Flambeau fires.

The first predictions concern the environment for a nominal large urban fire (with a 10 km radius). The sensitivity of the predictions to changes in model parameters is then considered. An experimental Flambeau fire (of radius ~ 0.25 km) is also analyzed. The results show reasonable agreement in all parameters when inflow horizontal velocities are selected to correspond to those observed.

Numerical simulation also shows that the type of plume observed over the Flambeau fire (i.e., with a width comparable to that of the fire) can be established only if turbulent mixing plays a major role in the combustion region dynamics. We anticipate that turbulence will play such a role in large urban fires.